

nn 0201

no 707

C

no 707

THE MULTISPECTRAL  
REFLECTANCE OF SHORTWAVE  
RADIATION BY AGRICULTURAL  
CROPS IN RELATION WITH  
THEIR MORPHOLOGICAL AND  
OPTICAL PROPERTIES

N. J. J. BUNNIK

NN08201.707

Dit proefschrift met stellingen van

**NICOLAAS JOHANNES JOZEF BUNNIK**

natuurkundig ingenieur, geboren te Rijswijk (Z.H.) op 22 juni 1942, is goedgekeurd door de promotoren, dr. ir. C. T. de Wit, buitengewoon hoogleraar in de theoretische teeltkunde, en ir. H. G. de Winter, hoogleraar in de technische natuurkunde aan de Technische Hogeschool te Twente.

*De Rector Magnificus  
van de Landbouwhogeschool,*

H. C. VAN DER PLAS

*Wageningen, 27 oktober 1977*

N. J. J. BUNNIK

THE MULTISPECTRAL  
REFLECTANCE OF SHORTWAVE  
RADIATION BY AGRICULTURAL  
CROPS IN RELATION WITH  
THEIR MORPHOLOGICAL AND  
OPTICAL PROPERTIES

*(with a summary in Dutch)*

PROEFSCHRIFT

TER VERKRIJGING VAN DE GRAAD  
VAN DOCTOR IN DE LANDBOUWWETENSCHAPPEN  
OP GEZAG VAN DE RECTOR MAGNIFICUS,  
DR. H. C. VAN DER PLAS,  
HOOGLERAAR IN DE ORGANISCHE SCHEIKUNDE,  
IN HET OPENBAAR TE VERDEDIGEN  
OP WOENSDAG 18 JANUARI 1978,  
DES NAMIDDAGS TE VIER UUR  
IN DE AULA VAN DE LANDBOUWHOGESCHOOL TE WAGENINGEN

H. VEENMAN & ZONEN B.V. – WAGENINGEN – 1978

## STELLINGEN

### I

Een mathematische beschrijving van de reflectie van kortgolvlige straling door gewassen uitgaande van een vooraf aangenomen drastische vereenvoudiging van de gewasstructuur volgens Suits, of door het achteraf invoeren van vereenvoudigingen in het gedetailleerde model volgens Goudriaan leidt tot vergelijkbare resultaten.

Dit proefschrift.

SUITS, G. H., 1972. The calculation of the directional reflectance of a vegetative canopy. Remote sensing of environment, 2: 117-125.

GOUDRIAAN, J., 1977. Crop meteorology: a simulation study. Pudoc, Wageningen, pp. 25-32.

### II

Chance en LeMaster (via het Suits model) en Goudriaan (via zijn numeriek model) vonden onafhankelijk van elkaar voor gewasreflectie de Helmholtz reciprociteitsrelatie tussen de richtingen van invallende straling en observatie.

Deze reciprociteitsrelatie berust op symmetrierelaties van de voor een gewaslaag geldende verstrooiingsfuncties voor directe en diffuse flux.

Met inachtnaam van de reflectiebijdrage van de bodem kan voor een gewas, opgebouwd uit een of meerdere uniforme lagen, deze reciprociteitsrelatie vanuit het Suits model algemeen bewezen worden.

Dit proefschrift.

CHANCE, J. E. and E. W. LEMASTER, 1977. Suits reflectance models for wheat and cotton; theoretical and experimental tests. Applied Optics, 16(2): 407-412.

GOUDRIAAN, J., 1977. Crop meteorology: a simulation study. Pudoc, Wageningen, pp. 36-39.

### III

Teledetectie-apparatuur en het gebruik ervan kunnen verbeterd worden door meer dan voorheen de aan de apparatuur te stellen kwaliteitseisen af te leiden uit de fysische relaties tussen de gezochte eigenschappen van de waargenomen objecten en de daarvan afkomstige straling.

### IV

Wanneer bij het beschouwen van een uniform gewas instralings- en observatie-richting samenvallen (waarbij de zgn. heiligenschijn optreedt) bestaat bij

zenith-hoeken van  $0^\circ$  en ongeveer  $52^\circ$  een nagenoeg lineair verband tussen de gemeten gewasreflectie en de bij deze richtingen behorende bedekkingsgraad. Deze relatie is geldig voor het zichtbare licht en het nabije infrarood.

Dit proefschrift.

MINNAERT, M., 1940. De natuurkunde van 't vrije veld I. W. J. Thieme & Cie, Zutphen, pp. 226-230.

## V

Door meting van de heiligenschijn onder een zenith-hoek van ongeveer  $52^\circ$  in het groene, het rode en het nabije infrarode deel van het spectrum, kunnen gegevens worden afgeleid welke in nagenoeg eenduidige relatie staan met de bladoppervlakte-index, de bedekkingsgraad, de bladkleur en het vochtgehalte van de oppervlaktelaag van de bodem.

Dit proefschrift.

## VI

Een door Jaggi voorgestelde beschrijving van de stralingsverdeling binnen niet gesloten gewassen met rijenstructuur, via voor drie orthogonale richtingen van elkaar onafhankelijke stelsels Duntley vergelijkingen, gaat voorbij aan de voor die richtingen geldende onderlinge afhankelijkheid van de diffuse flux.

JAGGI, R. K., 1972. A mathematical model concerning reflectance from a row crop. Rice University, Houston.

## VII

Uitspraken omtrent discriminatie tussen gesloten groene gewassen, gebaseerd op in het laboratorium gemeten reflectie-eigenschappen van op elkaar gestapelde bladeren, hebben weinig praktische betekenis.

RICHARDSON, A. J., *et al.*, 1969. Discrimination of vegetation by multispectral reflectance measurements. Proceedings of the 6th international symposium on remote sensing of environment, Ann Arbor, Michigan, pp. 1143-1156.

## VIII

De natuurkunde van het vrije veld en haar betekenis voor het toepassingsonderzoek in andere disciplines verdienen bij het wetenschappelijk onderwijs meer aandacht.

## IX

Het toepassen van resultaten bereikt via innoverend onderzoek aan de universiteiten dient te worden bevorderd door het leggen van meer en betere contacten met het bedrijfsleven.

## X

De koehandel rondom het Joint European Torus project bevestigt ogenschijnlijk, doch ten onrechte, de indruk dat een gezamenlijke inspanning voor het aanboren van nieuwe energiebronnen nog weinig urgent is.

## XI

De vrij hoge correlatie tussen de toename van het aantal huisdieren en de daling van het humane geboortecijfer lijkt een bij uitstek geschikt onderwerp voor multidisciplinair universitair onderzoek.

## VOORWOORD

Gedurende de periode januari 1971 tot januari 1977 is vanuit het Beleidsruimteproject NIWARS (Nederlandse Interdepartementale Werkgemeenschap voor het Applicatie-onderzoek van Remote Sensing technieken) onderzoek verricht naar de toepasbaarheid van moderne aardwaarnemingstechnieken.

Sedert eind 1972 tot aan de afsluiting van het NIWARS-project ben ik in dienst van NIWARS betrokken geweest bij het onderzoek betreffende de reflectie van licht en nabije infrarood straling door gewassen. Het doel van dit werk was het verkrijgen van achtergronds-kennis over deze verschijnselen en de resultaten aan te wenden voor het aangeven van praktische toepassingen van moderne luchtopnametechnieken ten behoeve van de landbouw.

Ik ben de voormalige Stuurgroep van de NIWARS erkentelijk voor de geboden faciliteiten om mijn onderzoek in dit proefschrift vast te leggen.

Het bestuderen van een natuurkundig verschijnsel, zoals reflectie van elektromagnetische straling in het genoemde golflengtegebied door levende systemen zoals gewassen, heeft mij vanaf het eerste begin ongemeen geboeid. In het bij mij aanvankelijk ontbreken van noodzakelijke landbouwkundige kennis werd voorzien door het onderzoek uit te voeren in multidisciplinair verband. De samenwerking binnen de onderzoeksgroep waarvan ik deel uit maakte, samengesteld uit fysici en landbouwkundigen, heb ik als zeer vruchtbaar ervaren.

Mijn dank gaat uit naar dr. ir. G. P. de Loor van het Fysisch Laboratorium TNO. Hij heeft een belangrijke bijdrage geleverd tot het opzetten van het onderzoek. Zijn ervaring op het gebied van remote sensing resulteerde in waardevolle adviezen, waarbij hij mij in het bijzonder heeft gestimuleerd tot het schrijven van dit proefschrift. Voorts mijn waardering voor het vele en vooral goede werk van mijn directe collega ing. W. Verhoef. Voor zijn inzet bij het veldexperimentele werk, het theoretisch onderzoek en zijn steun bij het schrijven van de gebruikte computerprogramma's ben ik hem in het bijzonder zeer erkentelijk.

Ir. Th. A. de Boer van het CABO heeft als leider van genoemde onderzoeksgroep en vanuit zijn landbouwkundige ervaring veel bijgedragen tot het sturen van het onderzoek en het evalueren van de potentiële toepassingsmogelijkheden van de bereikte resultaten. In de afgelopen periode heeft hij mij veel bij dit werk van belang zijnde landbouwkundige kennis bijgebracht. Ir. H. W. J. van Kasteren en de heer D. Uenk van het CABO wil ik bedanken voor het vele werk dat zij hebben verricht voor het verzamelen van gewasgegevens tijdens het spectrometeronderzoek te Wageningen in 1973 en 1974 en voor hun inbreng aan landbouwkundige kennis. Aan het samen met hen en ing. Verhoef verrichte veldwerk bewaar ik, mede dankzij de goede onderlinge verstandhouding, plezierige herinneringen.

Bij het verkrijgen van de over dit nog nieuwe onderwerp bestaande literatuur is ir. J. A. C. Holle van het documentatiecentrum van de NIWARS onmisbaar geweest.

Het in het veld meten van de reflectie van straling door gewassen, met behulp van een daartoe door de Technisch Fysische Dienst TNO & TH gebouwde veldspectrometer, is mede te danken aan de door het CABO en het Bureau Gemeenschappelijke Diensten op proefboerderij 'Droevendaal' te Wageningen beschikbaar gestelde faciliteiten. Het Fysisch Laboratorium TNO heeft steun verleend bij het gebruiksgereed maken van de apparatuur en bij computerverwerking van de meetgegevens. Het Nationaal Lucht- en Ruimtevaartlaboratorium kon voorzien in een voorlopige oplossing voor het vastleggen van de uitvoer van de veldspectrometer op magneetband. De direct hierbij betrokkenen wil ik voor hun aandeel hiertoe hartelijk danken. Bij de bouw van een speciaal voor de veldspectrometer geschikt registratiesysteem en de bijbehorende software heeft ir. P. W. H. Blansjaar van de Dienst Informatieverwerking van de Rijkswaterstaat een belangrijke bijdrage geleverd. De heer Th. Hirsch, eveneens werkzaam bij genoemde dienst, heeft de software voor en de verdere computerverwerking van de spectrometergegevens gerealiseerd.

Dr. ir. J. Goudriaan van het CABO heeft eigen modelsimulaties van gewasreflectie ter vergelijking met het door mij gebruikte model beschikbaar gesteld.

Mijn bijzondere dank gaat uit naar prof. dr. ir. C. T. de Wit en prof. ir. H. G. de Winter wegens hun bereidheid als promotoren op te treden en naar prof. dr. ir. J. Schenk, vanaf het begin actief betrokken bij het leggen van de daarbij noodzakelijke contacten. Dankzij de regelmatig met hen gevoerde voortgangsbesprekingen zijn, vooral gericht op bruikbare toepassingen van stralingsreflectie-metingen van gewassen, vele nieuwe aspecten ingebracht.

Veel werk is verricht door mej. A. H. van Rossem van het CABO voor het waar nodig corrigeren van het Engels en het typewerk. Mej. M. Sprengers, mevr. C. v. d. Velden en mej. J. v. d. Kruk van het Centraal Bureau NIWARS en mevr. A. E. Ch. van Vliet en mej. J. J. van der Wal van het Bureau Gemeenschappelijke Diensten wil ik bedanken voor hun bijdrage tot het typen van het manuscript.

Ten slotte mijn dank aan de Landbouwhogeschool om de verschijning van dit proefschrift mogelijk te maken.



# CONTENTS

## LIST OF SYMBOLS

1. INTRODUCTION . . . . .	1
1.1. General . . . . .	1
1.2. Motivation and objectives of the described investigation . . . . .	4
2. MULTISPECTRAL REFLECTANCE OF CROPS IN THE VISIBLE LIGHT AND THE NEAR INFRARED . . . . .	6
2.1. Detection of reflected radiation . . . . .	6
2.2. Spectral reflectance and transmittance of single leaves . . . . .	10
2.2.1. Leaf morphology and interaction with electromagnetic radiation . . . . .	10
2.2.2. Calculation of leaf reflectance and transmittance with the ray tracing method of Willstätter and Stoll . . . . .	12
2.2.3. Leaf reflectance and transmittance by the Kubelka and Munk theory . . . . .	13
2.2.4. The plate model for leaf reflectance and transmittance of Allen . . . . .	17
2.2.5. Directional reflectance and transmittance by single leaves . . . . .	18
2.2.6. Variation in reflectance and transmittance of leaves as a function of growth and senescence . . . . .	20
2.3. Spectral reflectance of soils . . . . .	22
2.4. Reflectance of radiation by a vegetation canopy . . . . .	24
2.4.1. Geometrical structure of a leaf canopy . . . . .	25
2.4.2. Radiative transfer within a canopy according to Ross and Nilson . . . . .	26
2.4.3. The canopy radiation model of Goudriaan and De Wit . . . . .	26
2.4.3.1. Geometry of the canopy and incident radiation . . . . .	27
2.4.3.2. Calculation of the radiant flux profile within the canopy . . . . .	27
2.4.3.3. Possible simplifications . . . . .	29
2.4.4. Canopy reflectance model of Smith and Oliver . . . . .	31
2.4.5. Calculation of canopy reflectance by application of the Duntley equations . . . . .	33
2.4.6. Plant canopy reflectance according to Suits . . . . .	34
2.4.6.1. Simplification of the geometrical structure of a vegetation canopy . . . . .	34
2.4.6.2. Calculation of the radiant flux profile within the canopy layers . . . . .	37
2.4.6.3. Calculation of directional reflectance . . . . .	41
2.4.7. Evaluation of the canopy reflectance models of Goudriaan and Suits . . . . .	42
2.4.8. Reciprocity relations . . . . .	45
2.4.9. Examples of canopy reflectance spectra . . . . .	46
3. SENSITIVITY OF MULTISPECTRAL REFLECTANCE DATA DUE TO VARIATION IN CROP PARAMETERS . . . . .	52
3.1. Distribution of information in the visible light and near infrared region. . . . .	52
3.2. Distribution of spectral information in canopy and soil contributions . . . . .	56
3.3. Calculation of the information distribution for simulated and measured reflectance spectra . . . . .	56
3.4. Relations between spectral bandwidth, variance and covariance of multispectral reflectance data in the visible light and near infrared due to crop parameter variations . . . . .	63
4. MEASUREMENTS OF CANOPY REFLECTANCE DATA . . . . .	70
4.1. Canopy reflectance measurements on the test site at Wageningen . . . . .	70
4.2. Description of the field spectrometer . . . . .	72
4.3. Measurements of crop parameters . . . . .	76
4.4. Collection of multispectral reflectance data at remote distance by means of MSS . . . . .	80

5. MULTISPECTRAL REFLECTANCE IN RELATION TO PLANT CANOPY PROPERTIES . . . . .	84
5.1. Introduction . . . . .	84
5.2. Canopy reflectance in the red and near infrared . . . . .	85
5.3. Analysis of model results and measurements by means of two-colour diagrams . . . . .	89
5.4. Relation between reflectance parameters and plant canopy structure . . . . .	98
5.5. Determination of the leaf colour . . . . .	114
5.6. The canopy hot spot and its applications for the detection of canopy properties . . . . .	118
6. SELECTION OF OPTIMUM WAVELENGTH BANDS FOR DISCRIMINATION BETWEEN VEGETATIVE CANOPIES . . . . .	127
6.1. Introduction . . . . .	127
6.2. An algorithm for optimum selection of spectral bands . . . . .	130
6.3. Calculation of optimum wavelength bands using Suits' model . . . . .	135
6.3.1. Passive detection . . . . .	137
6.3.2. Active detection . . . . .	141
6.4. Experimental results . . . . .	145
6.5. Intra- and interclass variations in multispectral reflectance data in relation with misclassification . . . . .	150
6.5. Summary and conclusions . . . . .	154
SUMMARY . . . . .	157
ACKNOWLEDGEMENTS . . . . .	165
REFERENCES . . . . .	166
APPENDIX A. BIDIRECTIONAL SCATTERING OF DIRECT RADIANT FLUX . . . . .	169
APPENDIX B. THE RECIPROCITY RELATION FOR BIDIRECTIONAL CANOPY REFLECTANCE . . . . .	172

## LIST OF SYMBOLS

### SECTION 2.1. TO 2.3.

Symbol	Description	SI-unit
$A$	Parameter for the state of the atmosphere	—
$a$	$(1 + \beta)/(1 - \beta)$	—
$b$	$\exp(\alpha)$	—
$E$	Global irradiance	$\text{W/m}^2\text{nm}$
$F(R_\infty)$	Kubelka-Munk function = $k/s$	—
$h$	Distance between object and sensor	$\text{m}$
$I$	Downward diffuse radiant flux	$\text{W/m}^2\text{nm}$
$J$	Upward diffuse radiant flux	$\text{W/m}^2\text{nm}$
$k$	Absorption coefficient	—
$L$	Spectral radiance	$\text{W/m}^2\text{sr nm}$
$L_A$	Apparent radiance	$\text{W/m}^2\text{sr nm}$
$L_I$	Intrinsic radiance	$\text{W/m}^2\text{sr nm}$
$L_p$	Path radiance	$\text{W/m}^2\text{sr nm}$
$LAI$	Leaf area index	—
$m$	Optical thickness	—
$N$	Total leaf area index	—
$n$	Cumulative leaf area index	—
$R_\infty$	Hemispherical reflectance of an infinitely thick diffusing medium	—
$R_g$	Hemispherical reflectance of the soil	—
$r$	Hemispherical reflectance of a single leaf	—
$r$	Directional spectral reflectance	$\text{sr}^{-1}$
$T$	Atmospheric transmittance	—
$s$	Scattering coefficient	—
$t$	time	$\text{s}$
$t$	Hemispherical transmittance of a single leaf	—
$\alpha$	$\{k(k + 2s)\}^{1/2}$	—
$\beta$	$\{k/(k + 2s)\}^{1/2}$	—
$\theta_o$	Zenith observation angle	—
$\theta_s$	Zenith solar angle	—
$\lambda$	Wavelength	$\text{nm}$
$\rho'$	Directional reflectance of single leaves	$\text{sr}^{-1}$
$\tau'$	Directional transmittance of single leaves	$\text{sr}^{-1}$
$\psi$	Azimuth angle	—
$\omega_D$	Solid view angle of the sensor	$\text{sr}$

SECTION 2.4.3. TO 2.4.5.

Symbol	Description	SI-unit
$B$	Backscatter coefficient for diffuse flux	—
$B'$	Backscatter coefficient for direct flux	—
$B_i(\beta', \lambda)$	Distribution function for flux scattered into direction, $\beta$ , by leaf fraction, $F(\lambda)$	—
$B_u(\beta')$	Weighting factor for angular scattering	—
$F(\lambda)$	Leaf angle distribution function	—
$F'$	Forward scatter coefficient for direct flux	—
$I_s(\lambda)$	Scattered amount of flux by fraction, $F(\lambda)$	W/m <sup>2</sup> nm
$I_n$	Direct flux as a function of cumulative leaf area index	W/m <sup>2</sup> nm
$I_0$	Incident direct flux	W/m <sup>2</sup> nm
$K_b(\beta)$	Canopy extinction coefficient for direct flux	—
$K_d$	Canopy extinction coefficient for diffuse flux	—
$K_f$	Canopy extinction coefficient	—
$K_h$	Extinction coefficient for a canopy with horizontal leaves	—
$LAI, LAI'$	Leaf area index	—
$L_s$	Leaf area index of an incremental canopy layer	—
$M_i(\beta, \lambda)$	Intercepted flux from direction, $\beta$ , by leaf fraction, $F(\lambda)$	W/m <sup>2</sup> nm
$M_i(\beta)$	Intercepted flux from direction, $\beta$	W/m <sup>2</sup> nm
$n$	Cumulative leaf area index	—
$O(\beta, \lambda)$	Average projection of leaves within inclination class, $\lambda$ , into direction, $\beta$	m <sup>2</sup>
$\bar{O}(\beta)$	Average projection of leaves into direction, $\beta$	m <sup>2</sup>
$q'$	Extinction coefficient for direct flux	—
$q'_0$	$q' \cos \xi$	—
$S_b$	Direct irradiance at the canopy top	W/m <sup>2</sup> nm
$s$	Degree of random distribution of leaves	—
$s$	Upward diffuse flux	W/m <sup>2</sup> nm
$t$	Downward diffuse flux	W/m <sup>2</sup> nm
$\beta, \beta'$	Inclination angle	—
$\lambda$	Leaf inclination interval	—
$\xi$	Solar zenith angle	—
$\mu$	Absorption coefficient for diffuse flux	—
$\mu'$	Absorption coefficient for direct flux	—
$\rho_f(\beta)$	Hemispherical canopy reflectance for incident flux from direction, $\beta$ , according to a simple formula	—
$\rho_f'(\beta)$	Hemispherical canopy reflectance for incident flux from direction, $\beta$ , with neglectance of multiple scattering, according to a simple formula	—

Symbol	Description	SI-unit
$\rho_h$	Hemispherical canopy reflectance for large LAI and horizontal leaves	—
$\rho_m$	Hemispherical canopy reflectance according to the numerical model of Goudriaan	—
$\hat{\rho}_m$	Hemispherical canopy reflectance, estimated by a regression between $\rho_m$ and $\rho_f$	—
$\rho_s$	Hemispherical soil reflectance	—
$\sigma$	Leaf scatter coefficient	—
$\tau$	Hemispherical leaf transmittance	—
$\phi_d(\beta)$	Downward diffuse flux from zone, $\beta$	$W/m^2nm$
$\phi_u(\beta)$	Upward diffuse flux from zone, $\beta$	$W/m^2nm$

#### SECTION 2.4.6. – 5.6.

Symbol	Description	SI-unit
$A$	Integration constant	$W/m^2nm$
$\bar{A}$	Average leaf area	$m^2$
$A_c$	Aperture area	$m^2$
$a_h$	Average area of horizontal canopy components	$m^2$
$a_v$	Average area of vertical canopy components	$m^2$
$a$	Canopy extinction coefficient for diffuse flux	$m^{-1}$
$B$	Diagonal matrix with diagonal elements, $B_{kk} = \pi^{-1} E_i(\lambda_k) T(\lambda_k)$	$W/m^2nm$
$B$	Integration constant	$W/m^2nm$
$B$	Soil cover	—
$C$	Integration constant	$W/m^2nm$
$C_i(k)$	Information contribution of original spectral band, $i$ , to a syntetic band, $k$	—
$C$	Diagonal matrix with diagonal elements, $E(L_{kj})$	$W/m^2sr nm$
$D$	Integration constant	$W/m^2nm$
$D^*(\lambda)$	Detectivity	$ms^{-1/2}W^{-1}$
$E$	Expectation value	—
$E(\lambda)$	Standard CIE illuminant	$W/m^2nm$
$E_-$	Downward diffuse flux	$W/m^2nm$
$E_-(0)$	Sky irradiance	$W/m^2nm$
$E_+$	Upward diffuse flux	$W/m^2nm$
$E_i$	Total irradiance	$W/m^2nm$
$E_s$	Direct solar flux	$W/m^2nm$
$E_s(0)$	Incident direct solar flux	$W/m^2nm$
$E_s^0$	Incident direct solar flux perpendicular to the sun rays	$W/m^2nm$

Symbol	Description	SI-unit
$F(\psi, \theta_s)$	Azimuthal variation function of bidirectional canopy scattering	—
$f(\theta_L)$	Cummulative leaf angle inclination distribution function	—
$f'(\theta_L)$	Probability density function of leaf angle, $\theta_L$	—
$f$	Focal length	m
$G(\theta_L, \theta_o)$	Factor for non-Lambertian variation of radiant intensity of canopy layer, $\Delta x$	$m^{-1}$
$g(\theta_o)$	Weighting factor for the average leaf area projection into direction, $\theta_o$	—
$H$	Total horizontally projected leaf area index	—
$H'$	Horizontal leaf area density	$m^{-1}$
$h$	$(a+m)/\sigma = \rho_{0\infty}^{-1}$	—
$h$	Flight altitude	m
$I(k)$	Relative information content of syntetic band, $k$	—
$I_i, i$	Relative information content of original band, $i$	—
$I$	Unity matrix	—
$I$	Radiant intensity	$W/m^2 sr nm$
$K(\theta_o)$	Extinction coefficient	$m^{-1}$
$k(\theta_s)$	Extinction coefficient	$m^{-1}$
$L(\lambda)$	Spectral radiance	$W/m^2 sr nm$
$\underline{L}$	Radiance vector	$W/m^2 sr nm$
$L_I(\lambda)$	Intrinsic spectral radiance	$W/m^2 sr nm$
$L_i$	Radiance of a uniform overcast sky	$W/m^2 sr nm$
$L_c$	Radiance from canopy components	$W/m^2 sr nm$
$L_c^o$	Radiance from canopy components, leaving the canopy without interception	$W/m^2 sr nm$
$L_s$	Radiance contribution from the soil	$W/m^2 sr nm$
$L$	Canopy leaf area index parameter	—
$L_p$	Atmospheric path radiance	$W/m^2 sr nm$
$LAI$	Leaf area index	—
$M$	Canopy emittance	$W/m^2 nm$
$m$	$(a^2 - \sigma^2)^{1/2}$	$m^{-1}$
$N$	Number of features	—
$n$	Normal vector	—
$NEP(\lambda)$	Noise equivalent power	W
$NER(\lambda)$	Noise equivalent radiance	$W/m^2 sr nm$
$P(\lambda)$	Spectral power	W
$P$	Spectral parameter	—
$P_t, P_m$		—
$P_r$		—
$p(x)$	Probability for penetration upto depth, $x$	—
$p$	Synthetic feature	—

Symbol	Description	SI-unit
$\underline{p}$	Spectral parameter vector	—
$q$	Ratio of intensities	—
$R_c$	Canopy hemispherical reflectance	—
$R_\infty$	Infinite hemispherical canopy reflectance	—
$r_b$	Bidirectional reflectance	$\text{sr}^{-1}$
$r_c$	Directional canopy reflectance	$\text{sr}^{-1}$
$r_\infty$	Directional infinite canopy reflectance	$\text{sr}^{-1}$
$r$	Directional reflectance	$\text{sr}^{-1}$
$\underline{r}$	Directional reflectance vector	$\text{sr}^{-1}$
$r_c(0)$	Directional canopy reflectance for a black soil	$\text{sr}^{-1}$
$r'_c(0)$	Differential canopy reflectance for a black soil	$\text{sr}^{-1}$
$S/N$	Signal to noise ratio	—
$s$	Forward scatter coefficient for direct flux	$\text{m}^{-1}$
$s'$	Backscatter coefficient for direct flux	$\text{m}^{-1}$
$S_i$	Reflectance signal in spectral band, $i$	—
$t_D$	Detector dwell time	$s$
$T(\lambda)$	Atmospheric transmittance	—
$u(\theta_o)$	Canopy scattering coefficient for upward diffuse flux	$\text{m}^{-1}$
$\underline{u}$	Transformed data vector	—
$V$	Total vertically projected leaf area index	—
$V'$	Vertical leaf area density	$\text{m}^{-1}$
$v(\theta_o)$	Canopy scattering coefficient for downward diffuse flux	$\text{m}^{-1}$
$v$	Velocity	$\text{ms}^{-1}$
$w(\theta_o, \theta_s, \psi)$	Bidirectional canopy scattering coefficient for direct flux	$\text{m}^{-1}$
$x$	Canopy depth	$\text{m}$
$\Delta x$	Incremental canopy layer	$\text{m}$
$X$	Tristimulus value	$\text{W}/\text{m}^2$
$x_1$	Canopy thickness	$\text{m}$
$x$	Chromaticity coordinate	—
$\bar{x}(\lambda)$	Weighting factor of CIE primary	—
$\underline{x}$	Feature vector	—
$Y$	Tristimulus value	$\text{W}/\text{m}^2$
$Y$	Eigenvector matrix	—
$y$	Chromaticity coordinate	—
$\bar{y}(\lambda)$	Weighting factor of CIE primary	—
$y$	Eigenvector	—
$Z$	Tristimulus value	$\text{W}/\text{m}^2$
$z$	Chromaticity coordinate	—
$\bar{z}(\lambda)$	Weighting factor of CIE primary	—
$\alpha$	Constant	—
$\alpha_L$	Leaf angle	—

Symbol	Description	SI-unit
$\beta$	Constant	—
$\delta_{mp}$	Kronecker delta function	—
$\delta(\theta_L)$	Dirac delta function	—
$\Delta\nu$	Electronic bandwidth	$s^{-1}$
$\theta_L$	Canopy leaf angle parameter	—
$\bar{\theta}_L$	Average canopy leaf angle	—
$\theta_o$	Zenith observation angle	—
$\hat{\theta}_o$	Zenith angle for the hot spot condition	—
$\theta_s$	Solar zenith angle	—
$A$	Covariance matrix	—
$\lambda$	Wavelength	nm
$\lambda_c$	Dominant wavelength	nm
$\lambda_i$	Eigenvalue	—
$\mu$	Mean value	—
$\underline{\mu}$	Mean vector	—
$\xi$	$(H^2 + V^2)^{1/2}/LAI$	—
$\xi'$	$(H + V)/LAI$	—
$\rho$	Hemispherical leaf reflectance	—
$\rho_o$	Hemispherical canopy reflectance for diffuse irradiance	—
$\rho_h$	Hemispherical canopy reflectance for large $LAI$ and horizontal leaves	—
$\rho_{hs}$	Hot spot reflectance for large $LAI$ and horizontal leaves (Goudriaan)	$sr^{-1}$
$\rho_s$	Hemispherical soil reflectance	—
$\rho'$	Bidirectional reflectance	$sr^{-1}$
$\Sigma$	Covariance matrix	—
$\sigma^2$	Variance	—
$\sigma_{mp}$	Matrix element of $\Sigma$	—
$\sigma$	Canopy back scattering coefficient for diffuse flux	$m^{-1}$
$\sigma$	Leaf scatter coefficient (Goudriaan)	—
$\tau$	Hemispherical transmittance of a single leaf	—
$\tau_o$	Optical transmittance	—
$\Phi(\psi)$	Azimuthal variation function of radiant intensity	—
$\phi_o$	Azimuthal view angle	—
$\phi_s$	Solar azimuth angle	—
$\phi_L$	Azimuthal angle of leaf orientation	—
$\psi$	Azimuthal angle between sun and sensor	—
$\omega$	Instantaneous view angle	—
$\omega'$	Rotation frequency of scanning mirror	$rad\ s^{-1}$
$\omega_o$	Solid angle for detection	sr
$\omega_s$	Solid angle for incident radiation	sr



# CHAPTER 6

Symbol	Description	SI-unit
$C_i$	Crop category (class) $i$	—
$C(x_i)$	Information contribution of spectral band, $x_i$ , to the total information present in feature vector, $\underline{x}$	—
$E$	Expectation value	—
$E_-(0)$	Sky irradiance	W/m <sup>2</sup> nm
$E_s(0)$	Incident direct solar flux	W/m <sup>2</sup> nm
$f_s$	Fraction of shadow observed inside a homogeneous canopy and on the visible fraction of the soil	—
$I(\underline{x})$	Information content of feature vector, $\underline{x}$	—
$K$	Extinction coefficient	m <sup>-1</sup>
$k$	Extinction coefficient of penetrating direct flux	m <sup>-1</sup>
$L$	Canopy leaf area index parameter	—
$LAI$	Leaf area index	—
$l(\underline{x})$	Relative loss of information	—
$M$	Number of crop clusters	—
$M$	Regression matrix	—
$N$	Number of spectral bands or dimension of feature vector, $\underline{x}$	—
$P(C_i)$	Probability for category, $C_i$	—
$P(C_i \underline{x})$	Conditional probability of $C_i$ , given $\underline{x}$	—
$P(\underline{x} C_i)$	Conditional probability of $\underline{x}$ , given $C_i$	—
$p(\underline{x} C_i)$	Conditional probability density of $\underline{x}$ , given $C_i$	—
$p(\underline{x}_1, \underline{x}_2 C_i)$	Joint conditional probability density of subvectors, $\underline{x}_1$ and $\underline{x}_2$ of $\underline{x}$ , given $C_i$	—
$p(\underline{x}_1 \underline{x}_2 C_i)$	Conditional probability density of subvector, $\underline{x}_1$ , given $\underline{x}_2$ and category, $C_i$	—
$q$	Dimension	—
$r(\lambda_i)$	Directional canopy reflectance at wavelength, $\lambda_i$	sr <sup>-1</sup>
$\underline{x}$	Feature vector, $\underline{x}$	—
$\underline{x}_1, \underline{x}_2$	Subvectors of $\underline{x}$	—
$\underline{x}^T$	Transposed feature vector	—
$\hat{\underline{x}}_1$	Estimation of $\underline{x}_1$ by linear regression between $\underline{x}_1$ and $\underline{x}_2$	—
$x_i$	Element of $\underline{x}$	—
$x_{ik}$	Element of $\underline{x}_k$ of crop category, $k$	—
$x'$	Relative canopy depth	—
$\Gamma_i$	Volume in feature space, containing feature vectors, $\underline{x}_i$ , of class, $C_i$	—
$\varepsilon$	Probability of error due to misclassification	—
$\theta_L$	Canopy leaf angle parameter	—
$\theta_o$	Zenith angle of observation	—

Symbol	Description	SI-unit
$\theta_o$	Zenith angle of observation for the hot spot condition	—
$\theta_s$	Solar zenith angle	—
$\Lambda$	Covariance matrix	—
$\lambda$	Eigenvalue	—
$\lambda_i$	Center wavelength value of spectral band, $i$	nm
$\mu$	Mean vector of feature vectors, $\underline{x}$	—
$\mu_1, \mu_2$	Mean vectors of subvectors $\underline{x}_1$ and $\underline{x}_2$	—
$\mu^{(1/2)}$	Bhattacharyya distance	—
$\rho$	Correlation coefficient	—
$\rho$	Hemispherical reflectance of a single leaf	—
$\rho_s$	Hemispherical reflectance of the soil	—
$\Sigma$	Covariance matrix	—
$\Sigma_{ij}$	Subcovariance matrix	—
$\Sigma_{11.2}$	Residual covariance matrix of subvector, $\underline{x}_1$ , relative to the linear regression space between $\underline{x}_1$ and subvector, $\underline{x}_2$	—
$\Sigma_a$	Covariance matrix of feature vectors obtained by active detection in the hot spot	—
$\Sigma_p$	Covariance matrix of feature vectors obtained by passive detection	—
$\sigma_{ii}^2$	Variance of element, $x_i$ , of feature vector, $\underline{x}$	—
$\sigma_{ii}$	Standard deviation of element, $x_i$ , of feature vector, $\underline{x}$	—
$\sigma_{ij}$	Covariance between elements, $x_i$ and $x_j$ , of feature vector, $\underline{x}$	—
$\sigma_{11.2}^2$	Residual variance of element, $x_1$ , relative to the regression line between $x_1$ and element, $x_2$	—
$\tau$	Hemispherical transmittance of a single leaf	—
$\chi^2_{N,P}$	Chi-square distribution with $N$ degrees of freedom	—
$\psi$	Azimuth angle between sun and sensor	—

# 1. INTRODUCTION

## 1.1. GENERAL

In agricultural and ecological management and research there is an increasing need to obtain information on the inventory and the condition of crops. Especially, in time determining differences due to diseases, plagues and deficiencies in crops and early assessment of crop yield are of economic importance.

Existing organizations at local, national and international level, based on the actual degree of efficiency, apply methods to collect necessary information on acreage assessment. Inspections of the state of crops provide required information about crop vigour and the expected yield.

For extended areas and those difficult of access, aerial surveys and recently observations from space, offer a valuable addition and in some cases it is the best method to supply management or research with the information required.

Long before World War II, aerial photography was applied for earth sciences.

Photo interpretation is the discipline for deriving useful information from a visual study of photographic images. Keys of interpretation make use of spatial features like size, shape, pattern, texture, shadow and spectral features, like tone and colour together with logical relations between details on the image.

Moreover useful stereo information is available, by photographing the observed ground under two different angles. Gray levels on black and white images or colours on colour photographs with spatial patterns are useful to a photo interpreter to recognize crop type, state of growth or local differences related with plant diseases, pests or stress.

Both gray level and colour are determined by the distribution of the light reflected by the features present on the earth's surface. The distribution and absolute magnitude of reflected light depend on many variable factors, like spectral composition of the incident solar radiation, reflection properties of the reflecting material itself, influence of the direct environment, solar altitude, direction of observation, flight altitude, state of the atmosphere, cloud cover percentage and weather conditions. Moreover, film density and resulting colour are affected by the camera used, the emulsions applied and the photographic processing afterwards.

After World War II, black and white and colour emulsions, sensitive to near infrared radiation between 700 and 900 nm, were made available for civil use. From laboratory experiments it was already known that spectral reflectance of well-developed green vegetation is characterized by relatively low reflectance in the red part of the visible light region and high reflectance in the near infrared. This specific high reflectance in the near infrared is a useful discrimina-

tive tool, when compared with other natural features like rocks, bare soil and especially water.

The colour infrared or false colour film widely applied today consists of an infrared-sensitive layer with cyan dye, a red-sensitive layer with yellow dye and a green-sensitive layer with magenta dye. A yellow filter prevents film exposure by blue light. By reversion after processing and the principle of colour subtraction, green vegetation will appear with a red colour on the false colour image due to dominant infrared reflectance.

One of the first experiments with false colour photography and other emulsions applied to vegetation studies, disease and stress detection was performed by COLWELL (1956).

In addition, multiband photography has been adopted to aerial survey. By photographing the earth's surface simultaneously through a series of different filters determining separated spectral bands in the visible light and the near infrared part, spectral reflectance differences present on separated images can be studied. Making use of colour additive techniques to compose a new colour image out of a selection of different spectral bands, a photo interpreter is capable of enhancing differences between features of interest and of improving discrimination exploiting differences in spectral reflectance.

In particular in vegetation studies by means of aerial survey, monitoring of variations during time, provides essential information, concerning plant growth, early detection of diseases, human control etc. The frequency of and the moments of survey desired depend on the vegetation categories dealt with. For agricultural crops, like cereals the requirements are different compared with those for forest land, range land, meadow land or marsh land. Otherwise, the varying climatological conditions also restricting a successful execution of aerial surveys, influence mission planning and the usefulness of information obtained.

Especially, as a result of applications for military purposes, also non-photographic imaging techniques have been developed. By means of electro-optical sensors or microwave detectors, the radiation emanating from the earth's surface is converted in electrical signals. These electrical signals either may be used for generating a photographic image directly or to apply computer data handling on the signals recorded on magnetic tape. Afterwards, systematic errors may be eliminated and these data are processed to new imagery accomplishing with user requirements.

Such modern earth observation techniques are known as Remote Sensing techniques, however, in a general sense this concept implies more.

An essential improvement of aerial survey as a consequence of remote sensing is related with the much larger extent of the electromagnetic spectrum of reflected or emitted radiation utilized in the observation of phenomena at the earth's surface. A limiting factor is the wavelength dependent transparency of the atmosphere for electromagnetic radiation.

Besides methods for detection of emitted radiation, within the atmospheric windows, in the thermal infrared between 3 to 5  $\mu\text{m}$  and 8 to 14  $\mu\text{m}$  and the

passive microwave range to about 1 m, solar radiation or an artificial source of electromagnetic radiation (laser and radar systems) may be used to detect reflected radiation.

The remote sensing technique to which attention is paid in this manuscript is based on the measurement of reflected shortwave radiation in the visible light and the near infrared, originating from the sun or an artificial source within the wavelength range from about 400 to 2500 nm.

This remote sensing technique, familiar under the name of multispectral scanning (MSS), detects reflected radiation by the earth's surface simultaneously within a discrete number of wavelength bands, distributed within the atmospheric windows, by means of solid state electro-optical sensors.

An opto-mechanical scanner, usually a rotating mirror in combination with an imaging telescope, is applied to collect radiation entering into the momentaneous field of view and line by line. After spectrometric dispersion and imaging the momentarily observed ground elements in different spectral 'colours' on the effective apertures of the sensors determining the number of spectral bands, the generated electrical signals are recorded on magnetic tape.

The principle of multispectral scanning is comparable to the method of multiband photography mentioned before.

Besides the drawback of the absence of stereo information, the coarser spatial ground resolution and some geometrical image distortions, inherent to MSS, the advantages are better spectral resolution, the use of signal calibration to obtain physically well-defined radiation values and the improved sensitivity to radiation intensity level discrimination.

Because of the availability of MSS data on magnetic tape, these data are appropriate for direct processing by means of computers or special purpose devices.

When important keys for image interpretation are related with spectral reflectance differences, like in agricultural areas, a large part of the interpretation by the user can be done automatically, unbiased and rapidly by means of image processing techniques.

Otherwise, it is possible to employ data processing procedures to produce imagery which improves or simplifies visual interpretation. Moreover, machine processing can be exploited in so far as small differences between intensity and spectral distribution of reflected radiation are concerned, which can hardly be distinguished or not by a human interpreter.

On the other hand, for multitemporal studies corrections could be required to eliminate systematic differences between data related to the actual state of the atmosphere or the position of the sun. Calibrated MSS data on magnetic tape are most suitable in applying correction algorithms.

Especially, in the United States the first experimental airborne multispectral scanners were manufactured since the early sixties. Today, several multispectral scanners with data processing facilities are commercially available. In the near future, earth observations by means of spaceborne multispectral scanners will be of increasing importance. In 1972, the first experimental satellite for

earth observations, Landsat-1, equipped with MSS, was launched by NASA, followed by Landsat-2 in 1975.

For more general information, the reader is referred to the Manual of Remote Sensing, volume 1 and 2 of the American Society of Photogrammetry (1975).

## 1.2. MOTIVATION AND OBJECTIVES OF THE DESCRIBED INVESTIGATION

From the first experiments with MSS for civil applications, much attention has been paid to aspects related with data processing to provide potential users with useful and reliable end products. Application of MSS for agricultural purposes mainly was directed at classification and inventory of standing crops in wide areas. Also early detection of diseases and stress has been subject of great efforts. In a later stage, the applicability of growth monitoring with the use of multitemporal reflectance data has been studied and will be continued (see COLWELL and SUITS, 1975 and NALEPKA *et al.*, 1977).

When only crop type discrimination is considered, differences present between spectral reflectance of agricultural crops registered with MSS are regarded as input data to be processed with a classification programme.

By means of cluster analysis (unsupervised classification) or data selected from features already known (supervised classification) and methods adopted from pattern recognition techniques, MSS data are assigned to known categories or classified as unknown. The final result is presented by a (usually colour coded or alpha numeric) map with a legenda and auxiliary data giving statistical information and ground cover percentages.

If scanner output is considered as input for data processing, background knowledge on the physical relations between crop properties, like state of growth, biomass, leaf colour etc. and the resulting spectral distribution of reflected radiation, does not play an essential role.

In this, the question is disregarded to what extent spectral reflectance (or spectral signature) can be used as a crop property from which intrinsic parameters can be deduced.

In relation with efficiency and cost factors concerning data collection and processing, it is important to know beforehand in which and in how many spectral bands reflected radiation from crops has to be detected to characterize spectral distribution and dynamic behaviour of reflected radiation sufficiently.

In addition, such spectral bands should produce reflectance data useful to determine reliable relations between scanner input and the crop variables to be detected.

A multidisciplinary approach of this problem is most suitable and must be based on background knowledge on physical and plant physiological relationships describing spectral reflectance of shortwave radiation by vegetative canopies.

Beyond a purely empirical approach, a more fundamental approach is

preferred. If an experimentally verified mathematical model describing these relations is available together with the acquisition of experimental data, potential application and optimized use of MSS data for agricultural purposes could be investigated in a more direct way.

These motives gave rise to the present study. The objectives of the investigation and the contents of this manuscript may be summarized as follows.

1. To investigate relations between crop variables and spectral reflectance of vegetative canopies by means of an appropriate mathematical model and experimental data. Variables of uniform canopies, like total leaf area index, leaf angle distribution, optical constants of the leaves and spectral reflectance of the bounding soil have been studied in relation with geometrical variables of incoming radiation and the direction of detection of reflected radiation.
2. To determine spectral bands producing useful relations between reflectance data and canopy variables. Further, suitable combinations of reflectance data from different spectral bands have been studied which provide a simplified and better defined relationship with canopy structure, leaf colour or moisture content variations of the upper surface layer of the bounding soil. As a result of this study, a non-destructive method became available for monitoring crop growth, crop senescence, detection of changes probably related to stress or diseases and to produce data useful to crop yield estimation techniques.
3. To determine the spectral bandwidth allowed of selected wavelength bands in relation with a minimized loss of sensitivity of the mensuration of spectral reflectance variations due to variations in crop structure.
4. To determine directions of incoming and reflected radiation producing a drastic simplification in the complicated relation between crop reflectance and crop variables. On account of the conditions found, monitoring of dynamic behaviour of crop properties could be carried out with increased accuracy.
5. To determine the position and a minimum number of spectral bands with a minimum loss of spectral information for between-crop type discrimination.

## 2. MULTISPECTRAL REFLECTANCE OF CROPS IN THE VISIBLE LIGHT AND THE NEAR INFRARED

### 2.1. DETECTION OF REFLECTED RADIATION

Remote sensing in the wavelength region from the visible light up to and including the near infrared is based on the remote measurement of electromagnetic radiation reflected by the earth's surface. In this way information is gathered from characteristic differences in the spectral composition.

Essential to the optimum use of remote sensing techniques is a good understanding of the way in which the detected observable is achieved, how this process depends on the physical properties of the reflecting object and the impinging radiation; moreover, the influence of the earth's atmosphere and the environment and the geometry of observation.

A crop is considered of which the reflected radiation is detected by a remote sensor present in an aeroplane or a satellite. Since generally detection occurs through a certain solid angle with a variable angle of observation, spectral radiance is the adequate physical quantity. Spectral radiance is defined by the radiative power emitted by a unit of the reflecting area projected in the direction of observation, per unit of solid angle and per unit of wavelength increment.

As a function of the geometry of observation and the scattering and absorbing properties of the earth's atmosphere, acting as the transferring medium between the crop under observation and the sensor, the detected radiance as a function of wavelength is given by the equation

$$L_A(\theta_o, \theta_s, \psi, A, h, \lambda, t) = L_I(\theta_o, \theta_s, \psi, A, \lambda, t) T(\theta_o, A, h, \lambda, t) + L_p(\theta_o, \theta_s, \psi, A, h, \lambda, t) \quad (2.1.)$$

$L_A$  = apparent radiance detected by the remote sensor.

$L_I$  = intrinsic radiance of the crop at surface level.

$T$  = transmittance through the atmosphere.

$L_p$  = atmospheric path radiance.

$A$  = general parameter representing the state of the atmosphere.

$h$  = distance between the sensor and the earth's surface.

$\theta_o$  = zenith angle of observation.

$\theta_s$  = solar zenith angle.

$\psi$  = azimuth angle between the direction of observation and the position of the sun.

$\lambda$  = wavelength.

$t$  = time.

Fig. 1. illustrates the geometry of bidirectional reflection from the earth's surface when an airborne scanning system is used in remote sensing.



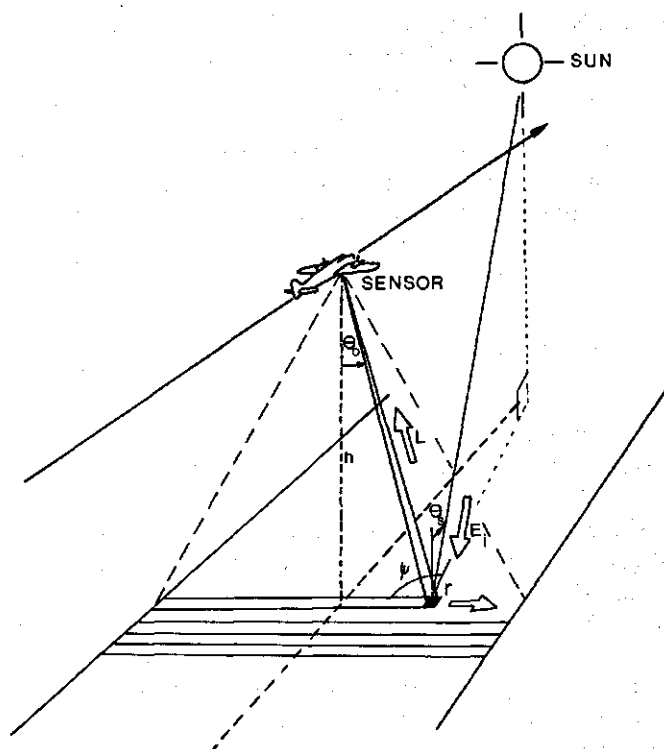


FIG. 1. Detection of electromagnetic radiation from the earth's surface with an airborne remote sensor.

With respect to the influence of the atmosphere on the measured spectral radiance, many data are available. Both the loss caused by transmittance and the scattering properties are determined mainly by the atmospheric composition and the distribution of the aerosol, the flight altitude and the direction of momentaneous detection.

These quantities are closely dependent on the meteorological conditions and the location on the earth, besides they may vary along the flight track of the sensor system. In the quantitative determination of the influence of the atmosphere upon the remote detection of reflected radiation empirical methods as well as mathematical models are available. The latter models are based on equations for radiative transfer of electromagnetic radiation through the atmosphere (see TURNER, 1974). Using measured input parameters of the state of the atmosphere, such a model can be applied in correcting remote sensing data for the systematic influence of the intervening atmosphere.

In general, a contrast reduction is caused by the additive scattered radiance and the advanced amount of signal noise. In view of the subject proper of this study, no detailed description will be given of the physics of the rather complex behaviour of the atmosphere which acts as a transfer medium for radiation to

be detected at a remote distance. When a quantitative analysis of remote sensing data is needed, the interaction of the atmosphere usually may not be neglected, if accuracy is required (MALILA *et al.* 1972).

The information deduced from the measured radiance is given by the intrinsic surface radiance,  $L_I$ . This radiance depends on the impinging global irradiance and the reflectance properties of the object itself. Analogous to an ideal diffuse scattering (Lambertian) surface, the following definition has been introduced

$$L_I(\theta_o, \theta_s, \psi, A, \lambda, t) = \frac{1}{\pi} r(\theta_o, \theta_s, \psi, \lambda) E(\theta_s, A, \lambda, t) \quad (2.2)$$

$r$  = directional spectral reflectance.

$E$  = hemispherical (global) spectral irradiance.

Irradiance consists of a component emanating from the direct solar radiation and a component given by the diffuse radiation of the sky. Irradiance is mainly determined by the solar zenith angle,  $\theta_s$ , meteorological conditions, cloud distribution, state of the atmosphere and is dependent on wavelength and diurnal variation.

Fig. 2. gives an example of the spectral irradiance for different solar angles. Fig. 3. shows an example of the ratio between diffuse sky irradiance and direct solar irradiance as measured.

The reflectance coefficient,  $r$ , contains the de facto spectral information about the object under observation. It is known that vegetation canopies in reality do not act as Lambertian reflectors, because crop reflectance depends on the direction of observation. Apart from this, reflectance changes due to vegetative growth, human management and ecological influences.

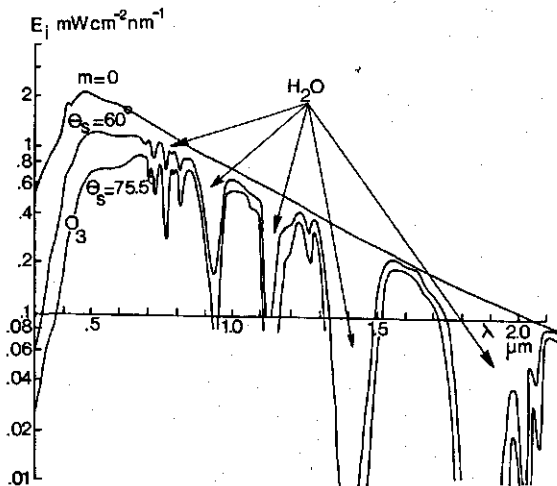
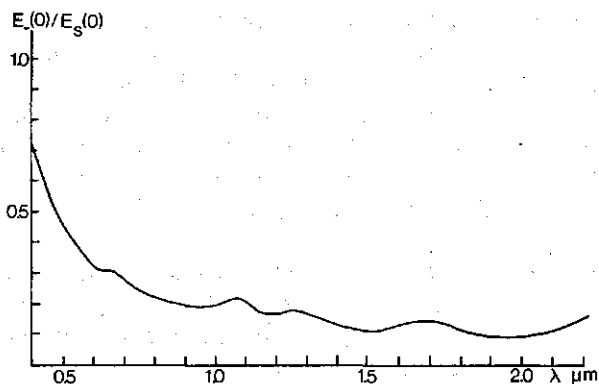


FIG. 2. Examples of the spectral distribution of solar irradiance. The irradiance outside the atmosphere is given by the optical thickness,  $m = 0$ .

FIG. 3. Ratio between diffuse sky and direct solar irradiance as measured at Lelystad (May 1975).



A vegetation canopy can be considered as an ensemble of scattering elements, very large compared with the wavelength of radiation, bounded by the soil. Striking radiation will be scattered by components like leaves, stems, flowers etc., through which a part of this scattered radiation will leave the canopy in upward direction. If, like in Fig. 4. a canopy is observed under zenith angle,  $\theta_o$ , with a sensor with a solid view angle,  $\omega_D$ , an amount of radiative power,  $P_o(A_o, \theta_o, \lambda)$ , emanating from the area,  $A_o$ , is seen by the detector and reaches the aperture of the sensor system.

This power originates from the canopy components and the fraction of the soil with direct lines of free sight into the aperture.

It is assumed that in most cases the leaves of the canopy are the dominant reflectors in comparison with the remaining plant components. With direct sunlight, directly irradiated leaves or a surface fraction of them and in case of an incomplete soil coverage a part of the soil area under direct illumination are observed. On the other hand, the complement in the field of view is filled by the observed leaves and soil elements present in the shadow.

The spatial distribution of the leaves, their reflectance and transmittance properties for electromagnetic radiation, as a function of wavelength and the

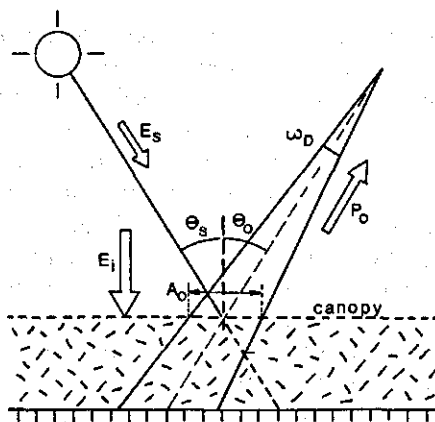


FIG. 4. Detection of plant canopy radiance under a zenith view angle,  $\theta_o$ , with a solid angle,  $\omega_D$ .

spectral reflectance of the soil determine the radiant flux profile within the canopy. The present amount of shadow inside the canopy is related to the solar angle and the leaf orientation distribution.

The local irradiance level on the observed canopy components and the soil follows from the radiant flux profile and the distribution of shadow inside the canopy. The quantity and location of the observed components and soil elements depend on the angle of view. Under perpendicular view, the observed fraction of the underground will be at a maximum, provided that soil cover percentage is less than 100%. Under oblique view, the largest fraction of observed components is present in the upper layers of the canopy, while the soil is more screened. For agricultural crops with a clear row structure an extra complicating factor is involved. Row structure presents a new parameter which determines radiation penetration and observed fractions of leaves, soil and amount of shadow.

After this qualitative introduction into the parameters of crops important to remote sensing, it will be clear that the relations between physical and morphological properties of a plant canopy do not correspond in a unique way, nor in a simple way with the observable quantity.

This study proceeds from the concept that measurable reflectance values at a given number of wavelengths form a unique feature of a crop. This feature could be used in distinguishing between different species and in detecting changes due to growth, stress etc. In order to be able to report on measured spectral reflectance behaviour, knowledge is required on all the factors determining spectral reflectance itself.

Before describing the interaction of global irradiance in the visible light region and the near reflectance infrared with a plant canopy, it is necessary to consider first the spectral optical behaviour of plant components like leaves and the underground.

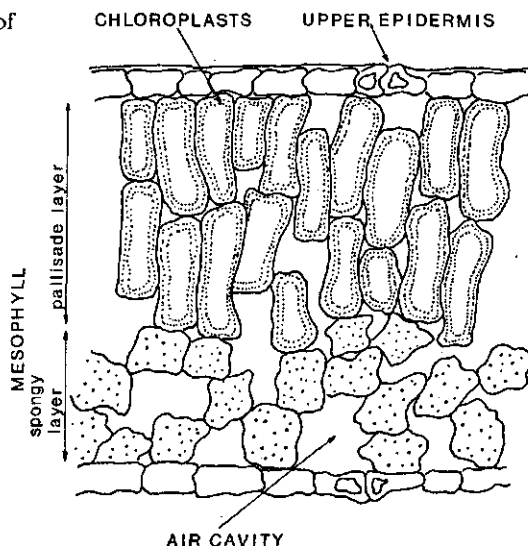
## 2.2. SPECTRAL REFLECTANCE AND TRANSMITTANCE OF SINGLE LEAVES

### 2.2.1. *Leaf morphology and interaction with electromagnetic radiation*

With respect to reflectance and transmittance properties of single leaves many studies have been performed in recent times, directed at bringing this behaviour into relation with physical properties. When a cross section of a normal green leaf is considered, see Fig. 5. the following components are present. The leaf is bounded on the upper (ventral) side and the under (dorsal) side by the epidermis. Between these layers is the mesophyll which, for most leaves, can be subdivided into the pallsade mesophyll at the ventral side and the spongy mesophyll at the dorsal side. This mesophyll tissue contains the pigments which are devided into plastids and dissolved vacuoles in the cellsap.

The most important plastids are the green chloroplasts containing chlorophyll inside the grana. Chlorophyll is created by light interaction out of prochlorophyll. Besides chloroplasts the carotenoides are present which deter-

FIG. 5. The morphological structure of a normal green leaf.



mine the colour of a leaf in the absence of chlorophyll. Inside the mesophyll structure air cavities are present filled with air with saturated water vapor.

If the reflectance spectrum of a normal green leaf is studied between 400 and 2500 nm, see Fig. 6, it can be subdivided into three regions.

a. The visible light: 400–700 nm.

Reflectance is characterized by a relative maximum in the green part at 550 nm and minima at 400 and 670 nm caused by maximum absorption of radiation by chlorophyll.

b. The near infrared: 700–1300 nm.

Reflectance in this region is relatively high and approximately constant. This is related to the low absorption by the leaf. Minor relative minima are present at 950 nm and 1160 nm due to selective absorption by the present water.

c. The waterabsorption region: 1300–2500 nm.

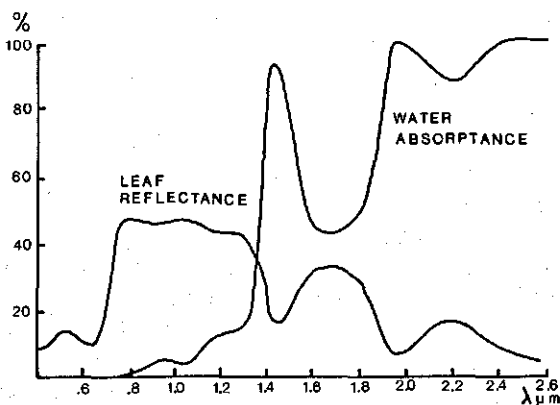


FIG. 6. Reflectance spectrum of a normal green leaf and absorbance spectrum of water.

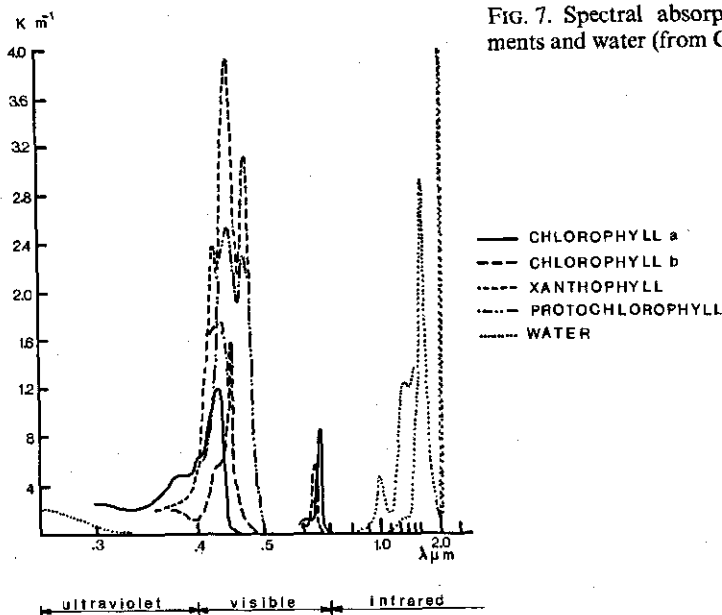


FIG. 7. Spectral absorption of leaf pigments and water (from GATES *et al.*, 1965).

In this wavelength region leaf reflectance is mainly determined by the water present in the leaf.

Reflectance behaviour of a leaf is closely connected with the absorption properties of the pigments and the water in the leaf as described by GATES *et al.* (1965).

Fig. 7 gives the absorbance spectrum of the regular leaf pigments and water. It is observed that in the interval between 400 and 450 nm, both chlorophyll and carotenes absorb radiation, while between 600 and 690 nm only the chlorophyll types a and b show maximum absorption.

After 690 nm the absorbing properties of the pigments disappear suddenly, while the water gives two minor absorption maxima at 950 and 1160 nm. After 1300 nm the absorbance by water plays a dominant role with maxima at 1450 and 1950 nm. This results in reflectance minima at these wavelength values and two relative maxima at 1675 and 2240 nm.

#### 2.2.2. Calculation of leaf reflectance and transmittance with the ray tracing method of Willstätter and Stoll

In different ways theories and models have been developed to describe reflectance and absorbance of leaves physically and to relate them with the morphology of the leaf. For a good review reference is made to SINCLAIR *et al.* (1973). The high reflectance as well as transmittance in the near infrared plateau between 700 and 1300 nm is explained by multiple reflections in the internal mesophyll structure, caused by the transitions of refraction index between the cell walls and the intercellular air cavities.

WILLSTÄTTER and STOLL (1918) assumed that multiple reflection is caused

by total or critical reflection at the cell walls through the change in the higher refraction index inside the cells to the lower (refraction index) of air within the cavities. According to the ray-tracing method the pathway of light rays within the leaf is calculated, effecting the intensity of the total amount of radiant flux leaving the upper and underside of the leaf. This method recently has been applied by ALLEN *et al.* (1973), resulting in an underestimation of leaf reflectance and an overestimation of its transmittance. Since this method approaches the physical reality quite well, KUMAR and SILVA (1973) were motivated to improve the ray tracing method by taking into account the influence of the chloroplasts and the cell sap. Reflectance at the cell wall and air cavity boundaries for angles of incidence smaller than the critical angle has also been included. The extinction along the path way was neglected. The results of their calculations approximated the experimental values very closely. Furthermore, they proved that Rayleigh and Mie scattering in the first order contribute negligibly to total reflectance and transmittance behaviour.

### 2.2.3. Leaf reflectance and transmittance by the Kubelka and Munk theory.

In 1968 a model to describe reflectance and transmittance by a plant canopy for isotropic light was published by ALLEN and RICHARDSON (1968). This model has been based on the theory of KUBELKA and MUNK (1931) which describes the transfer of radiation in diffuse scattering media. The first verification of the canopy reflectance model of Allen and Richardson was applied to single leaves. Whereas the model to be used later in this manuscript is also founded on the theory of Kubelka and Munk, a summary of the approach by Allen and Richardson is given. The Kubelka-Munk theory was published in 1931 with the aim to describe reflectance of dull painted surfaces and is an extension of the theory of SCHUSTER (1905) for the propagation of diffuse light in a star atmosphere. The Kubelka-Munk theory is a two parameter theory to describe the transfer of diffuse radiation into one dimension. The one parameter theory of Bouguer-Lambert for the extinction of radiation in a diffuse scattering medium follows directly from the K-M theory.

Allen and Richardson applied the K-M theory as follows. A plant canopy is considered with uniformly distributed leaves with total leaf area index (*LAI*). *N*. The total leaf area index is defined as the total one-sided leaf area per unit soil area. The canopy is extended infinitely into the lateral directions and at the underside bounded by the soil. The dimension along the vertical is formed by the cumulative leaf area index, *n*. This cumulative leaf area index is defined as the leaf area index present between the top of the canopy and the corresponding depths, see Fig. 8.

The relations between the upward diffuse radiant flux, *J*, and the downward diffuse radiant flux, *I*, are given by the differential equations of Kubelka and Munk.

$$\frac{dI}{dn} = -(k + s)I + sJ \quad (2.3.a.)$$

$$\frac{dJ}{dn} = (k + s) J + sI \quad (2.3.b.)$$

$k$  = phenomenological absorption coefficient.  
 $s$  = phenomenological (back)-scattering coefficient.

The boundary conditions are given by:

$$n = 0 : I(0) = I_0 = 1, J(0) = R \quad (2.4.a.)$$

$$n = N : J(N) = R_g I(N) \quad (2.4.b.)$$

$R$  = diffuse radiant flux reflected by the canopy.  
 $R_g$  = hemispherical reflection coefficient of the soil.

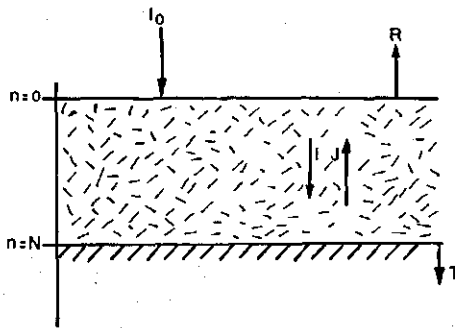


FIG. 8. The transfer of diffuse radiant flux in the plant canopy model of ALLEN and RICHARDSON.

From the Kubelka-Munk equations and the substitution of the boundary conditions follow the expressions for the fluxes  $J$  and  $I$ :

$$J = \frac{(1 - \beta^2) (e^{\alpha(N-n)} e^{-\alpha(N-n)}) - Rg \{ (1 - \beta)^2 e^{\alpha(N-n)} - (1 + \beta)^2 e^{-\alpha(N-n)} \}}{(1 + \beta)^2 e^{\alpha N} - (1 - \beta)^2 e^{-\alpha N} - Rg (1 - \beta^2) (e^{\alpha N} - e^{-\alpha N})} \quad (2.5.a.)$$

$$I = \frac{(1 + \beta)^2 e^{\alpha(N-n)} - (1 - \beta)^2 e^{-\alpha(N-n)} - Rg (1 - \beta^2) (e^{\alpha(N-n)} - e^{-\alpha(N-n)})}{(1 + \beta)^2 e^{\alpha N} - (1 - \beta)^2 e^{-\alpha N} - Rg (1 - \beta^2) (e^{\alpha N} - e^{-\alpha N})} \quad (2.5.b.)$$

In the derivation of these formulas, the parameters  $\alpha$  and  $\beta$  have been defined as follows:

$$\alpha^2 = k(k + 2s) \quad (2.6.a.)$$

$$\beta^2 = k/(k + 2s) \quad (2.6.b.)$$

If one substitutes

$$\alpha = \ln b \quad (2.7.a.)$$

$$\beta = (a - 1)/(a + 1) \quad (2.7.b.)$$



in the equations (2.5.a.) and (2.5.b.) the following relation is found for a black soil:

$$\frac{J(N, n, Rg = 0)}{b^{N-n} - b^{-(N-n)}} = \frac{I(N, n, Rg = 0)}{ab^{N-n} - a^{-1}b^{-(N-n)}} = \frac{1}{ab^N - a^{-1}b^{-N}} \quad (2.8.)$$

An identical relation was derived by STOKES (1862) for reflectance and transmittance of a pile of  $N$  glass plates. The Stokes parameters  $a$  and  $b$  and the K-M parameters  $k$  and  $s$  are connected by the following equations:

$$k = \{(a-1)/(a+1)\} \ln b \quad (2.9.a.)$$

$$s = \{2a/(a^2-1)\} \ln b \quad (2.9.b.)$$

In the Kubelka-Munk theory the K - M function,  $F(R_\infty)$ , has been defined by

$$F(R_\infty) = \frac{(1-R_\infty)^2}{2R_\infty} = \frac{k}{s} \quad (2.10.)$$

Reflectance of an infinitely thick medium is given by  $R_\infty$ , which is an intrinsic property of the diffusing material. From equation (2.8.) follows that reflectance of an infinitely deep canopy is

$$R_\infty = a^{-1}$$

Since reliable field measurements of canopy reflectance were not available, Allen and Richardson applied their model to stacked single leaves. They measured the corresponding reflectance and transmittance with a Beckman DK-2 laboratory spectrometer, see Fig. 9.

From equation (2.8.) follows for a single leaf:

$$\frac{r}{a-a^{-1}} = \frac{t}{b-b^{-1}} = \frac{1}{ab-a^{-1}b^{-1}} \quad (2.12.)$$

$r$  = hemispherical reflectance of a single leaf.

$t$  = hemispherical transmittance of a single leaf.

The Kubelka-Munk parameters,  $k$  and  $s$ , have been inferred from relation (2.12.) and the relations (2.9.a.) and (2.9.b.).

It appears that for  $N \geq 8$  the theoretical value  $R_\infty$  is attained, while for  $N$  between 2 and 8 the reflectance changes only significantly in the infrared plateau, because of the transparency of the leaf in this wavelength region. Fig. 10 gives the absorption coefficient and Fig. 11 the scattering coefficient,  $s$ , as calculated by Allen for a mature cotton leaf. These coefficients were calculated also for dehydrated leaves.

The absorption coefficient,  $k$ , corresponds with the general course of the actual absorption by green leaves with maxima near 400 and at 670 nm, due to absorption of radiation by chlorophyll. Absorption between 700 and 1300 nm

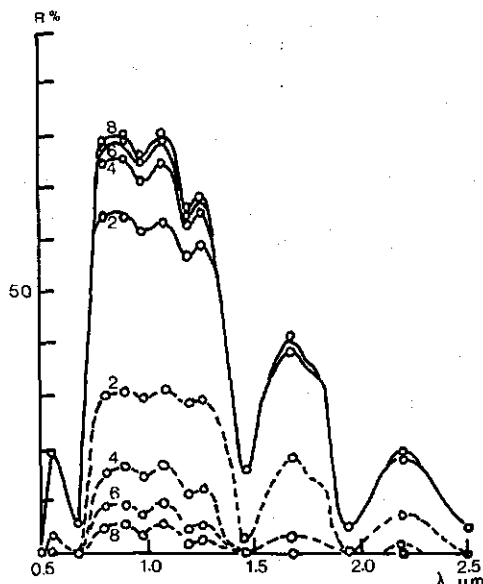


FIG. 9. Spectral reflectance and transmittance (dotted lines) of 2, 4, 6 and 8 stacked cotton leaves, as calculated with the K-M theory. The measured values are given by circles (from ALLEN and RICHARDSON, 1968).

is low, whereas absorption behaviour from 1300 to 2500 nm is identical with water absorption.

Though the K-M scattering coefficient,  $s$ , has no simple equivalent for easy interpretation, MYERS and ALLEN (1966) demonstrated that  $s$  can be approximated quite well in the near infrared by scattering at normal incidence of the incoming radiation by 35 air cavities along the mean optical pathway through the leaf.

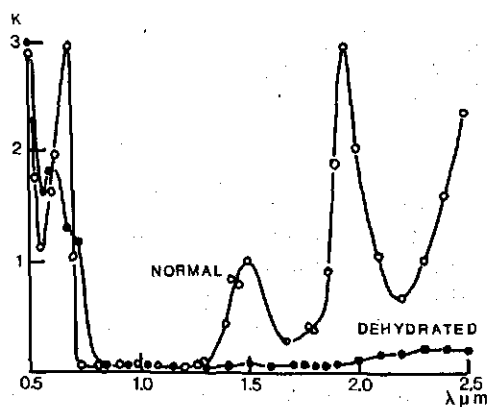


FIG. 10. The Kubelka-Munk absorption coefficient of a normal mature cotton leaf, compared with a dehydrated cotton leaf (from ALLEN and RICHARDSON, 1968).

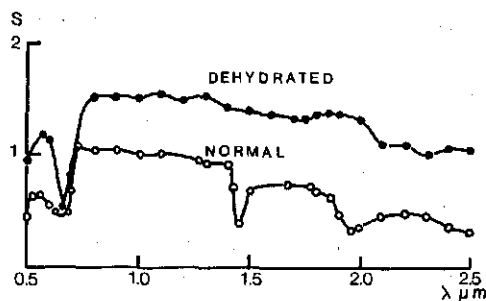


FIG. 11. The Kubelka-Munk scattering coefficient of a normal mature cotton leaf, compared with a dehydrated cotton leaf (from ALLEN and RICHARDSON, 1968).

#### 2.2.4. The plate model for leaf reflectance and transmittance of Allen

ALLEN *et al.* (1969) published a new theory for the reflectance and transmittance behaviour of a compact (no air cavities present) single leaf. This was based upon the scattering of isotropic light by a parallel plate with absorption coefficient,  $\kappa$ , and refraction index,  $n$ , with ideal diffuse scattering surfaces. This theory is an extension of the well-known expressions for multiple internal reflections between two interfaces assuming random polarisation. The effective dispersion and absorption, as a function of wavelength determined for a maize leaf using the plate model, are given in the Figs. 12 and 13.

Although no effective values of the refraction index of leaves are known, the value as indicated in Fig. 12 at 500 nm for carnauba wax is of the same order as that of the maize leaf. The effective absorption coefficient seems to be a composition of the absorption by chlorophyll and water, see also Fig. 7.

GAUSMAN *et al.* (1970) extended the plate model for leaves with air cavities. The leaf is built up by  $P$  compact layers separated by air. The void area index,

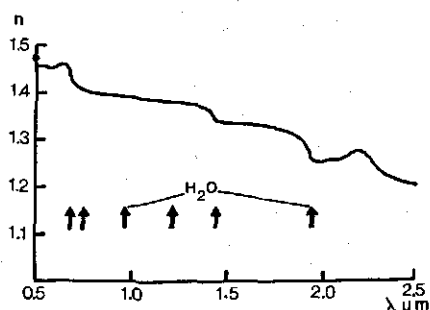


FIG. 12. Effective refraction index of a maize leaf as calculated with the plate model of ALLEN. The arrows are indicating selective absorption by chlorophyll and water (from ALLEN *et al.*, 1969).

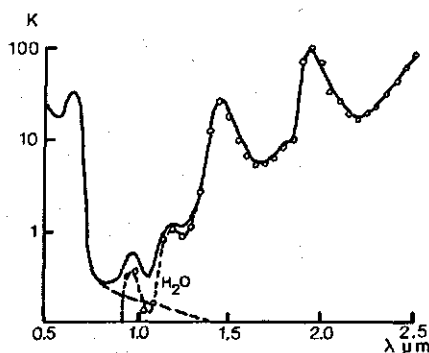


FIG. 13. Effective absorption coefficient of a maize leaf as calculated with the plate model of ALLEN. The measurement points correspond with those of water (from ALLEN *et al.*, 1969).

$VAI = P - 1$ , has been introduced to estimate the number of air cavities passed by a light ray during its mean pathway through the leaf.

For the water absorption region, the equivalent water thickness has been defined which is in accordance with the actual leaf thickness. Also in 1970, ALLEN *et al.* published an investigation, comparing the results of reflectance models for single leaves according to the Kubelka-Munk theory, the plate theory and the theory of MELAMED (1963). Melamed described the reflectance and transmittance of a diffuse scattering medium by representing this medium as a pile of identical spheres with optical constants,  $n$  and  $k$ , which scatter the incident and outgoing radiation ideally diffuse. The interaction of radiation, like for the plate model, is described with the relations of Fresnel and Lambert. An important result of the comparison between the plate theory and the K-M theory is that the K-M scattering coefficient,  $s$ , is approximated by the ratio  $r/t$  for a single leaf, when the absorptance is low. From the plate model it could be derived that leaf reflectance and transmittance for most plant species are of the same magnitude in the near infrared plateau, as stated earlier by DE WIT (1965).

#### 2.2.5. Directional reflectance and transmittance by single leaves.

Little attention has been paid to the spatial distribution of reflected or transmitted radiation by single leaves. In the preceding paragraphs only total reflectance and transmittance were considered. Directional measurements were performed by BREECE and HOLMES (1971) on soybeen and maize leaves.

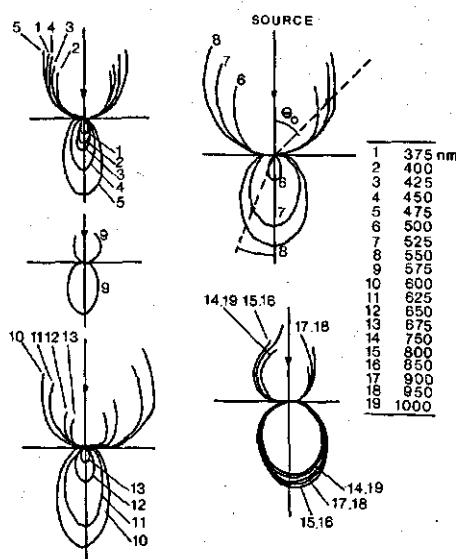


FIG. 14. Polar diagrams of the directional reflection coefficient,  $\rho' \cos \theta_o$ , and transmission coefficient,  $\tau' \cos (\pi - \theta_o)$ , as a function of wavelength at perpendicular incidence (from BREECE and HOLMES, 1971).

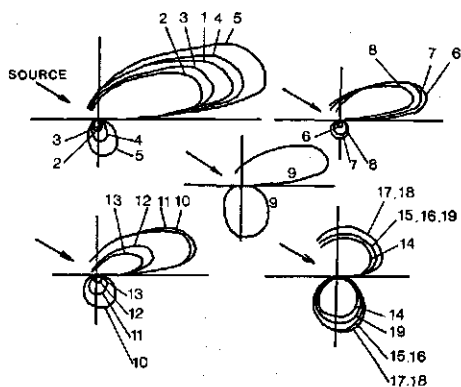


FIG. 15. Polar diagrams of the directional reflection coefficient,  $\rho' \cos \theta_0$  and transmission coefficient,  $\tau' \cos (\pi - \theta_0)$ , as a function of wavelength at a zenith angle of incidence of  $60^\circ$  (from BREECE and HOLMES, 1971).

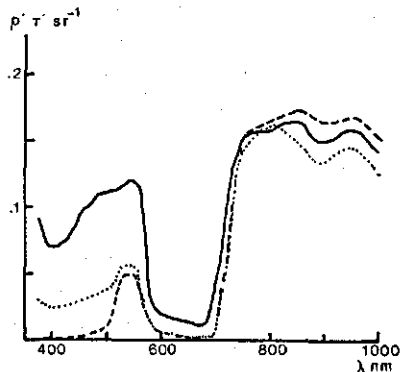


FIG. 16. Directional reflection and transmission coefficient,  $\rho'$ , for  $\theta_0 = 45^\circ$  (—) and  $\theta_0 = 0^\circ$  (...) and  $\tau'$ , for  $\theta_0 = 180^\circ$  (- -) at an angle of incidence of  $45^\circ$  (from BREECE and HOLMES, 1971).

Some of the results are given in Figs. 14, 15 and 16. It was found that the specular contribution, in particular for reflectance, increased with the angle of incidence of the collimated impinging radiation. Transmittance in all wavelengths approached Lambertian scattering.

At maximum absorptance, the non-Lambertian reflectance was maximum. The specular character could be explained in a qualitative way using the plate model of Allen, because in wavelengths where the chlorophyll absorbs heavily, only the upper layers in the model interact with the penetrating radiant flux. In this case, the reflected radiation will have a shorter optical pathway with a reduced probability of internal multiple scattering than with leaf transmission or at wavelengths with a low absorptance. This can be concluded directly from Fig. 16, in which the relative difference between the directional reflectance of  $\theta_0 = 45^\circ$  or  $0^\circ$  is small in the near infrared compared with the large variation in the visible light region.

This short review dealing with models for single leaf transmittance and reflectance clearly shows that detailed data on the process of scattering of shortwave radiation by plant leaves and on the relations with some physiological properties are available.

Because of the importance in practice of remote sensing applications some attention will be paid to the influence of growth and senescence on reflectance and transmittance of leaves.

#### 2.2.6. Variation in reflectance and transmittance of leaves as a function of growth and senescence

Reflectance and transmittance depend on the concentration of pigments and water, together with the internal cell structure of each leaf species. These physiological quantities depend on leaf type, average diurnal exposure to direct sunlight and the stage of maturing. GAUSMAN *et al.* (1970) carried out measurements on cotton leaves during a period of twelve days after tagging, see Figs. 17 and 18.

They found that reflectance increased, while transmittance decreased at all wavelengths. This is to be seen in relation to the increase of the water content and the number of intercellular air spaces. Application of the plate model provides the *VAI* which gives in comparison with the measured percentage of air cavities a correlation of 0.92, see Fig. 19.

The ratio between the equivalent water thickness and the required amount of layers in the plate model is at a minimum, when reflectance in the near infrared is maximum. When the void area index attains its stationary value, only leaf thickness keeps increasing due to continuing leaf growth. This leads to an increasing ratio between the equivalent water thickness and the number of layers. The plate model predicts for this stage a decrease in reflectance corresponding quite well with the experimental values given in Fig. 17.

SINCLAIR *et al.* (1971) measured the variation of leaf reflectance during a longer period of the growing season, from the final stage of development up to and including senescence, see Fig. 20.

During a period of a month after complete leaf maturing reflectance hardly changed within the entire wavelength interval. During senescence of the leaf, reflectance increased at all wavelengths as shown by the curves of 11–16 September. Especially in the red from 600–680 nm, there is a considerable increase in reflectance, because of the breakdown of chlorophyll. In this spectral region absorption by chlorophyll plays a dominant role. According to investigations of SHULL'GIN and KLISHING (1959) reflectance tends to increase.

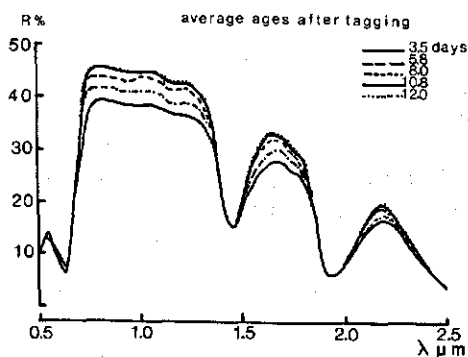


FIG. 17. Spectral reflectance of the ventral side of cotton leaves during a period from 3.5 to 12.0 days after tagging (from GAUSMAN *et al.*, 1970).

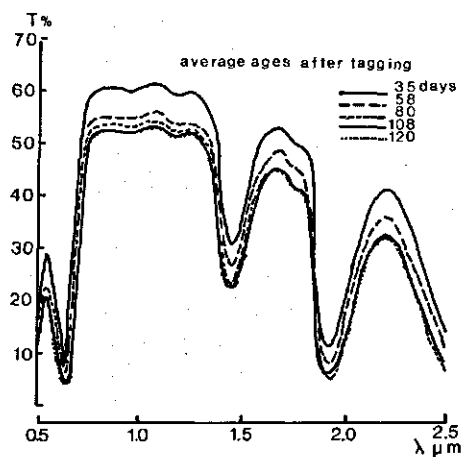


FIG. 18. Spectral transmittance of cotton leaves during a period from 3.5 to 12.0 days after tagging (from GAUSMAN *et al.*, 1970).

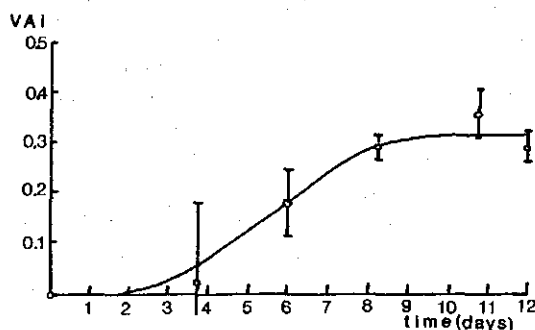


FIG. 19. The void area index of cotton leaves as a function of time. The measured values of the percentage of air cavities are indicated with their spread (from GAUSMAN *et al.*, 1970).

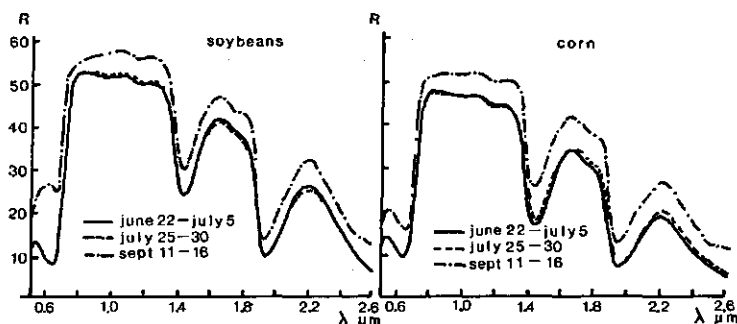


FIG. 20. Spectral reflectance of soybean and maize during the periods of 22 June – 5 July, 25–30 July and 11–16 September (from SINCLAIR *et al.*, 1971).

when the concentration of chlorophyll drops below 3 mg per 100 cm<sup>2</sup> leaf area. Normally the chlorophyll concentration is much higher. By senescence and a decrease in cell sap, the mesophyll structure collapses into more compact horizontal layers.

However, the measured increase in reflectance in the near infrared cannot be explained when using the plate model or the Willstätter-Stoll theory.

Sinclair proceeded from the hypothesis that the cell walls are scattering radiation highly diffuse, caused by the microfibril structure of the cell walls. This hypothesis has been affirmed by experiments in which a laser beam was used to trace the internal interaction of a light ray with cell walls. Dependent on the number of cell walls interacting with the incident radiation, total leaf reflectance is about 50%, if individual cell walls have a reflectance of 15% and a transmittance of 85%.

### 2.3. SPECTRAL REFLECTANCE OF SOILS

Spectral reflectance of a vegetative canopy is influenced by reflectance of the soil present and in particular for crops with incomplete covers. It is obvious that, especially in wavelength regions with a maximum contrast between leaf and soil reflectance, the influence of soil type on canopy reflectance can be considerable. For this reason, the most important physical properties of soils affecting reflectance will be reviewed in this paragraph.

As for single leaves, much work has been done on the relations between spectral reflectance of soils and their properties. Fig. 21 gives a comparison between reflectance of a mature wheat leaf and a dry and wet sandy loam soil. The wavelength interval from 400 to 2500 nm cannot be subdivided into smaller discrete regions, because selective absorbing materials are not always present.

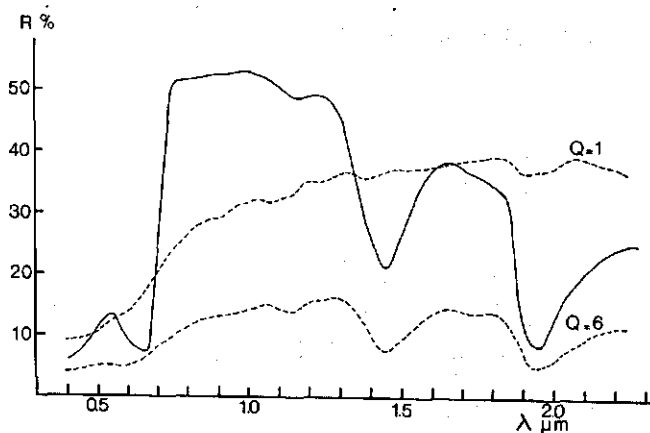


FIG. 21. Spectral reflectance of a green wheat leaf compared with reflectance of a dry ( $Q = 1$ ) and a moist ( $Q = 6$ ) sandy loam soil.



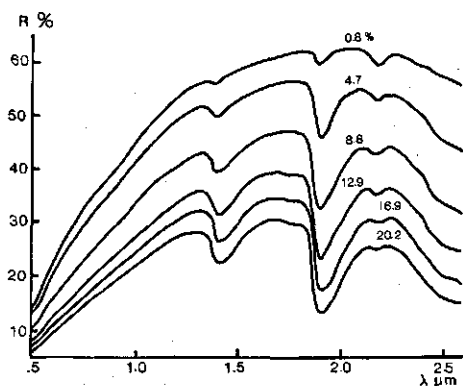


FIG. 22. Effect of moisture content on spectral reflectance of Newtonia silt loam (from BOWERS and HANKS, 1965).

Almost all soils show an increase of reflectance from 400 nm up to 2200 nm with a decrease afterwards. As with leaves, reflectance minima occur at 1450 and 1950 nm due to selective absorption by the water present.

It is not possible to subdivide soil reflectance curves into different classes for similar shape and magnitude in a simple way. However, it is well-known which properties determine soil reflectance, viz.: mineral composition, texture (particle size), structure (aggregates), moisture content and percentage of organic matter. Especially the last three factors are the most important.

The structure determines the percentage of shadow generated at soil surface. Moisture is retained in the pores between the particles by the capillary process, which is amplified by the hydro-attractive properties of organic matter present. An increasing moisture content in the top layer will induce reflectance to drop at all wavelengths, as shown in Fig. 22 (BOWERS and HANKS, 1965).

This decrease in soil reflectance with increasing moisture content can be easily explained by the gradual penetration of water into the inter-particle spaces decreasing the number of surface elements with a transition of refraction index from particle to air. More penetrating radiation will be absorbed. The decrease of the reflectance of the soil is at a relative maximum in the water absorption bands at 1450 and 1950 nm. When a soil is desiccated there usually is crust formation at the surface. The moisture present below this crust hardly affects reflectance (CIPRA *et al.*, 1971).

Soils with a low percentage of humus like sandy soils depend for their reflectance behaviour much more on moisture differences than clay soils (LARS BULLETIN, 1970). In the absence of soil structure various investigations have been performed on the influence of particle size on reflectance. Without exception it appeared that an increase in particle size was associated with a practically exponential decrease in reflectance (BOWERS and HANKS, 1965).

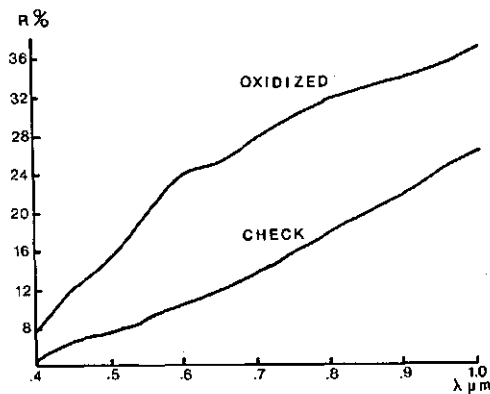


FIG. 23. The influence of organic matter on spectral reflectance of a summit silty clay (from BOWERS and HANKS, 1965).

Structure which is connected with the formation of aggregates at the soil surface dominates the influence of texture under field conditions, because of its major effect on the amount of shadow present and the orientation of the reflecting planes.

When the organic matter exceeds a volume percentage of 2% at the surface level, the absorptance properties dominate the effect of the mineral composition of the soil. At all wavelengths reflectance drops with increasing percentage of organic matter, because it has no selective spectral absorptance. Fig. 23, taken from BOWERS and HANKS (1965), shows reflectance of a summit silty clay sample before and after oxidization.

#### 2.4. REFLECTANCE OF RADIATION BY A VEGETATION CANOPY

For the study of photosynthesis and growth of a crop, models have been developed to relate the penetration of direct solar radiant flux and diffuse sky radiation into a leaf canopy with optical properties of components, the soil and architecture of the canopy. Useful references on this subject are, e.g. MONSI and SAEKI (1953), MONTEITH (1965), WARREN WILSON (1965), DE WIT (1965), NILSON (1971) and GOUDRIAAN (1977). The fraction of incident radiation on the canopy which is reflected upwards in these models is a derived quantity. As described in paragraph 2.1., the information on which the application of remote sensing techniques is based, is determined by the observed characteristic spectral differentiation in reflectance of the vegetative features on the earth surface.

During the past ten years, several investigators have developed mathematical models to predict spectral reflectance of a vegetative canopy and to explore potential applications of multispectral remote survey.

Most of these models show no fundamental differences. Their value for prac-

tical application however depends substantially on the required input parameters. The way in which architecture of the canopy is modelled plays an important role in all models. Input parameters dealing with reflectance and transmittance properties of canopy components, like leaves and reflectance of the soil, that can be measured separately, are taken from the literature. They can be interpreted with the relations as described in the preceding paragraphs.

Before reviewing the more important canopy reflectance models existing and in more detail the model used in this manuscript, an introduction is given into the usual methods of describing the architecture of a crop.

#### 2.4.1. Geometrical structure of a leaf canopy

Depending on the morphology of single plants present in a monoculture, a canopy can usually be subdivided into a number of horizontal layers with different structure and leaf density. A maturing wheat canopy for instance can be modelled by a first layer containing ears and stalks, a second layer with green leaves and a third layer bounded by the soil with senescent leaves.

If a homogeneous canopy layer is considered, consisting of a spatial distribution of leaves, adequate modelling requires an appropriate definition of such a leaf ensemble. A commonly used description starts from the experimentally determined random distribution of leaves in relation to the azimuth. For the leaves or their surface elements a frequency distribution or cumulative frequency distribution of the inclination can be defined, as introduced by DE WIT (1965). Based on possible distributions present in nature, the following classes for leaf angle distributions are defined.

- Planophile: horizontally oriented leaves are most frequent.
- Erectophile: vertically oriented leaves are most frequent.
- Plagiophile: leaves with an oblique angle are most frequent.
- Extremophile: leaves with an oblique angle are less frequent.

Furthermore, a uniform distribution can be defined for leaf angles,  $\theta_L$ , with equal probability of occurrence. Of theoretical importance is the spherical distribution for which the frequency of leaf angles is equal to the distribution of the inclination of surface elements of a sphere. Some erectophile canopies

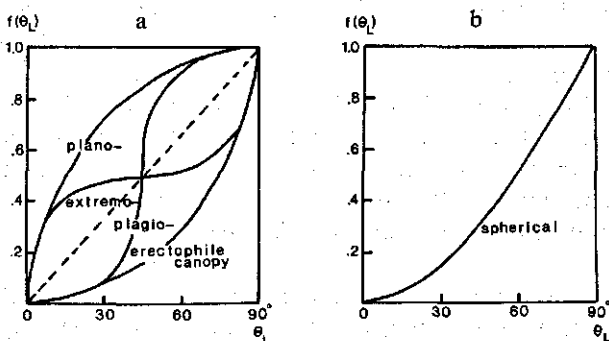


FIG. 24. a. Cumulative leaf angle distribution functions by De Wit.  
b. The spherical leaf angle distribution function.

have a leaf angle distribution which approximates the spherical distribution. Fig. 24 gives examples of cumulative frequency distributions for the classes introduced by DE WIT.

Interaction of incident radiant flux with the components of a canopy is related with the leaf inclination distribution, spatial distribution and total leaf area per unit of soil area  $LAI$ . Spatial distribution corresponds with the local leaf area density. Monsi and Saeki gave a definition for the number of horizontal leaf layers,  $LAI/s$ , of a canopy with horizontal leaves only. The definition of the quantity,  $s$ , has been extended to the presentation of the degree of random leaf distribution within a canopy layer. The larger  $s$  is the smaller the probability will be of a light ray penetrating through a layer without interaction. If  $s$  approaches zero, the spatial distribution of the components will be a Poisson distribution, OLIVER and SMITH (1974). The practical value of  $s$  is in the order of 0.1. GOUDRIAAN (1977) showed that  $s$  corresponds with the ratio between the leaf width and the mutual distance between the leaves.

#### 2.4.2. Radiative transfer within a canopy according to Ross and Nilson

The distribution of radiant flux within a leaf canopy was derived by ROSS and NILSON (1974) from the general theory on radiative transfer in a diffuse scattering medium, as described by CHANDRESEKHAR (1950). This theory is based on an energy balance for an elementary volume within the scattering medium. It is supposed that in a canopy the leaves are distributed at random, while the leaf angle distribution has been taken into account. The transfer equation is an integro-differential equation due to the terms for energy loss and volume scattering. The boundary conditions are given by the incident radiant flux at the top of the canopy and reflectance by the soil. In this model the probability is included of direct solar and diffuse sky irradiance penetrating to a certain depth, before being scattered. The equations can be solved using iterative methods. Radiation leaving the canopy in upward direction can be calculated, from which directional reflectance can be derived.

#### 2.4.3. The canopy radiation model of Goudriaan and De Wit

De Wit developed a model to simulate photosynthesis of crops (1965). In 1970 the model of De Wit was used by IDSO (1970) to simulate diurnal reflectance variations of a corn crop.

Goudriaan extended and improved this model. From a general description of the radiant flux profile within the canopy and the resulting reflection coefficient, more simplified relations were found for the extinction of radiation in the canopy, as well as for reflectance. These quantities were based on properties of crops with horizontal leaves and on crops with equal architecture, but with ideally black leaves.

In order to evaluate the model of Goudriaan in comparison with the model used in this manuscript, to be discussed later, the method to determine canopy reflectance according to Goudriaan's model will be summarized.

#### 2.4.3.1. Geometry of the canopy and incident radiation

A uniform distribution of leaves is assumed. The canopy is subdivided into horizontal infinitely extended layers. According to Monsi and Saeki it is assumed that the number of layers,  $m$ , is determined by the criterion that mutual shading of leaves in such a layer with leaf area index,  $L_s$ , can be neglected. For the leaf angle distribution, nine inclination intervals from  $0^\circ$  to  $90^\circ$  are introduced with fractions,  $F(\lambda)$ , belonging to each interval,  $\lambda$ . The average projection,  $O(\beta, \lambda)$ , of the leaves of inclination interval,  $\lambda$ , into the direction with inclination angle,  $\beta$ , is an important quantity; it is assumed that the azimuthal orientation of the leaves is at random. The diffuse flux within the canopy, divided into two fluxes in the upper and lower hemisphere, is calculated using a distribution in both hemispheres of nine equal zones. The incident radiation is subdivided into the direct solar flux and the diffuse sky radiation emanating from nine equal zones. A uniform sky radiation distribution is supposed, which means that the radiance of the sky is constant over the entire hemisphere. The contributions,  $B_u(\beta)$ , from each segment of the sky to the total diffuse irradiance on a horizontal plane has been calculated.

#### 2.4.3.2. Calculation of the radiant flux profile within the canopy

A simplified model to calculate the reflection coefficient of a canopy with horizontal leaves with large  $LAI$ , assuming equal leaf reflectance,  $\rho$ , and transmittance,  $\tau$ , and exponential extinction, gives the following results for extinction,  $K_h$  and reflection coefficient,  $\rho_h$ :

$$K_h = \sqrt{1-2\rho} \quad (2.13.)$$

$$\rho_h = (1 - \sqrt{1-2\rho}) / (1 + \sqrt{1-2\rho}) \quad (2.14.)$$

If in a canopy with leaf angle distribution,  $F(\lambda)$ , a layer with leaf area index,  $L_s$ , is considered, the fraction,  $M_i(\beta, \lambda)$ , of radiant flux from direction,  $\beta$ , will be intercepted by the leaves within the leaf angle interval,  $\lambda$ , and is given by.

$$M_i(\beta, \lambda) = L_s F(\lambda) O(\beta, \lambda) / \sin \beta \quad (2.15.)$$

A fraction,  $M_i(\beta)$ , of the incident flux,  $\phi(\beta)$ , leaves the layer without interception in direction  $\beta$ .

$$M_i(\beta) = 1 - \sum_{\lambda=1}^9 M_i(\beta, \lambda) = 1 - \frac{L_s}{\sin \beta} \bar{O}(\beta) \quad (2.16.)$$

It is assumed that the leaves act as Lambertian scatterers. This behaviour is not valid for the layer,  $L_s$ , because  $M_i$  still depends on  $\beta$ .

The distribution function,  $B_i(\beta', \lambda)$  of the flux scattered by the leaf fraction,  $F(\lambda)$ , can be written using the weighting factor,  $B_u(\beta')$ :

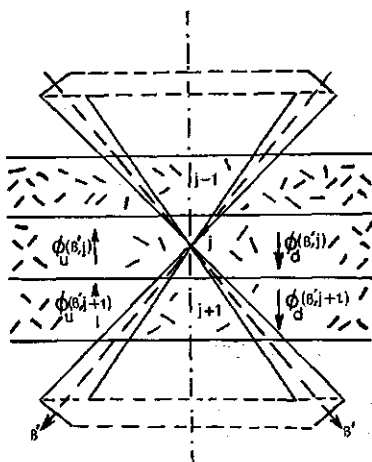


FIG. 25. Exchange of radiant flux between canopy layers,  $j$  and  $j+1$ , according to Goudriaan.

$$B_u(\beta') = \int_{\beta_1}^{\beta_2} 2 \sin \beta'' \cos \beta'' d\beta'' \quad (2.17.a.)$$

$$B_i(\beta', \lambda) = \frac{B_u(\beta') M_i(\beta', \lambda)}{\sum_{\beta=1}^9 B_u(\beta) M_i(\beta, \lambda)} \quad (2.17.b.)$$

In Fig. 25 two successive layers,  $j$  and  $j+1$ , are considered.

The intercepted amount of flux,  $I_i(\lambda, j)$ , in layer,  $j$ , is determined by the interception in layer,  $j$ , by the leaf fraction,  $F(\lambda)$ , of incident flux from all directions,  $\beta$ .

$$I_i(\lambda, j) = \sum_{\beta=1}^9 M_i(\beta, \lambda) (\phi_d(\beta, j) + \phi_u(\beta, j+1)) \quad (2.18.)$$

$\phi_d(\beta, j)$ : downward diffuse flux from zone,  $\beta$ , in layer,  $j$ .

$\phi_u(\beta, j+1)$ : upward diffuse flux from zone,  $\beta$ , coming from layer,  $j+1$ .

For the up- and downward flux the next equations hold:

$$\phi_d(\beta', j+1) = M_t(\beta') \phi_d(\beta', j) + \frac{\sigma}{2} \sum_{\lambda=1}^9 F(\lambda) B_t(\beta', \lambda) I_i(\lambda, j) \quad (2.19.a.)$$

$$\phi_u(\beta', j) = M_t(\beta') \phi_u(\beta', j+1) + \frac{\sigma}{2} \sum_{\lambda=1}^9 F(\lambda) B_t(\beta', \lambda) I_i(\lambda, j) \quad (2.19.b.)$$

with  $\rho = \tau = \sigma/2$ .

The boundary conditions of these equations are given by the impinging total

flux at the top of the canopy of  $m$  layers,  $m = LAI/s$  and by the soil with ideal diffuse reflectance. The upward flux at the soil level is given by:

$$\phi_u(\beta', m+1) = \rho_s B_u(\beta') \sum_{\beta=1}^9 \phi_d(\beta', m+1) \quad (2.20.)$$

$\rho_s$  = soil reflectance.

Radiation profile is calculated with a relaxation method as follows. First the leaves are supposed to be black by substitution of  $\sigma = 0$  into (2.19.). By a single series of calculations, first in downward and then in upward direction a good approximation for the flux profile is found. Then the calculation is started again from the first layer but now with taking into account the scattering terms. The calculations are repeated from the first layer, however, taking into account the scattering terms. By repeating the procedure of (2.19.) several times in upward and downward direction, by rapid convergence the limits of  $\phi_d$  and  $\phi_u$  in each layer are found.

The directional reflection coefficient in a certain direction is derived from the total radiance leaving the first layer in that direction.

#### 2.4.3.3. Possible simplifications

Goudriaan demonstrated that a simplification of equations (2.19.) leads to nearly the same results. The simplification implies that in calculating the intercepted flux in each layer, only the average leaf projection,  $\bar{O}(\beta)$ , in direction,  $\beta$ , is used.

All leaves are supposed to have the same radiance irrespective of their inclination. The scattered flux (the rightmost of equations (2.19.a.) and (2.19.b.) can be replaced by  $\sigma/2 B_i(\beta') I_t(j)$ , so that separate calculation of the scattered flux for each leaf angle is no longer necessary.  $B_i(\beta')$  and  $I_t(j)$  are calculated by the equations (2.17.b.) and (2.18.), whereby  $M_i(\beta, \lambda)$  should be replaced by  $M_i(\beta)$ , which is defined by:

$$M_i(\beta) = L_s \sum_{\lambda=1}^9 F(\lambda) O(\beta, \lambda) / \sin \beta = \frac{L_s}{\sin \beta} \bar{O}(\beta) \quad (2.21.)$$

With direct solar flux exponential extinction is obtained for low values of  $L_s$ .

$$\phi_d(LAI) = S_b \exp \{-K_b(\beta) LAI\} \quad (2.22.)$$

with

$S_b$ : direct irradiance at the canopy top

$K_b(\beta)$ : extinction coefficient

$LAI$ : cumulative  $LAI$  to a certain depth.

$$K_b(\beta) = \bar{O}(\beta) / \sin \beta \quad (2.23.)$$

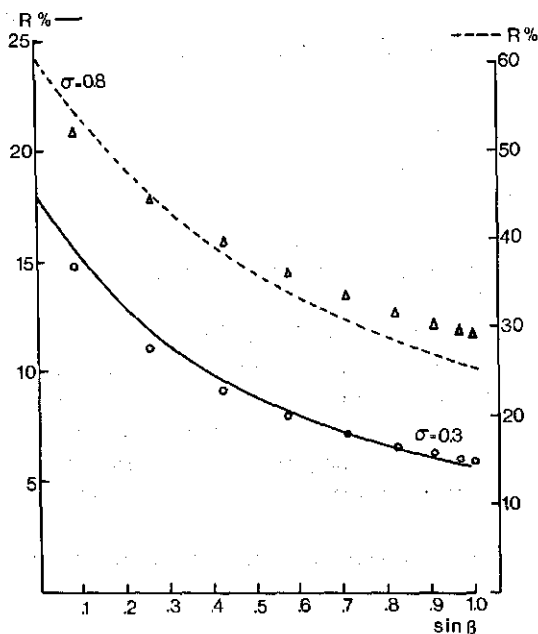


FIG. 26. Hemispherical reflectance of a canopy with spherical leaf angle distribution as calculated with the model of Goudriaan and for an exponential approximation as a function of  $\sin \beta$

$\rho_m$      $\hat{\rho}_m$   
 —     $\circ$      $\sigma = 0.3$   
 - - -     $\triangle$      $\sigma = 0.8$

Only with black or horizontal leaves is extinction purely exponential. Goudriaan showed that extinction of the net flux in most cases can be described with only one exponential function with 5% deviation at most. The extinction coefficient is defined as follows:

$$K_f = K_b \sqrt{1 - \sigma} = K_b K_h \quad (2.24.)$$

This extinction coefficient is the product of the extinction coefficient of a canopy with black leaves, but with actual leaf angle distribution and the extinction coefficient of a canopy with horizontal leaves only.

If multiple reflectance is neglected, hemispherical reflectance as a function of the inclination angle for incident direct flux is:

$$\rho_f'(\beta) = 2\rho_h \frac{K_b(\beta)}{1 + K_b(\beta)} \quad (2.25.)$$

By comparing the variation in the reflection coefficients, as calculated by the model as a function of  $\sin \beta$  and assuming an exponential character of the reflectance including multiple reflections hemispherical canopy reflectance,  $\rho_f(\beta)$ , becomes:



$$\rho_f(\beta) = 1 - \exp \left\{ -2\rho_h \frac{K_b(\beta)}{1 + K_b(\beta)} \left( 1 + L_s \frac{K_d}{1 + K_d} \right) \right\} \quad (2.26.)$$

The extinction coefficient,  $K_d$ , of diffuse flux is found from:

$$\exp(-K_d LAI) = \sum_{\beta=1}^9 B_u(\beta) \exp(-K_f(\beta) LAI) \quad (2.27.)$$

Fig. 26 illustrates for  $\sigma = 0.3$  and  $0.8$  the correspondence between reflectance value,  $\rho_m$ , found with the model and approximated reflectance,  $\hat{\rho}_m$ . The regression between  $\rho_m$  and  $\rho_f$ , for crops with various leaf angle distributions, gives for  $\hat{\rho}_m$ :

$$\hat{\rho}_m = 0.2057 + 1.1170 (\rho_f - 0.19414) \quad (2.28.)$$

It can be concluded that Goudriaan demonstrated the possibility of retaining accuracy of model output by introducing profound simplifications in a more detailed and realistic canopy model.

#### 2.4.4. Canopy reflectance model of Smith and Oliver

So far, the stochastic character of the model results has not been taken into consideration. In realistic plant canopies statistical fluctuations of all relevant parameters occur, caused by numerous environmental variables. The resulting statistical variation and the stochastic noise in actual remote sensing data are important in data processing and interpretation. A canopy reflectance model, especially, taking into account this statistical behaviour was developed by SMITH and OLIVER (1974).

In background studies for crop classification purposes it is important to obtain predictions about the inter and intra variations of multispectral data. The current statistical classification methods, like the maximum likelihood decision rule use the average response of a certain crop type in the different spectral bands and the corresponding covariance matrix. The model of Smith and Oliver can predict these data with varying directions of observation, given a solar zenith angle and canopy with known leaf area index and leaf angle distribution.

The model is based upon flux tracing through the canopy using the Monte Carlo principle of random choice.

The calculations are carried out by the following steps.

- a. Direct solar and diffuse sky radiation originating from 29 sectors give to reflected radiation in a certain direction an independent contribution, see Fig. 27.
- b. Like in the model of Goudriaan and De Wit the canopy has been subdivided into horizontal layers with a leaf angle distribution of leaves or their surface

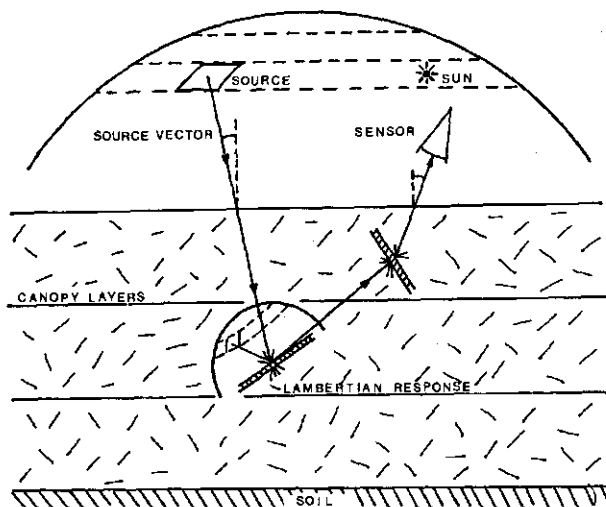


FIG. 27. Calculation of the directional reflectance of a plant canopy by Smith and Oliver. The leaves are distributed in horizontal layers and show Lambertian reflectance and transmittance.

elements which are distributed at random through each layer. The cumulative leaf angle distribution is subdivided into 10 intervals of equal probability. Equation (2.16.) has been applied to study the probability of finding a gap for light to penetrate through one layer from a certain radiation source in the sky hemisphere. By random generation of a number between 0 and 1 and by comparison with the given probability of finding a gap, the layer to which the flux penetrates without interaction can be determined. In this layer, selected at random, interaction must occur with a canopy element.

- c. The next step is formed by random generation of two numbers,  $r_1$ , and  $r_2$ , between 0 and 1, respectively. The first number determines the azimuthal orientation and the second the leaf angle interval of equal probability of the canopy element. Because of the Lambertian response of the element, secondary diffuse flux, belonging to the local co-ordinates of the canopy element, is scattered into its upper hemisphere by reflectance and into its lower hemisphere by transmittance.
- d. By means of a rotation of the Cartesian axes belonging to the canopy element towards the axes relative to the horizontal soil surface, it can be calculated how reflected and transmitted flux is distributed in the directions of the 20 sectors on the sky hemisphere. The random flux tracing procedure is continued until for each layer a threshold value is found by convergence, for all the radiating sources.

The bidirectional radiance of the canopy due to the first sky source is cal-

culated. The total radiance into a selected direction is determined by adding all the bidirectional radiance contributions. Directional reflectance is found by taking the ultimate radiance relative to the total irradiance at the canopy top.

#### 2.4.5. Calculation of canopy reflectance by application of the Duntley equations

In 1942 DUNTLEY extended the Kubelka-Munk theory to include the diffuse scattering of incident direct radiant flux. The absorption and scattering coefficients for direct and diffuse flux are different.

ALLEN, GAYLE and RICHARDSON applied the Duntley equations on a vegetation canopy with uniform leaf distribution (1970). Like in the K-M model, described in section 2.2.3, the radiative transfer is one-dimensional which means that the radiation profile is independent of the location above the canopy. The exchange of radiant flux into an infinitesimal layer,  $dn$ , is given by the following equations, see Fig. 28.

$$\frac{d}{dn} I_n' = -(\mu' + B' + F') I_n' \quad (2.29.a.)$$

$$\frac{d}{dn} t = -(\mu + B) t + Bs + F' I_n' \quad (2.29.b.)$$

$$-\frac{d}{dn} s = -(\mu + B)s + Bt + B' I_n' \quad (2.29.c.)$$

$I_n'$ : direct radiant flux

$s$ : upward diffuse flux

$t$ : downward diffuse flux

$\mu^*$ : absorption coefficient

$B^*$ : backscatter coefficient

$F^*$ : forward scatter coefficient

$n$ : cummulative leaf area index

\*) primed symbols in formulas (2.29.) stand for direct flux

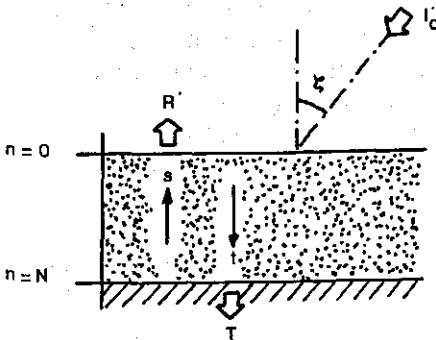


FIG. 28. Scattering of incident direct radiant flux by a plant canopy according to the model of Allen, Gayle and Richardson.

The solutions for the radiant flux are found in an analogous way to the K-M equations. From the value of the upward diffuse flux,  $s$ , for  $n = 0$  the hemispherical canopy reflectance is found. The daily cycle of the canopy reflectance is modelled by making the extinction coefficient of the direct flux proportional to the effective cumulative leaf area index for oblique sunrays.

$$q'_0 = \mu' + B' + F' \quad (2.30.a.)$$

$$q' = q'_0 \sec \xi \quad (2.30.b.)$$

$$I_n = I_0 \exp (-q'_0 n \sec \xi) \quad (2.30.c.)$$

The five Duntley parameters  $\mu'$ ,  $B'$ ,  $F'$ ,  $\mu$  and  $B$  are unknown and have to be derived from five independent measurements. Another disadvantage of this A.G.R.-model for remote sensing purposes is that only hemispherical reflectance can be predicted instead of the directional reflectance, while the Duntley parameters are not directly related with crop parameters.

#### 2.4.6. Plant canopy reflectance according to Suits

In 1972, G. H. SUITS published a new canopy reflectance model based on the Duntley equations similar to the A.G.R. model. In the Suits' model, however, the Duntley parameters are expressed in optical properties of the canopy components, parameters for architecture of the crop and important geometrical parameters for remote sensing purposes. Directional reflectance depends on the position of the sun and the observation direction from which the non-Lambertian behaviour can be predicted. Because the reflectance model of Suits is applied in this study for reasons dealt with in paragraph 2.4.7., the theory of this model will be summarized in the next sections.

##### 2.4.6.1. Simplification of the geometrical structure of a vegetation canopy

The canopy, in horizontal directions infinitely extended, can be subdivided into one or more distinct layers with a homogeneous composition. Within these layers, the canopy components are distributed uniformly and at random.

An essential simplification for the present scattering elements is their substitution by their orthogonal projections as shown in Fig. 29.

Surfaces with much curvature can be subdivided into smaller elements to be distributed at random within a canopy layer. The flux intercepted by these elements should be equal to the effective interception by their orthogonal projections.

A layer with thickness,  $x_1$ , is considered filled with canopy components with volume density,  $n$ , and average area,  $\bar{A}$ . The LAI of this layer is given by:

$$LAI(x_1) = n\bar{A}x_1 \quad (2.31.)$$

The total horizontal and vertical projected area per unit soil area for a given

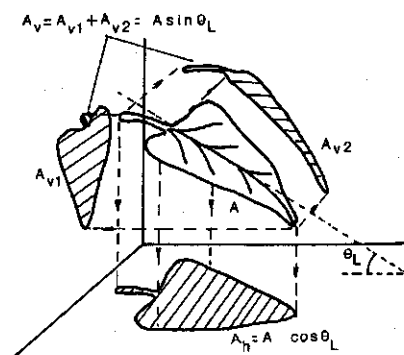


FIG. 29. The three orthogonal projections of a canopy component which substitute the actual components in the Suits' model.

leaf angle distribution is calculated using the probability density function,  $f'(\theta_L)$ , of the leaf angle,  $\theta_L$ , by:

$$H(x_1) = \int_0^{\pi/2} x_1 n f'(\theta_1) \bar{A} \cos \theta_L d\theta_L \quad (2.32.a.)$$

$$V(x_1) = \int_0^{\pi/2} x_1 n f'(\theta_1) \bar{A} \sin \theta_L d\theta_L \quad (2.32.b.)$$

The relation between the projected leaf area indices,  $H(x_1)$ ,  $V(x_1)$  and  $LAI(x_1)$ , is determined by the leaf angle distribution. A factor,  $\xi$  or  $\xi'$ , can be introduced to quantify this relation.

$$\xi = (H^2(x_1) + V^2(x_1))^{1/2} / LAI(x_1) \quad (2.33.a.)$$

$$\xi' = (H(x_1) + V(x_1)) / LAI(x_1) \quad (2.33.b.)$$

The average leaf angle of a given leaf angle distribution follows from integration of the probability density function multiplied by the angle,  $\theta_L$ , itself.

$$\bar{\theta}_L = \int_0^{\pi/2} f'(\theta_L) \theta_L d\theta_L \quad (2.34.)$$

From both projections,  $H(x_1)$  and  $V(x_1)$ , an effective leaf angle,  $\theta_L$ , is derived:

$$\theta_L = \arctg(V(x_1)/H(x_1)) \quad (2.35.)$$

The following examples of leaf angle distributions are introduced and given by Figs. 30 and 31.

a: Planophile:  $f'(\theta_L) = \frac{2}{\pi} (1 + \cos 2 \theta_L)$

b: Erectophile:  $f'(\theta_L) = \frac{2}{\pi} (1 - \cos 2 \theta_L)$

c: Plagiophile:  $f'(\theta_L) = \frac{2}{\pi} (1 - \cos 4 \theta_L)$

d: Extremophile:  $f'(\theta_L) = \frac{2}{\pi} (1 + \cos 4 \theta_L)$

e: Spherical:  $f'(\theta_L) = \sin \theta_L$

f: Uniform:  $f'(\theta_L) = 2/\pi$

Table I gives  $H$ ,  $V$ ,  $\xi$ ,  $\xi'$ ,  $\bar{\theta}_L$  and  $\theta_L$  for these distributions with  $LAI(x_1) = 1$ .

TABLE I. The canopy structure parameters of the Suits' model derived from leaf angle distribution functions.

	$H$	$V$	$\xi$	$\xi'$	$\bar{\theta}_L$	$\theta_L$
a	0.849	0.424	0.949	1.273	26.8°	26.6°
b	0.424	0.849	0.949	1.273	63.2°	63.4°
c	0.679	0.679	0.960	1.358	45°	45°
d	0.594	0.594	0.840	1.188	45°	45°
e	0.500	$\pi/4$	0.931	1.285	57.29°	57.52°
f	0.637	0.637	0.900	0.900	45°	45°

From this table it can be concluded that the factor  $\xi$  gives a better approach of the actual leaf area index per layer, except for extremophile canopies. This seems contradictory, because the Suits' canopy itself is an extreme example of an extremophile canopy; however, factor  $\xi'$  gives a minimum deviation from one in the extremophile case (the uniform distribution not included). It ap-

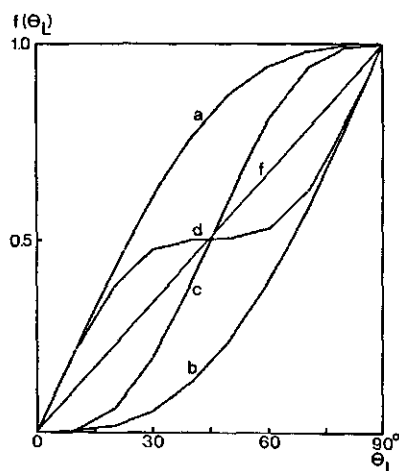


FIG. 30. Examples of cumulative leaf angle distributions.

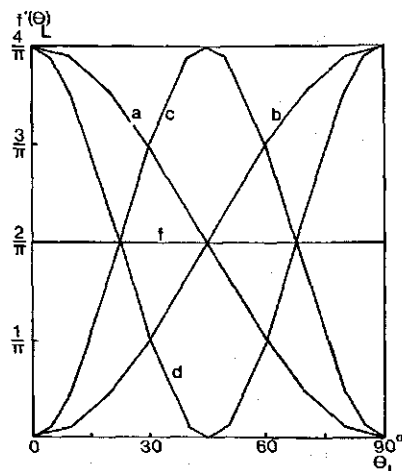


FIG. 31. Probability density functions of the leaf angle distributions, see Fig. 30.

pears further that the effective leaf angle,  $\theta_L$ , is a very good approximation of the average leaf angle,  $\bar{\theta}_L$ .

Therefore, the following structure parameters have been introduced.

$$L = (H^2 + V^2)^{1/2} \quad (2.36.)$$

$$H = L \cos \theta_L \quad (2.37.a.)$$

$$V = L \sin \theta_L \quad (2.37.b.)$$

#### 2.4.6.2. Calculation of the radiant flux profile within the canopy layers

One of the canopy layers is considered with only one kind of canopy component with hemispherical reflectance,  $\rho$  and transmittance,  $\tau$ , equal on both sides. The theory can be generalized in case of different components with unequal optical properties on both sides, BUNNIK and VERHOEF (1974). It is assumed that the components are Lambertian scatterers without polarizing properties. (If polarization effects are included, the resulting degree of polarization can be neglected in first order for most crops, because of the random distribution of the components.)

An advantage of the simplified canopy structure is the possibility of deriving simple analytical expressions for the Duntley parameters.

The extinction coefficient of the canopy layer for upward and downward diffuse flux is proportional to the surface area density of the components. The extinction coefficient of diffuse flux,  $a(\lambda)$ , in a layer is:

$$a(\lambda) = H'(1 - \tau(\lambda)) + V' \left( 1 - \frac{\rho(\lambda) + \tau(\lambda)}{2} \right) \quad (2.38.)$$

$$H' = H/x_1 \quad (2.39.a.)$$

$$V' = V/x_1 \quad (2.39.b.)$$

The backscatter coefficient of diffuse flux,  $\sigma(\lambda)$ , is found in an analogous way by adding the backscatter contributions from the horizontal and vertical components.

$$\sigma(\lambda) = H'\rho(\lambda) + V'\frac{\rho(\lambda) + \tau(\lambda)}{2} \quad (2.40.)$$

Direct solar radiant flux incident on the canopy, at zenith angle,  $\theta_s$ , will be scattered into upward and downward direction.

Radiative transfer is described in one dimension only, along the vertical and upwards in the positive direction. Irradiance on a horizontal plane by the direct flux is given by projection on the vertical.

$$E_s = E_s^0 \cos \theta_s \quad (2.41.)$$

$E_s^0$  = solar irradiance on a plane perpendicular to the solar rays

The increase in downward and upward diffuse flux by the loss of scattered direct flux in infinitesimal layer,  $dx$ , is given by the differential equations

$$dE_- = - \left( H' \cos \theta_s \tau + \frac{2}{\pi} V' \sin \theta_s \frac{\rho + \tau}{2} \right) E_s^0 dx \quad (2.42.a.)$$

$$dE_+ = \left( H' \cos \theta_s \rho + \frac{2}{\pi} V' \sin \theta_s \frac{\rho + \tau}{2} \right) E_s^0 dx \quad (2.42.b.)$$

The random azimuthal orientation of the vertical components gives an average vertical projected area,  $2/\pi V'$ , perpendicular to the solar azimuth.

From (2.42.) the forward scatter coefficient,  $s$ , and backscatter coefficient,  $s'$ , of direct flux is defined as:

$$s = H' \tau + \frac{2}{\pi} V' \frac{\rho + \tau}{2} \operatorname{tg} \theta_s \quad (2.43.a.)$$

$$s' = H' \rho + \frac{2}{\pi} V' \frac{\rho + \tau}{2} \operatorname{tg} \theta_s \quad (2.43.b.)$$

The extinction coefficient,  $k$ , is only connected with interception of direct flux and therefore independent of wavelength. The expression for  $k$  is found in the same way as for the scattering coefficients.

$$k = H' + \frac{2}{\pi} V' \operatorname{tg} \theta_s \quad (2.44.)$$

An incremental layer,  $\Delta x$ , is considered. It is assumed that mutual shading between components within this layer can be neglected. The energy balance of the upward diffuse flux,  $E_+$ , the downward diffuse flux,  $E_-$  and the direct flux,  $E_s$ , in vertical direction within the incremental volume given by  $\Delta x$  can be approximated by the Duntley equations, see Fig. 32.

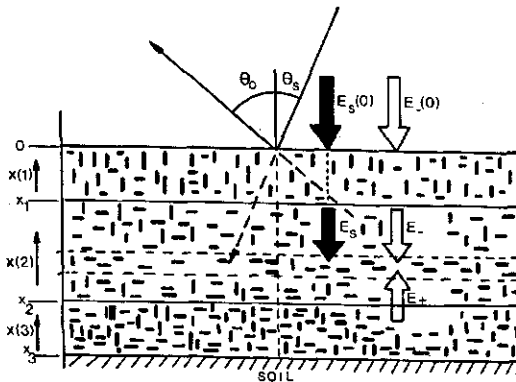


FIG. 32. Directional parameters and the balance of radiant flux in the Suits' canopy.



$$\frac{d}{dx} E_+ = -aE_+ + \sigma E_- + s'E_s \quad (2.45.a.)$$

$$\frac{d}{dx} E_- = -\sigma E_+ + aE_- - sE_s \quad (2.45.b.)$$

$$\frac{d}{dx} E_s = kE_s \quad (2.45.c.)$$

The general solution of these equations is:

$$E_+(x) = Ae^{mx} + Be^{-mx} + CE_s(0)e^{kx} \quad (2.46.a.)$$

$$E_-(x) = hAe^{mx} + h^{-1}Be^{-mx} + DE_s(0)e^{kx} \quad (2.46.b.)$$

$$E_s(x) = E_s(0)e^{kx} \quad (2.46.c.)$$

The following constants are introduced:

$$m = (a^2 - \sigma^2)^{1/2} \quad (2.47.)$$

$$h = (a+m)/\sigma \quad (2.48.)$$

$$C = \{s\sigma - s'(k-a)\}/(m^2 - k^2) \quad (2.49.a.)$$

$$D = \{s'\sigma + s(k+a)\}/(m^2 - k^2) \quad (2.49.b.)$$

The constants  $A$  and  $B$  are found by substitution of the boundary values at the canopy top, between the different layers and at soil level.

The incident flux is given by the direct flux,  $E_s(0)$ , and the diffuse irradiance from the sky,  $E_-$ .

$$E_s(0) = E_s^0(0) \cos \theta_s \quad (2.50.a.)$$

$$E_-(0) = E_- \quad (2.50.b.)$$

The solar flux outside the canopy perpendicular to the sun rays is  $E_s^0(0)$ . It is assumed that the fluxes are continuous between different layers. Local vertical coordinates,  $x(i)$ , are defined for each layer with thickness,  $x_i$ .

$$E_j(x(i+1) = 0) = E_j(x(i) = -x_i); j = s, +, - \quad (2.51.)$$

The soil bounding the deepest layer,  $n$ , reflects incident flux ideally diffuse.

$$E_+(-x_n) = \rho_s(E_-(-x_n) + E_s(-x_n)) \quad (2.52.)$$

$\rho_s$  = hemispherical reflectance of the soil.

The calculated diffuse fluxes are assumed to be isotropic. The radiant flux field is self-consistent, when this flux field acts as irradiating source to the components present in each layer and in another way the irradiated components form the flux field present. Actually the radiant diffuse fluxes are expected to be anisotropic and can be determined by the next iterative procedure.

The diffuse fluxes (2.46.a.) and (2.46.b.) are considered as first order approximations of the actual flux field.

Each incremental layer contains horizontal and vertical components with Lambertian scattering properties. These incremental layers have to be considered as radiative sources. If in each layer the radiance is calculated, non-Lambertian radiating sources are found, due to irradiance on the vertical components.

The radiance,  $\Delta L(x)$ , into the upward hemisphere from layer,  $\Delta x$ , with direction,  $(\theta_o, \phi_o)$ , does not depend only on the observation zenith angle,  $\theta_o$ , but also on the zenith angle,  $\theta_s$ , of the sun and on the differential azimuth angle,  $\psi (0 \leq \psi \leq \pi)$ , between the azimuth angle,  $\phi_o$ , of observation and  $\phi_s$ , of the sun. The canopy components scattering incident direct solar flux can be subdivided into a fraction of vertical components radiating by transmittance and the remaining fraction radiating by reflectance. This bidirectional effect is included, SURTS (1972). The radiance,  $\Delta L(x)$ , originates from the interaction of both diffuse fluxes and the direct flux with the components in layer,  $\Delta x$  and is given by:

$$\Delta L(\theta_o, \theta_s, \psi) = \frac{1}{\pi} (u(\theta_o)E_+ + v(\theta_o)E_- + w(\theta_o, \theta_s, \psi)E_s(\theta_s))\Delta x \quad (2.53.)$$

The weighting factors,  $u(\theta_o)$  and  $v(\theta_o)$ , respectively, belong to the contributions of the upward and downward diffuse flux; the bidirectional weighting factor,  $w(\theta_o, \theta_s, \psi)$ , contributes to  $\Delta L$  by scattering direct flux.

$$u(\theta_o) = H'\tau + V'\frac{\rho+\tau}{\pi} \text{tg } \theta_o \quad (2.54.a.)$$

$$v(\theta_o) = H'\rho + V'\frac{\rho+\tau}{\pi} \text{tg } \theta_o \quad (2.54.b.)$$

$$w(\theta_o, \theta_s, \psi) = H'\rho + V'F(\theta_s, \psi) \text{tg } \theta_o \quad (2.54.c.)$$

Factor,  $F(\theta_s, \psi)$ , allows for azimuthal variation due to the observed amount of vertical components radiating by transmittance or reflectance.

$$F(\theta_s, \psi) = \frac{1}{2\pi} \{ \rho(\sin \psi + (\pi - \psi) \cos \psi) + \tau(\sin \psi - \cos \psi) \} \text{tg } \theta_s \quad (2.55.)$$

The derivation of  $w(\theta_o, \theta_s, \psi)$  and the factor  $F(\theta_s, \psi)$  is given in appendix A.

The radiance of each layer as calculated with (2.53.) acts as a secondary source to the other layer. Allowance has to be made for interception of radiance by interjacent layers. The probability,  $p(x)$ , of interception into direction,  $\theta_o$ , along distance  $x$  is supposed to be exponential to the analogy of the extinction of direct solar flux.

$$p(x) = e^{Kx} \quad (2.56.a.)$$

$$K(\theta_o) = H' + \frac{2}{\pi} V' \text{tg } \theta_o \quad (2.56.b.)$$

By integration over all incremental layers a better approximation of the anisotropic flux field is found. The self-consistent flux field is determined by the convergence of radiance after repeated calculation of the new flux field on the basis of each preceding approximation.

Total radiance leaving the canopy in the direction of observation through gaps and emanating from the directly observed components, together with the contribution of radiance from the observed soil fraction, leads to the final result.

Suits assumes that in canopies without distinct non-Lambertian reflectance behaviour, the first calculated isotropic flux field already forms a good approximation of the actual flux field. This implies that the iteration required for obtaining the self-consistent field has to converge rapidly. This assumption simplifies the calculation of canopy reflectance.

#### 2.4.6.3. Calculation of directional reflectance

By substituting (2.46.) into (2.53.) the contribution  $\Delta L$  of increment,  $\Delta x(i)$ , in canopy layer,  $i$ , to the total directional radiance leaving the top layer, is found. The probability that the upper layers do not intercept radiance from layer,  $i$ , has to be included.

$$\Delta L^\circ(x(i)) = \prod_{i=1}^{i-1} \exp(-K_i x_i) \exp(K_i x(i)) \Delta L(x(i)) \quad (2.57.)$$

Integration of equation (2.57.) over all layers of the canopy and addition of the contribution from the observed fraction of the soil provides the total canopy radiance,  $L^\circ(\theta_o, \theta_s, \psi; \lambda)$ .

When a canopy is represented by one homogeneous layer of thickness,  $x_1$ , only, the radiance is:

$$\begin{aligned} L = & \frac{A}{\pi} (u + hv) \frac{1 - e^{-(K+m)x_1}}{K+m} + \frac{B}{\pi} (u + h^{-1}v) \frac{1 - e^{-(K-m)x_1}}{K-m} + \\ & + \frac{1}{\pi} (uC + vD + w) E_s(0) \frac{1 - e^{-(K+k)x_1}}{K+k} + \frac{\rho_s}{\pi} (hAe^{-(K+m)x_1} + \\ & + h^{-1}Be^{-(K-m)x_1} + (D+1)E_s(0)e^{-(K+k)x_1}) \end{aligned} \quad (2.58.)$$

Directional reflectance,  $r(\theta_o, \theta_s, \psi; \lambda)$ , is defined by:

$$r(\theta_o, \theta_s, \psi; \lambda) = \pi L(\theta_o, \theta_s, \psi; \lambda) / (E_s(0; \lambda) + E_-(0; \lambda)) \quad (2.59.)$$

From (2.58.) it is concluded that for homogeneous or multi-layer canopy models, all coefficients which are defined as linear combinations of the horizontal and vertical leaf area density,  $H'$  and  $V'$ , can be redefined by multiplying with the layer depth,  $x_i$ . This replaces  $H'$  and  $V'$  by the total horizontal and vertical leaf area index,  $H$  and  $V$ , per homogeneous layer.

If the direction of observation coincides with the direction of the sun rays, the observed shadows inside the canopy disappear. The probability of observing and the direct flux of reaching components at a certain depth are no longer independent of each other.

When the probability of the penetration of direct flux at depth,  $x$ , is taken into account, the probability of observing the directly illuminated components is equal to one. This implies that the probability function,  $\exp(K_i x(i))$ , in equation (2.57.) has to be replaced by one and that the bidirectional scattering term given by  $w$  in equation (2.58.) has to be modified by replacing  $(K+k)$  by  $K$  or  $k$  only, leading to maximum reflectance under this condition. This so called 'hot spot' effect is identical with the 'halo' effect.

#### 2.4.7. Evaluation of the canopy reflectance models of Goudriaan and Suits

The canopy reflectance models of Goudriaan and De Wit, Smith and Oliver and Suits for remote sensing applications have the advantage that spectral reflectance predicted, depends on the geometrical parameters of irradiance and observation, the ratio between direct and diffuse sky irradiance and physiological properties of the canopy itself. All these models have been evaluated and agreed well with field measurements, GOUDRIAAN (1977), SMITH and OLIVER (1973), SUITS and SAFIR (1972), BUNNIK and VERHOEF (1974), LEMASTER (1975). The accuracy of the necessary crop data, like leaf reflectance, transmittance, soil reflectance, leaf area index and leaf angle distribution ascertains to a great extent the conformity of absolute values.

On account of the availability of reflectance models it was decided to adopt one of these models and to improve it in some cases. Preference has been given to the model of Suits, because a drastic simplification for architecture of crops could be introduced directly without affecting the required correspondence between model results and measured data. This implies that additional field measurements on the geometrical structure of the crops considered could be simplified.

Another advantage was the analytical expression of crop reflectance. The physical relations between reflectance and observation geometry and the crop parameters are easily accessible for direct interpretation of their significance. This makes it also possible to obtain rapidly results using a small computer, while programming remains simple.

Application of the Smith-Oliver model has not been considered, because of the time consuming Monte Carlo method to be used. In this paragraph computations done with the model of Goudriaan are compared with results obtained with the Suits' model.

An elementary model of Goudriaan for horizontal leaves gives the same results as Suits' model. If only diffuse irradiance is assumed and the canopy hemispherical reflectance is defined by the ratio,  $E+(0)/E-(0)$ , it can be derived from (2.46.a.) and (2.46.b.) that for a homogeneous canopy with high LAI follows:

$$R_{\infty} = h^{-1} = \frac{1 - \tau - \sqrt{(1 - \tau)^2 - \rho^2}}{\rho} \quad (2.60.)$$

This result was found also by Goudriaan.

The same applies to the hemispherical reflectance of a canopy with horizontal leaves and soil reflectance,  $\rho_s$ . Substitution of the boundary conditions gives:

$$R_c = \frac{(1 - \rho_s h)e^{-mx_1} + (\rho_s h^{-1} - 1)e^{+mx_1}}{(\rho_s - h)e^{mx_1} + (h^{-1} - \rho_s)e^{-mx_1}} \quad (2.61.)$$

Calculations have been performed for diffuse irradiance, a black soil, a high leaf area index,  $LAI = 10$  and for different values of  $\rho = \tau$  of the leaves. The input parameters are summarized in Table 2.

TABLE 2. Input parameters for the canopy reflectance models of Goudriaan and Suits.

$\rho = \tau$	$\rho_s$	$LAI$	leaf angle distr.	$L$	$\theta_L$
0.15	0	10	50% hor./50% vert.	10	45°
0.40	0	10	50% hor./50% vert.	10	45°
0.15	0	10	100% : 45°	10	45°
0.40	0	10	100% : 45°	10	45°
0.15	0	10	spherical	9.31	57.52°
0.40	0	10	spherical	9.31	57.52°
0.15	0	10	100% : 85°	10	85°
0.40	0	10	100% : 85°	10	85°
0.15	0	10	100% : 0°	10	0°
0.40	0	10	100% : 0°	10	0°

Fig. 33, 34, 35 and 36 show the directional reflectance for variation of  $\theta_o$  between 0° and 85°.

Only when an extremophile leaf angle distribution in Goudriaan's model is substituted, both results are almost equal. For  $\theta_o > 75^\circ$  the reflectance values of Goudriaan are higher (see Fig. 33).

The probability of observing canopy components to a given depth with varying view angle is constant with leaves of a constant inclination between  $\theta_o = 0^\circ$  and  $\theta_o = \pi/2 - \theta_L$ . This results in a constant directional reflectance between 0° and 45° for leaves under 45°, as shown in Fig. 34. Because of the increasing influence of vertical components in the Suits' model, the corresponding directional reflectance is an increasing function. With a spherical leaf angle distribution, both reflectance functions show the same behaviour: for nearly vertical leaf angles the deviation between the two models is at a maximum. Both models illustrate the more pronounced non-Lambertian character which is amplified by the choice of a dark soil. With horizontal leaves only, both models predict Lambertian reflectance.

From these examples it can be concluded that the dynamic behaviour of the models of Goudriaan and Suits is very similar. With a spherical leaf angle

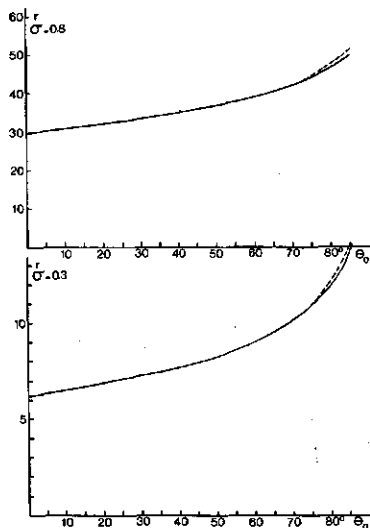


FIG. 33. Simulation of the directional reflectance with the canopy reflectance models of Goudriaan and Suits. The leaves are distributed over equal fractions of horizontal and vertical leaves only.  
 $LAI = 10$  —: Suits ---: Goudriaan.

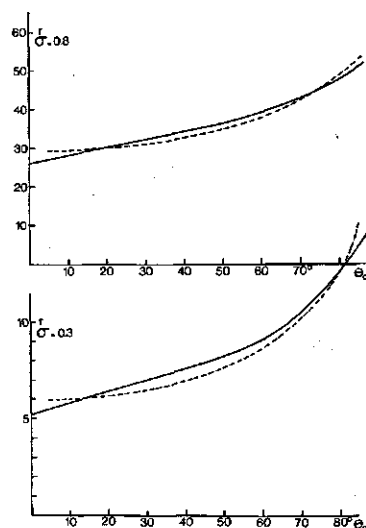


FIG. 34. Simulation of the directional reflectance with the canopy reflectance models of Goudriaan and Suits. The leaves have a constant inclination of  $45^\circ$ .  
 $LAI = 10$  —: Suits ---: Goudriaan.

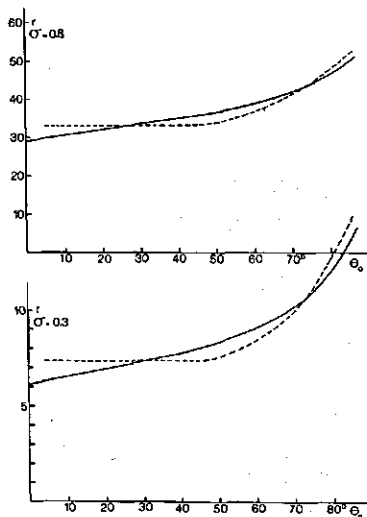


FIG. 35. Simulation of the directional reflectance with the canopy reflectance models of Goudriaan and Suits for a spherical leaf angle distribution.  
 $LAI = 10$  —: Suits ---: Goudriaan.

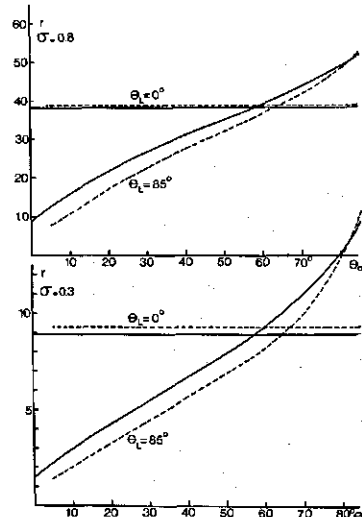


FIG. 36. Simulation of the directional reflectance with the canopy reflectance models of Goudriaan and Suits for leaves with inclination angles of  $85^\circ$  or  $0^\circ$ .  
 $LAI = 10$  —: Suits ---: Goudriaan.

distribution, which is quite a good approximation in erectophile canopies, the maximum deviation is observed at  $\theta_o = 0^\circ$ . With low leaf reflectance this deviation is about 13.5% and with high reflectance like in the near infrared at most 11.5%. The remarkable correspondence in the extremophile canopy simulated by assuming only horizontal and vertical leaves, proves the consistency of the Suits' model as a singular extremophile canopy.

Dealing with inaccuracies of the input parameters from field data, it may be concluded that the canopy reflectance model of Suits suffices for remote sensing applications. It has been demonstrated that immediate simplification of the crop structure in the first stage of modelling does not show a significantly different effect as approximations applied afterwards, as done by Goudriaan.

#### 2.4.8. Reciprocity relations

If no sky irradiance is present, Goudriaan's model yields for interchanging the direction of incident solar radiation and observation the following reciprocity relation:

$$r = (\theta_o, \theta_s, \psi) = r(\theta_s, \theta_o, \psi) \quad (2.62.)$$

CHANCE and LEMASTER (1977) have investigated this reciprocity in Suits' model. They proved this property in the case of an infinitely thick canopy, but model predictions and field reflectance measurements confirmed the general validity of relation (2.62.).

Using the equation (2.58.) this theorem was proved analytically in the general case of a single layer canopy with soil reflectance,  $\rho_s$ . The derivation of the reciprocity relation is summarized in appendix B. Simplified evidence of reciprocity of an infinite canopy is given. Suits' equation for the bidirectional reflectance in the absence of diffuse sky irradiance follows from (2.58.) and the boundary conditions:

$$r_\infty(\theta_o, \theta_s, \psi) = \frac{D}{h} + \frac{u + hv}{K + m} + \frac{uC + vD + w}{K + k} \quad (2.63.)$$

Substitution of the expressions (2.49.) for C and D into (2.63.) gives after some reductions:

$$\begin{aligned} r_\infty(\theta_o, \theta_s, \psi) = & \frac{\sigma\{us(K+k) + (a+m)(us+vs')\} + \sigma^2(us' + vs)}{(k+m)(K+m)(K+k)(a+m)} + \\ & + \frac{(a+m)\{us'(k+m) + vs(k+m)\}}{(k+m)(K+m)(K+k)(a+m)} + \frac{w}{K+k} \end{aligned} \quad (2.64.)$$

If the expressions for  $s$  and  $s'$  given by (2.43.) and for  $u$  and  $v$ , see (2.54.), are compared, reciprocity by interchanging  $\theta_o$  and  $\theta_s$  is found. The bidirectional

scatter coefficient,  $w$ , is symmetrical in  $\theta_o$  and  $\theta_s$ , while  $K$  and  $k$  also exchange. Using these properties proves the reciprocity of (2.64.).

Goudriaan has shown that as a consequence of this reciprocity relation, directional reflectance of a crop under diffuse irradiance from a uniform overcast sky is equivalent to the hemispherical reflectance resulting from a direct radiant flux. Hemispherical reflectance is defined by the ratio between upward emittance and downward irradiance. Emittance is found by integrating the radiant intensity,  $L_c \cos \theta_o$ , into the solid angle of  $2\pi$  steradians of the hemisphere. Canopy radiance,  $L_c(\theta_o, \theta_s, \psi)$ , as function of the radiant direction,  $\theta_o$ , the solar zenith angle,  $\theta_s$  and the azimuth angle,  $\psi$ , is given by Suits' model. Substitution gives for emittance,  $M$ :

$$M = \int_{2\pi} L_c(\theta_o, \theta_s, \psi) \cos \theta_o d\omega_o = \frac{E_s(0)}{\pi} \int_{2\pi} r(\theta_o, \theta_s, \psi) \cos \theta_o d\omega_o \quad (2.65.)$$

Canopy radiance,  $dL_c(\theta_o, \theta_s, \psi)$ , as a result of irradiance by an element given by the solid angle,  $d\omega_s$ , of a uniform overcast sky with constant radiance,  $L_i$ , is expressed by:

$$dL_c(\theta_o, \theta_s, \psi) = \frac{1}{\pi} r(\theta_o, \theta_s, \psi) L_i \cos \theta_s d\omega_s \quad (2.66.)$$

The total radiance is found by integration of (2.66.):

$$L_c(\theta_o, \phi_o) = \frac{L_i}{\pi} \int_{2\pi} r(\theta_o, \theta_s, \psi) \cos \theta_s d\omega_s \quad (2.67.)$$

When the reciprocity relation of the bidirectional reflectance, as shown in appendix B, is substituted in (2.65.) or (2.67.) the next identity follows:

$$R_c = \frac{M}{E_s(0)} = r_c(\theta_o, \phi_o) = \frac{1}{\pi} \int_{2\pi} r(\theta_o, \theta_s, \psi) \cos \theta_o d\omega_o \quad (2.68.)$$

#### 2.4.9. Examples of canopy reflectance spectra

To conclude this chapter, some examples of the calculated spectral reflectance and measured spectra are given. For the model, constant optical properties of the leaves have been assumed.

The reflection and transmission coefficients used are given in Fig. 37. The simulations have been carried out for a canopy consisting of one homogeneous layer. Constant values for the zenith angle of the sun,  $\theta_s = 30^\circ$ , and the observation angle,  $\theta_o = 0^\circ$ , have been chosen.

For simplicity a constant ratio between direct solar flux and diffuse sky irradiance has been applied, ( $E_d(0) = 0.5 E_s(0)$ , in all wavelengths).



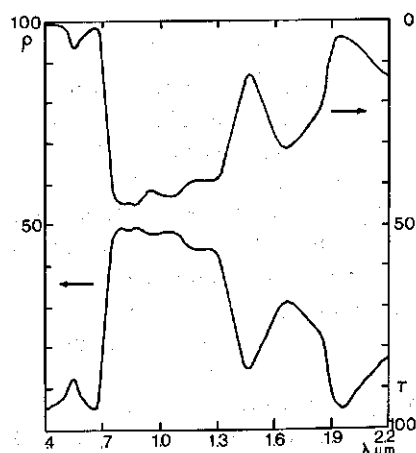


FIG. 37. Reflection and transmission coefficient of a single green leaf, used in canopy reflectance simulations.

FIG. 38. The spectral reflectance of a dry and moist sandy loam soil, used in canopy reflectance simulations (measured at test site Wageningen)  
dry soil: —, moist soil: ---

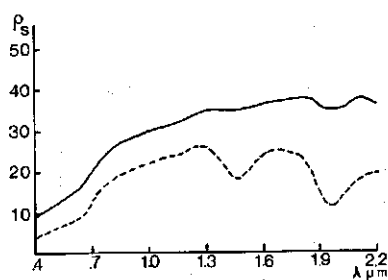


FIG. 39. Spectral reflectance of a one-layer canopy with a dry sandy loam soil.  
 $\theta_s = 30^\circ$ ,  $\theta_o = 0^\circ$ ,  $\theta_L = 15^\circ$   
 $L = 0.5$ : —,  $2$ : ---,  $8$ : -.-

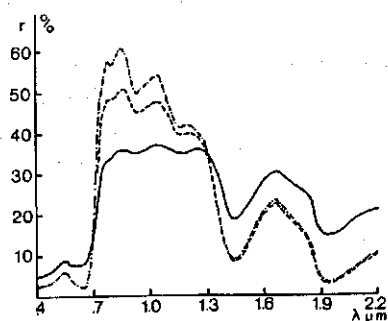
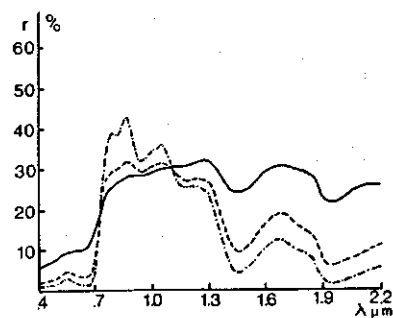


FIG. 40. Spectral reflectance of a one-layer canopy with a dry sandy loam soil.  
 $\theta_s = 30^\circ$ ,  $\theta_o = 0^\circ$ ,  $\theta_L = 75^\circ$   
 $L = 0.5$ : —,  $2$ : ---,  $8$ : -.-



The simulations have been done for a dry and moist sandy loam soil, their spectral reflectance is shown in Fig. 38.

Figs. 39 and 40 give results of varying leaf area indices with a constant average leaf angle of  $15^\circ$  and  $75^\circ$ , respectively, for a dry soil. These examples demonstrate that the relative variation of reflectance is at a maximum, where the contrast of leaf and soil reflectance is optimum. Increasing leaf area index leads to a relatively great decrease in reflectance at 670, 1450 and 1950 nm. Reflectance in the near infrared plateau increases (except at 1250 nm for vertically oriented leaves): the maximum variation in this case is observed at 870 nm, where maximum leaf-soil contrast and minimum leaf absorptance nearly coincide.

Fig. 41 gives canopy reflectance for varying leaf angle with a constant leaf area index.

If the average leaf angle,  $\theta_L$ , is the only varying canopy parameter, Fig. 41 shows that reflectance in the near infrared plateau and between 1500 and 1800 nm drops with increasing leaf angle. The probability of free lines of sight into the deeper canopy layers and of observing the soil increases. In the infrared regions mentioned, more of the reflecting soil contributes to canopy reflectance. At 670 nm, however, the soil contributes more than the single leaves leading to increased canopy reflectance. For higher values of the leaf area index, this increase disappears due to the simultaneously increased amount of shadow inside the canopy.

A different phenomenon occurs when soil moisture varies. As mentioned in 2.3. and shown in Fig. 38 soil reflectance decreases at all wavelengths with increasing moisture content in the top layer.

With an open canopy, as given in Fig. 42, the drop in reflectance is significant in all wavelengths. The percentage plant cover for  $L = 0.5$  and  $\theta_L = 45^\circ$  comes to 30%. When the leaf area index increases to  $L = 2$  as shown in Fig. 43, the plant cover percentage is already 76%. Reflectance variation in the visible light region is no longer significant, only in the near infrared plateau and at

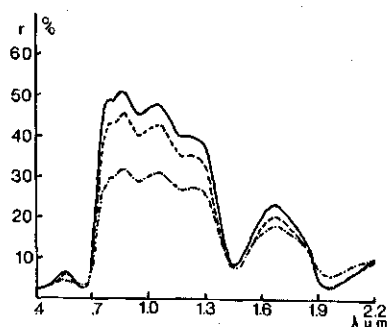


FIG. 41. Spectral reflectance of a one-layer canopy with a dry sandy loam soil.  
 $\theta_s = 30^\circ$ ,  $\theta_o = 0^\circ$ ,  $L = 2$   
 $\theta_L = 15^\circ$ : —,  $45^\circ$ : ---,  $75^\circ$ : -.-

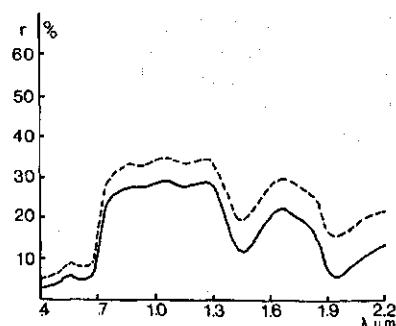
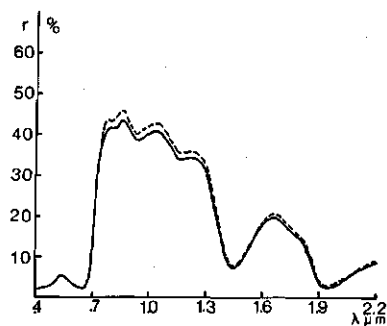


FIG. 42. Spectral reflectance of a one-layer canopy with a dry and a moist sandy loam soil.  
 $\theta_s = 30^\circ$ ,  $\theta_o = 0^\circ$ ,  $L = 0.5$ ,  $\theta_L = 45^\circ$   
dry soil: ---, moist soil: —

FIG. 43. Spectral reflectance of a one-layer canopy with a dry and moist sandy loam soil.  
 $\theta_s = 30^\circ$ ,  $\theta_a = 0^\circ$ ,  $L = 2$ ,  $\theta_L = 45^\circ$   
 dry soil: ---, moist soil: —



1700 nm some reflectance variation is present due to the more transparent character of the canopy.

Anticipating chapter 4, in which the reflectance measurements are described, some examples of measured spectra are included to compare them with model predictions.

Fig. 44 gives the average spectral reflectance of sugarbeets. The measurements have been performed with constant diffuse incident radiation using an artificial light source. All spectra have been measured under perpendicular view.

The dynamic behaviour of the time varying spectrum corresponds qualitatively quite well with Fig. 40, where an increasing leaf area index was simulated for vertically oriented leaves. Fig. 45 shows average spectral reflectance values

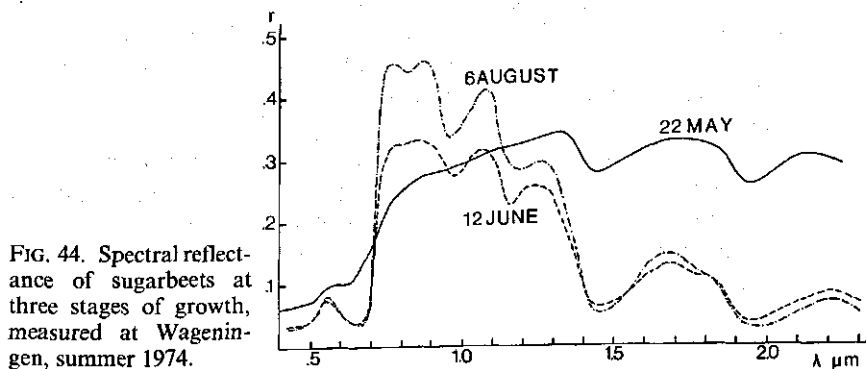


FIG. 44. Spectral reflectance of sugarbeets at three stages of growth, measured at Wageningen, summer 1974.

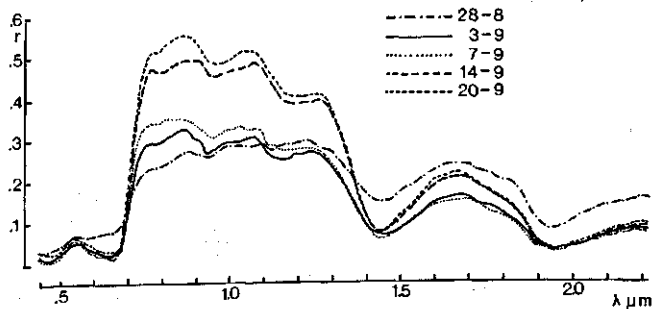


FIG. 45. Reflectance spectra of Perennial ryegrass during the growth cycle (Wageningen, summer 1973).

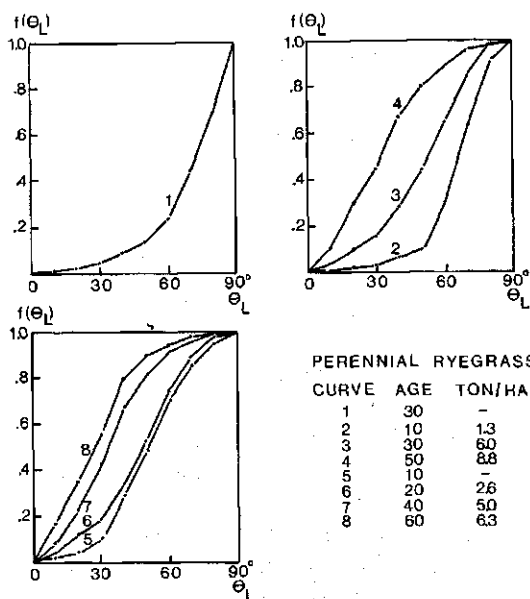


FIG. 46. Variation in the cumulative leaf distribution function of Perennial ryegrass during a growth cycle (taken from De Wit, 1965).

of Perennial ryegrass during one growth cycle. It is striking that the behaviour of the pasture is similar to that of sugarbeets, an interesting detail is the reflectance increase in the visible light region at the end of the cycle. This effect can be interpreted by following the changes in leaf angle distribution of pastures. Fig. 46 gives measurements taken from DE WIT (1965). The leaf angle distribution of grasses changes from erectophile to planophile when the leaves are flattening: this leads to an increase in canopy reflectance at all wavelengths, as shown in Fig. 41.

Fig. 47 gives some spectra of Perennial ryegrass measured with varying observation angles, a sun angle of  $\theta_s = 66^\circ$  and a clear sky. The grass canopy had an average thickness of 16 cm. The measured variations are merely due to canopy variation present in the field.

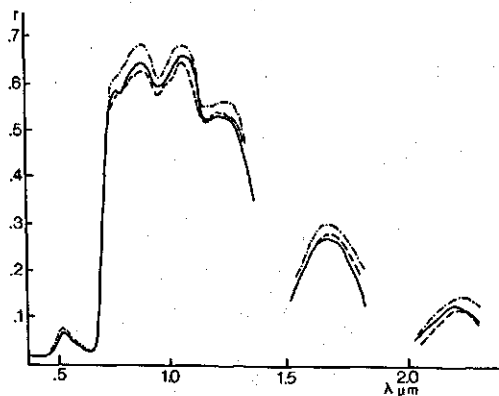


FIG. 47. Directional reflectance of Perennial ryegrass, measured at Wageningen, summer 1973.  
 $\theta_s = 66^\circ$ ,  $\theta_o = 15^\circ$ ,  $\psi = 153^\circ$ : —,  $\psi = 173^\circ$ : ---,  $\psi = 95^\circ$ : -.-.

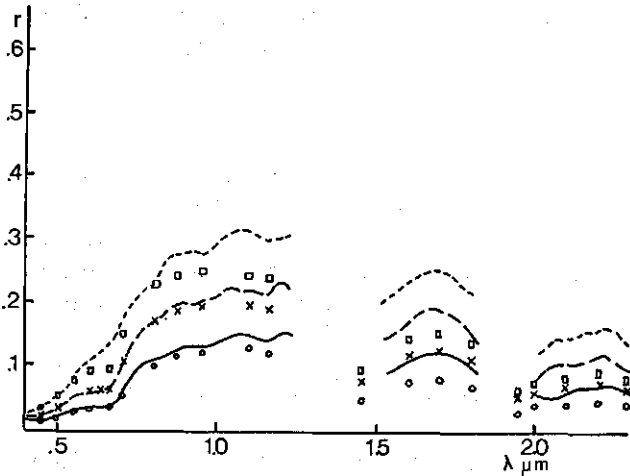


FIG. 48. Directional reflectance of mature wheat, measured at Wageningen, summer 1973.  $\theta_s = 50^\circ$ ,  $\psi = 45^\circ$ ,  $\theta_o = 0^\circ$ : —,  $\theta_o = 25^\circ$ : ---,  $\theta_o = 45^\circ$ : .... The spectra are simulated with a three layer Suits' model.  $\circ$ :  $\theta_o = 0^\circ$ ,  $\times$ :  $\theta_o = 25^\circ$ ,  $\square$ :  $\theta_o = 45^\circ$

An example of pronounced non-Lambertian canopy reflectance is shown in Fig. 48. These measurements were carried out in a mature wheat canopy with a dominant vertical structure. The soil mainly was covered by weeds. Therefore some selective absorption by chlorophyll is measured at an angle of  $0^\circ$ . When the view angle changes up to  $45^\circ$  a drastic spectral reflectance variation is measured, because at oblique view angles mainly stalks and ears are observed. These canopy components have different optical properties, especially in the visible light region.

A model simulation with a three layer structure has been carried out. Only the optical constants were available of the canopy components which were determined five days before these measurements taken in situ. This probably explains the deviation between model simulations and measurements, which are caused by a further decrease in the water content of the components.

### 3. SENSITIVITY OF MULTISPECTRAL REFLECTANCE DATA TO VARIATION IN CROP PARAMETERS

#### 3.1. DISTRIBUTION OF INFORMATION IN THE VISIBLE LIGHT AND THE NEAR INFRARED REGION

In chapter 2 the coherence has been treated between the reflectance spectrum of a crop and the structure, the optical properties of the phyto-elements and reflectance of the soil.

Differences between crops and dynamic changes due to growth, stress and diseases can give rise to differences between their reflectance spectra. In designing remote sensing equipment and its requirement, it is essential to know in which parts of the radiance spectrum maximum or minimum information is available relating to variations in crop parameters. For this it has to be known in which and in how many wavelengths bands the radiation reflected by a crop has to be measured.

In a given wavelength interval, for instance from 400 to 2400 nm, all information about the distribution of reflected radiation in this wavelength interval is available, if for each value within this interval reflectance is known.

The relations between physiological properties of leaves and their scattering behaviour and the non-spectral structure parameters of crops indicate that reflectance in different wavelength values is more or less closely correlated. As described in chapter 2, variation in a crop parameter like leaf area index or the moisture level of the soil indeed effects the canopy reflectance in all wavelengths.

Senescence of leaves is not only attended by degeneration of chlorophyll and yellowing, but the internal leaf mesophyll structure also changes. Because the leaves are shrinking, canopy structure changes drastically. This means that one cause does not always affect only one reflectance parameter, but that the response found in multispectral data often is closely interrelated in a rather complex manner.

Information obtained by measurement of the reflectance at a wavelength value is defined by the measured variance. When this information is compared with that of another wavelength, their correlation should be taken into account: in this way the covariance in reflectance at two different wavelengths is important.

It is possible to apply a linear transformation to multispectral reflectance data which eliminates this covariance. Variance may be compared directly and information distribution may be determined in these transformed (synthetic) data. The distribution in the original data can be found in a straight forward calculation.

The method, based on this linear transformation and used in the following analysis is a transformation of multivariate data to principal axes, HARALICK (1970), BEERS (1975) and FUKUNAGA (1972). In transforming, the symmetry

is applied of the covariance of a given set of datavectors. Assuming a set of  $M$  radiance spectra, sampled at  $N$  wavelength values. these values will form  $M$  datavectors,  $L_j$ .

$$L_j = Br_j + L_p, j = 1, 2, \dots, M \quad (3.1.)$$

The vector,  $L$ , with elements,  $L(\lambda_k)$ , is written as a matrixproduct of the diagonal matrix,  $B$  and the spectral reflectance vector,  $r$ , with an additive contribution by the path radiance vector,  $L_p$ , with elements,  $L_p(\lambda_k)$ . The diagonal  $N$  by  $N$  matrix is formed by diagonal elements.

$$B_{kk} = \frac{1}{\pi} E_i(\lambda_k) T(\lambda_k), k = 1, 2, \dots, N \quad (3.2.)$$

The magnitude of the variance of each element,  $L_{kj}$ , should be relative to the expectation value,  $E(L_{kj})$ . Since in general high radiance corresponds with a proportionally high variance, only the variance relative to the average is a useful measure of the information content. For this reason, all datavectors are transformed to an average zero value with weighting factors determined by the expectation values,  $E(L_{kj})$ .

The transformed radiance vector,  $L'_j$ , expressed in matrix-notation, is given by

$$L'_j = C^{-1} (L_j - E(L_j)) \quad (3.3.)$$

$$E(L_j) = B\mu + L_p \quad (3.4.)$$

$$C_{kk} = E(L_{kj}) = B_{kk}\mu_k + L_{pk} \quad (3.5.)$$

The expectation value of the reflectance,  $r$ ,  $E(r)$ , is defined as the average vector,  $\mu$ . The diagonal matrix,  $C$ , is formed by the  $N$  expectation values,  $E(L_{kj})$ , of the elements of datavector  $L_j$ .

From now on, it is assumed that the path radiance vector,  $L_p$ , is small compared with the apparent datavectors,  $L_j$ . This assumption simplifies all elements of the transformed datavectors,  $L'_j$ , as follows:

$$L'_{kj} = \frac{B_{kk}(r_{kj} - \mu_k)}{B_{kk}\mu_k + L_{pk}} \simeq \frac{r_{kj} - \mu_k}{\mu_k} = x_{kj} \quad (3.6.)$$

New datavectors,  $x_j$ , are obtained independent of the irradiance level and atmospheric transmittance and are only determined by the directional reflectance. In a similar way datavector,  $x_j$ , is written in matrix notation by the introduction of diagonal matrix,  $\mu$ .

$$x_j = \mu^{-1}(r_j - \mu) \quad (3.7.)$$

$$\mu_{kk} = E(r_{kj}) \quad (3.8.)$$

The transformation to principal axes in the feature space spanned by  $N$  orthonormal unitvectors starts from the covariance matrix,  $\Sigma$ , belonging to the set of  $M$  datavectors,  $\underline{x}$ .

$$\Sigma = E(\underline{x}\underline{x}^T) \quad (3.9.)$$

This matrix is symmetric because for its off-diagonal elements follows from (3.9.)

$$\sigma_{mp} = E(x_m x_p^T) = \frac{1}{M-1} \sum_{j=1}^M x_{mj} x_{jp} = \sigma_{pm} \quad (3.10.)$$

The eigenvalues of matrix,  $\Sigma$ , are calculated by solving the next equation:

$$\Sigma \underline{y} = \lambda \underline{y} \quad (3.11.)$$

The solution of these  $N$  linear equations is found if the following condition is fulfilled:

$$|\Sigma - \lambda I| = 0 \quad (3.12.)$$

Matrix,  $\Sigma$ , is hermitian. A property of hermitian matrices is that the eigenvalues,  $\lambda_j$ , are real and the corresponding set of eigenvectors,  $\underline{y}_j$ , form an orthogonal basis. The eigenvector matrix,  $Y$ , is formed by the normalized eigenvectors as columnvectors in an order corresponding with the descending absolute value of the eigenvalues. The original datavectors,  $\underline{x}$ , are spanned by the new basis by linear transformation with the transposed eigenvector matrix,  $Y^T$ .

$$\underline{u} = Y^T \underline{x} \quad (3.13.)$$

The covariance matrix,  $A$ , of the set of datavectors,  $\underline{u}$ , is diagonal which can be proved as follows

$$A = E(\underline{u} \underline{u}^T) = E(Y^T \underline{x} \underline{x}^T Y) = Y^T \Sigma Y \quad (3.14.a.)$$

$$A_{mp} = E(u_m u_p^T) = \underline{y}_m^T \Sigma \underline{y}_p = \delta_{mp} \lambda_p \quad (3.14.b.)$$

The eigenvalues,  $\lambda_p$ , are all positive because they are equal to the variance of the feature vectors,  $\underline{u}$ , into the 'synthetic' direction,  $p$ , given by  $\underline{y}_p$ . Covariances between elements of  $\underline{u}$  are all zero. The eigenvalues of covariance matrix,  $\Sigma$ , form the diagonal elements of the new covariance matrix,  $A$ .

A measure for the information distributed over the new  $N$  'synthetic' dimensions of the feature space is defined as the total variance of  $\underline{u}$  given by the trace of matrix,  $A$ .

The relative information content of synthetic feature,  $u_p$ , is defined as

$$I(p) = \lambda_p / \text{Tr}(A) \quad (3.15.)$$



The method of transformation to principal axes is illustrated by Fig. 49 where a set of two-dimensional data points has been transformed to an average of zero and to their principal axes.

The contribution,  $C_i$ , of an original axis,  $i$ , to the total information content is calculated from the given weighting factor to each of the  $N$  eigenvectors and their information contents.

$$C_i = \sum_{p=1}^N \frac{|y_{pi}|}{\sum_{j=1}^N |y_{pj}|} I(p) \quad (3.16.)$$

The distribution of information in the reflectance spectrum can be determined by calculating the ratio of information between the selected wavelengths and a fixed reference value, because the relative distribution is given by

$$I_{i,r} = \frac{C_i}{\sum_{j=1}^N C_j} = \frac{C_i/C_r}{\sum_{j=1}^N (C_j/C_r)} \quad (3.17.)$$

The information ratio between wavelength value,  $i$  and  $r$ , follows otherwise directly from the principal axis analysis for this band pair, which leads to the following result:

$$C_i/C_r = \frac{|y_{11}(i/r)| \lambda_1(i/r) + |y_{12}(i/r)| \lambda_2(i/r)}{|y_{12}(i/r)| \lambda_1(i/r) + |y_{11}(i/r)| \lambda_2(i/r)} \quad (3.18.)$$

$y_1(i/r)$ : eigenvector of  $\Sigma_{ir} = E(\underline{x}(i/r) \underline{x}^T(i/r))$

$\lambda_1(i/r), \lambda_2(i/r)$ : eigenvalues of  $\Sigma_{ir}$

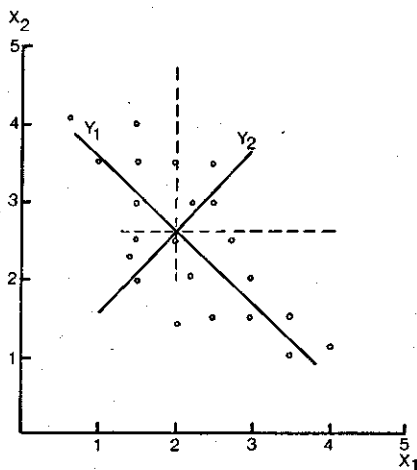


FIG. 49. Example of the principal axes of a two dimensional set of data points.

### 3.2. DISTRIBUTION OF SPECTRAL INFORMATION IN CANOPY AND SOIL CONTRIBUTIONS

The analysis of the canopy reflectance model of Suits has proved that the total reflectance can be considered as a linear combination of contributions emanating from the leaf canopy and the soil. To study the relative effect of both contributions to the information distribution, expression (2.58.) has been transposed to a new linear combination. The information distributions have been calculated for an uniform canopy for reasons of simplicity. If the boundary conditions (2.50.) and (2.52.) are substituted, (2.59.) can be written as:

$$r_c = r_c(0) + r'_c(0)\rho_s/(1 - \rho_o\rho_s) \quad (3.19.)$$

$r_c(0)$ : canopy reflectance for a black soil.

$$r'_c(0) = \lim_{\rho_s \rightarrow 0} \frac{d}{d\rho_s} r_c \quad (3.20.)$$

The factor,  $r'_c(0)$ , describes the relative increase in canopy reflectance, when the soil starts contributing to reflectance. Reflectance,  $\rho_o$ , is equal to the absolute reflectance for isotropic incident radiation which follows from the Kubelka-Munk equations, KORTUM (1969).

$$\rho_o = \frac{\sigma}{a + m \coth m} \quad (3.21.)$$

From equation (3.19.) and (3.20.) it follows directly that the soil contribution disappears with high leaf area index. The information distributions have been calculated for  $r_c$ ,  $r_c(0)$  and  $r_c - r_c(0)$ , respectively.

### 3.3. CALCULATION OF THE INFORMATION DISTRIBUTION FOR SIMULATED AND MEASURED REFLECTANCE SPECTRA

Information distribution functions have been calculated using model simulations and field measurements in order to determine wavelength values which are significant in detecting varying crop parameters.

The Suits' model has been used in calculating reflectance spectra for varying  $L$ ,  $\theta_L$ , soil moisture and optical properties of the leaves. The irradiance and observation parameters have been chosen constant in most situations. With varying  $L$ ,  $\theta_L$  or soil reflectance leaf reflectance and transmittance have been taken constant according to values given by GAUSMAN *et al.* (1971). Six soil reflectance spectra have been used for varying moisture content of a sandy loam soil at the test site at Wageningen, indicated with index  $Q = 1, 2, \dots, 6$ .

Reflectance of  $Q = 1$  (dry soil) and  $Q = 6$  (moist soil) are given in Fig. 21. To simulate varying canopy reflectance caused by yellowing leaves, six reflectance and transmittance spectra have been taken from the literature ( $K = 1, 2$ ,

TABLE 3. Variation in input parameters for model simulations of information distributions.

Fig.	$\theta_s$	$\psi$	$\theta_o$	Canopy parameter values	$L$	$\theta_L$	$Q$	$K$
50	30°	0°	0°	1, 1.5, 2, 2.5, 3, 3.5, 4, 4.5, 8, 16		30°	1	1
	30°	0°	0°	1, 1.5, 2, 2.5, 3, 3.5, 4, 4.5, 8, 16		30°	6	1
51	30°	0°	0°	1, 1.5, 2, 2.5, 3, 3.5, 4, 4.5, 8, 16		30°	1	1
	60°	0°	0°	1, 1.5, 2, 2.5, 3, 3.5, 4, 4.5, 8, 16		30°	1	1
	30°	90°	45°	1, 1.5, 2, 2.5, 3, 3.5, 4, 4.5, 8, 16		30°	1	1
52	30°	0°	0°	1, 1.5, 2, 2.5, 3, 3.5, 4, 4.5, 8, 16		30°	6	1
	30°	0°	0°	1, 1.5, 2, 2.5, 3, 3.5, 4, 4.5, 8, 16		60°	6	1
53	30°	0°	0°	1, 1.5, 2, 2.5, 3, 3.5, 4, 4.5, 8, 16		30°	1	1
	30°	0°	0°	3, 3.5, 4, 4.5, 5, 5.5, 6, 6.5, 7, 8		30°	1	1
54	30°	0°	0°	0°, 15°, 30°, 35°, 45°, 60°, 75°	3		1	1
	30°	0°	0°	0°, 15°, 30°, 35°, 45°, 60°, 75°	3		6	1
	30°	0°	0°	0°, 15°, 30°, 35°, 45°, 60°, 75°	1		1	1
55	30°	0°	0°	0°, 15°, 30°, 45°, 60°, 75°, 90°	3		1	1
	30°	90°	45°	0°, 15°, 30°, 45°, 60°, 75°, 90°	3		1	1
56	30°	0°	0°	1, 2, 3, 4, 5, 6	2	60°		1
	30°	0°	0°	1, 2, 3, 4, 5, 6	3	45°		1
	30°	0°	0°	1, 2, 3, 4, 5, 6	5	45°		1
57	30°	0°	0°	1, 2, 3, 4, 5, 6	1.5	58°	1	
	30°	0°	0°	1, 2, 3, 4, 5, 6	1.5	58°	6	
58	—	—	0°	1, 2, ....., 18	$\infty$	0°	—	

....., 6). An investigation into canopy reflectance variations caused by different green leaf types has been done using 18 single leaf spectra taken from GAUSMAN *et al.* (1971).

The input parameters for the model simulations are given in Table 3, the graphs of the information distributions are given in Fig. 50 to 58. With reference to these results, the following conclusions can be drawn:

a. The influence of the soil background is a dominating factor. With a light (dry) soil, maximum information on variation in leaf area index is found at wavelengths with maximum reflectance contrast, *viz.* at 670, 1450 and 1950 nm. With a dark (moist) soil, these maxima disappear and most information moves to the infrared plateau. The information distribution for a dark soil in the infrared region is similar to the distribution of  $r_c(0)$ . The information based on

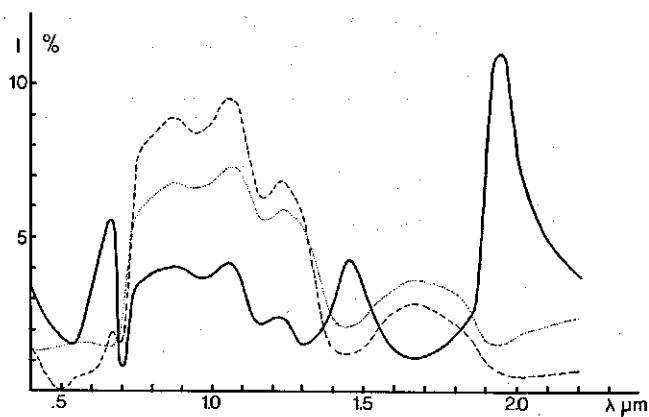


FIG. 50. Information distribution for variation in  $L$ .  
 $r_s(0)$ : ...,  $Q = 1$ : —,  $Q = 6$ : ---.

FIG. 51. Information distribution for variation in  $L$  and for varying sun and observation angles.

$\theta_o = 0^\circ$ ,  $\theta_s = 30^\circ$ : —,  $\theta_s = 60^\circ$ : ---,  $\theta_o = 45^\circ$ ,  $\theta_s = 30^\circ$ :  $\Delta$ .

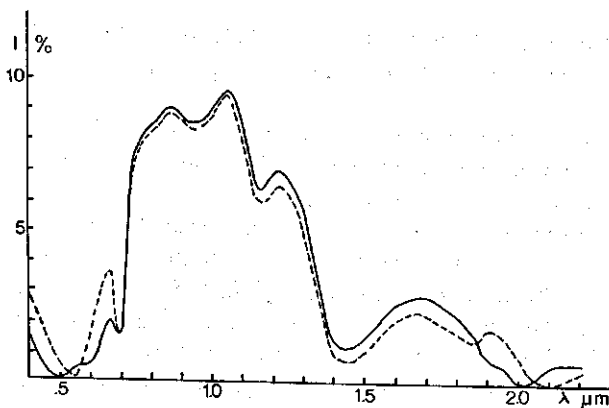
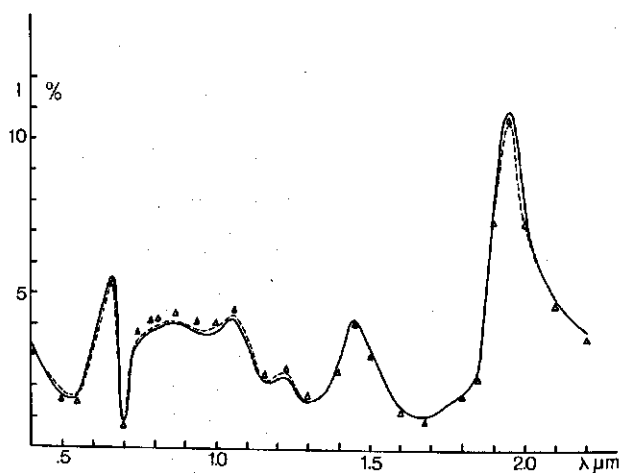


FIG. 52. Information distribution for variation in  $L$  and for a dark soil and different average leaf angles.

$\theta_L = 30^\circ$ : —,  $\theta_L = 60^\circ$ : ---.

FIG. 53. Information distribution for two different variations in  $L$ .

$L = 1, \dots, 16$ : —,  $L = 3, \dots, 8$ : ---.

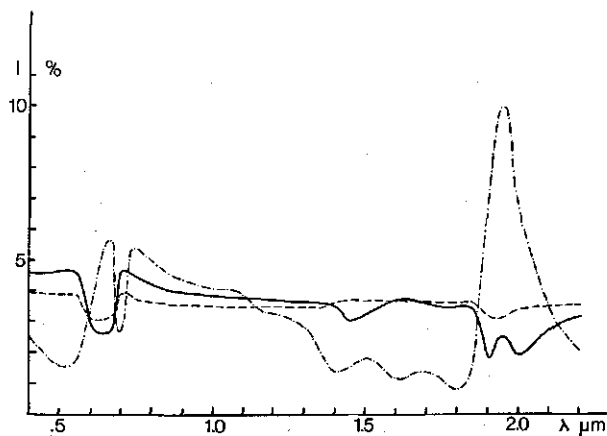
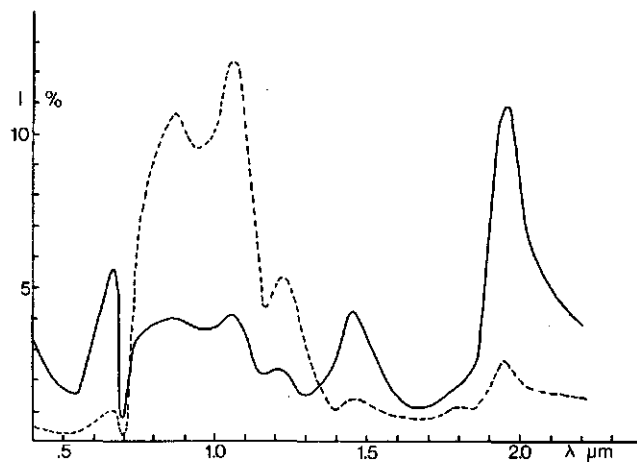
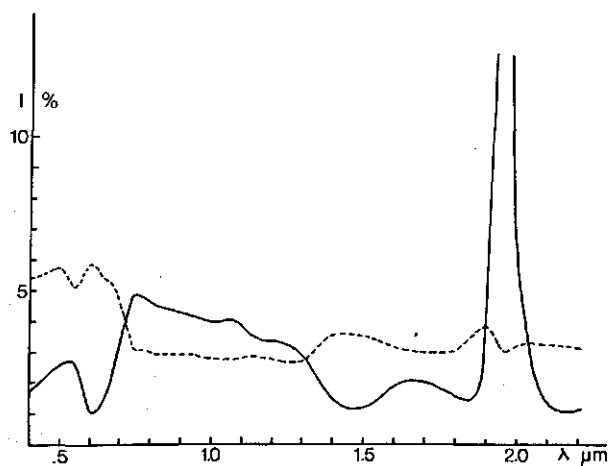


FIG. 54. Information distribution for variation in the average leaf angle,  $\theta_L$ , with different  $L$  and soil moisture,  $Q$ .

$(L = 3, Q = 1)$ : —,  $(L = 3, Q = 6)$ : ---,  $(L = 1, Q = 1)$ : - · - · -.

FIG. 55. Information distribution for variation in the average leaf angle,  $\theta_L$ , with perpendicular and oblique view angle.  $\theta_o = 0^\circ$ : —,  $\theta_o = 45^\circ$ ,  $\psi = 90^\circ$ : ---,  $Q = 1$ ,  $\theta_s = 30^\circ$ : - · - · -.



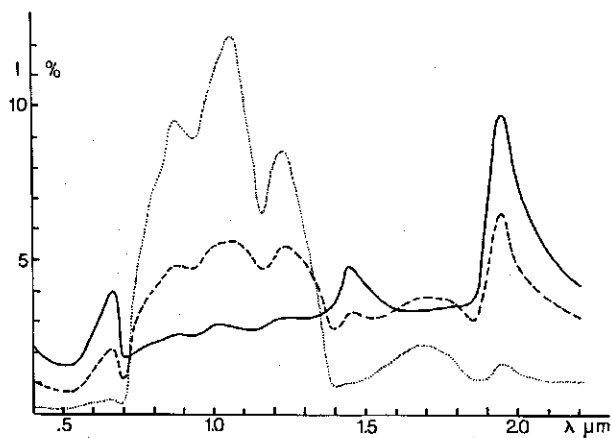


FIG. 56. Information distribution for varying soil moisture with different canopy structures.

( $L=2, \theta_L=60^\circ$ ): —  
 ( $L=3, \theta_L=45^\circ$ ): ---  
 ( $L=5, \theta_L=45^\circ$ ): .....

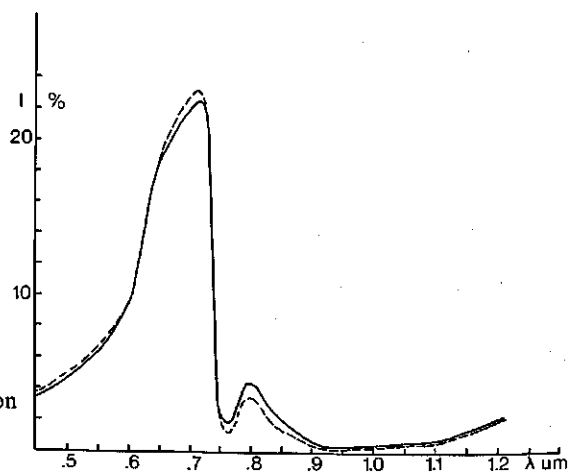


FIG. 57. Information distribution for variation in leaf senescence.  
 $Q=1$ : —,  $Q=6$ : ---.

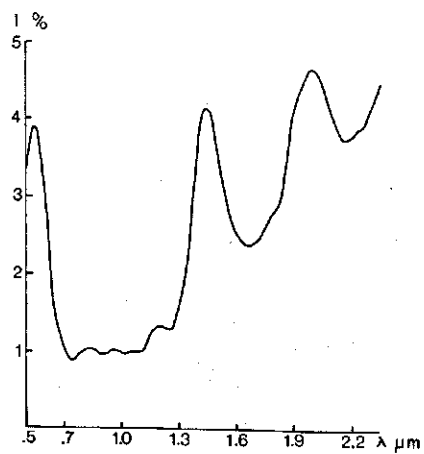


FIG. 58. Information distribution for variation in green leaf type. These spectra are calculated for diffuse irradiance; the canopy is supposed to be infinitely thick with horizontal leaves only.

leaf canopy reflectance,  $r_c(0)$ , is proportional to canopy reflectance itself.

Fig. 59 shows some examples of information distributions for measured field data. These data have been collected during one growth cycle of grasses and potatoes. The distributions for grasses correspond quite well with the simulation given in Fig. 50. The relatively highest contribution at 670, 1450 and 1960 nm for coach grass is caused by the relatively lower plant cover. The different function as measured in potatoes is caused by the high leaf area index values which were measured. The distributions given in Fig. 53 include a function which approximates the measured distribution of potatoes.

b. The influence of the solar zenith angle on the information distribution with varying leaf area index is not significant, see Fig. 51. This also applies to the effect of varying view angles, since even at  $\theta_o = 45^\circ$ , the apparent plant cover varies sufficiently to maintain information maxima at 670, 1450 and 1950 nm. These wavelengths correspond with maximum leaf absorptance caused by chlorophyll and water, see Fig. 13.

c. Information concerning leaf area index variation at an average high *LAI* value is mainly present in the near infrared plateau, see Fig. 53.

d. Variation in average leaf angle results in more uniform distribution of information. In this situation minimum values are found at 670, 1450 and 1950 nm, whereas at higher *LAI* the minimum value at 700 nm converges into a maximum.

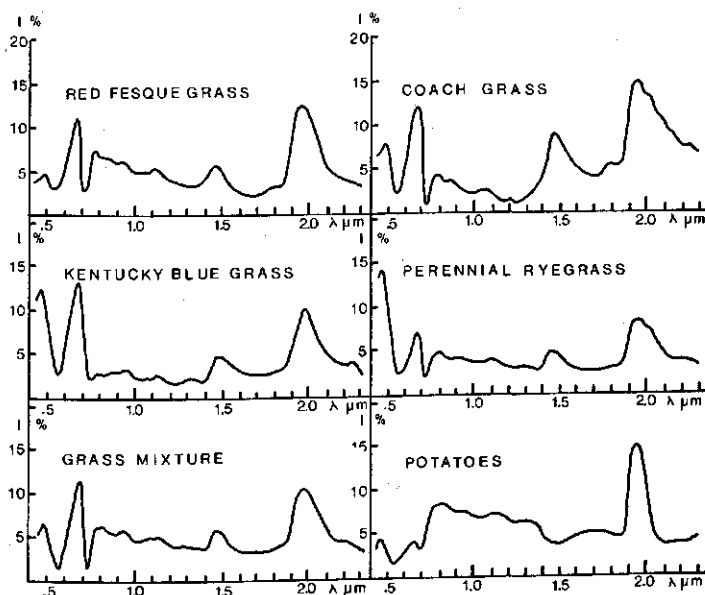


FIG. 59. Information distributions for grasses and potatoes as measured at Wageningen, summer 1973.

If the leaf angle variation is extended to the presence of vertical components only, the maximum at 550 nm will be more distinct and at 1950 nm the information increases drastically (Fig. 54 and 55). The information moves to the visible light region, when leaf angle variation with a constantly high leaf area index ( $L = 3$ ) is measured under oblique view.

e. As could be expected, the information about soil reflectance variation moves from the wavelengths with maximum leaf absorptance to the infrared plateau (Fig. 56).

f. The widest variation in leaf reflectance and transmittance at senescence occurs in the red part of the spectrum. Loss of absorbing chlorophyll leads to increasing reflectance as well as transmittance. The variation in the red is wider compared with the blue part of the visible light, because of the presence of other absorbing pigments, BUNNIK and VERHOEF (1974), see Fig. 7. The diffuse reflectance hypothesis of SINCLAIR (1973) predicts an increase in reflectance and a decrease in transmittance of dehydrated leaves in the near infrared, when the internal mesophyll structure collapses.

This results in a maximum information about leaf yellowing in the visible light region at 670 nm (see Fig. 57). The near infrared plateau hardly contributes, if a constant canopy structure is assumed. However, this is not the case in practice, because leaf senescence leads to falling leaves which implies a changing canopy structure.

g. If a variation only in green leaf type is assumed, maximum information is found at 550 nm and at the wavelength with maximum water absorptance, see Fig. 58. Variation in the infrared plateau is low compared with the visible light region.

It can be concluded that a unique combination of spectral bands for detecting varying plant canopy parameters does not exist, because such a set of different wavelengths depends on the variations usually occurring. For remote sensing applications, the atmospheric windows restrict the selection of spectral bands, as already shown in paragraph 2.1, Fig. 2. Within the available atmospheric windows, wavelengths which contribute maximum information are: 400, 550, 670, 730, 870, 1060, 1230, 1650 and 2200 nm.

Taking into account the correlations of the reflectance values at these wavelengths, a selection can be made of three spectral bands at 550, 670 and 870 nm. This selection is based on optimum information on the relevant crop parameter variation and on the performance of available solid state detectors like the widely used silicon photodiodes which are sensitive between 400 and 1100 nm.

For detection of variations due to water absorptance, these three spectral bands can be completed with one or two spectral bands in the water absorption region at 1650 and 2200 nm, respectively, applying infrared detectors. Besides the wavelength, attention will be paid to the bandwidth required, which is related to the detected radiant power and the spectral resolution.



### 3.4. RELATIONS BETWEEN SPECTRAL BANDWIDTH, VARIANCE AND COVARIANCE OF MULTISPECTRAL REFLECTANCE DATA IN THE VISIBLE LIGHT AND THE NEAR INFRARED DUE TO CROP PARAMETER VARIATIONS

In collecting remotely sensed multispectral data by means of electro-optical sensors, important factors are the spectral sensitivity, spectral detectivity, ground element observation time, spatial resolution on ground level and spectral bandwidth in relation to the desired spectral resolution and the signal to noise ratio of the sensors.

In the previous sections attention has been paid to the distribution of information in the spectral region including the visible light and the near reflectance infrared. The definition of information was based on the observed variance in the reflectance of canopies with variable crop and soil properties. It was concluded that most of the information distribution functions have some maxima within a small spectral bandwidth, like the frequently occurring maximum at 670 nm which is near an information minimum at 715 nm. The spectral bandwidth of sensors detecting at centre wavelength values, like the green, the red and the near infrared plateau has an important influence on the measured signal variance and the covariance. Otherwise, as mentioned before, a minimum bandwidth is required to obtain a sufficient signal to noise ratio in operations under practical conditions.

In this section, some relations between detected variance, covariance and the signal to noise ratio are considered.

Fig. 60 presents in a schematic way, the geometrical quantities of an electro-optical remote sensor. The spectral radiant power,  $P$ , entering the detector is determined by the instantaneous view angle,  $\omega$ , the aperture of the optical system,  $A_c$ , the intrinsic spectral radiance at groundlevel,  $L_I(\lambda)$ , the atmospheric transmittance and path radiance and the transmittance,  $\tau_o(\lambda)$ , of the optical system.

$$P(\lambda) = \omega^2 A_c \tau_o(\lambda) (L_I(\lambda) T(\lambda) + L_p(\lambda)) \quad (3.22.)$$

The signal to noise ratio in a given spectral band with bandwidth,  $(\lambda_2 - \lambda_1)$ , is determined by integration of the ratio of the radiant power,  $P(\lambda)$ , and the noise equivalent power,  $NEP(\lambda)$ , of the detector. This noise equivalent power of a detector corresponds with the output signal by absence of incoming radiant power. The  $S/N$  ratio determines the minimum detection level.

$$S/N = \int_{\lambda_1}^{\lambda_2} (NEP(\lambda))^{-1} P(\lambda) d\lambda \quad (3.23.)$$

The relation between the noise equivalent power, the signal observation time which is inversely proportional to the bandwidth,  $\Delta\nu$ , of the electronic system and the spectral detectivity,  $D^*$ , of the detector, is given by:

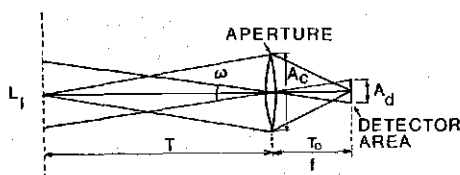


FIG. 60. Geometrical properties of an electro-optical remote sensor.

$$NEP(\lambda) = f\omega\Delta v^{1/2}D^*(\lambda)^{-1} \quad (3.24.)$$

$f$  = focal length of the collecting lens.

Combination of (3.22.) and (3.24.) gives with (3.23.) the following expression for  $S/N$ :

$$S/N \approx \frac{\omega A_c \tau_o}{f \Delta v^{1/2}} \int_{\lambda_1}^{\lambda_2} D^*(\lambda) \left\{ \frac{\rho(\lambda)}{\pi} E_i(\lambda) T(\lambda) + L_p(\lambda) \right\} d\lambda \quad (3.25.)$$

It is assumed that the system transmittance,  $\tau_o$ , is constant throughout the bandwidth.

The signal to noise ratio,  $S/N$ , increases with the bandwidth, the detectivity, the ground reflectance and the irradiance level. The detectivity,  $D^*(\lambda)$ , of silicon photodiodes is on a logarithmic scale proportional to the increasing wavelength between 400 and 950 nm.

If a small bandwidth is desired for feature discrimination of optimum variance detection, this causes a loss of detected power leading to a decreased signal to noise ratio. By using criteria for the permitted bandwidth for the detection of canopy property variations, the signal to noise ratio could be maximized or the instantaneous view angle could be made smaller to increase the spatial resolution at groundlevel.

To find some useful indications to determine criteria for maximum bandwidth values in relation to the detection of crop variety, model calculations have been carried out to investigate the variance and covariance in the green, the red and the near infrared as a function of increasing bandwidth. Analyses have been performed for varying leaf area index, varying average leaf angle, soil moisture content and the level of leaf yellowing. Results referring to varying leaf area indices and leaf angles are given.

Fig. 61 gives the covariance in 14 wavelength values in the interval between 400 and 1160 nm as a function of wavelength with varying  $L$  only. All the data have been calculated with transformed reflectance values according to equation (3.6.) All the wavelengths in the visible light region show a positive covariance with a minimum at 550 nm and a maximum in the red. All the covariances with wavelengths in the near infrared are negative. If the leaf angle only is varied, all the covariances at 550 nm are small but positive, see Fig. 62.

Experimental data resulting from fieldspectrometer measurements are given in Fig. 63. These data have been calculated for green canopies and with transformed reflectance values. The behaviour corresponds well with the theoretical

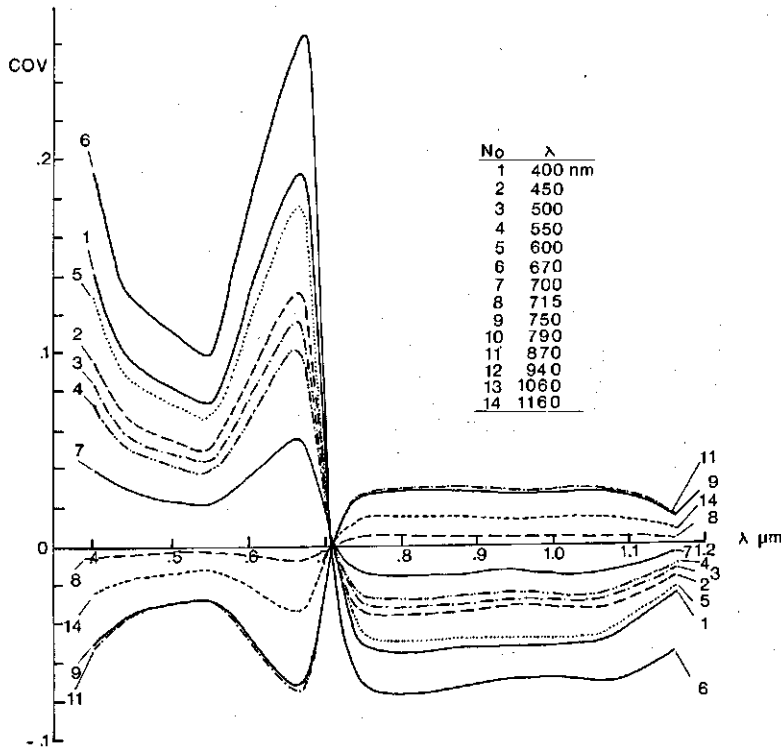


FIG. 61. Calculated covariance as a function of wavelength in transformed reflectance data caused by varying leaf area index.

$\theta_s = 30^\circ$ ,  $\theta_o = 0^\circ$

Leaf type: wheat

Soil type: dry sandy loam.

$L = 0.25, 0.5, 1, 1.5, 2, 2.5, 3, 3.5, 4, 4.5, 6, 10$

$\theta_L = 57.52^\circ$ .

predictions, however, they are based on simplified canopy variations compared with field conditions.

Multispectral scanner data collected from training areas have been used in calculating the covariance matrix of the transformed data in the nine recorded spectral bands. These data have been collected on a testfarm in Eastern Flevoland in July 1975 and refer to potatoes, sugar beets, bare soil and cereals in a maturing stage. The covariance of channels in the green (4), the red (7) and the near infrared (9) is presented in Fig. 64. The trend in these curves corresponds with the model predictions for leaf area index variation.

To calculate the variance and covariance as a function of increasing bandwidth, covariances have been calculated between 480 and 920 nm for a spectral resolution of 10 nm. It is assumed that the bandwidth of the green, the red and the near infrared increases proportionally to both sides of the centre wavelengths at 550, 670 and 870 nm with steps of 10 nm. The variance and covariance

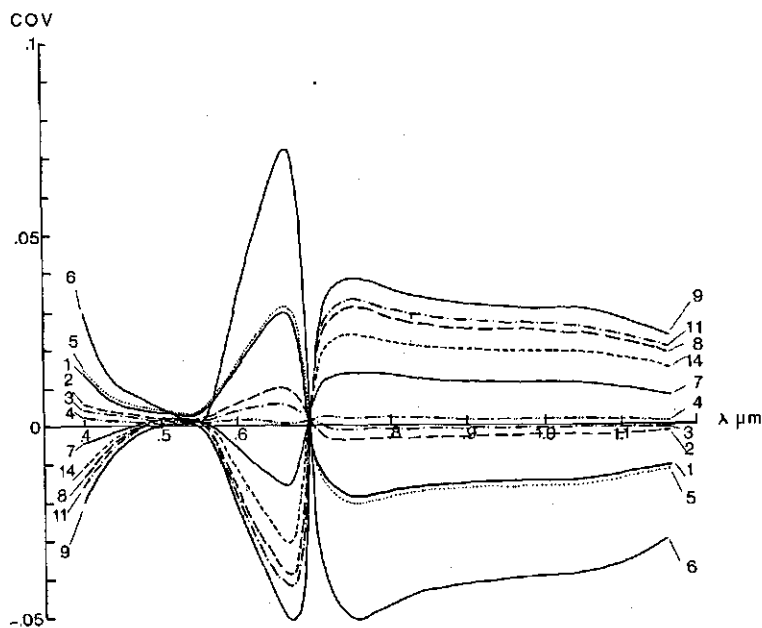


FIG. 62. Calculated covariance as a function of wavelength in transformed reflectance data caused by varying leaf inclination angles.

$\theta_s = 30^\circ$ ,  $\theta_o = 0^\circ$ .

Leaf type: wheat

Soil type: dry sandy loam.

$\theta_L = 0^\circ, 30^\circ, 45^\circ, 57.52^\circ, 75^\circ$

$L = 1$

FIG. 64. Covariance in the green (band 4), the red (band 7) and the near infrared (band 9) as a function of wavelength in transformed MSS-data. Eastern Flevoland - Testfarm - 30 July 1975.

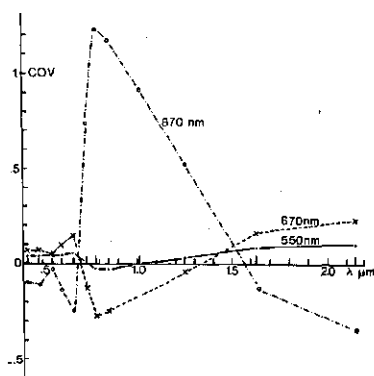
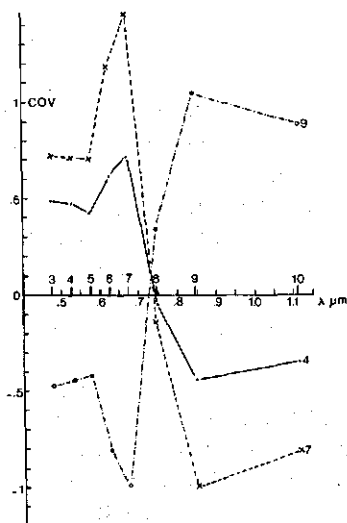


FIG. 63. Covariance in the green, the red and the near infrared of transformed field reflectance data as a function of wavelength. Wageningen, summer 1974.



of wide bands are found from variance and covariance values of the incremental bands. This is proved with the assumption of average equal response in each band.

If  $N$  features are measured in a spectral band with centre wavelength,  $\lambda_i$  and a width of  $2l\Delta\lambda$  and assuming  $l$  increments in both directions, the variance,  $\sigma^2(\bar{S}_i)$ , of the average response,  $\bar{S}_i$ , is given by:

$$\sigma^2(\bar{S}_i) = \frac{1}{N} \sum_{j=1}^N (\bar{S}_i(j) - \bar{S}_i)^2 \quad (3.26.a.)$$

$$\bar{S}_i = \frac{1}{N} \sum_{j=1}^N \bar{S}_i(j) \quad (3.26.b.)$$

The band response,  $\bar{S}_i(j)$ , for signal,  $j$ , is approximated by numerical integration into the  $2l$  wavelength increments.

$$\bar{S}_i(j) = \frac{1}{2l} \sum_{n=-l}^{n=l-1} S_i(j, n) \quad (3.27.)$$

Substitution of (3.27.) in (3.26.) gives for  $\sigma^2(\bar{S}_i)$

$$\sigma^2(\bar{S}_i) = \frac{1}{4l^2} \left\{ \sum_{n=-l}^{n=l-1} \sigma^2(S_i(n)) + 2 \sum_{\substack{n'=-l \\ n' \neq n}}^{l-1} \sum_{\substack{n=-l \\ n < n}}^{l-1} \sigma(S_i(n'), S_i(n)) \right\} \quad (3.28.)$$

$\sigma(S_i(n'), S_i(n))$ : covariance between  $n'$ ,  $n$ .

The covariance between spectral bands with bandwidth,  $2l\Delta\lambda$  and  $2m\Delta\lambda$  is found in the same way and presented by the equation (3.29.)

$$\sigma(\bar{S}_i, \bar{S}_k) = \frac{1}{4lm} \sum_{n'=-l}^{l-1} \sum_{n=-m}^{m-1} \sigma(S_i(n'), S_k(n)) \quad (3.29.)$$

The results for a maximum bandwidth of 100 nm of the variation in the average variance, are given in Fig. 65. Fig. 66 presents the correlation coefficient. The variance in reflectance in the green slowly increases when bandwidth exceeds 60 nm both with  $L$  and  $\theta_L$  variation. This is caused by the increased detection of spectral reflectance into the directions of greater soil-leaf contrast. The correlation between the green and the red remains close and constant with increasing bandwidth. This seems surprising, but is explained by the behaviour of varying canopies, as presented in Fig. 85 in chapter 5. Variation in leaf angle only leads to very low correlations with a small leaf area index. It is remarked that this also depends on the soil-leaf contrast. This low correlation was found. Fig. 66 shows that a minimum is attained with a bandwidth of 20 nm, whereas with further increase in both bandwidths the correlation increases rapidly.

The variance in the red is both with varying  $L$  and  $\theta_L$  a decreasing function of the bandwidth. The correlation between the red and the near infrared with leaf angle variations is higher than with leaf area index variations, but the magnitude is not greatly affected by the bandwidth.

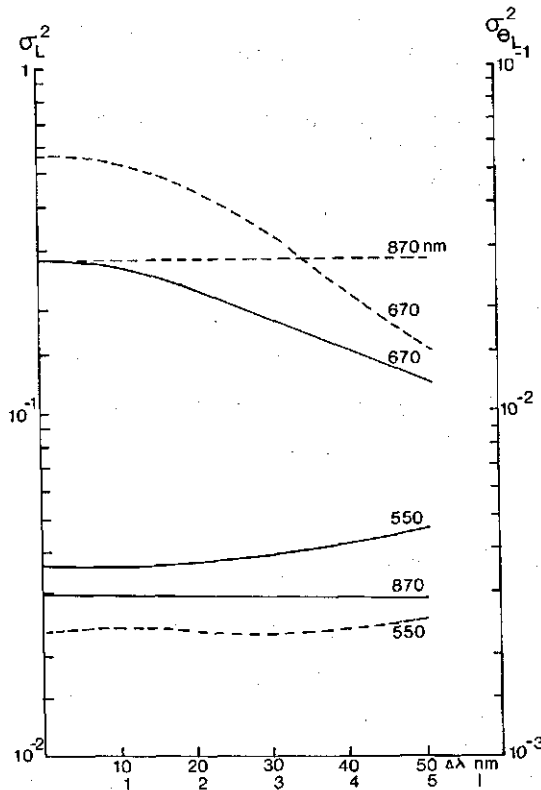


FIG. 65. Changing variance as a function of increasing bandwidth in the green, the red and the near infrared.

—: variance caused by varying  $L$  ( $\theta_L = 57.52^\circ$ )

---: variance caused by varying  $\theta_L$  ( $L = 1$ )

$\theta_s = 30^\circ$ ,  $\theta_o = 0^\circ$

Leaf type: wheat

Soil type: dry sandy loam.

Finally, it is observed that the variance in the near infrared is almost insensitive to the chosen bandwidth.

If the relative decrease in variance at 670 nm may not exceed 5%, a bandwidth of 20 nm in the red is required. The correlation between the red and the infrared due to leaf angle variations should decrease in this case. The bandwidth in the near infrared may be larger, because of the rather uniform optical constants of green leaves in this wavelength region.

It is concluded that the bandwidth in the red has to be chosen small. The resulting  $S/N$  ratio at varying bandwidth determines the compromise between the required width of 20 nm and the noise level in the red caused by the generally low intrinsic radiance in green canopies. The bandwidth in the green can be equal to that in the red. In the infrared a larger width can be specified, e.g. 100 nm, provided that the water absorption band at 940 nm (see Fig. 2),

is excluded. Such a larger bandwidth is also advantageous, because of the lower spectral irradiant power in the near infrared.

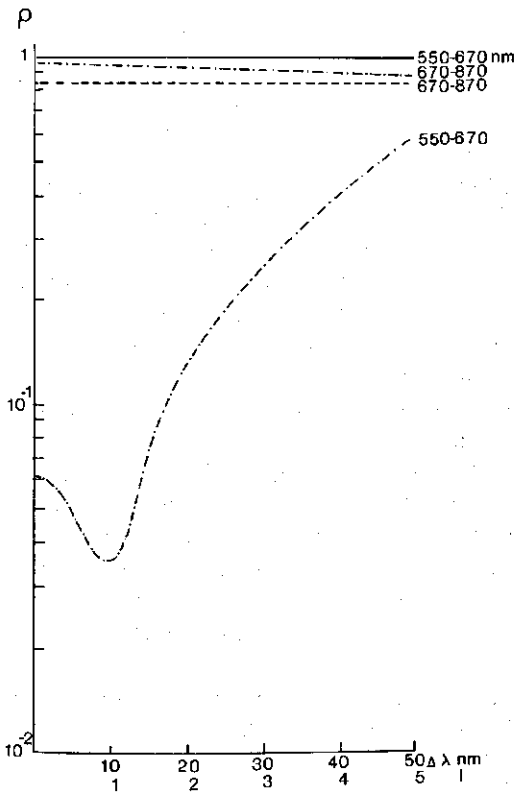


FIG. 66. Changing correlations in the green and in the red and the near infrared, as a function of increasing bandwidth.

-----: correlation caused by varying  $L$  ( $\theta_L = 57.52^\circ$ )

- · - · -: correlation caused by varying  $\theta_L$  ( $L = 1$ )

$\theta_s = 30^\circ$ ,  $\theta_o = 0^\circ$ .

Leaf type: wheat

Soil type: dry sandy loam.

## 4. MEASUREMENTS OF CANOPY REFLECTANCE DATA

### 4.1. CANOPY REFLECTANCE MEASUREMENTS ON THE TEST SITE AT WAGENINGEN

A field measurement program was started in July 1973, for the purpose of collecting crop spectral reflectance data in situ over a long period of the growing season. These spectra were collected with a reflectance spectrometer, specially designed for this purpose. With this spectrometer the measured field target reflectance can be sampled in 153 points within a wavelength interval from 361 nm at the end of the ultraviolet region to 2360 nm in the reflectance infrared. The radiant intensity of the resolution element of an object, observed by the spectrometer is measured relative to the intensity of a standard reflector exposed to the same irradiance as the object. Signal fluctuations due to varying irradiance are eliminated by a comparative method. Details concerning the spectrometer used are described in section 4.2.

In chapter 2, sections 4.5. and 4.6. it has been shown that the apparent canopy reflectance in situ depends on many variables, like observation direction, solar angle, the azimuth angle between sun and position of the observer, weather conditions and actual crop properties. For a number of reasons, a measurement method was applied to standardize the data collection procedure to obtain data which could be compared with each other independent of varying view angle and with or without direct solar flux.

Measurements performed during a long period of several months or at different moments of the daily cycle are influenced by the occurrence of days with a relatively low cloud cover or days with an overcast sky. These climatological influences may vary rather widely in the Netherlands. To overcome these

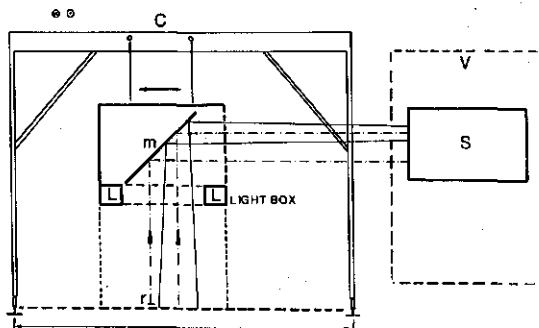


FIG. 67. Measurement of canopy reflectance under standardized conditions. The spectrometer, S, placed inside van, V, looks through mirror, m, at the canopy and the standard reflector, r. Both canopy and standard reflector are artificially illuminated by the lamps and TL-tubes at L.

The light box is moved along the test fields by means of the carrier, C.



difficulties and to ensure a great number of crop reflectance data throughout a growing period, an artificial illumination method was used, while crop reflectance was only measured under perpendicular view angle.

A light box containing four wide-flood bulbblamps and eight TL-tubes mounted on the four sides of the open part at the under side of the box provided the canopy top with a sufficiently homogeneous irradiant flux. To prevent incoming direct solar or diffuse sky flux on the canopy volume under the light box, a movable square screen mounted around the lamp house was lowered into the canopy. A motor driven mirror, oriented under a mean inclination of  $45^\circ$ , mounted inside the box above the lamp house was used to observe the canopy and the standard reflector, was adjusted at the canopy top, under perpendicular view.

The spectrometer was placed inside a van together with the control and data registration units. The light box could be adjusted in vertical direction to maintain a constant distance between the light source and the canopy. The box was moved along the test fields by way of a special carrier placed on rails at both sides of the fields. A simplified scheme of the measurement set up is presented in Fig. 67.

In spite of the advantage of constant illumination throughout the measurement campaign, a serious drawback of such a light source occurred, when cereals attained a high canopy height at the maturing stage. The vertical movement of the light box was limited and this brought about unequal irradiation of the canopy and the standard reflector, when this standard was placed near the underside of the box at the level of the canopy top.

Other problems were encountered with the light screen, when it was introduced into the lower layers of high crops. Besides this method of artificial illumination, measurements were performed with solar illumination on a wheat canopy and a grass canopy to collect data for different view angles and solar angles. These measurements have been used in investigating non-Lambertian directional reflectance at different stages of crop growth. These data were not used in this manuscript. The results were reported in BUNNIK and VERHOEF (1974) and VERHOEF and BUNNIK (1976).

The test field prepared for 1973, used for measurements with the light box, consisted of eleven plots of  $6 \times 6$  m each. The sandy loam soil was carefully homogenized. Monocultures, representative of agricultural crops in the Netherlands were cultivated. The crop types are given in Table 4. Based on experience obtained during the first year, it was decided to repeat a similar program in 1974. The same light box with carrier on rails and provided with an improved light screen was used. The strip with test plots was set out in another area to avoid soil differences caused by cultivation of the test plots in 1973. For practical reasons, the size of the test plots in the new strip was enlarged to  $6 \times 10$  m and 11 different crops were chosen. Instead of beans, one test plot was sown with alfalfa to take advantage of the three growth cycles possible during the summer season. Due to the failure of obtaining a sufficiently homogeneous coach grass canopy, this plot was used to seed a second barley and a second

TABLE 4. Crop types of the 1973-test area used for spectral reflectance measurements.

Plot no.	Crop type
1	Red Fescue (grass) ( <i>Festuca rubra</i> )
2	Coach grass ( <i>Elytrichia repens</i> )
3	Kentucky Blue grass ( <i>Poa pratensis</i> )
4	Perennial ryegrass ( <i>Lolium perenne</i> )
5	Mixture of Lp, Pp and Fr
6	Potatoes
7	Sugarbeets
8	Beans
9	Barley
10	Oats
11	Wheat

TABLE 5. Crop types of the 1974-test area used for spectral reflectance measurements.

Plot no.	Crop type
1	Orchard grass ( <i>Dactylis glomerata</i> )
2	Creeping bent grass ( <i>Agrostis stolonifera</i> )
3	Perennial ryegrass
4	Maize
	Barley
5	Alfalfa
6	Potatoes
7	Sugarbeets
8	Barley
9	Oats
10	Wheat

maize plot.

The crops cultivated during 1974, are summarized in Table 5.

#### 4.2. DESCRIPTION OF THE FIELD SPECTROMETER

The principle of the field spectrometer used, designed and constructed by the Laboratories of the Institute of Applied Physics TNO, Delft, is based on the simultaneous measurement of the radiant intensity of a standard reflector and the object. Fluctuations in the irradiant flux impinging on reference and object are eliminated by taking the ratio of the output signals corresponding with both intensity values. Referring to the phenomenon of varying shadow inside a plant canopy in relation with the ratio of diffuse sky irradiance and the direct solar flux, it is remarked here that compensation for irradiance fluctuations is only valid for flat reflectors. However, first order effects due to varying irradiance are eliminated and the measured field reflectance is standardized to the known reflectance of the used reference.

Using expression (2.66.), the radiant intensity of object and reference entering the spectrometer can be written as:

$$I(\theta_o, \phi_o, \lambda) = \cos \theta_o \int_A dx dy \int_{2\pi} \rho'(\theta_o, \phi_o, \theta_i, \phi_i; x, y, \lambda) * L_i(\theta_i, \phi_i) \cos \theta_i d\omega_i \quad (4.1.)$$

The intensity is measured from direction,  $(\theta_o, \phi_o)$  and is due to the reflected power from area,  $A$ , with local coordinates,  $(x, y)$ , seen by the view angle of the instrument. It is assumed that the bidirectional reflection coefficient depends on the direction of view, the direction,  $(\theta_i, \phi_i)$ , of the incoming radiance,  $L_i(\theta_i, \phi_i)$ , the coordinates of the radiating surface and the wavelength.

With dominating diffuse reflection, the general expression for radiant intensity may be given by the introduction of the product of total irradiance and directional reflectance. From (4.1.) it can be derived that the directional reflectance,  $r_L$ , of a Lambertian surface is equal to total absolute reflectance,  $R_L$ . If a comparative measurement with a Lambertian reflector is performed, the ratio of the intensities from object and reference is given by:

$$q(\theta_o, \phi_o, \lambda) = r_o(\theta_o, \phi_o, \lambda)/R_L \quad (4.2.)$$

Adapting this concept, the main advantage of this requirement for the reference results from the direct relation between the directional properties of reflectance of the object and the measured ratio. Only a calibration for absolute reflectance of such a Lambertian reflector is sufficient in the laboratory and no directional reflectance properties of the standard have to be taken into account.

After some preliminary experiments it was found that Eastman Kodak White Reflectance Paint based on  $\text{BaSO}_4$  met the requirements for field use. With careful handling, it was shown that reflectance properties hardly changed during a whole measurement period and it appeared that also the near ultra-violet reflectance was satisfactorily constant.

Several reference panels, sprayed with the Kodak paint were used in the field. These panels were calibrated with a standard panel with known absolute reflectance, see Fig. 68.

A general description of the principle of the field spectrometer is given. A scheme of the optical system is presented in Fig. 69.

The beams of radiant flux coming from object and reference are focussed by two off-axis parabolic mirrors (1) and (2) inside an opto-mechanical beamsplitter (4). Introduction of an auxiliary parabolic mirror (3) into the object beam enlarges the field of view of the object beam. Due to the focal length of both equal parabolic mirrors 1 and 2 and a field stop, the field of view for object and reference is 5 mrad. Mirror (3) enlarges the object field of view to  $8^\circ \times 20^\circ$ . Both beams sequentially enter the rotating beamsplitter through two half circular splits. In the center of this cylindrical beamsplitter two half circular flat mirrors are mounted. They rotate in the same direction and reflect either

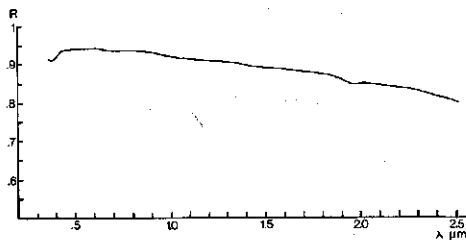


FIG. 68. Absolute hemispherical reflectance of the standard used. (Eastman Kodak White Reflectance Paint.)

the object beam or the reference beam to the focal plane which coincides with the cylinder radius. The focus is chopped by the rotating cylinder with square teeth on the edge of both splits. The sequency for object and reference beam is  $6 \frac{2}{3}$  Hz, the chopper frequency is 400 Hz. The light beams are modulated to provide the fotodetectors and the preamplifiers with an AC signal. When both beams leave the chopping and beam splitting system sequentially, they are collimated by the parabolic mirror (5) which provides the reflecting diffraction grating (6) with a parallel incoming beam. A special off-mounting of the grating according to WERNER (1970) is applied to optimize the grating efficiency for higher order spectra. In this case, the incoming beam is almost in the plane parallel to the blazed groves.

Due to this special mounting, the reflected spectra of first and higher order almost coincide. The dispersed paralalled beams are reflected by a flat mirror perpendicular to the grating plane and focussed by parabolic mirror (7) on the front of a spectral order splitter (8). Three round diaphragms split the overlapping spectra into three beams containing lines of the first, second and third

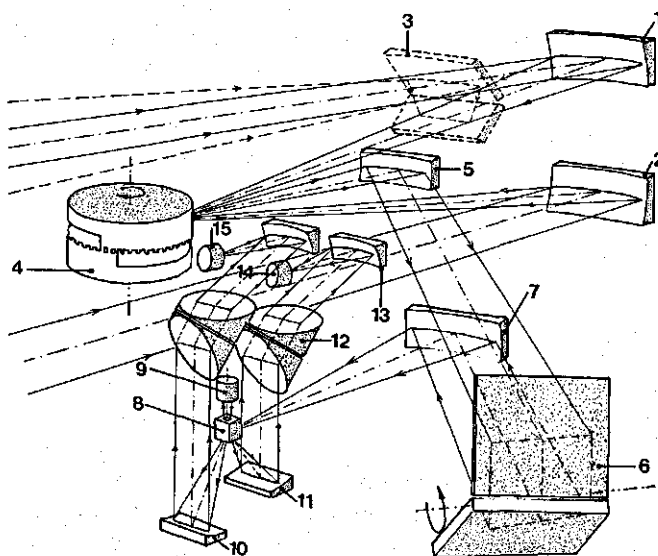


FIG. 69. Optical system of the field spectrometer.

order spectrum, respectively. Inside section (8) three differently oriented small flat mirrors reflect the incident beams into three different directions. The beam centred around the first order spectral lines is filtered by a high pass filter to avoid detection of lines of the second order spectrum. This filter has a cut off wavelength at 1150 nm. Detector (9) behind this filter is a PbS detector used in measuring the radiant intensity in the first order spectrum in the reflectance infrared between 1165 and 2360 nm.

Since the amount of solar energy available is relatively small in this wavelength region compared with the visible light region, see Fig. 2, the high efficiency of the first order diffraction spectrum of the grating is used in the measurement in the large wavelength region by a PbS detector at outdoor temperature within the required range of the signal to noise ratio.

The lines of the second order spectrum overlapped by a part of the first and the third order spectrum are present in a second beam, reflected downwards and collimated by a parabolic mirror (11).

To detect second order lines only, the parallel beam needs a higher dispersion which is realized by a prism (12). Finally, parabolic mirror (13) focusses second order lines on the aperture of a Si detector (14). An identical system is used in providing a second Si detector (15) with third order wavelengths.

In the second order spectrum, wavelengths are measured between 629 and 1226 nm. The third order spectrum, available with a high diffraction efficiency due to the off-axis mounting of the grating, is used in detecting within the visible wavelength region beginning at 361 nm in the far ultraviolet and ending at 753 nm in the near infrared.

A scan through the whole spectrum is obtained by moving the grating over 51 discrete positions. This is realized by a controlled stepping motor driving the grating by way of a specially designed curved disk. Because all 51 wavelength bands must be detected by both Si detectors, in the second and third order spectra respectively, the two prisms have a variable deviation angle. This is realized by varying the top angle of the prisms. Both prisms are partitioned in two equal parts which rotate around the same axis, but in opposite directions. The rotation mechanisms are directly coupled by way of another curved disk with the same stepping motor.

The total scantime can be varied between 1 and 128 min. The signal produced by the three photodiodes consists of 30 periods of the sequentially modulated signals from either the object or the reference. The rotation frequency of the feed-back system chopping cylinder is controlled by a feed-back system using a fixed oscillator frequency of 400 Hz. The signal of this oscillator is multiplied with the signal. The phase of both detector signal and oscillator signal is equalized. A positive signal with a 800 Hz frequency is obtained for object and reference. After common amplification, the signals corresponding with reference and object are split, ratioed and displayed. The common amplification is adjusted automatically by measuring the power of the signal belonging to the radiant intensity of the reference. The amplification is increased or decreased with steps of 10 dB. The total range is 70 dB. The scale

value of the reflectance ratio is also adjusted automatically between full scale values of 100, 30, 10 and 3% relative reflectance.

A three channel analog recorder for displaying the ratio signals of the three wavelength intervals is used as quick look facility. The output signals of the spectrometer are stored on magnetic tape after digitization by a specially designed datalogging system. Auxiliary library data are added before and after each data block belonging to one scan of the spectrometer. A computer program has been used to convert the spectrometer data on cassette tape to a computer compatible format. For all 153 spectral channels a correction factor has been determined. This correction is applied to the ratio between object and reference signal to obtain the directional reflectance of the object only. The correction factor contains the absolute hemispherical reflectance of the standard reflectors used and an equalizing factor to compensate systematic differences between the output of the object and the reference optics and signal processing sections.

A reflectance spectrum is determined after correction of the object-reference ratio and by means of a wavelength calibration of the three spectral intervals for all the grating positions. The final result is stored on magnetic tape for further processing. A hard copy of each spectrum presented by a table and a plot print is made.

The accuracy specified is equal to 1% absolute relative reflectance for the whole spectral interval, assuming more than 50 W/m<sup>2</sup> total irradiance. If the stochastic and systematic errors are taken into account, the estimated absolute error comes to 5%. Some specifications of the field spectrometer are given in Table 6.

TABLE 6. Specifications of the spectral resolution of the field spectrometer.

Interval	Detector	Spectral order	Spectral range	Bandwidth
1	Si	3	361– 753 nm	17 nm
2	Si	2	629–1226 nm	25 nm
3	PbS	1	1165–2360 nm	42 nm

#### 4.3. MEASUREMENTS OF CROP PARAMETERS

During the field measurement campaigns in 1973 and 1974, several crop parameters were collected to study their relations with reflectance data. Mostly crop parameters directly affecting or closely related with crop reflectance were measured. In addition, hemispherical leaf reflectance and transmittance spectra determined with a Zeiss PMQ-II laboratory spectrometer with an integrating sphere and directional reflectance spectra of the bare soil measured with the field spectrometer in situ were collected incidentally.

Leaf area indices have been measured by taking each time two samples of  $\frac{1}{4}$  m<sup>2</sup> each of canopies with large leaves, like for instance potatoes and

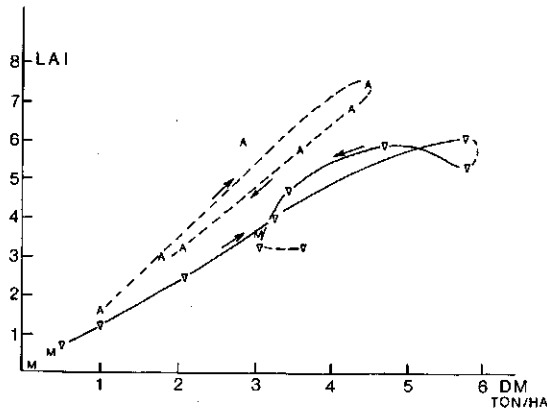


FIG. 70. Relation between dry biomass, (DM) and leaf area index, (LAI), for potatoes (A), sugarbeets (∇) and Maize (M), measured at Wageningen, summer 1974.

sugarbeets. Because of the difficulties associated to *LAI* determinations of grass canopies, only their biomass was measured. The dry biomass, (DM) and the percentage of moisture content was determined by drying the crop samples. The soil cover percentage was measured directly in the field by means of an optical sampling method and also afterwards using colour slides obtained by photographing the canopies into the nadir direction.

The in situ method makes use of a small telescope mounted on a movable horizontal carrier placed between two tripods. The telescope was looking vertically down to the canopy and could be moved over a distance of one meter along the carrier. By equidistant movement of the telescope it was decided for each position, if a canopy component or bare soil was observed in the

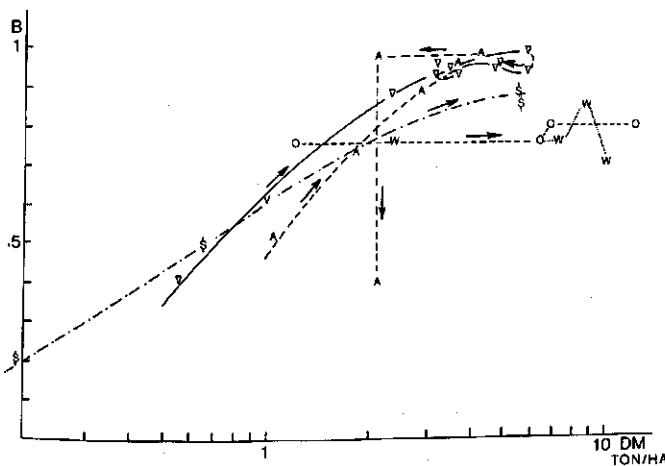


FIG. 71. Relation between dry biomass, (DM) and soil cover, (B), for potatoes (A), sugarbeets (∇), barley (\$), wheat (W) and oats (O), measured at Wageningen, summer 1974.

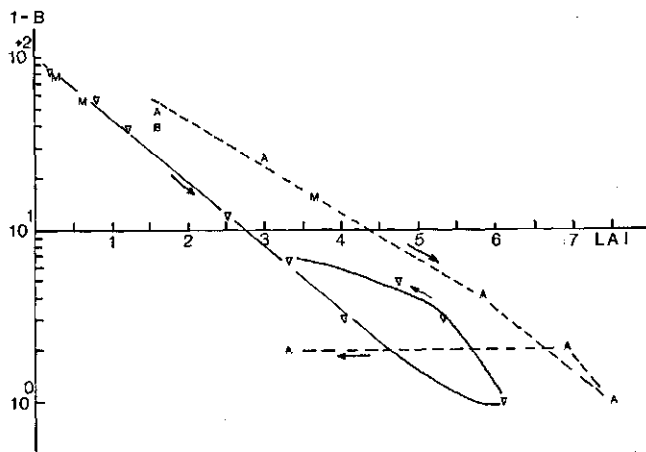


FIG. 72. Percentage of bare soil, ( $1-B$ ), as a function of leaf area index, ( $LAI$ ), for potatoes, beets and maize, measured at Wageningen, summer 1974.

the centre of the field of view. By repeating this procedure in different places an estimate of the soil cover percentage was attained. Diapositives were analysed in a similar way.

Each slide was projected on a grid consisting of 400 equidistant points. Only the central part of the image was selected to avoid the influence of oblique view caused by the wide view angle of the camera used. The actual soil cover percentage was estimated by counting the number of grid points coinciding with bare soil.

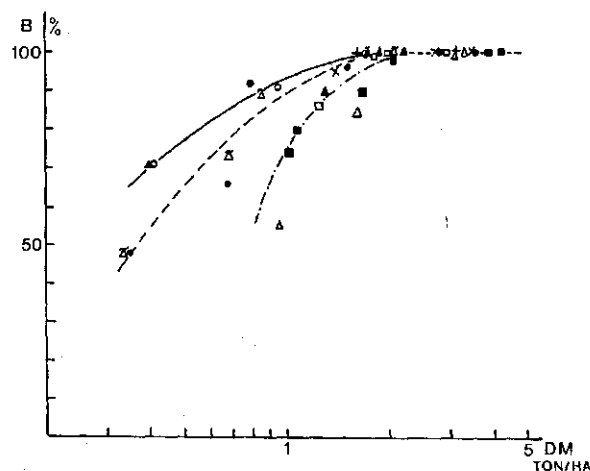


FIG. 73. Soil cover percentage, ( $B$ ), as a function of the dry biomass, ( $DM$ ), for pastures and alfalfa. Orchard grass (0:1,  $\bullet$ :2). Creeping bent grass ( $\times$ :1,  $+$ :2). Perennial ryegrass ( $\square$ :1,  $\blacksquare$ :2). Alfalfa ( $\Delta$ :1,  $\blacktriangle$ :2,  $\triangleleft$ :3).



Efforts with limited success were made to estimate some leaf angle distributions of canopies in situ. The distribution of the inclination of leaf elements were determined on calm days using a leaf graduator, DE WIT (1965). This instrument applied by NICHIPOROVICH (1961) consists of two parallel protractors connected by an axis through both centres. This axis can rotate only in a horizontal position. The rotation is caused by the moment resulting from the weight of two parallel pointers fixed on the axis. When the base of the graduator was placed parallel to a leaf element, the pointers indicated the actual leaf angle at both sides. After a sufficiently large number of random samples, a rather smooth distribution could be obtained.

Finally, examples are presented of relations between crop data as measured in 1974.

Fig. 70 gives the leaf area index as a function of the dry biomass for potatoes, sugarbeets and some data obtained on maize. Both the curves of potatoes and of sugarbeets affirm the assumption of a linear relation between total leaf area and corresponding biomass. At the end of the growing period, both curves reverted due to falling and shrinking of the leaves. This was especially so in potatoes, when *Phytophthora* occurred. The relation between soil cover percentage and dry mass of some field crops is presented in Fig. 71. Cereals with a more vertical leaf structure and mainly in rows did not attain complete soil cover. When the potato-test plot was infected by *Phytophthora*, the lower leaf layers shrank first which led to a decreasing biomass, whereas the upper layers still maintained a complete cover. Afterwards almost all green matter disappeared. The remaining biomass consisted of plant stalks and shrunken leaves.

For potatoes, sugarbeets and maize 100 minus soil cover percentage as a function of the *LAI* measured is presented in Fig. 72. The exponential relation between soil cover and *LAI*, as assumed by Suits, agrees satisfactorily with measurements between exponential growth and the stage of a well developed crop with complete soil cover percentage. Leaf shrinking and falling in the lower canopy layers no longer correspond with the assumption of a random distribution of canopy components in one homogeneous layer. This was especially so at the initial stage of the *Phytophthora* infection in the potato field.

The test plots with grass canopies and alfalfa were mown on 19 July and 20 August. Fig. 73 presents the soil cover percentage as a function of dry biomass for three growth cycles of alfalfa and two of the grasses after mowing. A wide spread between these functions is found due to crop type differences, variations in the leaf angle distribution during growth, a variable amount of visible dead biomass after mowing and the wide spread in the measured field data.

These examples of own field measurements and other data available from the literature demonstrate the mutual relations between the crop structure parameters, like leaf area index, soil cover and biomass. In the next chapter, relations between multispectral reflectance data and crop parameters are discussed. If the variation of one crop parameter during growth could be monitor-

ed by detection of reflectance data, correlations between crop data could be used in predicting the variation during growth of other crop parameters of agricultural interest.

#### 4.4. COLLECTION OF MULTISPECTRAL REFLECTANCE DATA AT REMOTE DISTANCE BY MEANS OF MSS

For reasons of completeness an introduction is given into the general principles of the technique used to collect multispectral reflectance data with remote sensors. For a more detailed review, reference is made to the Manual of Remote Sensing and a report prepared for ESRO by HIGHAM *et al.* (1972).

A multispectral scanner is a device used in measuring the radiance distribution of an observed scene in a number of spectral bands.

The position of the spectral bands may encompass the visible light region, the near reflectance infrared and the thermal infrared within the available atmospheric windows. The scene of the earth's surface is surveyed from a remote distance with an aeroplane or an orbiting satellite acting as platform.

Several techniques can be applied in collecting the electromagnetic radiation coming from ground level into the direction of the remote sensor, to separate the electromagnetic radiation into its spectral components and to convert the electromagnetic power into electrical signals.

Fig. 74 presents a simplified scheme of a linear multispectral scanner.

The resolution element on the ground is determined by the area of the field stop (3) imaged on the ground by the optical system. A system, usually applied in airborne scanners, consists of a rotating mirror (1) with a flat reflecting area under  $45^\circ$  with the optical axis and a Dall-Kirkham telescope (2).

The radiation is collimated by a lens (4) and dispersed in a spectrum by prism (5). A lens (6) focusses this spectrum on a detector array (7).

The number and position of spectral bands is specified by the images of the field stop (3) on the available detectors and the position of the array in the focal plane. By one rotation of the mirror (1) the beam is swept over the earth's surface within a total angle  $2\theta_{om}$  determined by an entrance slit present below the scanning mirror. During the same rotation, calibration values are measured from section (8). Internal calibration sources are provided by a black radiator

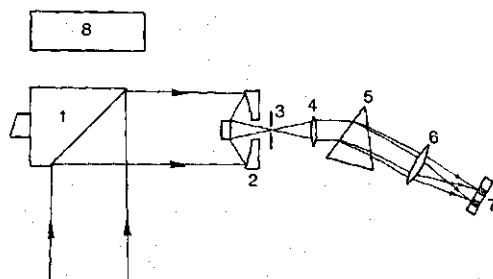


FIG. 74. Scheme of a linear multispectral scanner. The earth scene is scanned via a rotating mirror.

for zero level and a calibrated lamp to measure a reference radiance level.

By means of fiber optics, collecting radiance from a diffusor installed at the top of the platform, total irradiance at flight level can be sensed also. Through the forward movement of the platform, multispectral radiance values from the earth's surface are collected line by line. The electrical signals from the detectors are amplified and stored, together with auxiliary flight data, in analog or digital form on a magnetic tape. When a satellite is used as a platform a transmission system to provide ground stations with data is applied.

Due to the forward movement and rotation velocity of the scanning mirror systematic distortions of the image obtained are introduced.

Finally, some attention is paid to the limitations with respect to scanner and detector performance. The resolving power of MSS in terms of spectral and intensity resolution is limited by the noise level. In section 3.4. equations presenting signal to noise ratio have been introduced to qualify the influence of spectral bandwidth. The scanning technique produces signals of varying frequency caused by spatial variations on the ground scene. For correct data recording a sufficiently high response time of the detectors used and a minimum bandwidth of pre-amplifiers and amplifiers is required.

Fig. 75 shows a scanner at height,  $h$ , with instantaneous view angle,  $\omega$ , scanning the earth's surface between scan angles,  $-\theta_{om}$  and  $\theta_{om}$ . The rotating frequency of the scan mirror is  $\omega'$ , the platform velocity is  $v$ . It is assumed that adjacent scan lines do not overlap.

Signal variation is directly related to the spatial resolution of the scanner. The dwell time,  $t_D$ , of a detector corresponds with the time for a point on a scan line passing through the instantaneous field of view. The sampling theorem of Shannon gives a direct relation between the minimum bandwidth,  $\Delta v$ , of the electronic equipment and minimum dwell time.

$$\Delta v \geq (2t_{Dmin})^{-1} \quad (4.3.)$$

For view angle,  $\theta_o$ , dwell time,  $t_D$ , is given by:

$$t_D = \frac{\omega}{\omega'} \sec \theta_o \quad (4.4.)$$

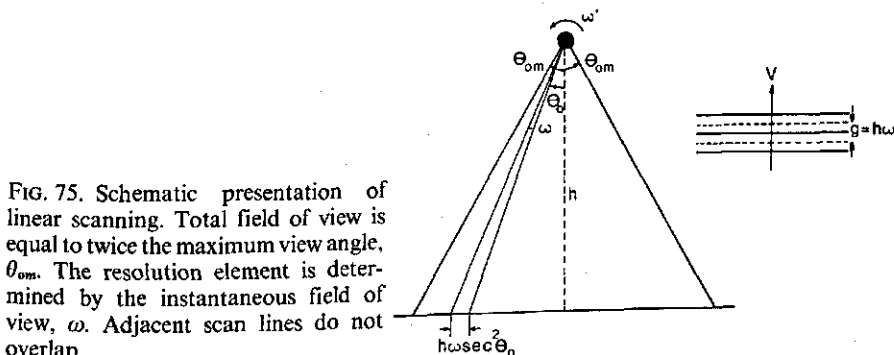


FIG. 75. Schematic presentation of linear scanning. Total field of view is equal to twice the maximum view angle,  $\theta_{om}$ . The resolution element is determined by the instantaneous field of view,  $\omega$ . Adjacent scan lines do not overlap.

From the relation between the minimum dimension of the ground resolution element,  $h\omega$ , the adjacency of scan lines, platform height,  $h$ , and velocity,  $v$ , follows a condition for the  $v/h$  ratio:

$$\frac{v}{h} = (2\pi)^{-1}\omega\omega' \quad (4.5)$$

Equation (4.3.) gives for the minimum bandwidth,  $\Delta\nu$ :

$$\Delta\nu = \pi v/h\omega^2 = 1/2 \left( \frac{\omega'}{\omega} \right) \quad (4.6.)$$

When noise equivalent power,  $NEP(\lambda)\Delta\lambda$ , in spectral bandwidth,  $\Delta\lambda$ , is caused by noise equivalent radiance,  $NER(\lambda)\Delta\lambda$ , equations (3.22.) and (3.24.) give a relation between  $NER(\lambda)$  and scanner parameters.

$$NEP(\lambda)\Delta\lambda = NER(\lambda)\Delta\lambda\omega^2 A_c\tau_o T = f\omega D^{*-1}(\lambda)\Delta\nu^{1/2} \quad (4.7.)$$

Substitution of (4.5.) in (4.7.) gives for  $NER(\lambda)$ :

$$NER(\lambda) = \frac{f}{A_c\tau_o TD^*(\lambda)\Delta\lambda} \left( \frac{\omega'}{2\omega^3} \right)^{1/2} = \frac{(\pi)^{1/2}f}{A_c\omega^2\tau_o TD^*(\lambda)\Delta\lambda} \sqrt{\frac{v}{h}} \quad (4.8.)$$

From this equation it is concluded that detection level is limited by a compromise between spatial resolution, spectral resolution, effective optical aperture,  $A_c$ , detector performance expressed by detectivity,  $D^*$ , atmospheric

TABLE 7. Some specifications of the DS-1250 multispectral scanner manufactured by Daedalus Enterprises Inc.

Operating parameters	
Optical aperture (effective) $A_c$	3"
Focal length $f$	6"
Scan rate $\omega'/2\pi$	80 s <sup>-1</sup>
Gated field of view $2\theta_{om}$	77°20'
Instantaneous field of view $\omega$	2.5 mrad
$v/h$ (constant value)	0.2
Spectral bands	Wavelength
1	380– 420 nm
2	420– 450 nm
3	450– 500 nm
4	500– 550 nm
5	550– 600 nm
6	600– 650 nm
7	650– 690 nm
8	700– 790 nm
9	800– 890 nm
10	920–1100 nm

transparency,  $T$ , and optical efficiency,  $\tau_o$ . The well-known flight parameter  $v/h$  determines  $NER(\lambda)$  and post detection bandwidth,  $\Delta\nu$ .

Some specifications of an airborne multispectral scanner, manufactured by Daedalus Enterprises Inc. are presented in Table 7. This scanner has been applied for investigations into the applicability of airborne MSS in The Netherlands, see BUNNIK *et al.* (1977).

## 5. MULTISPECTRAL REFLECTANCE IN RELATION TO PLANT CANOPY PROPERTIES

### 5.1. INTRODUCTION

Reflectance of a plant canopy at a number of different wavelengths includes information about the optical properties of canopy components and structure. Due to such causal relations, the spectral distribution of the reflected radiation may be regarded as a feature, through which remote sensing techniques can be applied to recognize crops in relation with their environment.

Multispectral pattern recognition exploits specific information from measured spectral reflectance in a given number of wavelength bands. The number and position of spectral bands is determined primarily by the atmospheric windows, the differences between the crops themselves and other field conditions.

In chapter 3, in which only crop structure, leaf colour and soil reflectance variations have been studied, it has been shown that a unique selection of wavelength bands for optimum information extraction is not possible. However, spectral bands with a frequent occurrence of maximum information have to be considered for permanent selection. In addition correlations between reflectance values in different spectral bands have to be taken into account. They will be higher, when reflectance behaviour is determined by similar properties of the leaves. The correlation, for example, between reflectance is high at 400 and 670 nm, 800 and 1100 nm and 1600 and 2200 nm, respectively, since the chlorophyll content, internal cell structure and water content have a prevailing effect on reflectance and transmittance in the mentioned wavelength intervals.

On the other hand, an evident assumption is that, if spectral reflectance of a crop in its characteristic points, like maxima and minima is known, already much information is available.

In practice, the number and position of spectral bands of existing multispectral scanners, usually is determined by the used sensor types, the physical properties and the limitations of the data recording systems. The applied methods of automatic multispectral pattern recognition have been improved to a high degree of perfection during the last decades. If a given crop has been already recognized using such automatic classification techniques or by available groundtruth, a new point of view originates. Can causal relations between crop properties and multispectral reflectance be applied in an opposite way to extract information on a crop parameter of interest? Actually a new feature derived from reflectance in one or more spectral bands should be required to show optimum sensitivity to variations in the crop property looked for, but remain invariant to non-relevant crop parameters.

## 5.2. CANOPY REFLECTANCE IN THE RED AND NEAR INFRARED

The results from the information distribution analysis require a more detailed study of canopy reflectance in the red and near infrared part of the spectrum. Systematic behaviour in relation with varying crop properties can give rise to the definition of new multispectral features related to crop parameters. The optical properties at 670 nm in the red and at 870 nm in the infrared have been chosen for an analysis using Suits' model. Only a homogeneous canopy with invariable optical constants of the leaves has been assumed. SINCLAIR *et al.* (1971) stated that spectral reflectance and transmittance of normal green leaves does not vary significantly during the main part of the growing cycle.

Table 8 shows the optical data used for the following calculations with Suits' model.

TABLE 8. Optical properties of the leaves, the soil and the ratio  $E_{-}(0)/E_s(0)$  between diffuse sky and direct solar irradiance at 670 and 870 nm,

$\lambda$	$\rho$	$\tau$	$\rho_s$	$E_{-}(0)/E_s(0)$
670 nm	7%	1%	13%	0.4
870	50	45	20	0.2

A constant solar zenith angle,  $\theta_s = 30^\circ$ , and perpendicular observation have been chosen. As varying parameters,  $L$ ,  $\theta_L$  and the percentage ground cover have been considered. The ground cover depends on  $L$  and  $\theta_L$  and in agriculture is defined as the percentage of soil screened by plant elements as observed in perpendicular view. According to the exponential assumption of Suits for the probability of soil observation,  $B$  is defined as:

$$B = 1 - \exp(-L \cos \theta_L) \quad (5.1.)$$

Figs. 76 and 77 give crop reflectance as a function of the average leaf angle,  $\theta_L$ , with  $L$  as a parameter for 670 and 870 nm.

In the discussion about the examples of canopy reflectance spectra given in section 2.4.9., most of the occurring variations in both figures have been illustrated already. An important phenomenon is shown in Fig. 76, where with  $L \leq 4$  crop reflectance increases at increasing values of  $\theta_L$ . This effect is due to higher reflectance of this soil type compared with leaf reflectance. If the average leaf inclination changes to a more vertical value, more of the brighter soil will be visible leading to increasing crop reflectance. Only with a high leaf area index the increasing percentage of shadow inside the canopy will dominate, resulting in a monotonous decrease of crop reflectance with increasing leaf inclination.

Crop reflectance in the near infrared decreases with increasing value of  $\theta_L$  for all values of  $L$ . If  $L$  and  $\theta_L$  are exchanged, the relations between red and near

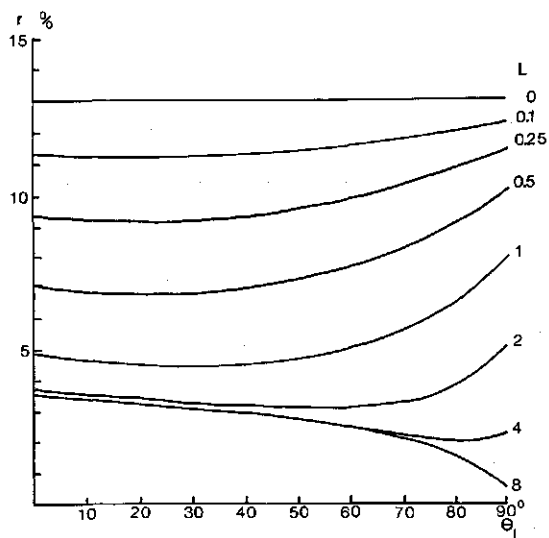


FIG. 76. Crop reflectance in the red at 670 nm as a function of the average leaf angle,  $\theta_L$ , with  $L$  as a parameter.

infrared reflectance and  $L$  are as shown in Fig. 78 and Fig. 79.

It appears that reflectance in the red decreases drastically with increasing  $L$ , whereas dependent on  $\theta_L$  a stationary value between  $L = 1.5$  and 3 is attained in most canopies.

Crop reflectance in the chlorophyll absorption band can be simplified, if the generated diffuse radiant flux is neglected. With an infinitely thick canopy, reflectance  $r_\infty$  is:

$$r_\infty \approx \frac{w}{K + k} = \frac{\rho \cos \theta_L + F \sin \theta_L \operatorname{tg} \theta_o}{\cos \theta_L + \frac{2}{\pi} \sin \theta_L (\operatorname{tg} \theta_s + \operatorname{tg} \theta_o)} \quad (5.2.)$$

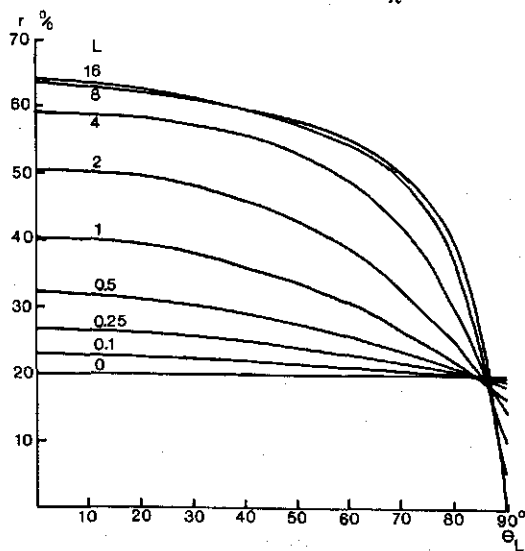
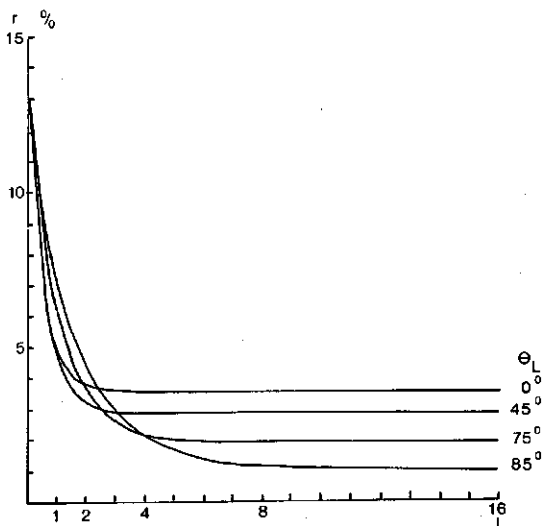


FIG. 77. Crop reflectance in the near infrared at 870 nm as a function of the average leaf angle,  $\theta_L$ , with  $L$  as a parameter.



FIG. 78. Canopy reflectance in the red at 670 nm as a function of  $L$  with  $\theta_L$  as a parameter.



By substitution of (5.2.) in (2.58.) canopy reflectance is approximated by:

$$r \simeq r_{\infty} + (\rho_s - r_{\infty})e^{-L(\cos \theta_L + \frac{2}{\pi} \sin \theta_L (\tan \theta_s + \tan \theta_s) x_1)} \quad (5.3.)$$

Reflectance as a function of  $L$  is exponential, as shown in Fig. 78. The dynamic behaviour in the near infrared is opposite, while saturation occurs for larger values of  $L$ , which is due to the high transparency of the leaves in this wavelength region.

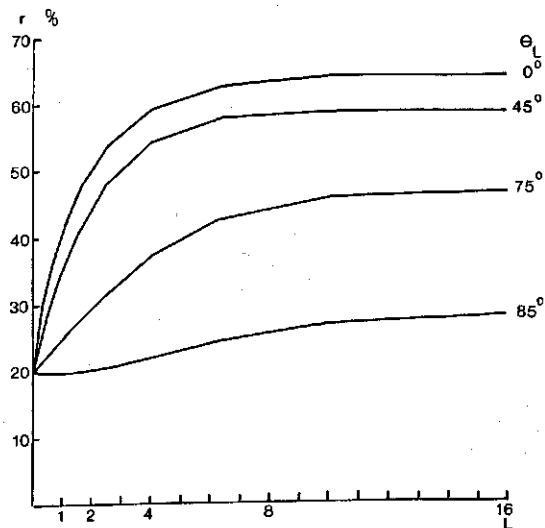


FIG. 79. Canopy reflectance in the near infrared at 870 nm as a function of  $L$  with  $\theta_L$  as a parameter.

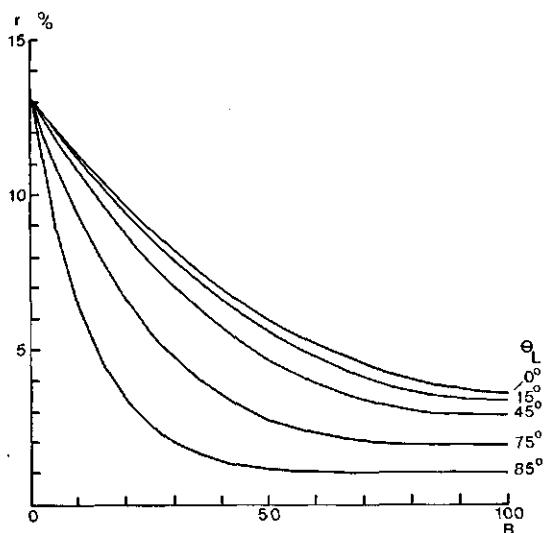


FIG. 80. Canopy reflectance in the red at 670 nm as a function of the percentage of ground cover with  $\theta_L$  as a parameter.

Figs. 80 and 81 represent the relations between reflectance in the red and infrared and the percentage of ground cover.

In the red, the decrease in canopy reflectance still depends on the average leaf inclination,  $\theta_L$ . For high inclinations, reflectance is already stationary for lower cover percentages, because of the relatively greater amount of observed shadow.

The small effect of leaf angle,  $\theta_L$ , for values between  $0^\circ$  and  $45^\circ$  on the increase of near infrared reflectance is surprising. Only with highly vertically oriented leaves, when physical reflectance behaviour is dominated by shadow effects,

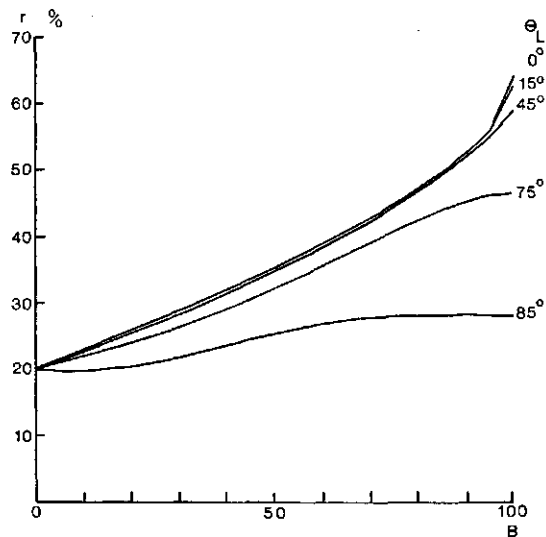


FIG. 81. Canopy reflectance in the near infrared at 870 nm as a function of the percentage of ground cover with  $\theta_L$  as a parameter.

will reflectance increase with high cover percentages, owing to the greater sensitivity of reflectance to high values of  $L$  in the near infrared plateau.

Apart from the influence of  $L$  and  $\theta_L$  on canopy reflectance, also reflectance behaviour of the bounding soil and the intrinsic optical properties of the leaves play an important role, but in most cases they do not change the illustrated systematic behaviour significantly.

### 5.3. ANALYSIS OF MODEL RESULTS AND MEASUREMENTS BY MEANS OF TWO-COLOUR DIAGRAMS

Multispectral reflectance can be described by a vector presentation as used in section 3.1. The distribution of the data points belonging to different crops in the multidimensional feature space are found within a volume bounded by hyperplanes. These hyperplanes are determined by extreme conditions of the crop parameters, like leaf area index, leaf angle distribution, leaf colour and spectral reflectance of the soil. This concept was also adopted by KAUTH and THOMAS (1976) for a graphical description of the spectral-temporal development of agricultural crops, as measured by Landsat.

Model simulations and field reflectance data can be used in determining the dynamic behaviour of reflectance vector. This dynamic behaviour originates from time dependent and geometrical dependent variables, like crop growth, observations of different crops, variation in solar zenith angle and observation angle. To investigate the definition of new spectral observables out of reflectance values at different wavelengths, the relations between elements of the reflectance vector are required. These relations are present in subspaces of the multidimensional feature space. In this paragraph some two-dimensional presentations are given to illustrate fundamental properties of agricultural crops with green leaves, as valid for different combinations of two wavelength values.

Fig. 82 gives the relation between reflectance in the red at 670 nm and in the infrared at 870 nm for the data used in section 5.2.

The point S in this 'two-colour' diagram belongs to the soil. If constant leaf and soil reflectance characteristics are assumed, lines of varying leaf area index are emanating from S. Point H gives the infinite reflectance of a crop with horizontal leaves only. Line OH refers to crops with varying average leaf angle,  $\theta_L$ , with very high leaf area index. Line OS represents crops with vertical leaves only. This line shows increasing shadow proceeding from S, while the origin, O, is equivalent to a black body, which is an extreme case included in Suits' model. From this figure it can be concluded that each homogeneous canopy is presented by a point within the area OHS, with two remaining degrees of freedom formed by soil reflectance and optical properties of the single leaves.

If a reflectance parameter,  $P_i(r, ir)$ , is defined by taking a linear combination of the red and infrared reflectance, it follows from Fig. 82 that a large variety

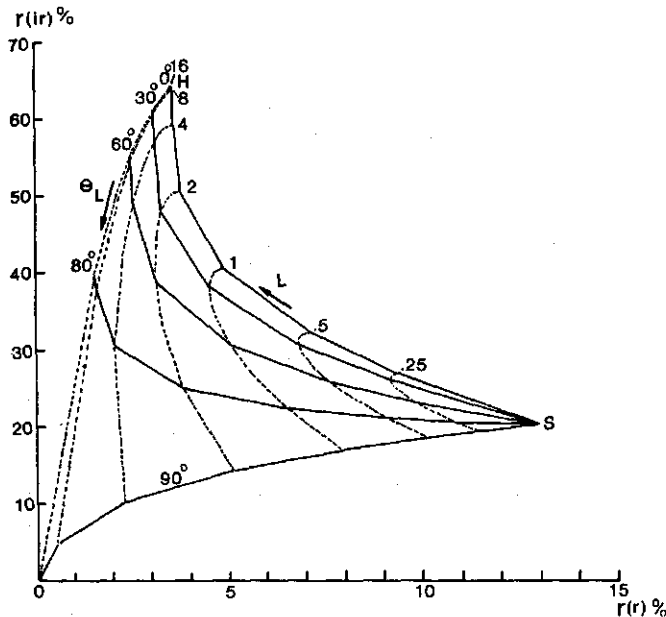


FIG. 82. Relation between red and infrared red reflectance with constant leaf and soil colour as a function of the canopy structure.  
 $\theta_o = 0^\circ$ ,  $\theta_s = 30^\circ$ .

of crops with different structures will meet equation (5.4.).

$$P_l(r, ir) = \alpha r(r) + \beta r(ir) \quad (5.4.)$$

However, the spectral discrimination can be optimized between features at the bases of such linear combinations of two or more reflectance values, as applied in the principle component analysis of multispectral data from different crops. No useful relation between such algorithm and one crop parameter has been found.

A frequently applied method of multispectral data processing is based on ratios between different spectral bands. This reflectance parameter for the red and near infrared wavelengths is defined as:

$$P_r(r, ir) = r(ir)/r(r) \quad (5.5.)$$

From Fig. 82 it can be concluded that a small value of  $P_r(r, ir)$  is related to a low leaf area index, whereas a large ratio is related to a high value of the leaf area index. A drawback of this ratio defined by equation (5.5.) consists of the remaining degree of freedom caused by the large range of the average leaf angle,  $\theta_L$ , which keeps a given ratio invariant.

Variations in reflectance of the soil, as caused by the surface moisture con-

tent, are eliminated in the first order which makes parameter  $P_r(r, ir)$  less dependent on the position of point  $S$ , see Fig. 82.

From Suits' model it can be inferred that for both wavelengths canopy reflectance as a function of reflectance of the soil is almost linear. Equation (3.19.) may be approximated by:

$$r_c = r_c(0) + r'_c(0) \rho_s \quad (5.6.)$$

Substitution of (5.6.) in (5.5.) gives:

$$P_r(r, ir) = \frac{r_c(0, ir)}{r_c(0, r)} \cdot \frac{1 + \frac{r'_c(0, ir)}{r_c(0, r)} \rho_s(ir)}{1 + \frac{r'_c(0, r)}{r_c(0, r)} \rho_s(r)} \quad (5.7.)$$

Variations in the soil moisture content always affect soil reflectance as shown in Fig. 22. The positive correlation between the variations in the red and infrared makes  $P_r(r, ir)$  insensitive, which follows from (5.7.). Another advantage of ratioing remotely sensed radiance values comes from the compensation of variations in surface irradiance, atmospheric transmittance and additive path radiance.

A reflectance parameter,  $P_m(r, ir)$ , defined by multiplying reflectance in the red and infrared, see (5.8.), remains in the first order invariant to different values of the leaf area index, when small variations of the leaf angle,  $\theta_L$ , are assumed.

$$P_m(r, ir) = r(r) \cdot r(ir) \quad (5.8.)$$

Differences in soil reflectance are amplified, which follows from (5.6.), while for radiance data the variations in irradiance, transmittance and path radiance are disadvantageously intensified.

To illustrate the dynamic behaviour of crop reflectance data, a plot of measured reflectance values of crops with green leaves in a red-infrared diagram has been given in Fig. 83.

These data were measured at the Wageningen test site during the summer of 1974 and have been transformed to zero mean values according to formula (3.7.). The distribution of reflectance data qualitatively agrees well with Fig. 82. To show the degree of correlation between the two spectral bands, an ellipse has been plotted with axes equal to the square root of the first and second eigenvalue of the covariance matrix. The principal directions are determined by the first and second eigenvector.

To analyse the influence of different leaf types, soil types and soil moisture level, model simulations were performed for homogeneous canopies. Reflectance and transmittance data for single leaves have been taken from GAUSMAN *et al.* (1971). Some measured soil reflectance data are used. These data and the wavelengths selected have been summarized in Table 9.

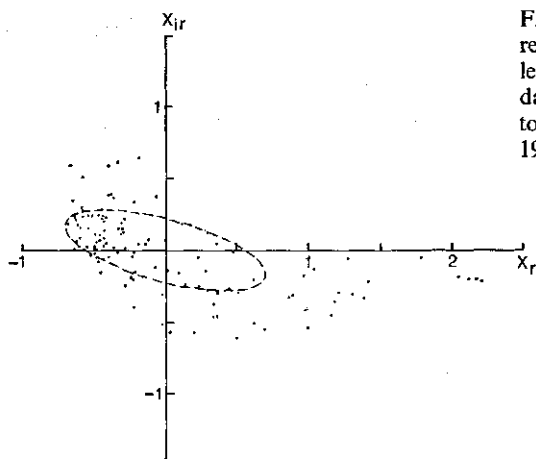


FIG. 83. Distribution of measured field reflectance data of crops with green leaves in the red-infrared diagram. The data points have been transformed to zero mean values. (Wageningen, 1974.)

TABLE 9. Optical constants of single leaves of wheat, beans and maize. Reflectance data of soil types used and the ratio between diffuse sky irradiance and direct solar irradiance.

$\lambda$	$\rho$			$\tau$			$\rho_s$		$E_-(0)/E_s(0)$	
nm	wheat	bean	maize	wheat	bean	maize	sandy loam dry*	sandy loam wet*	clay dry*	
550	0.135	0.185	0.162	0.055	0.109	0.098	0.126	0.051	0.107	0.388
670	0.075	0.102	0.091	0.007	0.035	0.007	0.175	0.065	0.116	0.299
870	0.520	0.567	0.476	0.440	0.420	0.510	0.286	0.126	0.159	0.200
1650	0.382	0.409	0.329	0.368	0.322	0.430	0.380	0.145	0.187	0.129
2200	0.244	0.240	0.198	0.247	0.197	0.303	0.370	0.115	0.168	0.157

\* Reflectance data on the sandy loam soil were measured at Wageningen, clay reflectance was measured at Lelystad.

First some two-colour diagrams and measured data are presented to compare variations in spectral reflectance in different bands with each other. The field data are averaged in the wavelength intervals indicated. The model results are calculated for standard conditions. A solar zenith angle of  $30^\circ$  and perpendicular observation have been chosen. Most diagrams are valid for the dry sandy loam soil and the optical leaf properties for wheat.

For the varying crop structure the following standard series have been used:

$L$ : 0.25, 0.5, 1.0, 1.5, 2.0, 2.5, 3.0, 3.5, 4.0, 4.5, 6, 10.

$\theta_L$ :  $0^\circ$ ,  $30^\circ$ ,  $45^\circ$ ,  $57.52^\circ$ ,  $75^\circ$ .

Fig. 84 shows the red-infrared diagram for dry and wet sandy loam soil. It is observed that changes in soil reflectance indeed influence canopy reflectance drastically at  $L < 3$ . The contrast variation in the red band is reduced

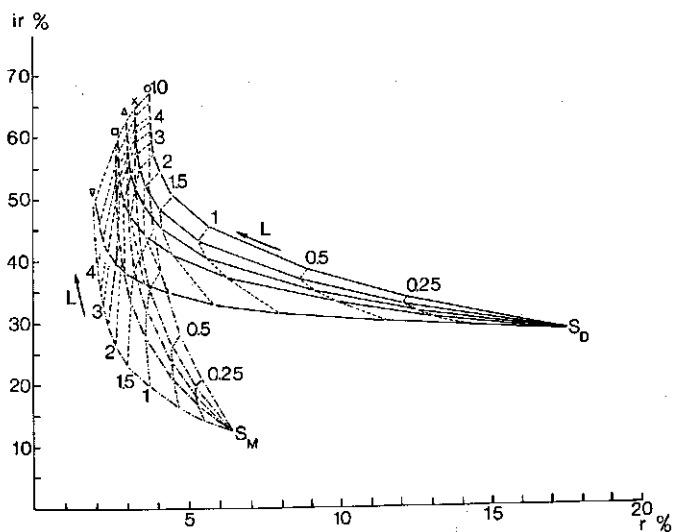


FIG. 84. Two-colour diagram of canopy reflectance in the red (670 nm) and near infrared (870 nm) wavelength regions for a dry and moist sandy loam soil.  $\theta_s = 30^\circ$ ,  $\theta_o = 0^\circ$ .  $\theta_L: 0^\circ$  ( $\circ$ ),  $30^\circ$  ( $\times$ ),  $45^\circ$  ( $\Delta$ ),  $57.52^\circ$  ( $\square$ ),  $75^\circ$  ( $\nabla$ ). Leaf type: wheat.

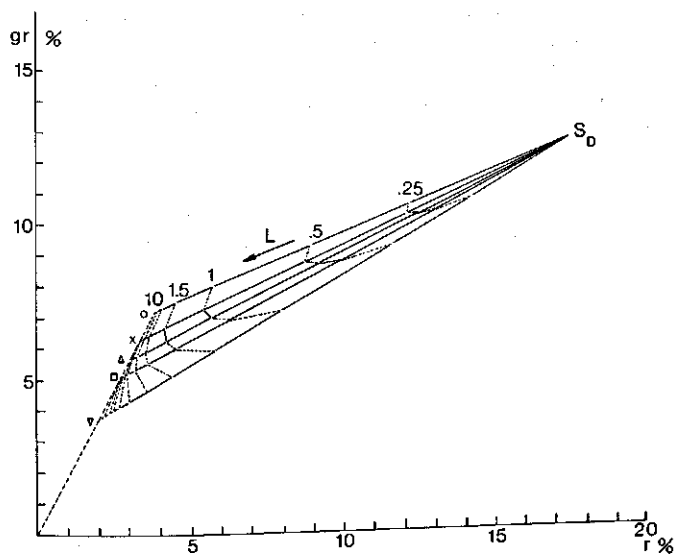


FIG. 85. Reflectance in the red-green diagram of canopies with varying structure.  $\theta_L = 0^\circ$  ( $\circ$ ),  $30^\circ$  ( $\times$ ),  $45^\circ$  ( $\Delta$ ),  $57.52^\circ$  ( $\square$ ),  $75^\circ$  ( $\nabla$ ).

*Meded. Landbouwhogeschool Wageningen 78-1 (1978)*

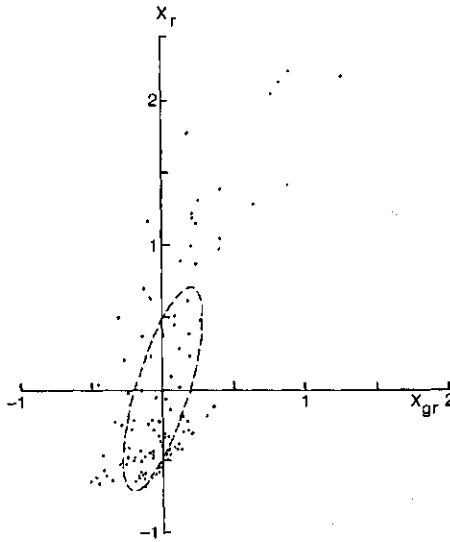


FIG. 86. Distribution of measured field reflectance data of crops with green leaves in the green-red diagram. The data points have been transformed to zero mean values.

considerably, but is increased in the infrared. This was already observed in section 3.3., see Fig. 50.

The relation between the red and green reflectance at 670 and 550 nm, respectively, with constant leaf angle,  $\theta_L$ , is linear in good approximation, see Fig. 85. It appears that the red/green ratio is independent of the leaf angle for high leaf area index. The same feature was found in the measured reflectance data shown in Fig. 86.

Also some relationships between green, red, near infrared and two wavelengths in the water absorption region have been investigated. For model calculations data have been used for 1650 and 2200 nm. Field reflectance data have been averaged for the respective intervals from 1550–1700 nm and from 2060–2240 nm, indicated as middle infrared 1 and middle infrared 2 (mir 1, mir 2).

If crop structure variations only are considered, it can be concluded from Figs. 85 and 88 that the green and middle infrared 1 region show similar

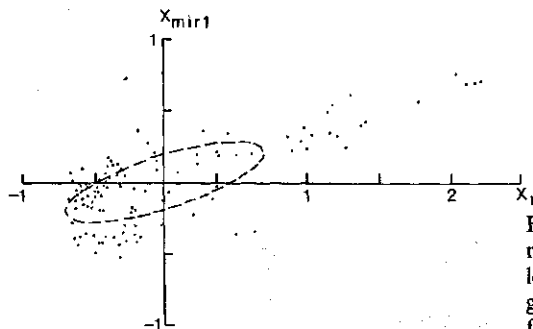


FIG. 87. Distribution of measured field reflectance data of crops with green leaves in the red-middle infrared 1 diagram. The data points have been transformed to zero mean values.



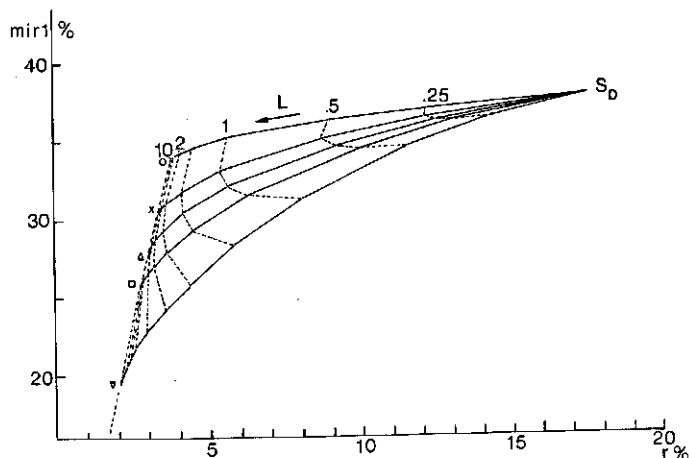


FIG. 88. Reflectance in the red-middle infrared 1 diagram of canopies with varying structure.  $\theta_L = 0^\circ$  (O),  $30^\circ$  (X),  $45^\circ$  ( $\Delta$ ),  $57.52^\circ$  ( $\square$ ),  $75^\circ$  ( $\nabla$ ).

behaviour. The red/middle infrared 1 ratio does not vary with the average leaf angle for high values of the leaf area index.

The relation between near infrared reflectance at 870 nm and middle infrared reflectance at 1650 nm is not essentially different from the relation between red and near infrared reflectance. Variations due to differences in leaf angle are of the same order as variations caused by changing *LAI*. This results in a lower correlation between reflectance in the near infrared plateau and the first band in the middle infrared. This is confirmed by the field measurements as shown in Fig. 90.

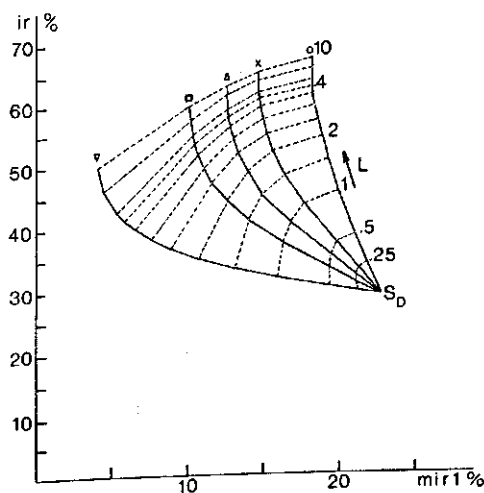


FIG. 89. Reflectance in the middle-infrared 1 - infrared diagram of canopies with varying structure.  $\theta_L = 0^\circ$  (O),  $30^\circ$  (X),  $45^\circ$  ( $\Delta$ ),  $57.52^\circ$  ( $\square$ ),  $75^\circ$  ( $\nabla$ ).

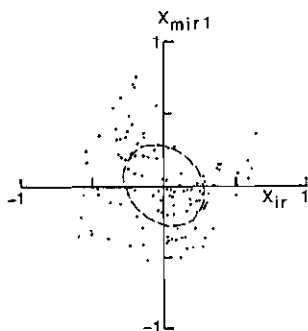


FIG. 90. Distribution of measured field reflectance data of crops with green leaves in the infrared-middle infrared 1 diagram. The data points have been transformed to zero mean values.

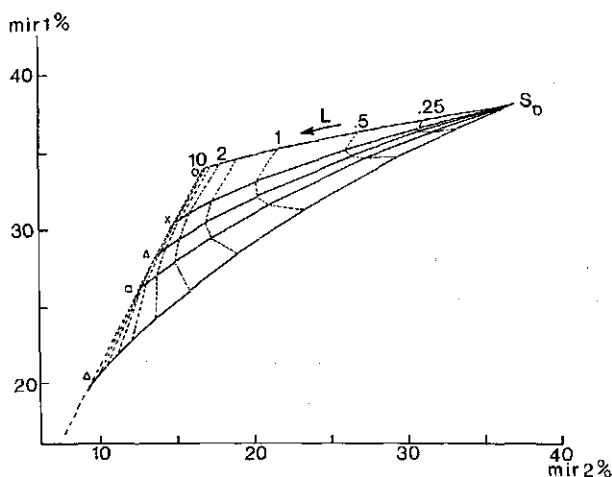


FIG. 91. Reflectance in the middle infrared 2-middle infrared 1 diagram of canopies with varying structure.  
 $\theta_L = 0^\circ$  (○),  $30^\circ$  (×),  $45^\circ$  (△),  $57.52^\circ$  (□),  $75^\circ$  (▽).

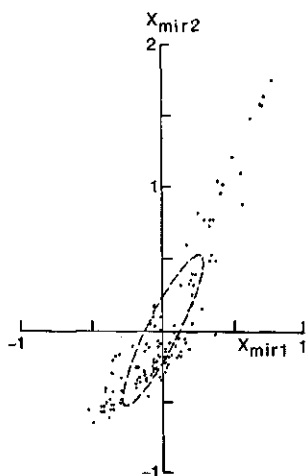


FIG. 92. Distribution of measured field data of crops with green leaves in the middle infrared 1 – middle infrared 2 diagram. The data points have been transformed to zero mean values.

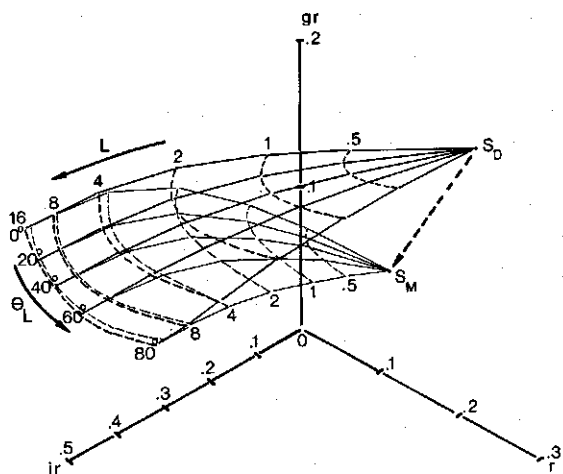


FIG. 93. Canopy reflectance variation in the green-red-near infrared feature space as a function of the structure parameters,  $L$  and  $\theta_L$ , for a dry and a moist soil.

If the reflectance magnitudes and the contrast between leaf and soil reflectance at 550 and 670 nm are compared with these quantities at 1650 and 2200 nm the same dynamic behaviour between 1650 and 2200 nm is predicted as was found between red and green, see Fig. 21 and Table 9. The ratio between reflectance in middle infrared 1 and 2 is constant and independent of the leaf angle for high  $LAI$  values. The measured data given in Fig. 92 are in good correspondence with the model predictions given in Fig. 91. The high correlation between both wavelength bands as shown by the excentric ellips along the first principal direction is due to the high correlation between reflectance or transmittance of the canopy leaves at both wavelength bands, where water absorption determines the interaction of radiant flux with the canopy.

It can be concluded that information from spectral bands other than green, red and near infrared does not contribute essential new information about the dynamics of canopy reflectance spectra caused by variations in the structure. Fig. 93 gives an example of the position of curved planes in the green-red-near infrared feature space formed by data points for varying crop structure parameters,  $L$  and  $\theta_L$ . Both planes originate from soil vector,  $S$ , and coincide with high value of  $L$ . In the special case of vertically oriented leaves only, both planes converge to the black body point in the origin.

Out of the two-colour diagrams treated in this paragraph, some useful parameters related with crop variables are defined in the next section.

#### 5.4. RELATIONS BETWEEN REFLECTANCE PARAMETERS AND PLANT CANOPY STRUCTURE

A spectral parameter is defined as a new observable derived from a chosen set of different spectral bands, which improves information extraction from multispectral data about the physical conditions of the observed features.

The feature vector is considered of a multispectral observation in a homogeneous canopy. The elements,  $x_i$ , of feature vector,  $\underline{x}$ , are functions of the wavelength dependent optical properties of canopy components and soil, canopy structure and geometrical parameters of incoming radiant power and observation direction.

$$\underline{x} = (x_1, x_2, \dots, x_N) = \{x_i\} = \{x_i(\rho(\lambda_i), \tau(\lambda_i), \rho_s(\lambda_i); L, \theta_L; \theta_s, \theta_o, \psi)\} \quad (5.9.)$$

A new observable,  $\underline{p}$ , is defined as a (preprocessed) feature vector with elements,  $p_r$ , which are functions of the original basis set,  $\{x_i\}$ .

$$\underline{p} = (p_1, p_2, \dots, p_M) = \{p_r\} = \{p_r(\{x_i\})\} \quad M \leq N \quad (5.10.)$$

If information is required about a canopy parameter, like e.g. soil cover,  $B$ , the average leaf angle,  $\theta_L$ , or soil variations, feature vector  $\underline{p}$  should be defined with the following properties.

$$\underline{p} = (p_1(B), p_2(\theta_L), p_3(\rho_s)) \quad (5.11.)$$

$$\begin{aligned} p_1(B) &= P_1(\{x_i\}) \\ p_2(\theta_L) &= P_2(\{x_i\}) \\ p_3(\rho_s) &= P_3(\{x_i\}) \end{aligned} \quad (5.12.)$$

To meet such requirements, the next criteria have to be accomplished.

1. The parameter is a predominant function of the canopy property of interest.
2. The parameter is invariant to the remaining variables of the canopy.
3. The parameter should be invariant to variations in the solar and observation angles.

If these conditions can be fulfilled, a considerable data-reduction could be obtained, if before data recording multispectral data from different channels have been transformed to preprocessed feature vectors with a reduced dimension. In addition, the elements of such feature vectors should have a better defined causal relationship with the physiological properties of the surveyed crops.

When crop growth monitoring is the object of multitemporal survey by means of a multispectral remote sensing technique, variation and development of canopy structure are dominant parameters. Remote measurement of the variations as a function of time of leaf area index or percentage soil cover of

agricultural crops in wide areas should offer a useful tool to agronomists for purposes, like inventory and yield prediction. The systematic behaviour of the multispectral reflectance vector as described in the previous sections of this chapter can be applied to such purposes, if canopy structure variations are dominant compared to variations in optical properties of single leaves. It has been stated before, that during the main part of the growing cycle of agricultural crops this condition is fulfilled, therefore it is assumed that leaves remain green before maturing or senescence. Otherwise, inherent to the concept of multispectral sensing, it is possible to derive criteria, whether the leaves of the canopy monitored are still green or not. Some suggestions for this requirement are given in sections 5.5. and 5.6.

A detailed analysis has been performed of the definition of useful spectral reflectance parameters from elements of a feature vector defined by the wavelengths given in Table 9. Using the dynamic behaviour displayed in two-colour diagrams, parameters as a function of leaf area index and soil cover percentage have been formed, which minimize the remaining degrees of freedom formed by average leaf angle, intrinsic properties of the single leaves and soil, solar zenith angle and direction of view. Some of these parameters are summarized in Table 10 and their main properties are discussed.

TABLE 10. Definition of reflectance parameters based on canopy reflectance in the green, red and near infrared wavelength region.

Parameter	Definition	Wavelength
$P_r(1)$	$r(ir)/r(r)$	$r$ : red 670 nm
$P_r(2)$	$r(r)/r(gr)$	$gr$ : green 550 nm
$P_r(3)$	$r(gr) \cdot r(ir)/r(r)$	$ir$ : infrared 870 nm
$P_r(4)$	$r(r) \cdot r(ir)/r(gr)$	
$P_r(5)$	$r(ir)/(r(r) \cdot r(gr))$	
$P_r(6)$	$(1 - P_r(2))/(1 + P_r(2))$	
$P_r(7)$	$(r(ir) - r(gr))/(r(ir) + r(gr))$	
$P_r(8)$	$P_r(6) \cdot r(ir)$	

a. *Parameter  $P_r(1)$*

The infrared/red reflectance ratio is a sensitive measure of the variation in  $L$  or  $B$ , as shown in Figs. 94 and 95.

When the average leaf angle of the canopy changes during growth, this parameter is not suitable because of the remaining influence of  $\theta_L$ . This is especially so with grass canopies in which leaf angle distribution changes from extremophyte to planophyte due to leaf flattening, see Fig. 46. Fig. 96 gives the parameter  $P_r(1)$  as measured in Perennial ryegrass during two growth periods. It will be shown later in this section that the difference between irradiance with direct solar flux or diffuse irradiance does not affect the trend in all the defined parameters essentially. The red-infrared diagram as measured is given in Fig. 97. The curvature at the end of the second growth period of line 2 is due to leaf flattening and corresponds with the decrease in parameter  $P_r(1)$ , as a function

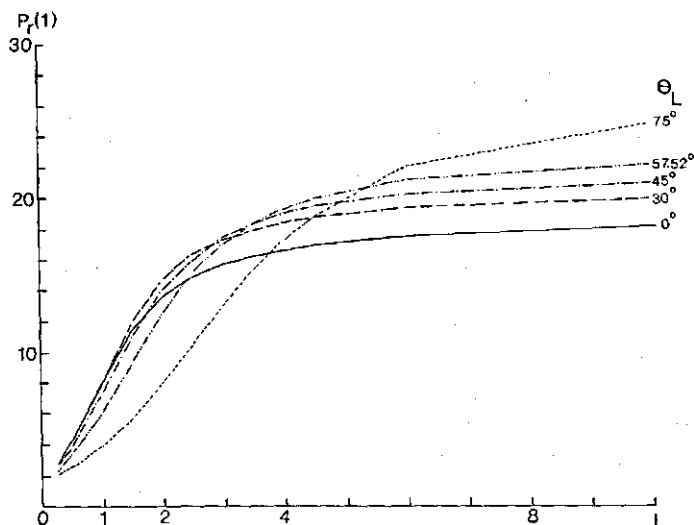


FIG. 94. Ratio of infrared and red reflectance as a function of  $L$ .  
 Leaf type: wheat.  
 Soil: dry sandy loam.  
 $\theta_s = 30^\circ$ ,  $\theta_o = 0^\circ$ .

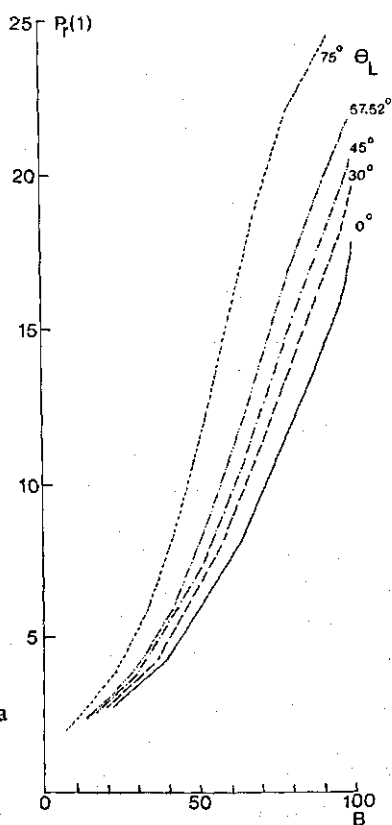
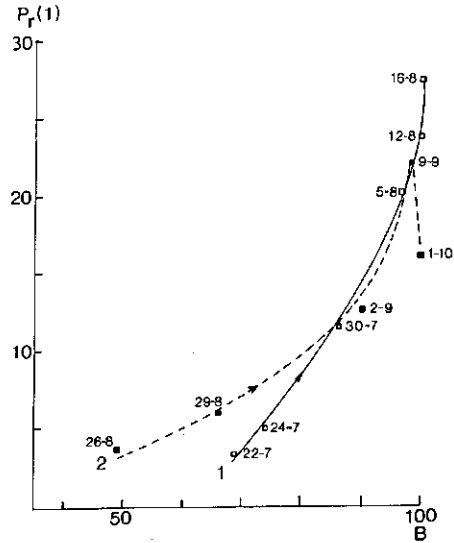


FIG. 95. Ratio of infrared and red reflectance as a function of the soil cover percentage.  
 Leaf type: wheat.  
 Soil type: dry sandy loam.  
 $\theta_s = 30^\circ$ ,  $\theta_o = 0^\circ$ .

FIG. 96. Infrared-red reflectance ratio of Perennial ryegrass, measured in two growth cycles at the Wageningen test site, summer 1974.



of the dry mass. It is assumed that the dry mass is proportional to the  $LAI$ .

To illustrate the reduction in the influence of soil reflectance, Fig. 98 gives an example of wheat and bean leaves forming a canopy with  $\theta_L = 57.52^\circ$  belonging to a spherical distribution, with a dry and a wet sandy loam soil. It is shown that soil reflectance is quite well eliminated at  $L > 1.5$ . Another conclusion is that  $P_r(1)$  does not reduce the difference between leaf types.

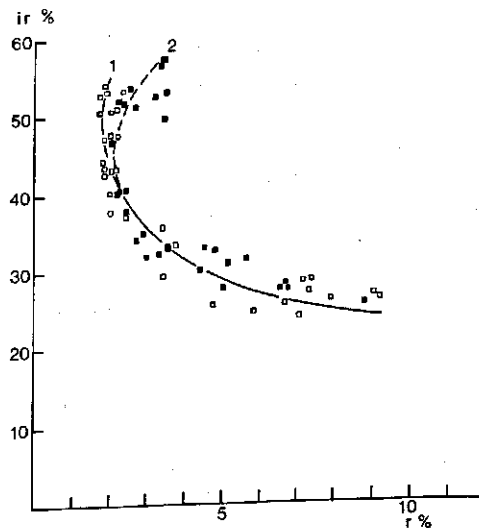


FIG. 97. Two-colour diagram for red and near infrared reflectance of Perennial ryegrass, as measured at Wageningen during two growth cycles in the summer of 1974.

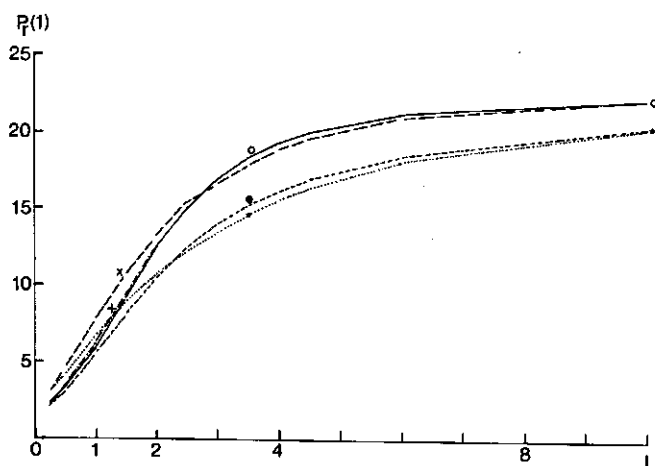


FIG. 98. Ratio of infrared and red reflectance for canopies consisting of wheat and bean leaves with different soil types, as a function of  $L$ .

$\theta_L = 57.52^\circ$

$\theta_s = 30^\circ$

$\theta_o = 0^\circ$

○: wheat – dry sandy loam

×: wheat – moist sandy loam

+: wheat – dry clay

●: bean – dry sandy loam

\*: bean – moist sandy loam

#### b. Parameter $P_r(2)$

In the previous section, it was concluded from Fig. 85 that the ratio of canopy reflectance in the red and green remains constant in canopies with a high leaf area index. Parameter  $P_r(2)$  does not depend on the average leaf angle of nearly infinitely thick canopies for wavelength values in the visible light region. If  $P_r(2)$  is plotted as a function of  $B$ , see Fig. 99, the influence of  $\theta_L$  is quite small compared with the variation of  $P_r(2)$  as a function of  $L$ . The influence of soil moisture, however, is quite considerable. Otherwise, model calculations have shown that canopy reflectance in this wavelength region is mainly determined by the single scattering of the direct radiant flux. In Suits' model, Lambertian reflectance and transmittance of the canopy components is assumed. The hemispherical reflectance and transmittance used, are measured by means of a spectrometer with an integrating sphere. The experiments of Breece and Holmes, described in section 2.2.5., have indicated that especially the bidirectional reflectance of normal green leaves is non-Lambertian, see Fig. 15.

Considering the polar diagrams of bidirectional reflectance in the green and the red, it can be concluded from their similar shape, that the ratio of hemispherical reflectance is almost equal to the ratio of bidirectional reflectance. This leads to the conclusion that a ratio of spectral reflectance values in the visible light region gives a correction to the model prediction, when non-Lambertian bidirectional reflectance is neglected.

Another property of interest results from the high positive correlation between leaf reflectance and transmittance in the green and in the red. This was found after an analysis of Gausman's data for various single green leaves.



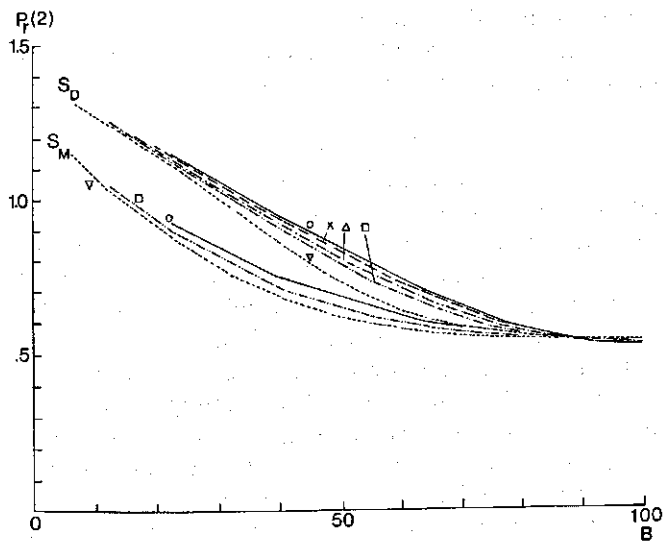


FIG. 99. Ratio of canopy reflectance in the red and in the green, as a function of the soil cover percentage for a dry and moist sandy loam soil.

$\theta_o = 0^\circ$ ,  $\theta_s = 30^\circ$

Leaf type: wheat.

$\theta_L = 0^\circ$  ( $\circ$ ),  $30^\circ$  ( $\times$ ),  $45^\circ$  ( $\Delta$ ),  $57.52^\circ$  ( $\square$ ),  $75^\circ$  ( $\nabla$ )

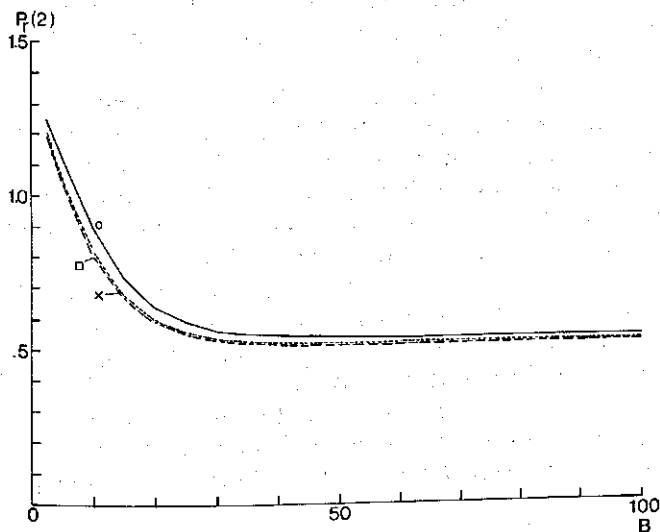


FIG. 100. Ratio of canopy reflectance in the red and in the green as a function of the soil cover percentage for different leaf types.

$\theta_L = 57.52^\circ$   $\theta_s = 30^\circ$   $\theta_o = 0^\circ$

Soil type: dry sandy loam.

$\circ$ : wheat

$\times$ : bean

$\square$ : maize

Parameter,  $P_r(2)$ , has been calculated for the different leaf types, as specified in Table 9 as a function of  $L$  for  $\theta_L = 57.52^\circ$ . The influence of the intrinsic scattering properties of the leaves is drastically reduced, see Fig. 100.

#### c. Parameter $P_r(3)$

An interesting correspondance between  $P_r(2)$  and near infrared reflectance as a function of  $B$  leads to a new and useful parameter. In Figs. 81 and 99 a positive correlation is found between the variation of  $P_r(2)$  and  $r(ir)$  as a function of  $\theta_L$  and as a function of soil moisture. This leads to the definition of parameter  $P_r(3)$ , in which the influence of variations in  $\theta_L$  and soil moisture could be minimized by ratioing of near infrared reflectance and  $P_r(2)$ . From Fig. 15 it is concluded that non-Lambertian reflectance of the canopy components in the near infrared can be neglected. Combination of near infrared reflectance with  $P_r(2)$  is not sensitive to non-Lambertian reflectance of single leaves. Otherwise, parameter  $P_r(3)$  is found by multiplying  $P_r(1)$  with  $r(gr)$ . The increase in  $P_r(1)$  caused by increased leaf inclination is compensated by decreasing reflectance in the green. Fig. 54 demonstrates that for higher values of  $L$ , the variation in  $r(gr)$  due to varying  $\theta_L$  is larger than the variation in  $r(r)$  for light soils as well as for dark soils.

Fig. 101 shows  $P_r(3)$  as a function of  $B$  for wheat leaves, a light soil and a solar angle of  $30^\circ$ . Due to the dispersion of infrared reflectance for different leaf angles at high values of  $B$ , parameter,  $P_r(3)$ , is still dependent on  $\theta_L$  for high soil cover percentages.

An analysis of this dispersion as a function of the solar angle,  $\theta_s$ , has shown that this dispersion increases with  $\theta_s$ , because more canopy components in shadow are being observed in the deeper layers.

Fig. 102 shows for  $\theta_L = 57.52^\circ$  the parameter,  $P_r(3)$ , as a function of  $B$  for  $\theta_s = 30^\circ, 45^\circ, 60^\circ$  and for diffuse irradiance. The influence of different moisture content in the soil surface layer is quite well eliminated. An example of the difference between the dry and moist sandy loam soil is included in Fig. 102.

The effect of differences between leaf types also has been analysed. From Fig. 58 it was concluded that reflectance differences of single leaves were minimum in the infrared plateau, whereas parameter,  $P_r(2)$ , is almost invariant for different single green leaves. When reflectance differences in the near infrared are negatively correlated with differences in  $P_r(2)$  for different single leaves parameter,  $P_r(3)$ , might be sensitive to this leaf type. This was particularly so for wheat and bean leaves, see Table 9 and Fig. 100. Fig. 103 gives measured  $B$ . Fig. 104 gives the relation between  $P_r(3)$  and  $B$  for *Dactylis glomerata* and Perennial ryegrass.

#### d. Parameter $P_r(4)$

Ratioing near infrared reflectance and  $P_r(2)$  does improve the sensitivity to varying cover percentage and compensates for soil moisture differences. It is expected that multiplying  $r(ir)$  with  $P_r(2)$  will give the opposite effects. Model

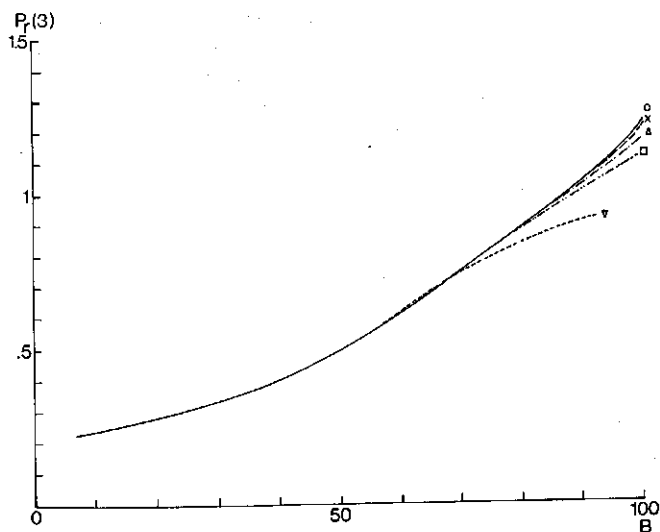


FIG. 101. Parameter,  $P_r(3)$ , as a function of the soil cover percentage.  
 $\theta_s = 30^\circ$   $\theta_o = 0^\circ$   $\theta_L = 0^\circ$  (○),  $30^\circ$  (×),  $45^\circ$  (Δ),  $57.52^\circ$  (□),  $75^\circ$  (▽)  
 Leaf type: wheat.  
 Soil type: dry sandy loam.

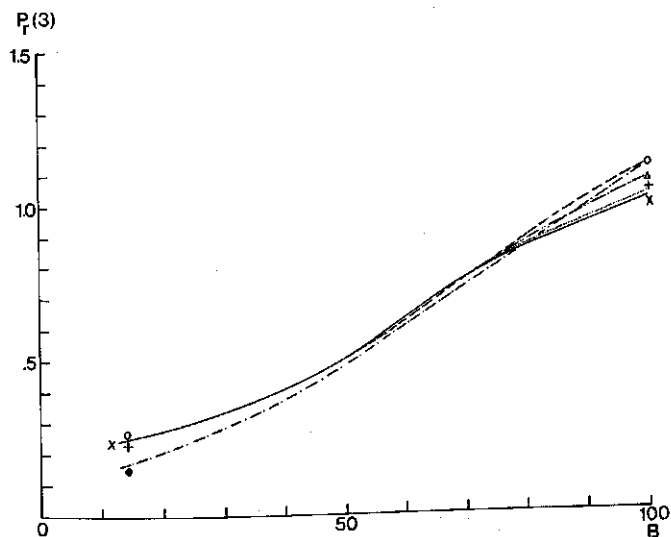


FIG. 102. Parameter,  $P_r(3)$ , of a canopy consisting of wheat leaves, as a function of the soil cover percentage,  $B$ , for different solar zenith angles and diffuse irradiance.  
 ○:  $\theta_s = 30^\circ$       ×:  $\theta_s = 60^\circ$       ●:  $\theta_s = 30^\circ$  moist sandy loam soil  
 Δ:  $\theta_s = 45^\circ$       +: diffuse irradiance ( $E_s = 0$ )

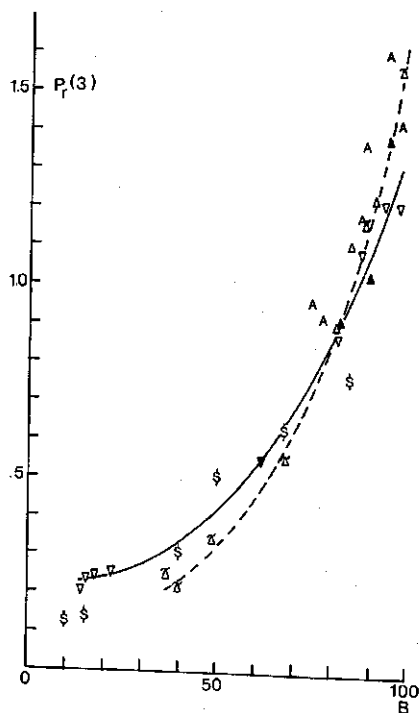


FIG. 103. Parameter,  $P_r(3)$ , as a function of soil cover percentage as measured for different crops at the Wageningen test site, in the summer of 1974.

A: potatoes  
 $\nabla$ : sugarbeets  
 $\Delta, \blacktriangle, \triangle$ : alfalfa  
 $\S$ : barley

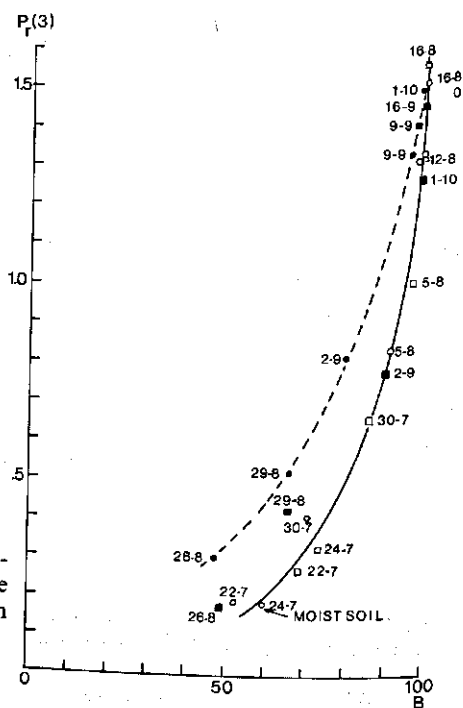


FIG. 104. Parameter,  $P_r(3)$ , of *Dactylis glomerata* and Perennial ryegrass as a function of the soil cover percentage during two growth cycles.

○, ●: *D. glomerata*  
 $\square$ , ■: Perennial ryegrass

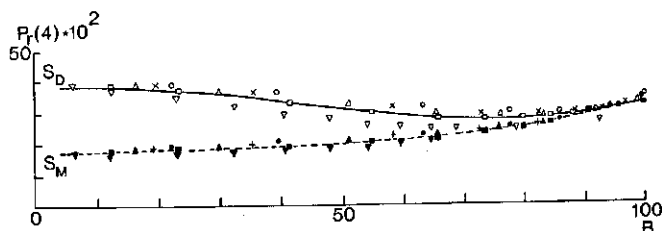


FIG. 105. Parameter,  $P_r(4)$ , of canopies on a dry and a wet sandy loam soil, as a function of soil cover percentage.

$\theta_s = 30^\circ$ ,  $\theta_o = 0^\circ$   $\theta_L = 0^\circ$  ( $\circ$ ),  $30^\circ$  ( $\times$ ),  $45^\circ$  ( $\Delta$ ),  $57.52^\circ$  ( $\square$ ),  $75^\circ$  ( $\nabla$ )

Leaf type: wheat.

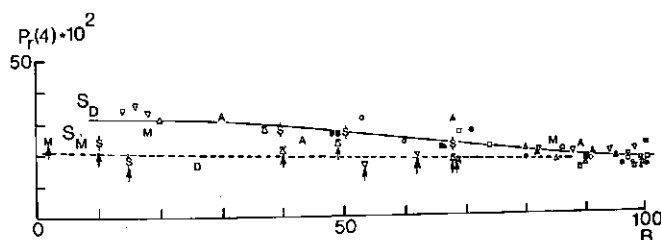


FIG. 106. Parameter,  $P_r(4)$ , as a function of the soil cover percentage for canopies as measured at the test site at Wageningen in the summer of 1974. Data points indicated by arrows have been measured on a moist soil.

$\nabla$ : sugarbeets

A: potatoes

§: barley

M: maize

$\Delta, \blacktriangle, \triangle$ : alfalfa

$\circ, \bullet$ : *D. glomerata*

$\square, \blacksquare$ : Perr. ryegrass

simulations have been performed for the standard set of canopy structure parameters and for the dry and moist sandy loam soil. The results are given in Fig. 105. If by means of  $P_r(3)$ , the soil cover percentage is determined, parameter,  $P_r(4)$ , can be used to estimate the moisture conditions in the upper soil layer. This suggestion applies to cover percentages below 60% and for small solar zenith angles. Measured reflectance data are given in Fig. 106. Measurements done with a moist dark coloured soil are indicated with arrows and can be distinguished quite satisfactorily.

#### e. Parameter $P_r(5)$

When canopies with high leaf area index ( $L > 4$ ) are considered, the product of red and green reflectance becomes mainly a function of the average leaf angle. An increasing leaf inclination angle causes a decreasing product,  $r(gr)$ . Leaf angle variations between  $\theta_L = 0^\circ$  and  $75^\circ$  give a relative variation of this reflectance product of about 250%.

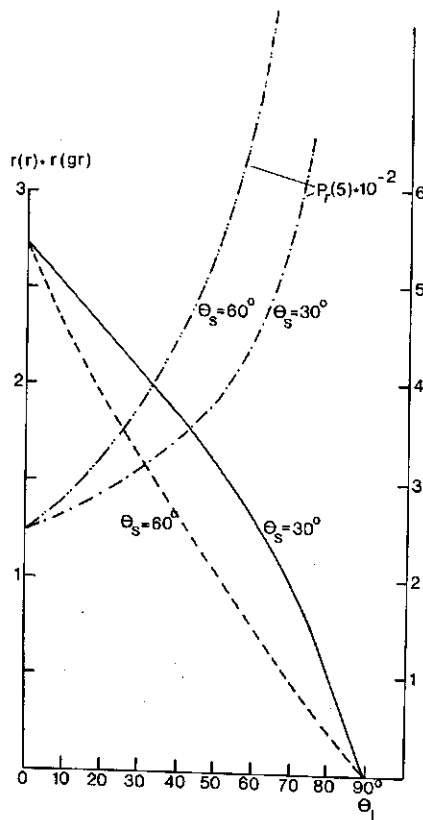


FIG. 107. Product of reflectance in the green and in the red and parameter,  $P_r(5)$ , as a function of the average leaf angle,  $\theta_L$ , for solar zenith angles of  $30^\circ$  and  $60^\circ$ .

$B = 1$

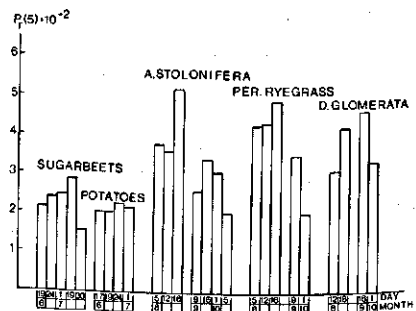
$\theta_s = 30^\circ$

$\theta_o = 0^\circ$

Leaf type: wheat. Soil type: dry sandy loam.

From Fig. 77 it was concluded that an increasing leaf angle results in a monotonous decrease in near infrared reflectance. Ratioing the near infrared and  $r(gr) \cdot r(r)$  gives for soil cover percentages near and equal to 100% an increasing function of  $\theta_L$ . This parameter depends on solar angle because relatively less radiant flux penetrates in the lower canopy layers in the green and the red wavelength bands as compared with the infrared. Both  $P_r(5)$  and the product of canopy reflectance in the green and in the red are given as a func-

FIG. 108. Parameter,  $P_r(5)$ , as a function of time of measured spectra of sugarbeets, potatoes, *A. stolonifera*, Perr. ryegrass (*Lolium perenne*), *D. glomerata* with 100% soil cover at the test site at Wageningen, in the summer of 1974.



tion of  $\theta_L = 30^\circ$  and  $60^\circ$  in Fig. 107. Some examples of measured data on crops with 100% cover are presented in Fig. 108.

The increase in  $P_r(5)$  for sugarbeets from 19 June till 19 July is the result of crop growth and increasing leaf area index, see Fig. 70. The more horizontal orientation and the yellowing of the older leaves of the beet plants results in a decrease in  $P_r(5)$ , as measured on 30 July. The data on potatoes between 17 June and 1 July indicate the steady crop structure which corresponds with the measured  $LAI$  values between 6 and 7.5. The relatively low value of  $P_r(5)$  agrees with the planophyle leaf angle distribution. The data on the grass canopies, during the last period of the first growing cycle, show a dominant extremophyle leaf distribution. After further plant growth during the second growing cycle leaf flattening is detected, especially for Perennial ryegrass.

#### f. Parameter $P_r(6)$

Since the difference between reflectance in the green and in the red wavelength band changes significantly with increasing leaf area index, this quantity can be used to enlarge the multispectral detectivity of soil cover variations. In most conditions, an increasing leaf area causes decreasing green reflectance. If a ratio between the difference and the sum of green and red reflectance is defined as parameter,  $P_r(6)$ , a monotonous increasing function of the leaf area index parameter,  $L$ , or the soil cover,  $B$ , is obtained. Fig. 109 gives the relation

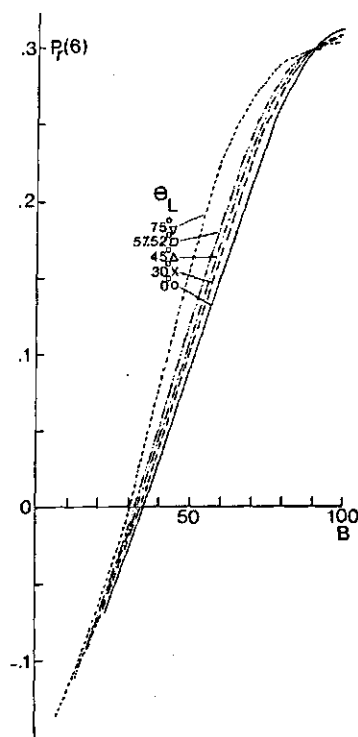


FIG. 109. Parameter,  $P_r(6)$ , as a function of soil cover percentage.

$\theta_s = 30^\circ$ ,  $\theta_o = 0^\circ$

Leaf type: wheat. Soil type: dry sandy loam.

between  $P_r(6)$  and the soil cover percentage for the standard series of structure parameters. Since  $P_r(6)$  has a direct relation with  $P_r(2)$ , this parameter still depends considerably on soil moisture differences.

g. Parameter  $P_r(7)$

From the two-colour diagrams, as e.g. Fig. 84, it is concluded that ratios between two different spectral bands still remain dependent on the leaf angle parameter,  $\theta_L$ . The dashed isolines for the leaf area index parameter,  $L$ , cause an inherent variation in reflectance ratio for constant  $L$  with overlapping intervals between significantly different values of  $L$ . This overlapping effect could be minimized, if one spectral band could be found with a small variation in reflectance due to varying leaf angle. Fig. 76 suggests that if the contrast between the green leaves and the soil is minimum, reflectance differences measured are caused by  $LAI$  variations only. The green wavelength band fits the best with this requirement. A combination of reflectance values in the green with the near infrared band could make this parameter also sensitive to higher leaf area index values. It has been found that a ratio between the difference and the sum of near infrared and green reflectance, defined as parameter,  $P_r(7)$ , is quite invariant for leaf angle variations. Fig. 110 shows  $P_r(7)$  as a function of  $L$ . It is observed that for high  $\theta_L$  values, some widening of the  $P_r(7)$  functions occurs between  $L = 0.25$  and  $L = 3$ . Another important property of  $P_r(7)$  is its insensitivity to soil moisture variations.

During the summer of 1974, the leaf area index of sugarbeets and potatoes was measured, see Fig. 70. Fig. 111 gives  $P_r(7)$  as a function of the  $LAI$ . The relationship found, corresponds satisfactorily with the predictions by Suits'

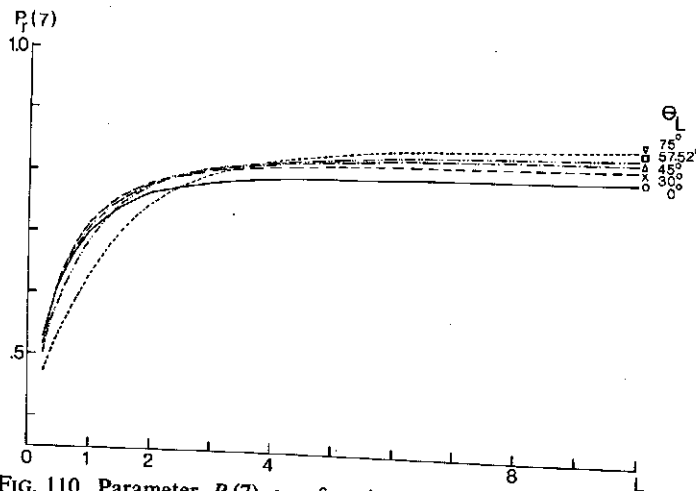


FIG. 110. Parameter,  $P_r(7)$ , as a function of  $L$ .  
Leaf type: wheat.  
Soil type: dry sandy loam.  
 $\theta_s = 30^\circ, \theta_o = 0^\circ$



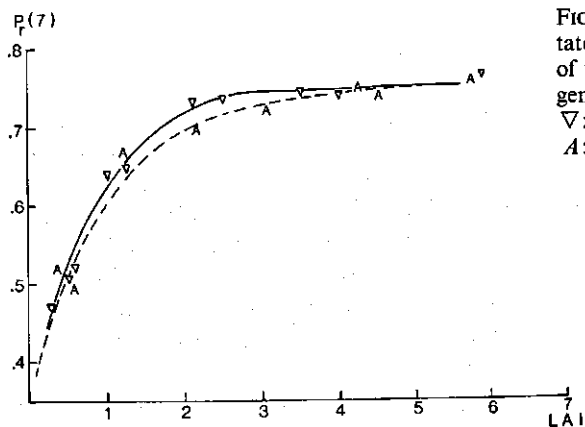


FIG. 111. Parameter,  $P_r(7)$ , for potatoes and sugarbeets, as a function of the LAI, measured at Wageningen, summer 1974.

▽: sugarbeets

△: potatoes

model. It was assumed that the dry green biomass of grass canopies is proportional to the LAI, which proportionality need not be equal for the different crops, as was found for potatoes and sugarbeets, see Fig. 70. Based on this assumption, parameter,  $P_r(7)$ , is plotted against the dry green biomass of three grass canopies in Fig. 112. It was found that the relation between  $P_r(7)$  and the dry mass for *Dactylis glomerata* is significantly different from that of *Agrostis stolonifera* and that of Perennial ryegrass for both growth cycles.

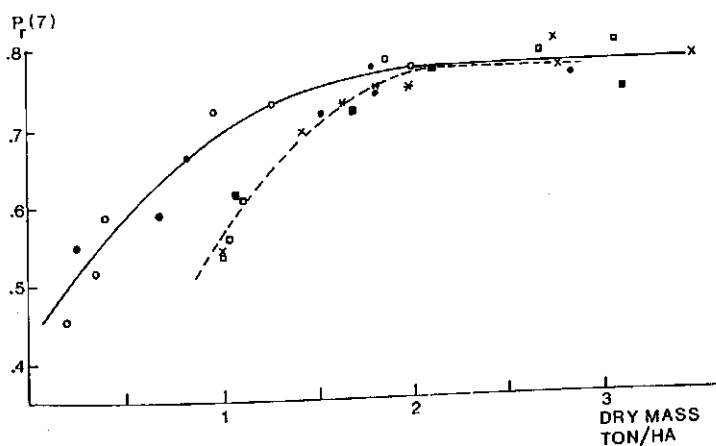


FIG. 112. Parameter,  $P_r(7)$ , for *D. glomerata*, *A. stolonifera* and Perennial ryegrass as a function of the dry biomass.

○, ●: *D. glomerata* (1, 2)

×, \*: *A. stolonifera* (1, 2)

□, ■: Perr. ryegrass (1, 2)

Wageningen, summer 1974.

g. Parameter  $P_r(8)$

The definition of  $P_r(3)$  is based on the negative correlation between near infrared reflectance and the red-green reflectance ratio,  $P_r(2)$ , as a function of the soil cover percentage,  $B$ . Fig. 109 shows  $P_r(6)$  as increasing with  $B$ . Model simulations predict a positive correlation between  $P_r(6)$  and soil moisture. These properties lead to the conclusion that analogous to  $P_r(3)$ , a product of  $P_r(6)$  and  $r(ir)$  yields a new parameter,  $P_r(8)$ , which should be a function of soil cover with insensitivity to soil moisture variations. As an additional advantage, it appeared that for soil cover percentages of over 90%, the dispersion of infrared reflectance due to leaf angle differences is compensated by the differences in  $P_r(6)$  caused by leaf angle variations. Parameter,  $P_r(8)$ , is given in Fig. 113 for wheat leaves and a solar angle of  $30^\circ$ .

Some experimental data on  $P_r(8)$  are given in Figs. 114 and 115. The difference between the amplitude of  $P_r(8)$  of potatoes and sugarbeets is probably due to the difference in single leaf reflectance in the infrared plateau. From the data on grass canopies and alfalfa it can be inferred that the dead material present after two growth periods influences the trend in  $P_r(8)$  during canopy growth. It is observed that  $P_r(8)$  of *Dactylis glomerata* and Perennial ryegrass coincides in the first measurement series. After cutting,  $P_r(8)$  has moved in an upward position and coincides with the data on alfalfa in which a layer of dead material was already present. Field measurements have pointed out that dead material has a significantly higher infrared reflectance than the soil type present at the test site.

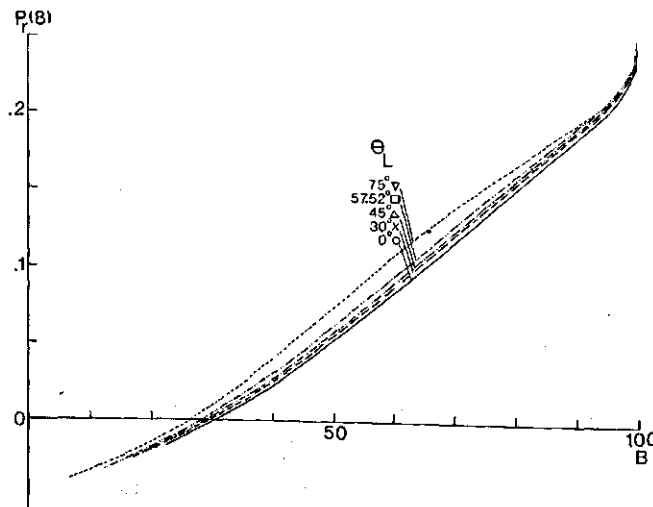


FIG. 113. Parameter,  $P_r(8)$ , as a function of the soil cover percentage.

Soil type: dry sandy loam.

Leaf type: wheat.

$\theta_s = 30^\circ$ ,  $\theta_o = 0^\circ$

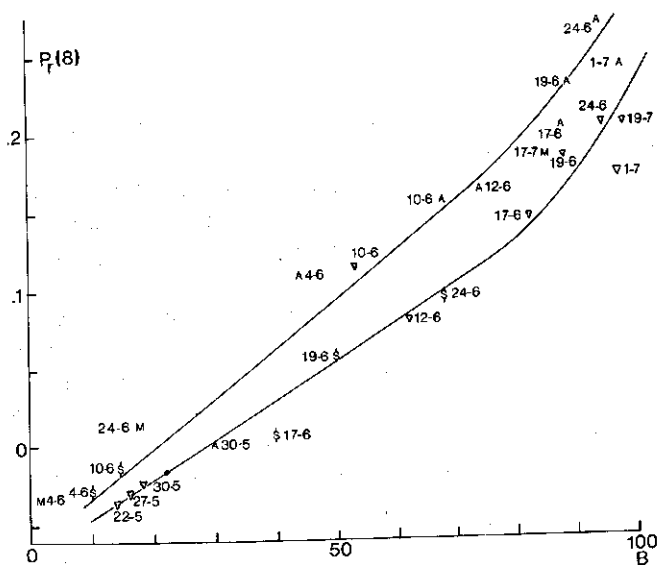


FIG. 114. Parameter,  $P_r(8)$ , for sugarbeets, potatoes, maize and barley, as a function of the soil cover percentage as measured at Wageningen in the summer of 1974.

A: potatoes  
M: maize  
∇: sugarbeets  
§: barley

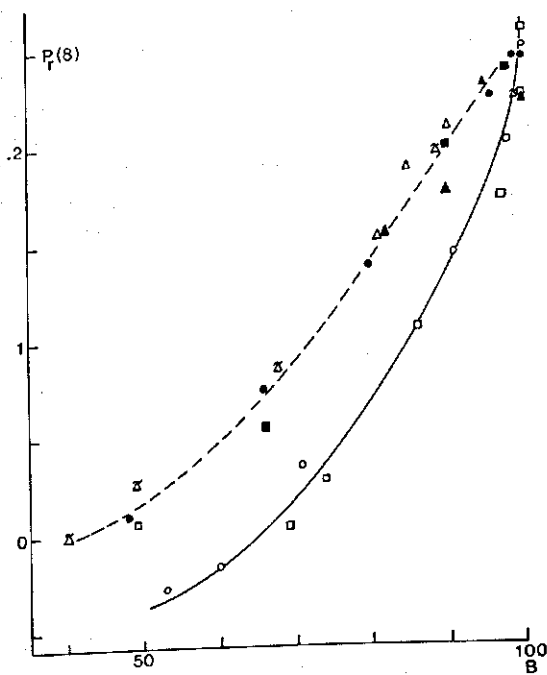


FIG. 115. Parameter,  $P_r(8)$ , for *D. glomerata*, Perennial ryegrass and alfalfa, as a function of the soil cover percentage. (Wageningen, summer 1974.)

○, ●: *D. glomerata* (1, 2)  
□, ■: Perr. ryegrass (1, 2)  
△, ▲, △: Alfalfa (1.2.3)

## 5.5. DETERMINATION OF THE LEAF COLOUR

In the previous section, it has been assumed that during crop growth the variations in the optical properties of the leaves or other canopy elements are small compared with structure variations.

All spectral parameters have been investigated on their causal relations with crop structure or soil moisture variations. Specific information about intrinsic leaf colour variations is useful, because of its relation with crop maturing or changes due to stress or crop diseases.

As a consequence of the use of multispectral remote sensing techniques, information closely related with colour becomes available. Instead of spectral parameters which are optimized for the detection of crop structure or soil reflectance variations, other parameters should be required which have a direct relation with leaf colour.

Since canopy reflectance is determined also by the spectral reflectance of the bounding soil, colour information on the leaves is improved, when the probability of observing fractions of the soil is small. This requirement can be met, if canopy radiance is detected under oblique view with a high probability of obtaining complete soil cover for a large variety of canopy structures. A drawback of oblique view is the decreased probability of detecting direct canopy radiance contributions from lower leaf layers, where leaf colour changes are usually initiated. When active sensing is applied, this drawback can be obviated. It has been demonstrated in a homogeneous canopy with a leaf area index varying between 0.25 and 4 and average leaf angles between  $0^\circ$  and  $75^\circ$  that a view angle of  $75^\circ$  is sufficiently large to observe soil cover percentages near 100%.

The colour of an observed object like a plant canopy is determined by the spectral power distribution of the radiant source and apparent reflectance. Colours today are uniquely specified by the CIE colour measurement system (Commission Internationale de l'Eclairage, 1931). This system is based on the definition of standard light sources and a standard observer. This standard observer (a normal human observer) determines colour perception by means of a linear combination of three component stimuli (primaries) in accordance with Grassmann's law.

The relation between colour and reflectance properties of an object is given by the tristimulus values  $X$ ,  $Y$ ,  $Z$  and defined by equation (5.13.a, b, c).

$$X = \int_0^\infty \bar{x}(\lambda) r(\lambda) E(\lambda) d\lambda \quad (5.13.a.)$$

$$Y = \int_0^\infty \bar{y}(\lambda) r(\lambda) E(\lambda) d\lambda \quad (5.13.b.)$$

$$Z = \int_0^\infty \bar{z}(\lambda) r(\lambda) E(\lambda) d\lambda \quad (5.13.c.)$$

The function,  $E(\lambda)$ , is a standard CIE-illuminant. For remote sensing applications standard source,  $S_e$ , is preferred, because of its colour temperature of

6770°K which belongs to average daylight. The weighting factors,  $\bar{x}(\lambda)$ ,  $\bar{y}(\lambda)$  and  $\bar{z}(\lambda)$ , determine the quantity of the three primaries to match the colour at each wavelength for the CIE standard observer and they correspond with the tristimulus values of the colour produced by unit density of radiant flux. The chromaticity ( $x, y, z$ ) is found from (5.13.) as follows:

$$x = X/(X+Y+Z) \quad (5.14.a.)$$

$$y = Y/(X+Y+Z) \quad (5.14.b.)$$

$$z = Z/(X+Y+Z) \quad (5.14.c.)$$

The ( $x, y$ ) values are plotted in the CIE chromaticity diagram, see Fig. 118. The dominant wavelength which provides information about the hue is found by projection of a colour point on the spectral locus from the white point. The spectral purity is found by ratioing the distance from the white point to the colour point and the distance from white to the projected point on the spectral locus.

Speaking in terms of colour, the relation between dominant wavelength and canopy reflectance seems useful. Due to the rather broad spectral reflectance curve of canopies, as measured in the visible light region, small purity is expected for green leaves with a dominant wavelength near 550 nm.

From the equations (5.14.a.) and (5.14.b.) it is concluded that a detailed spectral resolution is required to determine the chromaticity coordinates. In case of multispectral scanning, only a limited number of spectral bands is available in the visible light. Therefore, it has been investigated, whether a parameter defined by means of two or more spectral bands, yields information

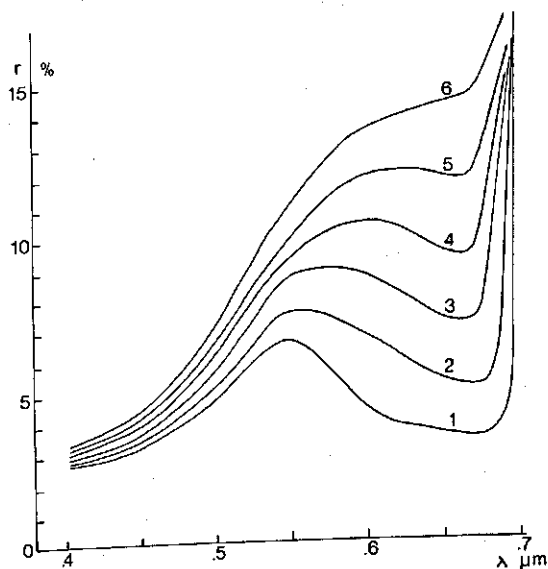


FIG. 116. Spectral directional reflectance of a one-layer canopy for varying stages of leaf yellowing.  
 $\theta_s = 30^\circ, \psi = 90^\circ$   
 $\theta_o = 75^\circ$   
 Soil type: dry sandy loam  
 $L = 1.5$   
 $\theta_L = 57.52^\circ$

closely correlated with the dominant wavelength,  $\lambda_c$ , and reflectance properties of the single leaves.

Using Suits' model, calculations have been performed for a uniform canopy with average leaf angle,  $\theta_L = 57.52^\circ$ ,  $L = 1.5$  and a dry sandy loam soil. A view angle of  $75^\circ$  has been used with a solar zenith angle of  $30^\circ$  and an azimuth angle of  $90^\circ$ . Six leaf types have been studied with increasing degree of yellowing. Reflectance and transmittance values have been taken from the literature and own measurements. In this data selection, the predominant variation occurs in the red, as confirmed by Gates (1965), SINCLAIR (1971) and GAUSMAN *et al.* (1976). The result of these model simulations is presented in Fig. 116.

The trend in the canopy reflectance curves suggests the suitability of the red/green ratio, because of its sensitivity and its positive correlation with the varying red/green reflectance and transmittance ratio of the single leaves. In section 5.4. it has been demonstrated that parameter,  $P_r(2)$ , is stationary at high LAI values and invariant to leaf angle variations. This property, quite fortunately, meets the requirement that a colour sensitive spectral parameter should be invariant to canopy structure variations. In this relation reference is made to section 5.6., where it has been found for  $\theta_o = \theta_s = \arctg 4/\pi$  and  $\psi = 0$ , that  $P_r(2)$  turns independent of the canopy structure and is a function of single leaf reflectance only.

For a varying set of canopy structure parameters, reflectance in the green and red has been calculated for green leaves, stage 1 in Fig. 116, for a view angle of  $75^\circ$  and solar zenith angle of  $30^\circ$ . The red-green two colour diagram is given in Fig. 117. It is concluded that the red/green ratio is not sensitive to structure variation with  $L > 1$ . This diagram also shows that the black body angle is not present, due to the oblique observation angle.

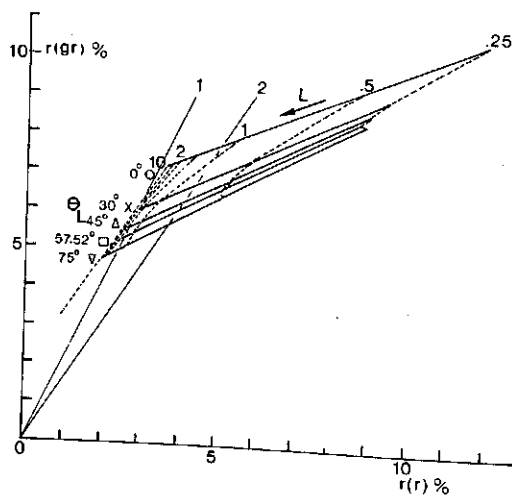


FIG. 117. Relation between red and green canopy reflectance at an oblique view angle of  $75^\circ$ .  
Leaf type: wheat.  
Soil type: dry sandy loam.  
 $\theta_s = 30^\circ$ ,  $\psi = 90^\circ$

Figure 1 is a color space diagram showing the color of green leaves and dead leaves. The diagram is a 2D plot with axes from 0 to 1. It features a large green curve on the left, a smaller yellow curve on the right, and a dashed line connecting them. Points 1 through 6 are marked along the yellow curve. Labels include 'green leaves', 'dead leaves', 'green', 'cyan', 'blue', 'red', 'orange', 'yellow', 'S.W.', 'C', '700nm', '400', '480', '500', '520', '540', '560', '580', '600', and '700nm'.

The calculated chromaticity coordinates, the dominant wavelength and the ratios of canopy reflectance between the red and green for 670 and 550 nm are presented in Table 11.

canopy stage	chromaticity		dominant wavelength $\lambda_c$	$\frac{r(670)}{r(550)}$	$\frac{\rho(670)}{\rho(550)}$
	$x$	$y$			
1	0.3182	0.3868	548 nm	0.511	0.576
1	0.3499	0.3922	561	0.673	0.710
3	0.3677	0.3970	570	0.818	0.865
4	0.3806	0.3958	575	1.010	1.000
5	0.3908	0.3950	578	1.212	1.120
6	0.3981	0.3980	579	1.325	1.134

*Meded. Landbouwhogeschool Wageningen 78-1 (1978)*

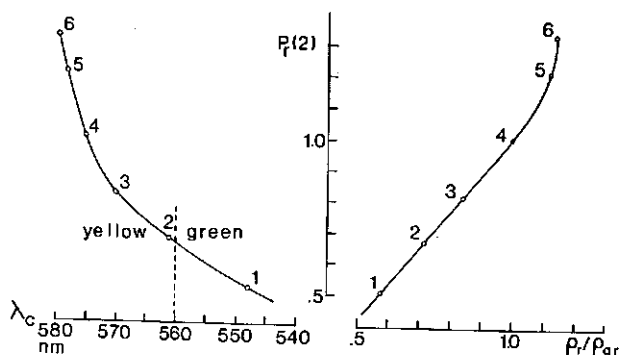


FIG. 119. Parameter,  $P_r(2)$ , of a yellowing canopy, observed under  $\theta_o = 75^\circ$  as a function of the dominant wavelength,  $\lambda_c$ , and the red/green reflectance ratio of the single leaves.

Finally, it is concluded that the spectral canopy parameter,  $P_r(2)$ , measured under oblique view large enough to obtain complete soil cover, is a useful multispectral observable to detect leaf colour variation. In Fig. 117 the lines of constant colour ratio for stage 1 and 2 are given. It appears that a variation of the dominant wavelength from 548 to 561 nm corresponds with the initiation of yellowing.

When the variation of  $P_r(2)$  is ascribed to structure variation only, there would have to be a drastic decrease in the leaf area index which seems quite unlikely.

#### 5.6. THE CANOPY HOT SPOT AND ITS APPLICATIONS IN THE DETECTION OF CANOPY PROPERTIES

Passive multispectral remote sensing techniques make use of the detection of reflected solar radiation. If multi-temporal canopy radiance measurements are performed over long periods during crop growth, the varying solar zenith angle can interfere with the previously suggested methods of information extraction about canopy structure. The observed amount of shadow inside plant canopies affects directional reflectance and depends on the momentaneous solar zenith angle which varies through the daily cycle and through the year. Because most of the operational multispectral systems in satellites, like Landsat, observe the earth's surface under perpendicular view, all spectral parameters as defined in the previous section were analysed for  $\theta_o = 0^\circ$  and for their sensitivity to varying solar angles.

To standardize crop reflectance measurements at Wageningen during the summer periods of 1973 and 1974, most data were collected with an artificial radiation source and with perpendicular view. To study systematic effects of directional reflectance on account of a varying view angle, measurements have



been performed on grass and wheat canopies during 1973 and 1974. A varying observation angle, necessary to airborne line scanners in collecting data from extended areas, adds even more variables to the apparent reflectance from non-Lambertian canopies. On the basis of the previous assumption used in Suits' model and verifications by field reflectance measurements, this non-Lambertian reflectance has a direct causal relation with the canopy structure. This leads directly to the suggestion that detection under different observation angles of the same features yields information on non-Lambertian reflectance. This concept was tested by MALILA (1974) using MSS data collected with a scanner mounted in two different positions.

Scan angle effects on directional reflectance of plant canopies have been studied in detail, VERHOEF and BUNNIK (1976): also the influence on the spectral parameters of section 5.4. The general conclusion of this study may be summarized as follows. Especially in multi-layer canopies with a predominant vertical structure, the influence of a varying observation angle on spectral reflectance is quite complex. No spectral parameters have been found which are invariant to the scan angle. On the basis of the canopy reflectance properties, as predicted by the model equations valid for the passive detection technique, it was proved that no systematic corrections of a given variety in the canopy structure for scan angle effects of spectral parameters are feasible.

If under certain conditions the physical complexity of plant canopy reflectance could be simplified, a better approach of the concept of information extraction using different observation directions should be possible. This desired simplification is offered by the special case of the so-called hot spot, described in section 2.4.6.3.

Hot spot reflectance as described by Suits' model requires only a modification of the bidirectional contribution to reflectance as given by equation (2.58). Bidirectional reflectance,  $r_b$ , originates from observed fractions of canopy components and soil which are directly illuminated. For  $\theta_o = \theta_s = \theta_o$  and  $\psi = 0$ , this bidirectional or single scattering term,  $r_b$ , is given by the equation

$$r_b = \frac{w}{K} (1 - e^{-K}) + \rho_s e^{-K} \quad (5.15.)$$

The coefficients,  $w$  and  $K$ , are expressed in terms of total horizontal and vertical leaf area index.

In wavelength bands where incident radiant flux is heavily absorbed, like in the chlorophyll and water absorption bands of green canopies, the contribution from the scattered diffuse flux can be neglected. Even in near infrared reflectance, the diffuse flux contribution remains small compared with the single scattering term up to  $LAI \approx 2.5$ . These properties make equation (5.15.) a good approximation and give a drastic simplification. In the hot spot, the canopy components observed radiate by reflectance of the incident flux only. After substituting factor,  $F(\theta_s, \psi)$ , in the bidirectional scattering coefficient,  $w$ , the ratio,  $w/K$ , as a function of the average leaf inclination angle is:

$$\frac{w}{K} = \rho \frac{1 + \frac{1}{2} \text{tg} \theta_L \text{tg}^2 \hat{\theta}_o}{1 + \frac{2}{\pi} \text{tg} \theta_L \text{tg} \hat{\theta}_o} \quad (5.16.)$$

From (5.15.) and (5.16.) it is concluded that the single scattering approach depends on the (apparent) cover percentage,  $B$ , and the average leaf angle,  $\theta_L$ .

The next analysis shows how  $r_b$  becomes independent of  $\theta_L$  for two view angles and how this further simplification is closely related with a canopy structure property already known.

The factor  $w/K$  does not vary with the average leaf angle, when the total differential as a function of  $H$  and  $V$  is zero.

$$d\left(\frac{w}{K}\right) = \frac{\partial}{\partial H} \left(\frac{w}{K}\right) dH + \frac{\partial}{\partial V} \left(\frac{w}{K}\right) dV = 0 \quad (5.17.)$$

Substitution of  $w$  and  $K$  and the use of the condition,  $d(H+V) = 0$ , in the case of the leaf angle variation leads to the relation

$$\frac{1}{\rho} d\left(\frac{w}{K}\right) = (H+V) \frac{dH}{K^2} \text{tg} \hat{\theta}_o \left(\frac{2}{\pi} - \frac{1}{2} \text{tg} \hat{\theta}_o\right) = 0 \quad (5.18.)$$

Two solutions for the view angle,  $\hat{\theta}_o$ , are found,  $\hat{\theta}_{o1} = 0^\circ$  and  $\hat{\theta}_{o2} = \arctg 4/\pi$  ( $\hat{\theta}_{o2} = 51.8^\circ$ ). The same result could be obtained directly from (5.16.) by making  $w/K$  independent of  $\text{tg} \hat{\theta}_o$ .

If the total differential of  $w/K$  is written in terms of partial differentials of  $w$  and  $K$ , another approach leads to a relation with an interesting phenomenon of plant canopies.

$$d\left(\frac{w}{K}\right) = -\frac{w}{K^2} \left(\frac{\partial K}{\partial H} dH + \frac{\partial K}{\partial V} dV\right) + \frac{1}{K} \left(\frac{\partial w}{\partial H} dH + \frac{\partial w}{\partial V} dV\right) \quad (5.19.)$$

Substitution of the hot spot condition in the azimuthal factor,  $F$ , gives a zero solution for both terms of (5.19) for view angles close to  $\hat{\theta}_{o2}$ . The total differential,  $dK$ , is zero for  $\hat{\theta}_{o3} = \arctg \pi/2$  ( $\hat{\theta}_{o3} = 57.5^\circ$ ) and  $dw = 0$  when  $\hat{\theta}_{o4} = \arctg \sqrt{2}$  ( $\hat{\theta}_{o4} = 54.7^\circ$ ).

When the azimuthal variation of the canopy is not taken into account, the bidirectional volume scattering coefficient,  $w$ , has to be averaged over  $\psi$ .

$$\bar{w} = \frac{1}{\pi} \int_0^\pi w(\theta_o, \theta_s, \psi) d\psi = H\rho + \frac{4}{\pi^2} V \frac{\rho + \tau}{2} \text{tg} \theta_o \text{tg} \theta_s \quad (5.20.)$$

The average scattering coefficient,  $\bar{w}$ , was introduced by Suits in his first paper concerning his canopy reflectance model. If this value is substituted in (5.19.) by assuming equal leaf reflectance and transmittance, the total differentials,  $dw$  and  $dK$ , make  $d(w/K)$  zero for the zenith view angle,  $\hat{\theta}_{o3} = \arctg \pi/2$ .

This angle was known earlier from the work of WARREN WILSON (1965). His inclined point quadrat method was used to determine the probability of light penetration under varying inclination angle. Long parallel needles were introduced into a canopy and the registration of hits with canopy elements as a function of penetration depth gave the mechanical equivalent of the probability of the penetration of direct radiant flux under a given inclination. Warren Wilson concluded that the penetration probability is much the same for all values of the leaf angle, when the inclination angle is  $32.5^\circ$ . This corresponds with the solution for  $\theta_{03}$ .

Another method to investigate this penetration probability was used by MILLER (1964) and OLIVER and SMITH (1974). Oliver and Smith have shown that the probability for light penetration in relation with the leaf angle distribution is given by a Fredholm integral equation.

This relation was used to determine the leaf angle distribution by taking angular photographs. The average projection of the total leaf area into direction,  $\theta_0$ , is given by the weighted average leaf projection using the leaf inclination density function,  $f'(\theta_L)$ .

$$LAIg(\theta_0) = LAI \int_0^{\pi/2} f'(\theta_L) d\theta_L \cdot \frac{1}{\pi} \int_0^\pi |\underline{n}_L \cdot \underline{n}_0| d\varphi_L \quad (5.21.)$$

The normal vector of a single leaf is given by  $\underline{n}_L$ , the direction vector of observation by  $\underline{n}_0$  with  $\varphi_0 = 0^\circ$ .

This integral equation is solved easily for a Suits' canopy. The leaf inclination density function for horizontal and vertical leaves is given by two Dirac functions.

$$f'(\theta_L) = \frac{H}{H+V} \delta(\theta_L), 0 \leq \theta_L < \alpha_L, 0 < \alpha_L < \frac{\pi}{2} \quad (5.22.)$$

$$f'(\theta_L) = \frac{V}{H+V} \delta(\theta_L - \frac{\pi}{2}), \alpha_L < \theta_L \leq \pi/2$$

Introduction of (5.22) and the solution of the kernel for horizontal and vertical leaves into equation (5.21) gives:

$$(H+V)g(\theta_0) = H \cos \theta_0 + \frac{2}{\pi} V \sin \theta_0 = K(\theta_L, \theta_0) \cos \theta_0 \quad (5.23.)$$

Oliver and Smith have shown that the solution of the Fredholm equation for a number of leaf inclination distributions is invariant for these distributions at a zenith view angle of  $57.5^\circ$ .

The average projected leaf area for a Suits' canopy according to (5.21.) for several values of  $\theta_L$  is given in Fig. 120.

The total differential,  $dw$ , is related with the average radiant intensity from a reflecting canopy layer into the observation direction. A canopy layer is considered with thickness,  $\Delta x$ , at depth,  $x$ . The average radiant intensity is given by a similar Fredholm integral equation.

$$\Delta I(\theta_o) = \int_0^{\pi/2} f'(\theta_L) d\theta_L \left\{ \frac{1}{\pi} \int_0^{\pi} a_L n(\theta_L) E_s^2(x) \frac{\rho}{\pi} |\underline{n}_L \cdot \underline{n}_o|^2 d\phi_L \right\} \Delta x \quad (5.24.)$$

When inclination distribution (5.22.) of a Suits' canopy is substituted in this integral equation, the intensity,  $\Delta I(\theta_o)$ , is:

$$\Delta I(\theta_o) = \frac{\rho}{\pi} E_s(x) \Delta x (H' \cos \theta_o + \frac{V'}{2} \cos \theta_o \operatorname{tg}^2 \theta_o) \quad (5.25.)$$

With condition,  $H' + V' = 1$ , and introduction of the average leaf angle,  $\theta_L$ , equation (5.25.) is:

$$\Delta I(\theta_o) = G(\theta_L, \theta_o) \frac{\rho}{\pi} E_s(x) \Delta x \quad (5.26.a.)$$

$$G(\theta_L, \theta_o) = (\cos \theta_L + \sin \theta_L)^{-1} \left( \cos \theta_L + \frac{\sin \theta_L}{2} \operatorname{tg}^2 \theta_o \right) \cos \theta_o \quad (5.26.b.)$$

Factor,  $G(\theta_L, \theta_o)$ , is given in Fig. 121. All functions are equal for  $\theta_{o4} = \arctg \sqrt{2}$ . Under this view angle, the radiant intensity is not influenced by the inclination distribution function of canopy components.

It has been shown that the minima of  $w$  and  $K$ , as a function of a varying leaf angle do not coincide. They are related with the minimum of the average

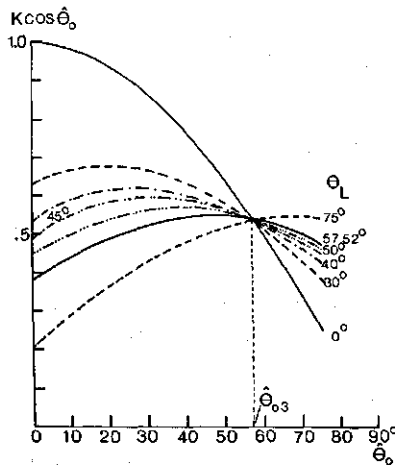


FIG. 120. Average projected total leaf area into direction,  $\theta_o$ , for varying leaf angle,  $\theta_L$ , of a Suits' canopy with  $H + V = 1$ .

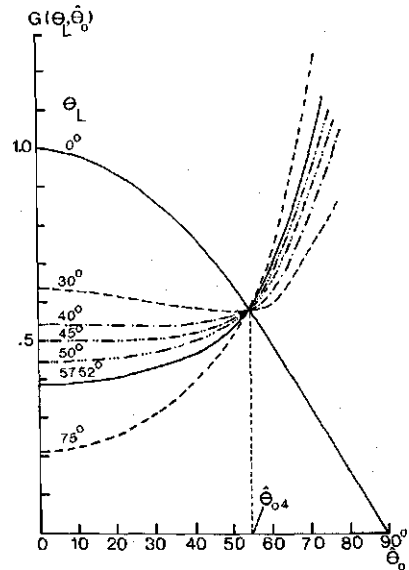


FIG. 121. Trend of radiant intensity from canopy layer with  $H' + V' = 1$ , into direction,  $\theta_o$ , for varying leaf angle,  $\theta_L$ .

projected leaf area, as a function of the view angle for varying leaf angles. The special oblique view angle for a simplified hot spot reflectance condition differs only  $5.7^\circ$  from the Warren Wilson angle of  $57.5^\circ$  for equal probability of light penetration into canopies with different leaf angle distributions.

From Goudriaan's model the following relation for hot spot reflectance of an infinitely thick canopy with horizontal leaves has been found:

$$\rho_{hs} = \rho_h + \frac{\sigma}{4} \quad (5.27.)$$

Only direct flux is present, the canopy hot spot reflectance is,  $\rho_{hs}$ . The same result follows from Suits' equation. If only horizontal leaves are present, expression (2.53.) for the canopy reflectance outside the hot spot is:

$$r_\infty = h^{-1} \frac{u + hv}{K + m} \quad (5.28.)$$

In this case,  $C = 0$  and  $D = -1$ .

In the hot spot, the infinite reflectance is given by:

$$r_{\infty hs} = r_\infty + \frac{2w - v}{2K} \quad (5.29.)$$

Substitution of,  $v$ ,  $w$  and  $K$  and the assumption,  $\rho = \tau = \sigma/2$ , leads to the result given in (5.27.).

With perpendicular view and with the special oblique view angle canopy reflectance is a linear function of the soil cover percentage determined by single leaf reflectance and soil reflectance.

$$r_b = \rho_s + (\rho - \rho_s)B \quad (5.30.)$$

The relation between  $r(\hat{\theta}_{o2})$  and  $B$  in the red and near infrared as calculated with Suits' model is given in fig. 122. From the function of  $r(\hat{\theta}_{o2})$  in the near infrared it is concluded that with  $LAI > 2.5$  the linear approximation is no longer valid. The two-colour diagrams for red-infrared and red-green are given in Figs. 122 and 123. The usefulness of multispectral reflectance detection in the hot spot under this oblique view angle is evident, because of the elimination of leaf angle differences. Fig. 124 shows the canopy lines in the green-red-infrared feature space. For perpendicular view, the canopy vectors are present along the same lines in the feature space, but at other positions due to the different soil cover percentage.

The spectral parameters,  $P_r(1)$ ,  $P_r(3)$  and  $P_r(4)$ , as a function of  $B$ , for wheat leaves and a dry sandy loam soil are given in Fig. 125. Parameters,  $P_r(1)$  as well as  $P_r(3)$ , now both are well defined functions of soil cover. The trend coincides of all spectral parameters for perpendicular view. When  $P_r(1)$  or  $P_r(3)$  are applied to determine the soil cover under  $\hat{\theta}_{o1}$  and  $\hat{\theta}_{o2}$ , both canopy struc-

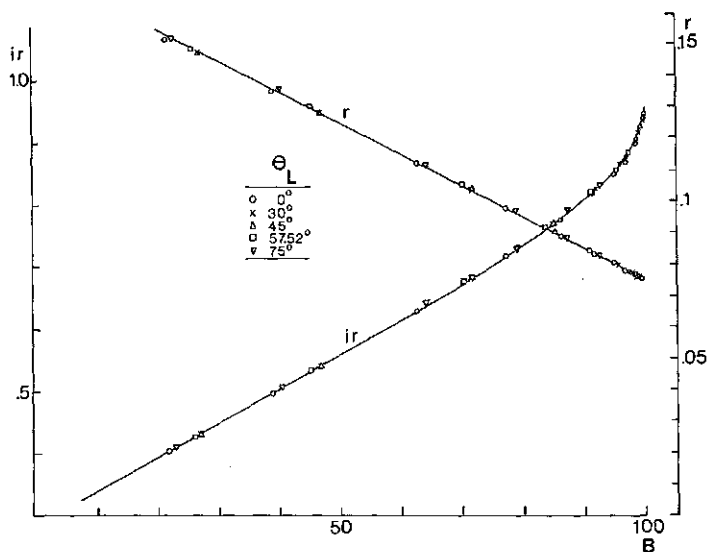


FIG. 122. Hot spot reflectance in the red and in the near infrared as a function of the soil cover percentage,  $\theta_o = \arctg 4/\pi$ .  
Leaf type: wheat. Soil type: dry sandy loam.

ture parameters,  $L$  and  $\theta_L$ , are known. Otherwise, both parameters have an increasing gradient, as a function of  $B$ , while  $P_r(3)$  has a higher sensitivity compared with  $P_r(2)$ .

The properties of  $P_r(4)$  can be used to detect soil differences. In spite of the increased coverage as a result of oblique view, a better detection of soil properties is possible due to the absence of observed shadows.

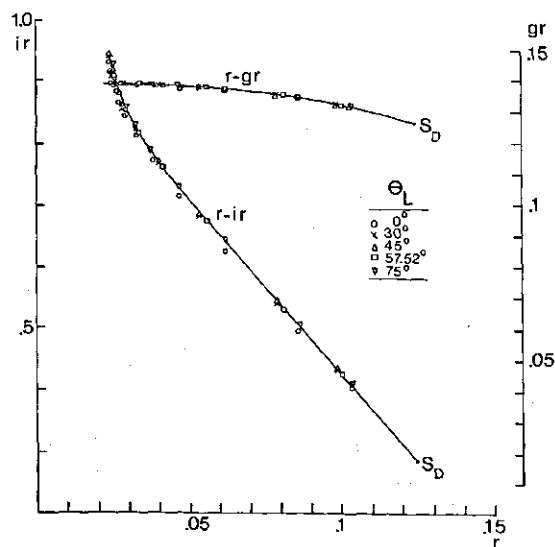
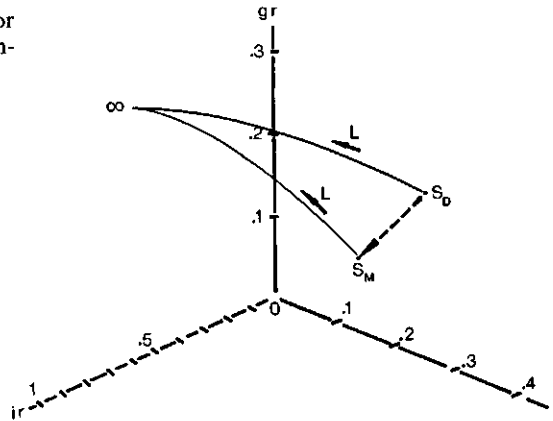


FIG. 123. Hot spot reflectance in the green, red and near infrared.  
 $\theta_o = \arctg 4/\pi$   
Leaf type: wheat. Soil type: dry sandy loam.

FIG. 124. Two canopy curves for grass leaves in the green, red, infrared feature space.

$S_D$ : dry sandy loam soil  
 $S_M$ : moist sandy loam soil  
 $\theta_o = \text{arctg } 4/\pi$



Data collection under an oblique view angle of  $\text{arctg } 4/\pi$  and in the canopy hot spot is possible, if an active conical scanning system is available.

If complete soil cover is detected, parameter,  $P_r(2)$ , becomes equal to  $\rho(r)/\rho(gr)$ . This is a function of the physiological properties of the single leaves only. This parameter yields direct information about leaf colour.

It has been found that the parameters mentioned almost coincide for different leaf angles, when they are plotted as a function of  $H + V$ . Fig. 126 gives  $P_r(3)$  for view angle  $\text{arctg } 4/\pi$  of wheat leaves. Another suggestion to apply the properties of canopy hotspot reflectance should be the combined use of active and passive scanning. If at a moment with solar zenith angle of  $\text{arctg } 4/\pi$  canopy reflectance is detected under the same view angle and simultaneously with reflectance of solar irradiance and with reflectance from an active radiant source, the diffuse contribution can be eliminated. Especially in the near infrared plateau, where the diffuse sky irradiance is small compared with the visible light region and reflectance and transmittance of single leaves are of the same order, this suggestion is feasible. Radiance originating from reflectance of solar radiation should be measured with the sun in opposite position. After adjustment to equalize the detected output signal from the response of a Lambertian reflector for passive and active irradiance, subtraction of the active and passive radiance from a plant canopy according to Suits' equations gives the following expression:

$$\Delta r(ir) = r_{act}(ir) - r_{pas}(ir) = (1/2\rho - \rho_s)B^2 + \rho_s B \quad (5.31.)$$

When complete coverage is attained, differential detection of passive and active scanning produces a signal which is a function of near infrared reflectance of the single leaves of the canopy only. Morphological changes in the internal mesophyll structure due to diseases or stress could be detected independent of variations in the canopy architecture.

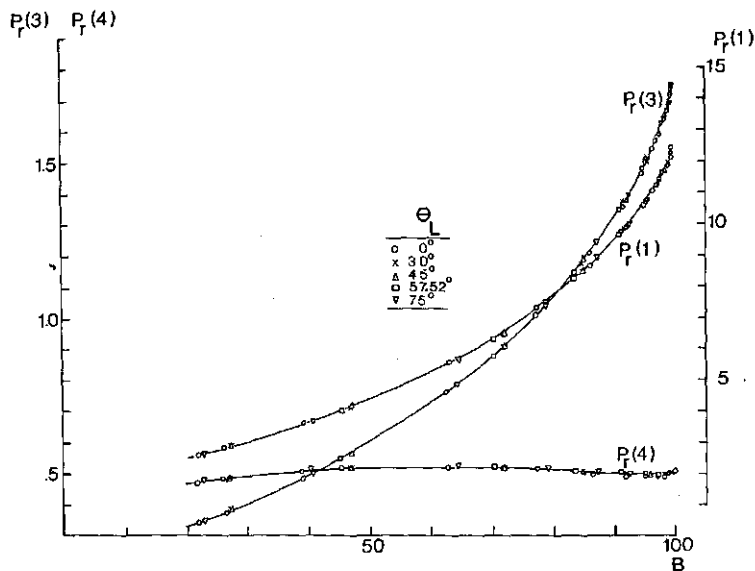


FIG. 125. Parameters,  $P_r(1)$ ,  $P_r(3)$  and  $P_r(4)$ , for the hot spot as a function of the soil cover percentage.  $\theta_o = \arctg 4/\pi$ .  
Leaf type: wheat. Soil type: dry sandy loam.

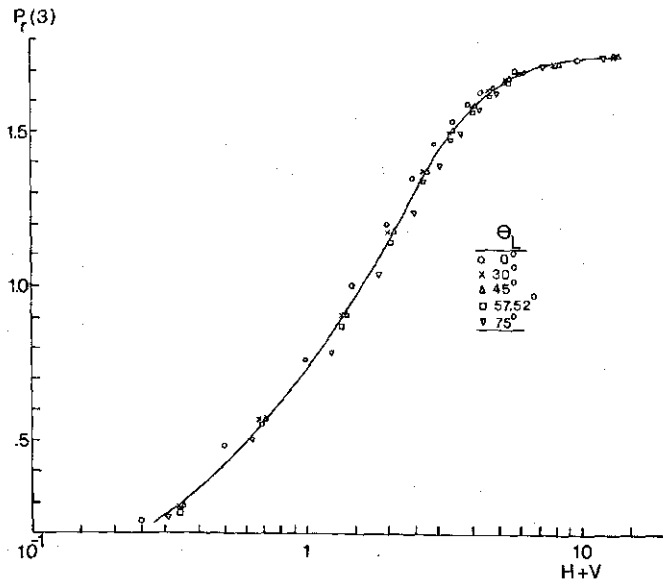


FIG. 126. Parameter,  $P_r(3)$ , for the hot spot as a function of  $H + V$ .  
 $\theta_o = \arctg 4/\pi$   
Leaf type: wheat. Soil type: dry sandy loam.



## 6. SELECTION OF OPTIMUM SPECTRAL BANDS FOR DISCRIMINATION BETWEEN VEGETATIVE CANOPIES

### 6.1. INTRODUCTION

In section 3.1., an analysis based on the variance within a given set of reflectance spectra has been described to determine those spectral regions in which maximum sensitivity to crop parameter variations is obtained.

After selection of a useful number of spectral bands in the visible light and the near infrared region, new parameters formed out of reflectance values at different wavelengths were found. These parameters have a causal relation with agricultural crop properties of interest, like the percentage of soil cover or leaf colour.

It was also demonstrated that such causal relations between spectral parameters and crop parameters can be highly improved, if detection takes place under hot spot condition and with carefully chosen view angles.

In this chapter, attention is paid to the question, how many and which spectral bands are necessary for discrimination between different crop types in relation with passive or active multispectral sensing techniques.

The methodology applied to automatic crop type (feature) discrimination using multispectral data is based on classification theory.

All canopy parameters, also with monocultures, like most agricultural crops, have stochastic properties. This holds for optical properties of the canopy components, leaf angle distribution, leaf density, reflectance of the bounding soil etc. Therefore the resulting directional spectral reflectance of each crop type shows stochastic variation. The statistical behaviour of reflected radiation by vegetative canopies plays an essential role.

Measurements of the radiation reflected by agricultural crops in  $N$  spectral bands within the wavelength region between 400 and 2500 nm are considered. These measurements are described by feature vectors,  $\underline{x}$ .

The performance of a classification algorithm depends on the initial choice of feature vector,  $\underline{x}$ , not only determined by the number of spectral bands, but also by their position and bandwidth.

Before the considerations leading to the analysis used in defining feature vector,  $\underline{x}$ , appropriate in discriminating between agricultural crops, are discussed, a basic principle of statistical feature classification is summarized.

In the so-called parametric method, applied in automatic feature discrimination, use is made of determined conditional probability functions of each feature and of decision rules.

Bayes' decision rule is given by the inequalities:

$$P(C_i|\underline{x}) \geq P(C_j|\underline{x}) \Rightarrow \underline{x} \in \begin{cases} C_i \\ C_j \end{cases} \quad j \neq i \quad (6.1.)$$

Category,  $C_i$ , is assigned to feature vector,  $\underline{x}$ , if the conditional probability of  $C_i$ , given  $\underline{x}$ , is greater than all the other conditional probabilities of categories,  $C_j$ , given  $\underline{x}$ .

Bayes' formula gives a relation between the conditional probability,  $P(C_i|\underline{x})$  and the conditional probabilities,  $P(\underline{x}|C_j)$  and the probabilities of the categories,  $P(C_j)$ , themselves.

$$P(C_i|\underline{x}) = \frac{P(\underline{x}|C_i)P(C_i)}{\sum_j P(\underline{x}|C_j)P(C_j)} = \frac{P(\underline{x}|C_i)P(C_i)}{P(\underline{x})} \quad (6.2.)$$

Substitution of Bayes' formula in Bayes' decision rule gives:

$$P(\underline{x}|C_i)P(C_i) \geq P(\underline{x}|C_j)P(C_j) \Rightarrow \underline{x} \in \begin{cases} C_i \\ C_j \end{cases} j \neq i \quad (6.3.)$$

For practical applications of Bayes' decision rule in automatic feature classification of remotely sensed data, without a priori knowledge about probabilities,  $P(C_j)$ , equal probabilities for all categories,  $C_j$  and continuous distribution functions for feature vectors,  $\underline{x}$ , are assumed. The maximum likelihood decision rule, based on these assumptions, expressed in conditional probability density functions is given by:

$$p(\underline{x}|C_i) \geq p(\underline{x}|C_j) \Rightarrow \underline{x} \in \begin{cases} C_i \\ C_j \end{cases} j \neq i \quad (6.4.)$$

Before assigning feature vector,  $\underline{x}$ , to one of the defined categories, a second condition must be fulfilled. The probability for  $\underline{x}$  to belong to a category,  $C_j$ , must exceed a threshold value.

For most homogeneous agricultural crops, the probability density functions,  $p(\underline{x}|C_j)$ , may be approximated by a multivariate Gaussian distribution, see ANDERSON (1958).

$$p(\underline{x}|C_j) = (2\pi)^{-N/2} |\Sigma_j|^{-1/2} \exp \left[ -\frac{1}{2} (\underline{x} - \underline{\mu}_j)^T \Sigma_j^{-1} (\underline{x} - \underline{\mu}_j) \right] \quad (6.5.)$$

Of each category,  $C_j$ , to be recognized automatically by processing multispectral data, mean vector,  $\underline{\mu}_j$  and covariance matrix,  $\Sigma_j$ , are calculated by means of samples selected from training areas. In practice, the maximum likelihood decision rule usually is not applied to the original data presented in the  $N$ -dimensional measurement space. When principal component analysis is applied on the training samples used, a number of principal axes, smaller than  $N$ , is determined with corresponding eigenvalues in descending order, representing significant information on the basis of feature variance. By accepting an upper bound of information loss, the dimension of the transformed decision space may be reduced drastically which improves processing efficiency; while displaying significant contrast variations along the principal axes in the feature space offers a useful tool for visual image interpretation.

The efficiency of a recording and processing system for remotely sensed multispectral data can be further improved, if the number of input data is

reduced by minimizing the number of spectral bands. If a minimum number of spectral bands is required, the accepted loss of information equivalent with information redundancy has to be determined. On the other hand, when a minimum number of already chosen spectral bands is required for crop parameter detection, the smallest increase with other spectral bands for crop discrimination purposes should be found, meeting the requirement of minimum information redundancy. Also, a reduction of spectral information could be employed to increase spatial information. Especially this aspect is of importance in remote sensing from satellites applied in agriculture, where a high ground resolution is required.

Information redundancy as an inherent property of feature vector,  $\underline{x}$ , consisting of  $N$  elements, is directly related with the existing correlations between the elements of  $\underline{x}$ , which may be made clear in the following way.

Divide feature vector,  $\underline{x}$ , into two subvectors,  $\underline{x}_1$  and  $\underline{x}_2$ .

$$\underline{x} = \begin{pmatrix} \underline{x}_1 \\ \underline{x}_2 \end{pmatrix} \quad (6.6.)$$

Subvector,  $\underline{x}_1$ , consists of  $q$  components, and  $\underline{x}_2$  of  $N-q$  components. Subvector,  $\underline{x}_1$ , does not contribute relevant information to  $\underline{x}$ , if  $\underline{x}_1$  can be well predicted from  $\underline{x}_2$ . In this case, the information redundancy of  $\underline{x}$  is mainly present in  $\underline{x}_1$ . If by deleting  $\underline{x}_1$  the upper bound of information loss is not exceeded, vector,  $\underline{x}$ , could be reduced to  $\underline{x}_2$  with dimension,  $N-q$ .

Principal component analysis as applied in chapter 3 to calculate the distribution of available information, due to crop parameter variation, over initially chosen wavelength bands, was used to exclude correlation present between the reflectance measured in spectral bands. With formula (3.16.), the contribution of each spectral band to the total variance of all bands together was found. As a consequence of this exclusion, the information content of each spectral band, relative to the total information content based on variance, should be defined by taking into account the variance in all other bands, predicted by the correlations present.

The usefulness of this approach is illustrated for the example of a two-band system with a high correlation between the two features  $x_1$  and  $x_2$ .

Transformation to principal axes is found by solution of quadratic equation (3.12.).

$$\begin{vmatrix} \sigma_{11}^2 - \lambda & \sigma_{12} \\ \sigma_{12} & \sigma_{22}^2 - \lambda \end{vmatrix} = 0 \quad (6.7.)$$

The correlation coefficient,  $\rho$ , is defined as:

$$\rho = \frac{\sigma_{12}}{\sigma_{11}\sigma_{22}} \quad -1 \leq \rho \leq 1 \quad (6.8.)$$

For a high correlation, the eigenvalues,  $\lambda_1$  and  $\lambda_2$ , found from (6.7.) are approximately equal to:

$$\begin{aligned}\lambda_1 &\approx \sigma_{11}^2 + \sigma_{22}^2 \\ \lambda_2 &\approx 0\end{aligned}\quad (6.9.)$$

After calculating both eigenvectors, a different information contribution of  $x_1$  and  $x_2$  is obtained.

$$\begin{aligned}C(x_1) &\approx \frac{\sigma_{11}|\rho|}{\sigma_{11}|\rho| + \sigma_{22}} (\sigma_{11}^2 + \sigma_{22}^2) \\ C(x_2) &\approx \frac{\sigma_{22}}{\sigma_{11}|\rho| + \sigma_{22}} (\sigma_{11}^2 + \sigma_{22}^2)\end{aligned}\quad (6.10.)$$

A high correlation between  $x_1$  and  $x_2$  is equivalent with high redundancy of information present in either  $x_1$  or  $x_2$ . The distribution of information, given by (6.10.), does not express redundancy due to its definition and is therefore not appropriate for determining the information content of each spectral band.

However, when either element,  $x_1$ , or element,  $x_2$ , of feature vector,  $\underline{x}$ , is known, the information content of  $\underline{x}$  can be determined due to the a priori knowledge of the high correlation between the elements of  $\underline{x}$ .

In the next section an algorithm is presented to calculate the information content of a subvector,  $\underline{x}_2$ , of feature vector,  $\underline{x}$ .

## 6.2. AN ALGORITHM FOR OPTIMUM SELECTION OF SPECTRAL BANDS

Small differences between canopy reflectance spectra, together with stochastic variations lead to misclassifications when automatic crop type discrimination is applied by means of decision rules. The probability of misclassification will increase, when the dimension of feature vector,  $\underline{x}$ , is reduced by deleting redundant spectral bands. For optimum spectral bands for discrimination between clusters of feature vectors, corresponding with a representative variety of green crop types, an upper bound for the increase of the probability of misclassification is required. The redundant spectral bands of  $\underline{x}$  are presented by subvector,  $\underline{x}_1$ , the optimum bands by subvector,  $\underline{x}_2$ .

The conditional probability density function of feature vector,  $\underline{x}$ , given crop category,  $C_j$ , is equal to the joint probability density function of subvectors,  $\underline{x}_1$  and  $\underline{x}_2$ , given  $C_j$ .

$$p(\underline{x}|C_j) = p(\underline{x}_1, \underline{x}_2|C_j) \quad (6.11.)$$

Because of the statistical dependence of  $\underline{x}_1$  and  $\underline{x}_2$ , a conditional probability density function,  $p(\underline{x}_1|\underline{x}_2|C_j)$ , for  $\underline{x}_1$  given  $\underline{x}_2$  and crop category  $C_j$  is introduced. The joint probability density function,  $p(\underline{x}_1, \underline{x}_2|C_j)$ , may be written as:

$$p(\underline{x}_1, \underline{x}_2|C_j) = p(\underline{x}_1|\underline{x}_2|C_j)p(\underline{x}_2|C_j) \quad (6.12.)$$

When the maximum likelihood decision rule is used for crop type classification, substitution of (6.12.) in (6.4.) gives:

$$p(x_1|x_2|C_i)p(x_2|C_i) \geq p(x_1|x_2|C_j)p(x_2|C_j) \Rightarrow x \in \begin{cases} C_i \\ C_j \end{cases} \quad (6.13.)$$

$M$  crop categories are considered. If  $p(x_1|x_2|C_j)$  is of the same order for all categories,  $j = 1, 2, \dots, M$ , the increase of the probability of misclassification by applying the maximum likelihood decision rule to subvector,  $x_2$ , could be minimized. This means that all  $M$  clusters are distributed closely in and around the regression space between  $x_1$  and  $x_2$ .

Otherwise, when the probability density of  $x_1$  can be predicted from  $x_2$ , independent of a priori knowledge of crop categories,  $C_j$ , the information content of  $x_2$ , relative to the information content of  $x$ , is high.

Due to the correlation between  $x_1$  and  $x_2$ , the variance of  $x_1$  and  $x_2$  is not statistically independent. Some variance of  $x_1$  can be predicted by a priori knowledge about the correlation between  $x_1$  and  $x_2$ . The information content of  $x_2$ , relative to the information content of  $x$ , expressed in terms of variance is thus defined as:

$$\frac{\text{variance of } x_2 + \text{variance of } x_1, \text{ predicted by } x_2}{\text{total variance of } x}$$

Only intercrop class variation is considered. Each feature vector,  $x$ , represents a crop category and is equal to the mean vector of a cluster of intraclass feature vectors. In section 6.5., attention will be paid to intraclass variation in relation to interclass variation and the occurrence of misclassifications using a Bayesian decision rule.

First, a formula for the information content of subvector,  $x_2$ , relative to the information content of feature vector,  $x$ , is derived for a two-dimensional feature space. The general result for a  $N$ -dimensional feature space is given afterwards.

The position of feature vectors,  $x$ , representing  $M$  clusters in the two-dimensional feature space spanned by  $x_1$  and  $x_2$  is presented in Fig. 127. The predicted value,  $\hat{x}_1$ , of  $x_1$  by means of the correlation between  $x_1$  and  $x_2$  follows from the regression equation:

$$\hat{x}_1 = \mu_1 + M(x_2 - \mu_2) \quad (6.14.)$$

The mean values of  $x_1$  and  $x_2$  are equal to  $\mu_1$  and  $\mu_2$ , respectively. The regression coefficient,  $M$ , is given by:

$$M = \frac{\sigma_{12}}{\sigma_{22}} = \frac{\sigma_{11}}{\sigma_{22}} \rho \quad (6.15.)$$

The regression coefficient is expressed in the covariance,  $\sigma_{12}$ , between  $x_1$  and  $x_2$  and the variance of  $x_2$ ,  $\sigma_{22}$ , or in the standard deviations,  $\sigma_{11}$ ,  $\sigma_{22}$  and the correlation coefficient,  $\rho$ .

The residual variance of  $x_1$ ,  $\sigma_{1.2}^2$ , relative to the regression line is found by substitution of (6.14.) in the definition equation for the variance.

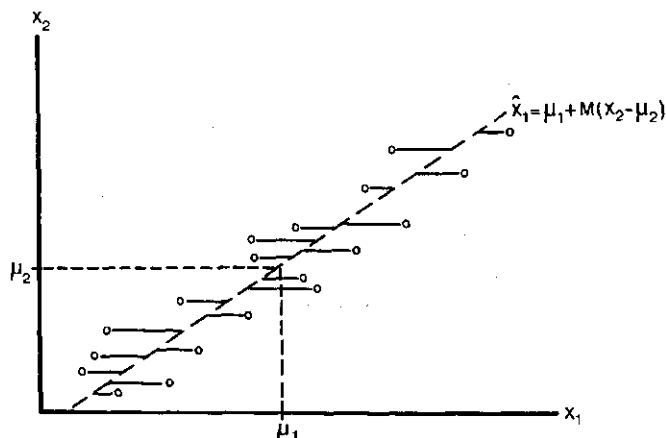


FIG. 127. Correlation between elements,  $x_1$  and  $x_2$ , of feature vector,  $\underline{x}$ . The free information of  $x_1$  is related with the residual variance of  $x_1$  relative to the regression line,  $\hat{x}_1 = \mu_1 + M(x_2 - \mu_2)$ .

$$\begin{aligned}\sigma_{11.2}^2 &= E[\{x_1 - \hat{x}_1 - E(x_1 - \hat{x}_1)\}^2] = \sigma_{11}^2 - \frac{\sigma_{12}^2}{\sigma_{22}^2} \\ &= \sigma_{11}^2(1 - \rho^2)\end{aligned}\quad (6.16.)$$

The variance of  $x_1$ , predicted by  $x_2$  by means of the correlation between  $x_1$  and  $x_2$  is defined by the difference between the variance of  $x_1$  and its residual variance.

The information content of  $x_2$ , relative to the information content of  $\underline{x}$ ,  $I(x_2)$ , is given by:

$$I(x_2) = \frac{\sigma_{22}^2 + \sigma_{11}^2 - \sigma_{11.2}^2}{\sigma_{11}^2 + \sigma_{22}^2} = \frac{\sigma_{22}^2 + \rho^2 \sigma_{11}^2}{\sigma_{11}^2 + \sigma_{22}^2} \quad (6.17.)$$

From this result it is concluded that a high correlation between  $x_1$  and  $x_2$  gives a high information content for  $x_2$ , whereas  $x_1$  contains redundant information. The information content of  $x_2$  in the absence of correlation with  $x_1$  is given by the variance of  $x_2$  relative to the variance of  $\underline{x}$ .

The information content of subvector,  $\underline{x}_2$ , of feature vector,  $\underline{x}$ , in the  $N$ -dimensional feature space is found in an analogous way. The predicted subvector,  $\hat{\underline{x}}_1$ , with mean value,  $\mu_1$ , as function of  $\underline{x}_2$  assuming linear regression is presented by the equation:

$$\hat{\underline{x}}_1 = \mu_1 + M(\underline{x}_2 - \mu_2) \quad (6.18.)$$

The regression matrix,  $M$ , with  $q$  rows and  $N-q$  columns is found by calculating the covariance matrix between  $\underline{x}_1 - \hat{\underline{x}}_1$  and  $\underline{x}_2 - \mu_2$ , which is equal to the zero matrix.

$$\begin{aligned}E\{(\underline{x}_1 - \hat{\underline{x}}_1)(\underline{x}_2 - \mu_2)^T\} &= 0 = E\{(\underline{x}_1 - \mu_1)(\underline{x}_2 - \mu_2)^T\} + \\ &- ME\{(\underline{x}_2 - \mu_2)(\underline{x}_2 - \mu_2)^T\}\end{aligned}\quad (6.19.)$$

The covariance matrix,  $\Sigma$ , of feature vector,  $\mathbf{x}$ , is partitioned into sub-matrices.

$$\begin{aligned} E\{(\mathbf{x} - \boldsymbol{\mu})(\mathbf{x} - \boldsymbol{\mu})^T\} &= E\left\{\begin{pmatrix} \mathbf{x}_1 \\ \mathbf{x}_2 \end{pmatrix} - \begin{pmatrix} \boldsymbol{\mu}_1 \\ \boldsymbol{\mu}_2 \end{pmatrix} \begin{pmatrix} \mathbf{x}_1 \\ \mathbf{x}_2 \end{pmatrix} - \begin{pmatrix} \boldsymbol{\mu}_1 \\ \boldsymbol{\mu}_2 \end{pmatrix} \right\}^T = \\ &= \begin{pmatrix} E\{(\mathbf{x}_1 - \boldsymbol{\mu}_1)(\mathbf{x}_1 - \boldsymbol{\mu}_1)^T\} & E\{(\mathbf{x}_1 - \boldsymbol{\mu}_1)(\mathbf{x}_2 - \boldsymbol{\mu}_2)^T\} \\ E\{(\mathbf{x}_2 - \boldsymbol{\mu}_2)(\mathbf{x}_1 - \boldsymbol{\mu}_1)^T\} & E\{(\mathbf{x}_2 - \boldsymbol{\mu}_2)(\mathbf{x}_2 - \boldsymbol{\mu}_2)^T\} \end{pmatrix} = \\ &= \begin{pmatrix} \Sigma_{11} & \Sigma_{12} \\ \Sigma_{21} & \Sigma_{22} \end{pmatrix} \end{aligned} \quad (6.20.)$$

Introduction of subcovariance matrices,  $\Sigma_{12}$  and  $\Sigma_{22}$ , defined by (6.20.) into (6.19.) gives for  $M$ :

$$M = \Sigma_{12}\Sigma_{22}^{-1} \quad (6.21.)$$

Analogous to equation (6.16.), the residual covariance matrix,  $\Sigma_{11.2}$ , of  $\mathbf{x}_1$  follows directly from substitution of (6.18.) in the equation:

$$\Sigma_{11.2} = E\{(\mathbf{x}_1 - \hat{\mathbf{x}}_1)(\mathbf{x}_1 - \hat{\mathbf{x}}_1)^T\} \quad (6.22.)$$

The residual covariance matrix, as a function of subcovariance matrices is presented by:

$$\Sigma_{11.2} = \Sigma_{11} - \Sigma_{12}\Sigma_{22}^{-1}\Sigma_{12}^T \quad (6.23.)$$

A measure for the information content of feature vector,  $\mathbf{x}$ , is defined by the total variance of  $\mathbf{x}$ , given by the trace of covariance matrix,  $\Sigma$ . The trace is equal to the sum of all diagonal elements,  $\sigma_{ij}^2$  and is invariant for an orthogonal basis transformation. This implies that the sum of the variances of the original elements of  $\mathbf{x}$  is equal to the sum of the eigenvalues of covariance matrix,  $\Sigma$ . The advantage of this property of the trace is that for determining the information content of  $\mathbf{x}$ ,  $\mathbf{x}_1$  or  $\mathbf{x}_2$  transformations to principal axes of  $\Sigma$ ,  $\Sigma_{11}$  or  $\Sigma_{22}$  are not demanded.

The predicted variance of  $\mathbf{x}_1$ , taking into account the statistical dependence of  $\mathbf{x}_1$  and  $\mathbf{x}_2$ , is defined by the trace of  $\Sigma_{11} - \Sigma_{11.2}$ . The final result for the information content of subvector,  $\mathbf{x}_2$ , relative to the information content of  $N$ -dimensional feature vector,  $\mathbf{x}$ , is presented by the following equation.

$$I(\mathbf{x}_2) = \frac{\text{Tr}\Sigma_{22} + \text{Tr}\Sigma_{12}\Sigma_{22}^{-1}\Sigma_{12}^T}{\text{Tr}\Sigma} \quad (6.24.)$$

When this algorithm is applied to spectral radiance or reflectance data of crops, some remarks concerning non-linear relations have to be made. In Section 5.3 it has been demonstrated that, when small variations in the average leaf inclination angle are assumed, the regressions between spectral bands either within the visible light region or within the near infrared plateau or within the water absorption region are in general linear. If a spectral band in the near infrared plateau is compared with a spectral band in the visible light or in the water absorption region, the regressions are non-linear. This is schematically illustrated by a two-colour diagram of green canopy reflectance in the red and near infrared, given in Fig. 128.

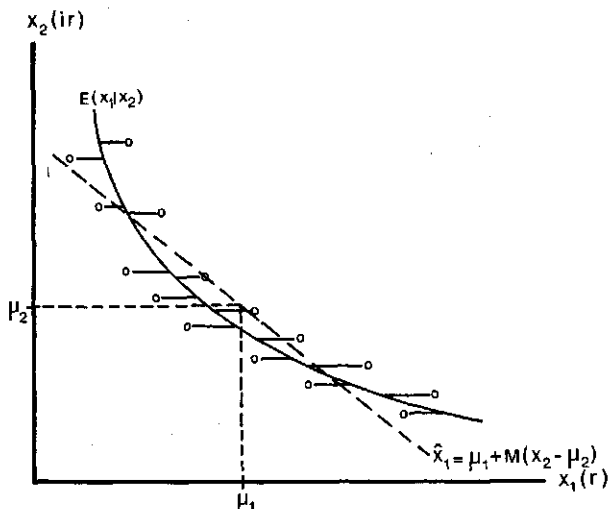


FIG. 128. Non-linear regression between  $x_1$  and  $x_2$  as present between red and near infrared reflectance of green canopies. The residual variance of  $x_1$  relative to the non-linear regression line,  $E(x_1 | x_2)$ , is smaller than the residual variance in case of linear regression.

The non-linear regression line has to be estimated by integration over  $x_1$  weighted by the conditional probability density function of  $x_1$ , when  $x_2$  is given.

$$\hat{x}_1 = \hat{x}_1(x_2) = E(x_1|x_2) = \int x_1 p(x_1|x_2) dx_1 \quad (6.25.)$$

As a result of such a non-linear regression analysis, the residual variance of  $x_1$ , given  $x_2$ , is smaller compared with the residual variance belonging to linear regression. This increases the information content of  $x_2$ . In a multi-dimensional case the trace of  $\Sigma_{11.2}$  is smaller, when non-linear regression analysis is applied, which effects an increase in the information content of subvector,  $\hat{x}_2$ . Therefore, it is expected that linear approximation of multi-spectral canopy reflectance behaviour deteriorates the information content found in sub-feature vector,  $x_2$ , with dimension,  $N-q$ .

The procedure of determining optimum spectral bands, presented by subvector,  $\hat{x}_2$ , for crop type discrimination meeting the requirements for maximum information and minimum dimension is as follows:

1. Initially,  $N$  spectral bands between 400 and 2500 nm and within the atmospheric windows are chosen based on physical and instrumental requirements.
2. A set of  $M$   $N$ -dimensional feature vectors, representing the mean vectors of  $M$  crop categories is chosen. The  $N \times N$  covariance matrix,  $\Sigma$ , of this set of feature vectors is calculated.
3. First, of each (one-dimensional) element,  $x_{2k}$ , out of  $\hat{x}_2$ , the information content,  $I(x_{2k})$ , is calculated with algorithm (6.24.).
4. When the maximum information content of the single spectral band,  $x_{2k}$ ,



is established, two-dimensional subvectors,  $\underline{x}_{2k}$ , are formed stepwise out of the best single band and another second band.

5. The two-dimensional subvector,  $\underline{x}_{2k}$ , with maximum information content is used to form three-dimensional subvectors,  $\underline{x}_{3k}$ , etc.
6. An upper bound for the loss of information, present in the  $N$ -dimensional feature vector,  $\underline{x}$ , is set.
7. When the information content of the  $N$ - $q$ -dimensional subvector,  $\underline{x}_{2k}$ , no longer satisfies this bound, the procedure stops. The subspace spanning  $\underline{x}_{2k}$  equivalent to optimum spectral bands is determined.

In Chapter 5 it has been demonstrated that reflectance measurements in the green, the red and the near infrared plateau are useful in extracting crop properties out of multispectral data. For that reason, the first subspace spanning,  $\underline{x}_{2k}$ , with three dimensions is based on this initial choice. The procedure of calculating the optimum subspace of  $\underline{x}_2$  is analogous to the method previously discussed. It is stated that  $\underline{x}_2$  spanned by the three initially chosen bands and others added afterwards by the algorithm (6.24.) should not be, a priori, the best choice for optimum crop class discrimination.

### 6.3. CALCULATION OF OPTIMUM WAVELENGTH BANDS USING SUITS' MODEL

The algorithm derived to obtain an optimum choice of spectral bands for crop type discrimination has been applied to spectra generated by means of Suits' model. Twelve spectral bands have been chosen in accordance with characteristic positions on the reflectance spectrum of green vegetation and outside regions of high absorption of electromagnetic radiation by the earth's atmosphere (see Fig. 2). The wavelength values selected for model simulations together with the band width of 12 spectral bands as applied to field reflectance data are indicated in Fig. 129. Spectral reflectance of a single wheat leaf as given by GAUSMAN *et al.* (1971) is presented with an example of the solar irradiance at ground level attenuated by the selective absorptance of the atmosphere.

The initially chosen wavelengths, based on the analysis treated in Chapter 5, are indicated as band 3, 5 and 8. In the visible light region, three extra bands have been chosen to characterize spectral reflectance in the blue, the blue-green and the yellow part of the visible light. Spectral bands 6 and 7 in the near infrared are positioned where usually optimum contrast occurs between reflectance of canopies with a high leaf area index and the bare soil. Spectral bands 8 and 9 coincide with the wavelength region of minimum radiation absorptance of single green leaves. At the end of the infrared plateau, where absorptance of radiation by the water in the canopy components grows significant, spectral band 10 has been chosen.

Reflectance behaviour in the water absorption region between 1300 and 2500 nm is sufficiently characterized by two wavelength values, which almost coincide with maximum atmospheric transparency and with relative minima of leaf absorptance.

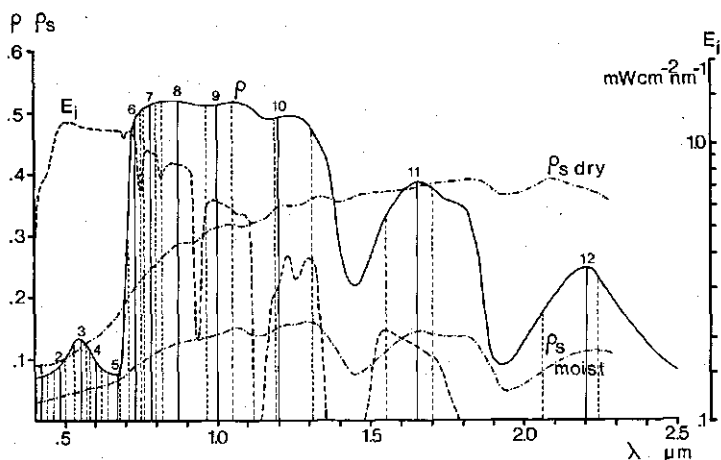


FIG. 129. Position of twelve selected wavelengths and wavelength bands relative to the reflectance spectrum of a single wheat leaf. An example of the trend in the solar irradiance at ground level and reflectance spectra of a dry and a moist sandy loam soil are included.

Variation of canopy reflectance has been simulated by taking 20 canopy structures obtained by combinations of two series of  $L$  and  $\theta_L$ .

Only homogeneous canopies have been assumed. The twelve-dimensional feature vectors have been calculated for the three green leaf types, wheat, bean and maize leaves with rather different optical properties, as chosen in Chapter 5. All spectra have been calculated substituting spectral reflectance of the standard dry and moist sandy loam soil. All canopy input parameters are presented in Table 12.

TABLE 12. Canopy input parameters used to calculate 12-dimensional feature vectors of canopies with varying structure, leaf colour and soil moisture content.

No.	Wave-length nm	Wheat		Bean		Maize		Sandy loam	Soil	$\frac{E-(0)}{E_s(0)}$
		$\rho$	$\tau$	$\rho$	$\tau$	$\rho$	$\tau$	$\rho_s$	$\rho_s$	
1	420	0.071	0.007	0.101	0.029	0.084	0.009	0.091	0.03	0.64
2	480	0.089	0.014	0.139	0.052	0.113	0.025	0.1	0.041	0.51
3	550	0.135	0.055	0.185	0.109	0.162	0.098	0.126	0.051	0.388
4	600	0.096	0.021	0.12	0.055	0.12	0.037	0.137	0.053	0.355
5	670	0.075	0.007	0.102	0.035	0.091	0.007	0.175	0.065	0.299
6	730	0.486	0.384	0.535	0.37	0.442	0.42	0.222	0.09	0.255
7	780	0.51	0.427	0.567	0.417	0.461	0.502	0.25	0.107	0.22
8	870	0.52	0.44	0.567	0.42	0.463	0.51	0.286	0.126	0.2
9	1000	0.512	0.446	0.562	0.422	0.457	0.512	0.315	0.141	0.2
10	1200	0.488	0.436	0.535	0.4	0.432	0.498	0.351	0.155	0.145
11	1650	0.382	0.368	0.409	0.322	0.329	0.43	0.38	0.145	0.129
12	2200	0.244	0.247	0.24	0.197	0.198	0.303	0.37	0.115	0.157
$L$	0.5	1	1.5	3	6					
$\theta_L$	30°	45°	57.52°	75°						

TABLE 13. Specifications of the covariance matrices 1 to 4 of passive detected feature vectors ( $\Sigma_p$ ) and 6 to 14 of active detected feature vectors ( $\Sigma_a$ ).

$\Sigma_p$	$Q^*$	$K^{**}$	$\theta_s$	$\theta_o$	$\Sigma_a$	$Q$	$K$	$\hat{\theta}_o$
1	1	3	30°	0°	6	1	3	51.8°
2	2	3			7	2	3	
3	1+2	3			8	1+2	3	
4	1	1			9	1	1	
5	2	1			10	2	1	
					11	1	3	30°
					12	1	3	40°
					13	1	3	60°
					14	1	3	75°

\*  $Q = 1$  : dry sandy loam soil,  
 $Q = 2$  : moist sandy loam soil.

\*\*  $K = 1$  : wheat leaf,  
 $K = 3$  : three leaf types.

This set of 120 feature vectors has been calculated simulating passive as well as active detection. For passive detection, a solar angle of 30° and a view angle of 0° have been chosen. The simulations for active scanning have been performed for oblique view angles of 30°, 40°, 51.8°, 60°, 75° and without diffuse sky irradiance.

Each feature vector as calculated with Suits' model is considered as the mean vector of the crop categories. Out of a set of available mean vectors, 14 covariance matrices have been calculated. The covariance matrices refer to passive and active detection, the assumption of a dry or a moist soil, a combination of the mean vectors for the three leaf types together, or combination of all spectra with a dry and a moist soil or spectra derived from one leaf type only.

The covariance matrices used, are specified in Table 13.

All covariance matrices have been calculated for transformed canopy reflectance data according to formula (3.7.). The following estimation for the matrix elements,  $\sigma_{ij}$ , has been applied.

$$\sigma_{ij} = \frac{1}{N-1} \sum_{k=1}^N x_{ik}x_{jk} = \frac{N}{N-1} \left\{ N \frac{\sum_k r_{ik} r_{jk}}{\sum_k r_{ik} \sum_k r_{jk}} - 1 \right\} \quad (6.38.)$$

#### 6.3.1. Passive detection

The information content of subvector,  $x_2$ , formed by spectral bands 3, 5, 8 and additionally selected bands has been calculated by means of a computer program written for algorithm (6.24). The maximum accepted loss of information relative to the information obtained from the 12 spectral bands is taken equal to 1%. Diagrams presenting the dimension and specifying the spectral bands belonging to the covariance matrices 1 to 5 are given in Fig. 130. The information content of  $x_2$  consisting of bands 3, 5 and 8 alone, in all cases exceeds 95% of the total information. When the leaf type varies with a dry or a

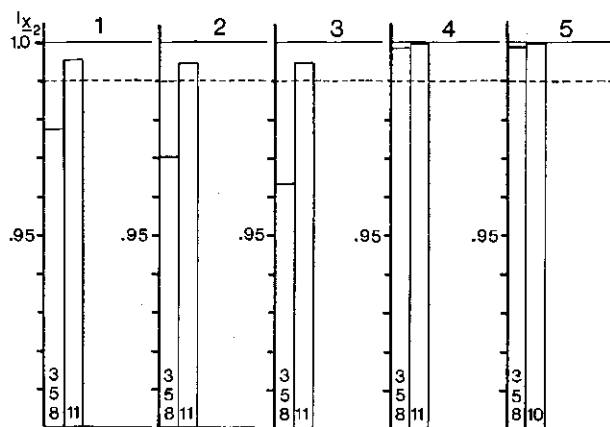


FIG. 130. Selection of vector,  $\underline{x}_2$ , from spectral bands 3, 5, 8 and the others for the covariance matrices 1 to 5 of passive canopy reflectance detection.

FIG. 131. Distribution of the contribution of the remaining spectral bands to vector,  $\underline{x}_2$ , for covariance matrix No. 3. The selected bands are indicated by a cross.

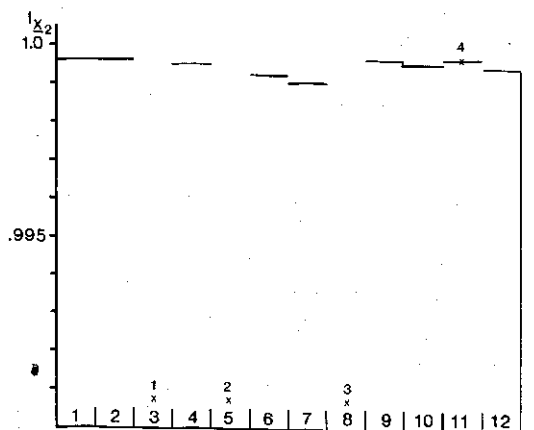
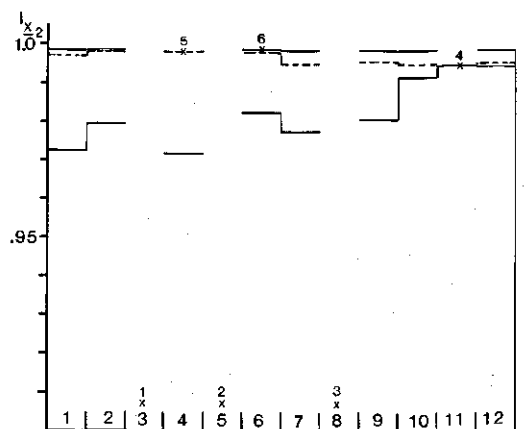


FIG. 132. Distribution of the contribution of a fourth band added to vector,  $\underline{x}_2$ , formed by bands 3, 5 and 8, for covariance matrix No. 4. The canopy structure is the only variable.

FIG. 133. Selection of vector,  $\underline{x}_2$ , by addition of optimum spectral bands for the covariance matrices 1 to 5 of passive canopy reflectance detection.

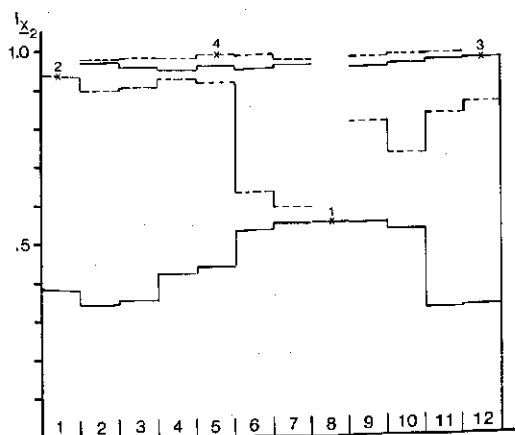
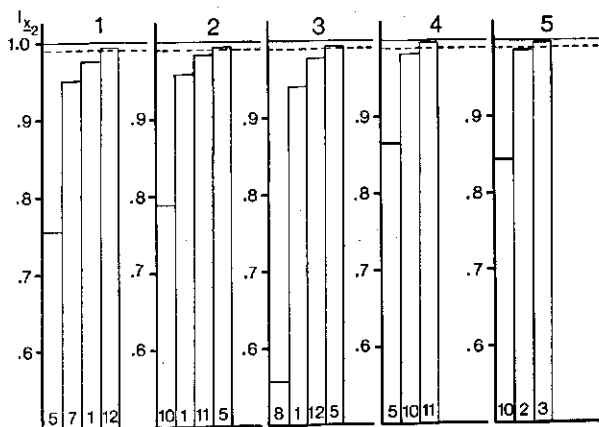


FIG. 134. Distribution of the contribution of added spectral bands to subvector,  $\underline{x}_2$ , for covariance matrix No. 3.

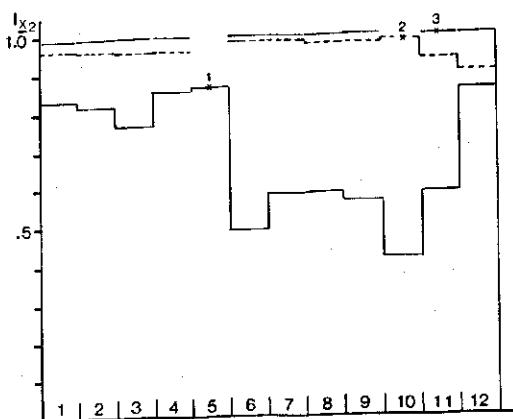


FIG. 135. Distribution of the contribution of added spectral bands to subvector,  $\underline{x}_2$ , for covariance matrix No. 4.

moist soil, spectral band 11 is added to bring the information content of this four-dimensional vector at a maximum value of over 99%. In the presence of one leaf type only, e.g. wheat leaves, the three wavelengths alone are sufficient to obtain more than 99% information.

The contribution of each remaining spectral band to the information content of  $x_2$  is shown in Fig. 131 for covariance matrix No. 3. Owing to the rather close correlations due to the simplified simulation of reality by means of the reflectance model, the contribution function, when the subvector,  $x_2$ , exceeds a dimension equal to 4, is almost invariant to the wavelength values.

Covariance matrix 4, based on spectra of a varying crop structure only and a dry soil, e.g. yields information distribution which is already invariant to the remaining wavelength bands, when bands 3, 5 and 8 are initially chosen. This distribution for the fourth band is presented in Fig. 132.

To investigate the difference between the results based on the, a priori, choice of bands 3, 5 and 8, combined with one or more remaining bands, calculations have been performed using the same covariance matrices, but starting from a dimension of  $x_2$  equal to one. The elements and the increase of the dimension of  $x_2$  are presented in Fig. 133.

With leaf type variation and a dry soil, band 5 in the red has been selected as the best spectral band followed by band 7 in the near infrared plateau. Due to the non-linear regression between band 5 and the bands in the near infrared plateau, one of these bands has been chosen. Band 5 and 7 together contain already 95% of the total information. The difference between the contribution of the spectral bands in the near infrared plateau, when band 7 is selected is at most 0.5%. Then, when band 1 is added, the difference between the contribution of band one and the others lies between 96.3% and 97.7%. Together with band 12 as the fourth band, these four bands contain over 99% of the information of  $x$ .

The second covariance matrix, concerning the same canopy variations, but with a moist soil leads to a different result. When band 10 in the near infrared plateau is chosen as a first band, with an information content of 78.8%, the information content of band 5 is only 17.8%; because the dark soil causes a considerable reduction in contrast in band 5. From the diagram it can be concluded that also four spectral bands are sufficient to obtain over 99% of the available information.

When the same calculations are repeated for covariance matrix No. 3, where spectra for a light and a dark soil were combined, the required dimension of  $x_2$  is also equal to four. Instead of bands 10 and 11, bands 8 and 12 are chosen. With a varying crop structure only, as simulated by covariance matrices 4 and 5, three spectral bands are sufficient to represent almost 100% of the total information. The distribution of the information over the chosen spectral bands for covariance matrix No. 3 is presented in Fig. 134. Combination of spectra of canopies with a light and dark soil yields maximum information in the infrared plateau (compare this distribution with the distribution given by Fig. 52 obtained by principal component analysis).

After selection of band 8, the optimum contribution comes from the visible light region with band 1 as the optimum one. Since there is a close correlation between band 8 and bands 6 and 7, the contribution of 6 and 7 combined with 8 are significantly lower than the contributions from bands of the visible light region with band 8. The distribution diagram for covariance matrix No. 4 is given in Fig. 135. The trend in the distribution in single bands may be compared with the curve of a dry soil in Fig. 50. Maximum information is present in the red spectral band, minimum information in band 10. A combination of both bands brings the information of a two-dimensional vector up to the maximum value of 98.3%.

### 6.3.2. Active detection

In section 5.6. it has been proved with model simulations that for (active) detection in the canopy hot spot under view angles of  $0^\circ$  and  $51.8^\circ$ , the spectral reflectance is a linear function of the soil cover percentage.

This property highly improved the relationship between spectral parameters formed by algebraic combinations of the canopy reflectance in different spectral bands and specific canopy properties.

It has been shown that the distribution of the feature vectors in the three-dimensional feature space of canopies with constant optical properties of the leaves, was transformed from curved planes to lines. It is obvious that such a useful simplification deteriorates discrimination between the feature vectors of different crops. Hot spot detection under these specific view angles drastically decreases the possibility of crop type discrimination, when great differences in the leaf angle distribution function are present and the canopies considered may be assumed as homogeneous. The loss of available information has to be related to the information content resulting from other bidirectional detection geometries. For practical reasons, the loss of information is taken relative to the information available from the passive detection geometry, used in the previous section. This relative loss,  $l_j(\underline{x})$ , is expressed by means of the traces of the  $12 \times 12$  covariance matrices transformed to their principal axes and concerning the same canopy parameter variations.

$$l_j(\underline{x}) = \frac{\text{Tr}A_{pj} - \text{Tr}A_{aj}}{\text{Tr}A_{pj}} = \frac{\text{Tr}\Sigma_{pj} - \text{Tr}\Sigma_{aj}}{\text{Tr}\Sigma_{pj}} \quad (6.39.)$$

$\text{Tr}\Sigma_{pj}$  = Trace of covariance matrix  $j$  calculated for passive detection  
( $\theta_s = 30^\circ$ ,  $\theta_o = 0^\circ$ )

$\text{Tr}\Sigma_{aj}$  = Trace of covariance matrix  $j$  calculated for active detection  
( $\theta_s = \theta_o = 51.8^\circ$ ,  $\psi = 0$ )

Table 14 presents the relative information loss for a comparison between covariance matrices 1 to 5 and 6 to 10.

From Table 14 it is concluded that for a moist soil the information loss is lower, because the relative contrast variation between open and closed canopies is high in all 7 bands in the infrared, see Fig. 129. Reducing the canopy variety to only one leaf type increases the information loss, especially with a dry soil.

TABLE 14. Relative loss of information on canopy discrimination by means of hot spot detection under a view angle of  $51.8^\circ$ .

j	$\Sigma_{pj}$	$\Sigma_{aj}$	$\text{Tr}\Sigma_{pj}$	$\text{Tr}\Sigma_{aj}$	$I(x)\%$
1	1	6	0.8825	0.3159	64.204
2	2	7	0.9721	0.6534	32.785
3	3	8	0.9195	0.4805	47.743
4	4	9	0.9485	0.2302	75.730
5	5	10	0.8182	0.4957	39.415

Crop discrimination using hot spot detection could be improved, when another view angle is chosen instead of  $\hat{\theta}_o = 51.8^\circ$ .

Feature vectors have been calculated for all three leaf types and assuming a dry soil, for the hot spot condition detected with view angles of  $30^\circ$ ,  $40^\circ$ ,  $60^\circ$  and  $75^\circ$ , respectively. The trace of the covariance matrix of the transformed reflectance data as a function of the angle of view is given in Fig. 136.

The trace has a minimum value for a view angle between  $60^\circ$  and  $70^\circ$ . This minimum could be determined by solving the equation:

$$\frac{\partial}{\partial \theta_o} \text{Tr}\Sigma = \sum_{i=1}^{12} \frac{\partial}{\partial \theta_o} [E(r^2(\lambda_i)) - \{E(r(\lambda_i))\}^2] = 0 \quad (6.40.)$$

By means of this example it is obvious that for oblique view angles, discrimination between crop categories using hot spot detection is more difficult than that with bidirectional detection under perpendicular view. This is caused by the disappearance of the observed amount of shadow inside the canopies. The amount of shadow observed inside a homogeneous canopy and on the visible fraction of the soil is given by:

$$\begin{aligned} f_s &= (1 - e^{-k})e^{-K} + \int_{-1}^0 (1 - e^{Kx'})e^{Kx'} dx' \\ &= (1 - e^{-k})e^{-K} + \frac{1 - e^{-K}}{K} - \frac{1 - e^{-(K+k)}}{K+k} \end{aligned} \quad (6.41.)$$

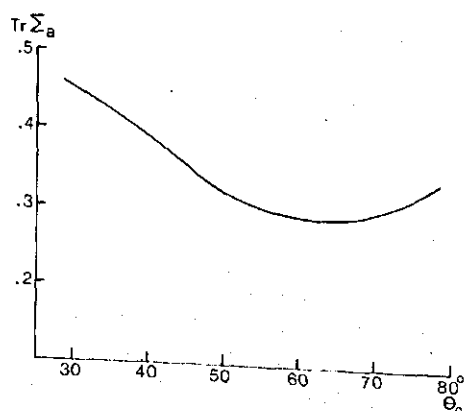


FIG. 136. Trace of covariance matrix,  $\Sigma_a$ , of hot spot detection as a function of view angle,  $\theta_o$ .  $\Sigma_a$  has been calculated for the three leaf types together and a dry sandy loam soil.



FIG. 137. Selection of vector,  $\mathbf{x}_2$ , by addition of optimum spectral bands for the covariance matrices 6 to 10 of active canopy reflectance detection.

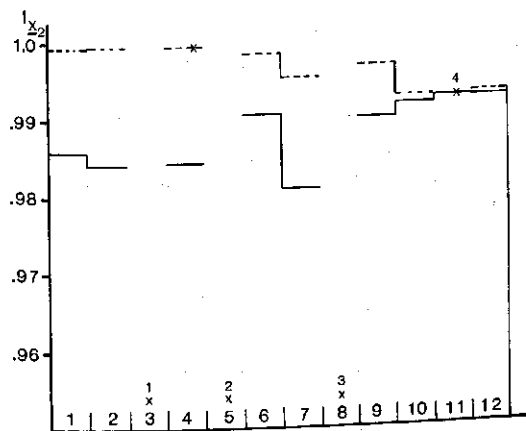
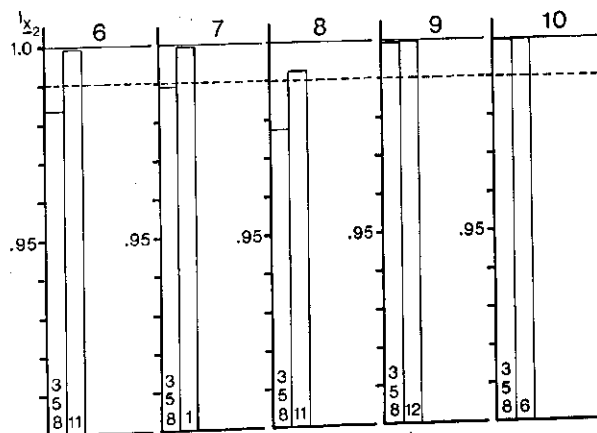
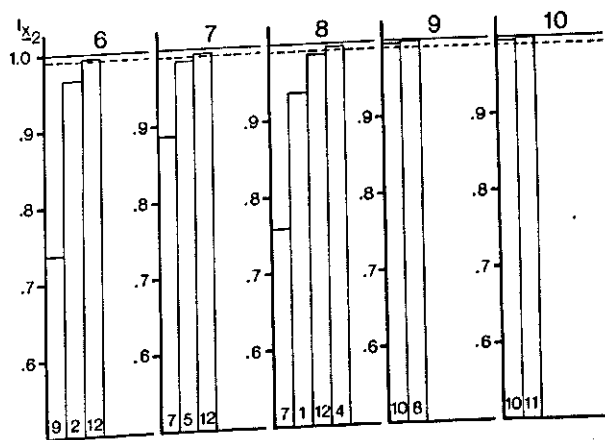


FIG. 138. Distribution of the contribution of the remaining spectral bands to the information of vector,  $\mathbf{x}_2$ , for covariance matrix 8.

FIG. 139. Selection of vector,  $\mathbf{x}_2$ , by addition of optimum spectral bands for the covariance matrices 6 to 10 of active canopy reflectance detection.



For the hot spot condition the joint probability,  $e^{-(K+k)}$ , becomes  $e^{-K}$ ; from (6.41.) it is seen that for this case the fraction of shadow,  $f_s$ , disappears. Average leaf inclination angle variations with a given leaf area index cause a variable amount of observed shadow. Due to this the feature vectors in the feature space belonging to bidirectional (passive) detection diverge, improving crop category discrimination.

Analogous to the examples shown for passive detection, Fig. 137 presents the subvectors,  $\underline{x}_2$  formed out of bands 3, 5, 8 and added ones containing more than 99% information of  $\underline{x}$  for the covariance matrices 6 to 10.

The selection of band 1 instead of 11 together with bands 3, 5 and 8 for covariance matrix 7 is based on a difference of only 0.01%. The distribution function of the information after selection of bands 3, 5 and 8 for covariance matrix 8 is presented in Fig. 138.

When the extraction of  $\underline{x}_2$  out of  $\underline{x}$  is started with the optimum single band, the results for the covariance matrices 6 and 10 are as given in Fig. 139. For a dry or a moist soil, only three spectral bands instead of four are necessary to obtain more than 99% of the total information. The best single band with a dry soil is not the red band as found for passive detection under perpendicular view, but band 9 in the near infrared.

This is explained by the reduced contrast variation in the red due to the oblique view angle by which the bounding soil is better screened by the canopy. When covariance matrix No. 8 of the reflectance data with a dry and moist soil together is used, a fourth band is needed to exceed 99%.

The distribution of the information of  $\underline{x}_2$  during addition of new selected bands is presented in Fig. 140. In the visible light, a relative maximum for band 3 is found due to leaf colour differences. An information analysis applied to covariance matrices 9 and 10, related to canopy structure variations only, gives one spectral band which is sufficient to obtain over 99% information.

This conclusion affirms the close correlations already found in section 5.6. between all spectral bands. Out of the dynamic behaviour of one spectral band, the response in all other bands is predicted with a high accuracy. The distribu-

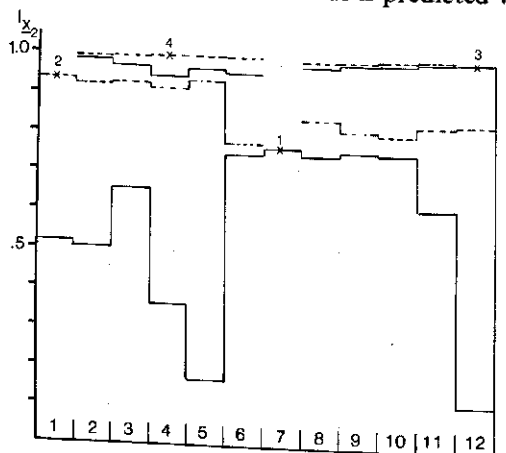
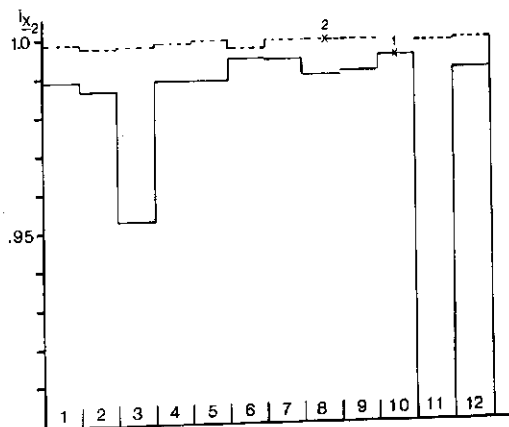


FIG. 140. Distribution of the contribution of selected subvectors,  $\underline{x}_2$ , to the total information content for covariance matrix 8.

FIG. 141. Distribution of the combination of selected subvectors,  $\lambda_2$ , to the total information content for covariance matrix 9.



tion of information for covariance matrix 9 is presented in Fig. 141. Band 11 alone contributes only 68.23%, because accidentally single leaf reflectance is almost equal to reflectance of the dry soil.

#### 6.4. EXPERIMENTAL RESULTS

A covariance matrix has been calculated of mean reflectance data obtained with the field spectrometer during the measurement campaign in 1974, at the test-site at Wageningen. From measurements on the 14 crop types, 120 mean reflectance vectors have been calculated of merely green leaf canopies. These mean reflectance vectors belong to different stages of growth of the crops and are estimated by taking average reflectance in the twelve spectral bands given in Table 15 and indicated in Fig. 129. All the mean vectors have been transformed to zero mean value and all the elements are weighted by ratioing by the corresponding mean of all the elements according to formula (3.7.).

TABLE 15. Spectral bands used to calculate mean reflectance value in 12 bands of the field spectrometer data.

Band	Bandwidth	Wavelength region
1	400- 440 nm	Visible light
2	460- 500	
3	530- 570	
4	580- 620	Near infrared plateau
5	640- 680	
6	710- 750	
7	760- 800	
8	820- 870	
9	965-1050	Water absorption
10	1190-1310	
11	1550-1700	
12	2060-2240	

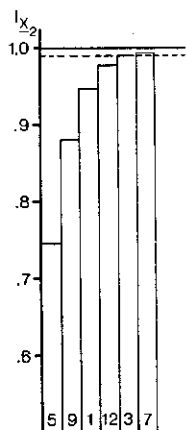


FIG. 142. Selection of vector,  $x_2$ , by addition of optimum spectral bands for the covariance matrix of 120 mean spectra measured with the field spectrometer.

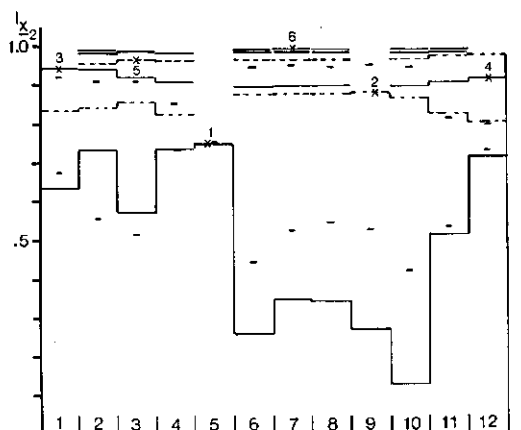


FIG. 143. Distribution of the contribution of added spectral bands to subvector,  $x_2$ , for the covariance matrix of field reflectance data. The distribution for covariance matrix 1 is indicated by dashes.

The optimum subvector,  $x_2$ , found, when the selection is started from the best single band is presented in Fig. 142.

The distribution of information during the increase of the dimension of  $x_2$  is given in Fig. 143.

The distribution of information as obtained from covariance matrix 1 with the simulated spectra by using Suits' model is included in Fig. 143 for the selection of the first and second band and presented by means of dashes. Both distributions correspond qualitatively quite well in spite of the differences due to the model input, like the presence of direct solar irradiance and the restriction of using homogeneous canopy models only. Band 5 in the red part of the visible light region is selected first, afterwards band 9, 1 and 12. From Fig. 143 it is concluded that the difference between the information increase by combining band 5 with 7 or 9 is hardly significant. The total variance or the trace of the covariance matrix of the field spectrometer data is equal to 2.0281. This larger value compared with the simulated values is due to the larger range of the varying leaf area index, the presence of spectra of dead biomass as obtained by measurements of recently mown grass canopies and the presence of some spectra of senescing canopies, like oats and wheat. This probably gives rise to the relatively higher information content of bands in the visible light region compared with the near infrared plateau. It is also expected that the larger variations within the leaf area index range of the experimental data, together with the larger heterogeneity within these data will increase the non-linear regressions between the elements of the mean vectors. The analysis applied and based on the assumption of linear regression, results into an increase in the dimension of subvector,  $x_2$ . After selection of band 12, band 3 and 7 are selected to obtain more than 99% of the total information available.

TABLE 16. Agricultural crops, selected to extract training data to calculate covariance matrices (Test farm – Proefstation voor de Akkerbouw, Lelystad – 30 July 1975).

Crop class	Crop type	Maturing stage
1	Oats	Senescing
2	Winter wheat	Senescing
3	Bare soil	—
4	Flax	Senescing
5	Poppy-seed	Mature
6	Sugarbeets	Mature
7	Summer barley	Senescing
8	Winter wheat	Senescing
9	Potatoes	Mature
10	Maize	Mature
11	Winter wheat	Senescing
12	Winter wheat	Senescing

Airborne multispectral scanner data have been used to test the algorithm for the extraction of an optimum number of spectral bands. Data obtained from an agricultural test farm, Proefstation voor de Akkerbouw, Lelystad, the Netherlands, collected at 6,000 feet flight height on 30 July 1975, have been selected (BUNNIK *et al.*, 1977).

The scanner used and manufactured by Daedalus Enterprises, Ann Arbor, Michigan, had 10 spectral channels as specified in Table 7. Training samples from 11 standing agricultural crops and bare soil have been used. These crops and their maturing stage are given in Table 16. Covariance matrices have been calculated using the signals from channels 3 to 10 for all 12 spectral classes together, for potatoes, sugarbeets, maize and poppy-seed and also for potatoes and sugarbeets alone. All covariance matrices are calculated with the scanner radiance data according to the transformation as given by formula (3.7.). This transformation also eliminates the signal gain factors which are different for each spectral channel.

For all twelve spectral categories, the calculation of  $\bar{x}_2$  and the distribution of information over the channels added to  $\bar{x}_2$  are presented in Figs. 144 and 145.

The original channel numbers 3 to 10 are renumbered from 1 to 8. A sub-vector formed by spectral bands in the red, the near infrared plateau and the green, already yields over 98% of the information relative to the total wavelength interval of the scanner. Five recorded channels out of a total of eight represent more than 99% of the information.

When the training data of crops in senescence are excluded, the total variance is drastically reduced. The traces of the covariance matrices for the 12 categories, for a combination of training data from potatoes, sugarbeets, maize and of poppy-seed and for training data from potatoes and sugarbeets only are presented in Table 17. Fig. 146 gives the selection of vector,  $\bar{x}_2$ , for the four crop categories. Fig. 147 shows the influence of restriction to two green canopies with 100% cover percentage on the selection of  $\bar{x}_2$ .

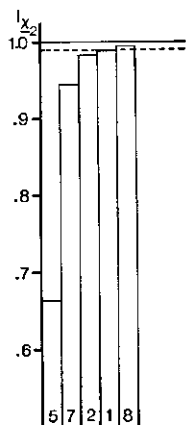


FIG. 144. Selection of vector,  $x_2$ , by addition of optimum spectral bands for the covariance matrix of scanner data of 12 spectral categories.

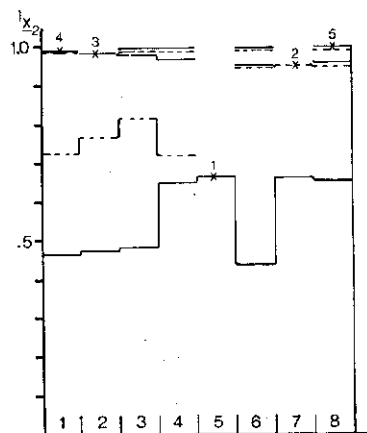


FIG. 145. Distribution of the contribution of added spectral bands to subvector,  $x_2$ , for the covariance matrix of multispectral scanner data of 12 spectral categories.

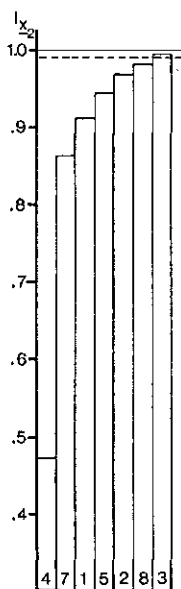


FIG. 146. Selection of spectral bands for subvector,  $x_2$ , for the covariance matrix of scanner data of 4 spectral categories.

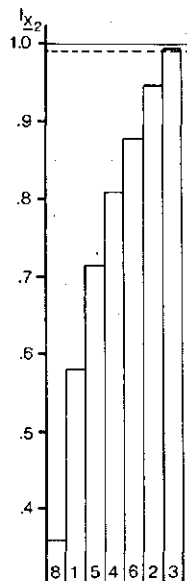


FIG. 147. Selection of spectral bands for subvector,  $x_2$ , for the covariance matrix of scanner data of 2 spectral categories.

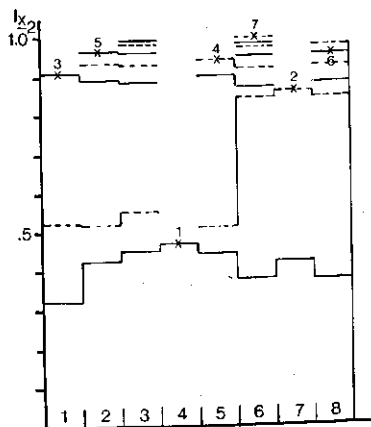


FIG. 148. Distribution of the contribution of added spectral bands to the information of subvector,  $\bar{x}_2$ , for the covariance matrix of multispectral scanner data of 4 spectral categories.

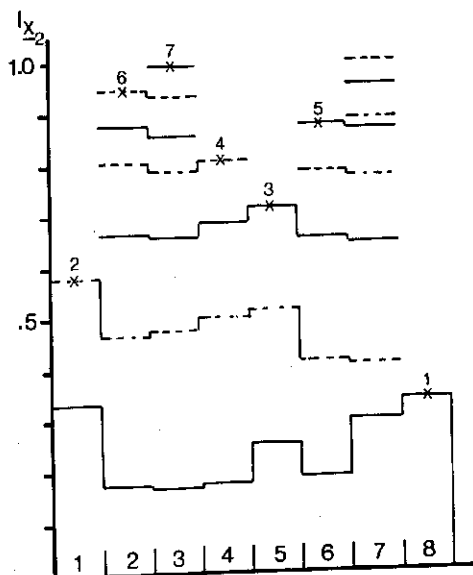


FIG. 149. Distribution of the contribution of added spectral bands to subvector,  $\bar{x}_2$ , for the covariance matrix of multispectral data of 2 spectral categories.

The distribution functions of the information of  $\bar{x}_2$  belonging to the 4 and 2 crop classes are shown in Figs. 148 and 149, respectively.

Both for 4 and only 2 crop types, 7 spectral bands are used out of the 8 available to obtain over 99% of the total information. The small amount of total variance is caused by the relatively small differences between the radiance spectra of the 4 green crops. Due to the larger colour variation within the 4 crops compared with colour variations between potatoes and sugarbeets, spectral band No. 4 has been selected as the best single band. The difference between potatoes and sugarbeets gives maximum information increase of  $\bar{x}_2$  is higher for the four spectral categories than for the very similar spectra of potatoes and sugarbeets, which was to be expected.

TABLE 17. Traces of the covariance matrices of multispectral scanner data for 12, 4 and 2 spectral categories.

$\Sigma$	$\text{Tr}\Sigma$
12	0.5969
4	0.0957
2	0.0219

## 6.5. INTRA- AND INTERCLASS VARIATIONS IN MULTISPECTRAL REFLECTANCE DATA IN RELATION WITH MISCLASSIFICATION

In section 6.3. interclass discrimination was considered only on the basis of differences between mean vectors generated with Suits' model. When multispectral reflectance data of samples of several crop categories are available, their statistical behaviour can be determined by calculating the mean vector,  $\mu$  and the covariance matrix,  $\Sigma$ , from these samples for each class.

Using a Bayesian classifier, automatic crop type discrimination can be executed successfully, if these samples are representative for the corresponding crop categories and their intraclass stochastic variations.

One of the major causes of misclassifications is due to overlapping of probability regions in the feature space. When intraclass stochastic variations are considered Gaussian, these regions for each class are presented by quadratic forms given by the argument of the exponential functions in the multivariate probability density functions defined by equation (6.11.). The quadratic forms present multidimensional ellipsoids containing clusters of multispectral reflectance data samples of crop classes. The effective volume of the ellipsoids is determined by a threshold distance corresponding with an assumed probability for feature vectors to be assigned to these classes.

Because of the stochastic character of feature vector,  $\underline{x}$ , the quadratic forms have a chi-square distribution,  $\chi^2_{N,P}$ . The degree of freedom,  $N$ , of the  $\chi^2$ -distribution is equal to the number of spectral bands (or the dimension of the feature space) and  $P$  is equal to the probability of being assigned (recognized) to this class.

Two crop types,  $C_i$  and  $C_j$ , are considered. Feature vectors,  $\underline{x}$ , are spanned by a choice of  $N$  spectral bands based on the analysis presented in sections 6.3. and 6.4. Measurement,  $\underline{x}$ , is assigned to crop type,  $C_i$  or  $C_j$ , by means of Bayes' rule. The effectiveness of Bayes' decision rule is determined by the actual probability of error closely related to the degree of overlapping of the corre-

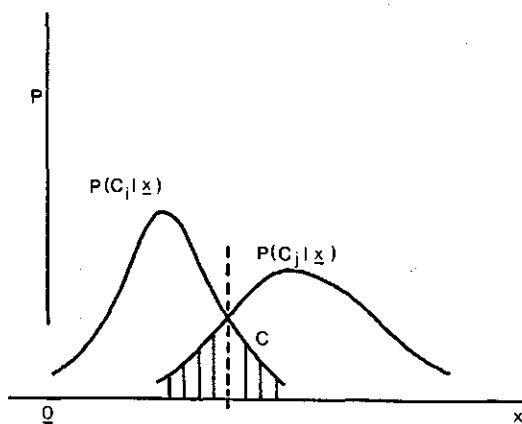


FIG. 150. Overlapping of conditional probabilities,  $P(C_i|\underline{x})$  and  $P(C_j|\underline{x})$ , for a one-dimensional example. The probability of error corresponds with area C.



sponding probability regions. Fig. 150 illustrates for a one-dimensional example the resulting probability of error.

Volume,  $\Gamma_i$ , contains feature vectors,  $\underline{x}$ , taken from class,  $C_j$ , but assigned to class,  $C_i$ , and volume,  $\Gamma_j$ , contains those feature vectors of class,  $C_i$ , assigned to class,  $C_j$ .

For volumes,  $\Gamma_i$  and  $\Gamma_j$ , follow the inequalities:

$$\begin{aligned}\Gamma_i: P(C_i|\underline{x}) &> P(C_j|\underline{x}) \\ \Gamma_j: P(C_j|\underline{x}) &> P(C_i|\underline{x})\end{aligned}\quad (6.30.)$$

Using Bayes' formula (6.2.), total probability of error,  $\varepsilon$ , is expressed by:

$$\begin{aligned}\varepsilon &= \int_{\Gamma_i} P(C_j)p(\underline{x}|C_j)d\underline{x} + \int_{\Gamma_j} P(C_i)p(\underline{x}|C_i)d\underline{x} \\ &= P(C_j)\varepsilon_j + P(C_i)\varepsilon_i\end{aligned}\quad (6.31.)$$

For Gaussian intraclass stochastic variation of  $\underline{x}$ , a measure of  $\varepsilon$  can be obtained in terms of mean vectors,  $\underline{\mu}_i$ ,  $\underline{\mu}_j$ , and covariance matrices,  $\Sigma_i$ ,  $\Sigma_j$ .

An upper bound of  $\varepsilon$  is given by:

$$\varepsilon \leq \{P(C_i)P(C_j)\}^{1/2} \exp \{ -\mu^{(1/2)} \} \quad (6.32.)$$

$$\begin{aligned}\mu^{(1/2)} &= 1/8 (\underline{\mu}_j - \underline{\mu}_i)^T \left( \frac{\Sigma_i + \Sigma_j}{2} \right)^{-1} (\underline{\mu}_j - \underline{\mu}_i) + \\ &+ 1/2 \ln \frac{|\Sigma_i + \Sigma_j|/2}{|\Sigma_i|^{1/2} |\Sigma_j|^{1/2}}\end{aligned}\quad (6.33.)$$

Function,  $\mu^{(1/2)}$ , is called the Bhattacharyya distance and is a direct measure of separability or divergence between two statistical populations.

For a more detailed description and the considerations leading to the definition of the Bhattacharyya distance, reference is made to BHATTACHARYYA (1943) and FUKUNAGA (1972).

Besides, small differences between properties of different crop categories, probability of error due to misclassification is mainly determined by the choice of spectral bands. Other causes of misclassification, like variations in ground illumination caused by cloud shadows, heterogeneities of the atmospheric state or local irregularities within the canopies are left out of consideration.

To illustrate the suitability of the Bhattacharyya distance in quantifying the performance of Bayes' decision rule for two crop categories, sugarbeets and potatoes, the probability of error during growth due to misclassification is presented. Reflectance data are used obtained with the field spectrometer during 1974. By taking between 6 and 12 samples on each field on the same day, the mean vector and intracovariance matrix of both crops are estimated for the 12 wavelength bands given in Table 15.

To analyse the coherence between the probability of error and the choice of elements of the feature vector, three calculations have been performed originating from a four-dimensional feature vector. Three dimensions of the feature

vector have been defined by spectral bands in the green, the red and in the near infrared, given by bands Nos. 3, 5 and 8. As fourth element, band No. 11 in the water absorption region, or band No. 9 adjacent to band No. 8 in the near infrared plateau, or band No. 4 in the yellow part of the visible light region have been chosen successively.

The combination of Nos. 3, 5, 8 and 11 is based on the analysis with Suits' model. In case of a restriction in the total spectral interval between 500 and 1100 nm, band No. 9 and band No. 4 have been chosen to be provided with a fourth band either with a high correlation with the near infrared band No. 8, or with the two wavelength bands Nos. 3 and 5 in the visible light.

Mean vectors,  $\mu_A$  (potatoes) and  $\mu_B$  (sugarbeets), formed out of the average response in each group of four selected bands are summarized in Table 18 for seven dates during the growth period. The spectral bands used for feature vectors,  $x_a$ ,  $x_b$  and  $x_c$ , are indicated in the same table.

Seven dates have been taken to characterize crop growth from the early stage, during the period of exponential growth and maturing and to monitor the first stage of the infection of *Phytophthora* in the potato test field.

With a computer program, the Bhattacharyya distance between the two crop types for the three feature vectors has been calculated during growth.

FUKUNAGA (1972) demonstrated that a maximum value of the probability of error, given by condition (6.32.), is obtained, when equal a priori probabilities  $P(C_i) = P(C_j) = 0.5$  are assumed. For the two crop categories dealt with, equal occurrence is assumed without other crop types. The maximum probability of error due to misclassification using the maximum likelihood decision rule is equal to:

$$\varepsilon = \frac{1}{2} \exp \{ -\mu^{(1/2)} \} \quad (6.34.)$$

Fig. 151 shows  $\mu^{(1/2)}$  during growth between 30 May and 6 August 1974. The percentage of  $\varepsilon$  with a limit of 50% is indicated by means of horizontal lines corresponding with the scale on the right side. The variation in LAI of sugarbeets and potatoes during growth is included and the scale of  $\mu^{(1/2)}$  is used as an ordinate.

In the initial stage, soil cover percentage did not exceed 20% for both crops. Spectral reflectance is mainly determined by the reflectance spectrum of the soil itself. The Bhattacharyya distance for the three feature vectors is in the same order. For  $x_a$ , the Bhattacharyya distance increases during crop maturing. It is concluded that sugarbeets can be well discriminated from potatoes, mainly because of the significant difference in reflectance in the water absorption region. In potatoes a dry mass percentage between 9.0% and 9.8% was measured during June, whereas in sugarbeets values between 7.3% and 9.0% were found. The higher water content in sugarbeet leaves probably causes a much lower canopy reflectance between 1000 and 2500 nm. It was found that this difference in reflectance level was significant during the whole growing period.

The infection by *Phytophthora* caused a decrease in green mass in the lower layers of the potato canopy. Especially, reflectance in band No. 8 in the near

infrared decreased, resulting in a smaller Bhattacharyya distance. However, a high interclass separability capacity of feature vector,  $x_a$ , was maintained because of the reflectance difference in band No. 11 which remained considerable.

If band No. 9 is used, instead of No. 11, probability of error increases throughout the growing period. With feature vector,  $x_b$ , optimum interclass discrimination was obtained when the *LAI* of potatoes attained its maximum value of approximately 7, whereas in sugarbeets the *LAI* was only about 3, and still growing. Ground cover percentage of both crops was already between 95% and 100%.

With band Nos. 3, 4 and 5 in the visible light region and band No. 8 in the near infrared, forming feature vector,  $x_c$ , probability of error increases during growth, attaining a maximum of 27% near 17 June. The Bhattacharyya distance between both crops on that day is at a minimum, because the mean vectors and covariance matrices for  $x_c$  are of the same order. Afterwards, during the period from 19 to 24 June, the Bhattacharyya distance first increased by an enhanced difference between the infrared reflectance. The distance increased up to 19 July, because of a greater difference in reflectance in the visible light. Yellowing and a more horizontal orientation of the leaves of sugarbeets, together with a decrease in the infrared reflectance of potatoes due to *Phytophthora* infection led to a greater probability of error in misclassification, measured on 6 August.

TABLE 18. Mean vectors of reflectance measurements on potatoes, (A) and sugarbeets, (B), (30-5-'74 to 6-8-'74, Wageningen).

Crop type	Date	Mean reflectance					
		Band 3	Band 4	Band 5	Band 8	Band 9	Band 11
1 A	30-5-'74	10.58	9.62	10.45	31.47	31.22	25.55
B		9.08	8.78	10.58	28.66	30.14	27.36
2 A	12-6-'74	6.59	3.90	2.87	40.87	36.59	15.83
B		6.97	4.73	4.20	32.84	29.24	11.60
3 A	17-6-'74	7.56	4.45	3.37	52.52	45.06	22.21
B		6.35	3.79	3.05	41.63	35.97	12.26
4 A	19-6-'74	8.17	4.75	3.18	53.04	46.67	22.04
B		7.03	4.17	2.99	45.98	38.58	11.38
5 A	24-6-'74	8.40	4.80	3.21	60.98	53.03	23.29
B		7.06	4.15	2.85	48.64	40.63	11.36
6 A	19-7-'74	7.9	4.73	3.24	48.62	45.12	20.41
B		6.43	3.85	2.63	49.10	39.43	12.36
7 A	6-8-'74	9.15	5.80	3.66	45.73	42.56	19.35
B		8.15	5.29	3.69	43.91	35.87	12.80
Mean vector							
$\mu_a$		$\mu_{a1}$		$\mu_{a2}$	$\mu_{a3}$		$\mu_{a4}$
$\mu_b$		$\mu_{b1}$		$\mu_{b2}$	$\mu_{b3}$	$\mu_{b4}$	
$\mu_c$		$\mu_{c1}$	$\mu_{c2}$	$\mu_{c3}$	$\mu_{c4}$		

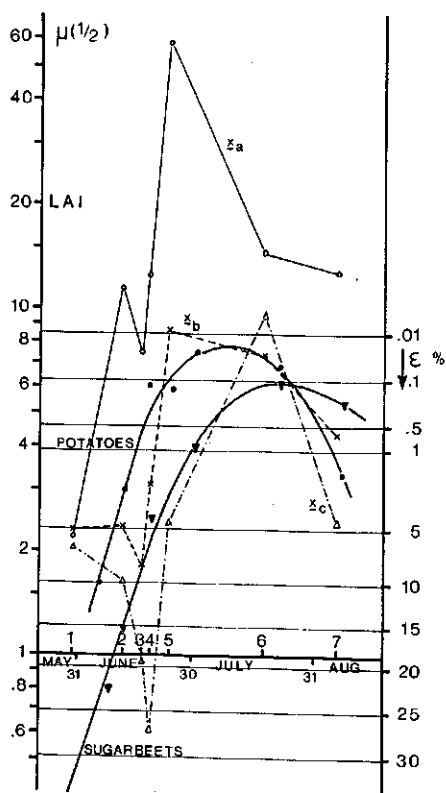


FIG. 151. Bhattacharyya distance,  $\mu^{(1/2)}$  and probability of error,  $\epsilon$ , in potatoes and sugarbeets during growth as measured at Wageningen in 1974. Fourdimensional feature vectors,  $x_a$ ,  $x_b$  and  $x_c$ , are used and specified in Table 18. The leaf area index of potatoes and sugarbeets as a function of time is included.

## 6.6. SUMMARY AND CONCLUSIONS

Crop type discrimination by means of decision rules applied to multispectral reflectance data requires a data collection technique which yields optimum information about the dynamic behaviour of the spectral distribution of radiation reflected by vegetative canopies.

The simultaneous measurement of the reflected radiation in a number of wavelength bands is presented by a feature vector,  $\underline{x}$ . The information content of a set of,  $\{\underline{x}\}$ , is defined as the total variance which is equal to the trace of the covariance matrix of  $\{\underline{x}\}$ .

This information content depends on the initial choice of the number and the position of the spectral bands and the bidirectional geometry of crop reflectance detection.

Optimum conservation of information with maximum elimination of redundant spectral bands, or elements of  $\underline{x}$  has been analysed for passive detection and active detection in the canopy hot spot. An algorithm has been used to estimate the information content of a subvector,  $\underline{x}_2$ , extracted from the elements of  $\underline{x}$ .

Suits' model has been applied to provide reflectance data of a representative variation of the parameters of uniform canopies. Experimental data have been analysed to verify model predictions.

Discrimination between crop classes using multispectral reflectance data is successful, if mutual differences between the stochastic parameters, like the mean vector and the covariance matrix are sufficiently large to minimize the probability of error due to misrecognitions. Under assumption of Gaussian intraclass stochastic variations, the Bhattacharyya distance has been adopted as a quantitative measure of interclass separability.

Referring to the previous sections of this chapter, the following is concluded.

a. It has been shown earlier that reflectance measurements in the green, the red and in the near infrared part of the electromagnetic spectrum are useful in non-destructive determination of canopy parameters. If data from these three spectral bands are required, a subvector,  $\underline{x}_2$ , from  $\underline{x}$ , containing these bands and others, is determined which represents more than 99% of the total information.

Simulations with Suits' model have shown that for variations in uniform canopies caused by varying *LAI*, leaf angle distribution, leaf colour and different soil reflectance, four spectral bands are sufficient to measure more than 99% of the information available from an original selection of 12 well-chosen spectral bands. The best fourth band in most cases is centered at 1650 nm in the water absorption region. This choice holds for most conditions simulated for passive detection under perpendicular view and for active detection under oblique view in the hot spot.

Whereas spectral bands in the violet or blue part of the visible spectrum are not selected with high priority, fewer problems will be encountered with respect to atmospheric scattering.

Fortunately, the same four spectral bands, as proposed in this manuscript are selected for a new generation of earth observation satellites, starting with Landsat-D to be launched in 1981.

b. When subvector,  $\underline{x}_2$ , is calculated by increasing order of the best spectral bands, the dimension of  $\underline{x}_2$  to exceed 99% of the total information is also equal to four. The order of selection, however, depends on the observed contrast between the canopy and the bounding soil.

c. Total variance based on mean values of crop reflectance data is decreased when detection takes place in the canopy hot spot, due to the absence of the observed variable amount of shadow related with different crop structures. For oblique view angles, the variance is further reduced because of the decreasing fraction of observed soil.

It is expected that stochastic within-class variations also decrease which compensates the deterioration of between-class separability.

d. Analysis of optimum band choice based on field spectrometer and scanner

data agree satisfactorily with model predictions. When interclass differences are small, more spectral bands are required to exceed 99% available information.

e. The probability of error for discrimination between crop categories depends highly on the initial choice of spectral bands. The Bhattacharyya distance, expressed in the corresponding mean vectors and covariance matrices, is a useful quantity to analyse the relation between the feature vector used and the resulting probability of error.

An example of potatoes and sugarbeets demonstrated the importance of a fourth spectral band in the water absorption region to use the characteristic difference between these crop types due to a significant difference in the water content of the leaves.

## SUMMARY

Relations between morphological properties of uniform canopies, optical properties of the leaves and reflection of shortwave radiation, in the visible light region and the near infrared, by crops are the subject of this thesis.

The aim of the study was a further investigation of potential applications of multispectral scanning for agricultural purposes by a fundamental approach. Multispectral scanning is a modern aerial survey technique, based on the simultaneous measurement of radiation reflected by the earth's surface within a discrete number of wavelength bands. These wavelength bands are distributed in the wavelength interval encompassing the visible light and the near reflectance infrared.

Applications of thermal infrared radiation and reflected or emitted microwave radiation are left out of consideration.

Chapter 1 gives a general introduction to the relation between aerial photography, remote sensing and multispectral scanning in particular. The objectives of the research are described and interrelated with potential applications in agriculture.

In chapter 2 attention is first paid to the physical relations dealing with the remote detection of radiation reflected by the earth's surface.

Current knowledge concerning reflection, transmission and absorption of shortwave radiation by single leaves is summarized. With this the optical behaviour is related to leaf anatomy, the present pigments and the leaf water.

After mentioning the predominating factors determining reflectance of bare soils, reflectance of homogeneous crops is treated.

Utilizing a description of crop structure and the optical properties of leaves as most important canopy components, several mathematical models of canopy reflectance are discussed. A deterministic model, published by G. H. SUITS in 1972, is adopted for this study and further elaborated. A comparison with a numerical model according to GOUDRIAAN (1977) showed that a drastic simplification of canopy structure introduced initially led to similar results as, when the realistic numerical model was simplified afterwards. The actual leaf angle distribution is characterized by one parameter only in Suits' model. The reflectance as function of canopy parameters and the directions of incoming radiation and observation is described by an analytical expression. This also holds for the reciprocity relations connected with and found earlier by Goudriaan. By means of Suits' model, a sensitivity analysis is performed in chapter 3 for the relation between reflectance as a function of wavelength and canopy variables, like leaf area index, leaf angle distribution, leaf colour and soil reflectance. Information distributions calculated from own measurements were confirmed by model predictions. Taking account of selective absorption

of radiation by the atmosphere, spectral bands with a high sensitivity of reflectance to variation in crop parameters have been chosen. Reflectance in the green at 550 nm and in the red at 670 nm in the visible light region and in the near reflectance infrared plateau at 870 nm and in the water absorption region at 1650 nm and 2200 nm were selected for a more detailed study. Canopy reflectance at these wavelengths has a direct relation with leaf pigments, leaf morphology and the water content of the leaf.

The sensitivity of the measured canopy reflectance to variations in canopy structure dependent on spectral bandwidth was investigated for the green, the red and the near infrared plateau.

In the red with 670 nm as centre wavelength, a bandwidth of 20 nm appeared to be acceptable, in relation to the loss of variance, as well as to the increased covariance with the spectral band in the green with equal width. In the near infrared, bandwidth is allowed to be larger, at least 100 nm, since the small spectral variation of the optical properties of the leaves in the infrared plateau.

Chapter 4 gives a description of the in situ canopy reflectance measurements during growth performed at Wageningen, with a specially designed spectrometer. By means of a comparative method canopy reflectance is measured at 153 wavelength values between 361 and 2360 nm.

The optical system and the principle of the spectrometer used is discussed. Examples of canopy variables measured, like soil cover percentage, leaf area index and biomass are presented.

Finally, the principle of multispectral scanning is explained in this chapter. Some attention is paid also to relations concerning ground resolution, spectral resolution, the radiation level, detector properties and limitations due to detector noise.

Chapter 2 shows the complex relation between reflectance of radiation by crops and the optical properties of canopy components and structure. In chapter 5 new spectral parameters are found by combining reflectance values of homogeneous green canopies of different spectral bands which show an optimum sensitivity to a canopy parameter under detection, with a high invariability to other parameters.

The systematic coherence between the reflectance at different wavelengths, caused by canopy structure and correlations between the optical properties of leaves and of soil is investigated. For 2 combinations of the reflectance in the green, the red and the near infrared plateau, a useful relation with the soil cover percentage has been found. This combination is insensitive to variations in the solar angle and in soil moisture content. Out of the same reflectance values combinations are made which, assuming an incomplete soil cover, are sensitive to detection of soil moisture variations only or, with a high soil cover, sensitive to actual differences in the leaf angle distribution.

By observing a crop under an angle of 75° relative to the vertical, the influence of the soil background on the reflectance in the visible light may be neglected



in most crops.

For the ratio of reflectance in the red and the green it is concluded that variation in this parameter during growth may be attributed uniquely to colour variation in the canopy components. By means of reflectance in the three wavelength bands mentioned, a structure parameter, a soil characteristic and a colour indication for the canopy components may be monitored during the growing season and employed for applications in agriculture.

Making use of the analytical expression for plant canopy reflectance it has been demonstrated that for detection in the canopy hot spot (directions of incoming radiation and of observation coincide), the relations between multispectral reflectance and canopy variables are simplified considerably. Detection perpendicular to the earth's surface or under a zenith angle of  $51.8^\circ$ , eliminates the influence of leaf angle distribution function on reflectance as a function of the apparent soil cover percentage. Combinations of reflectance values in the green, the red and the near infrared produce a well-defined relation with soil cover, the leaf area index and differences in soil moisture content. The ratio of reflectance in the red and the green wavelength band for these view angles is independent of canopy structure and is a function of leaf colour only.

Conical scanning under an angle of  $51.8^\circ$  using an active radiant source and appropriate sensors, from an airplane offers the facility to collect crop data under cloudy weather conditions, while the disturbing influence of the atmosphere can be eliminated considerably.

In chapter 6 an analysis is made on which and how many spectral bands, well-chosen within the atmospheric windows available, are needed at a minimum to discriminate between green crops of different structure, leaf colour and soil reflectance. In this a multi-regression analysis is used with the restriction that by deletion of redundant spectral bands not more than 1% of the information available is lost. Starting with the already chosen bands in the green, red and near infrared plateau, it appeared for both passive detection perpendicular to the earth's surface and active detection into the hot spot under  $51.8^\circ$ , that addition of a fourth band at 1650 nm in the water absorption region produced more than 99% of the information available.

The preferred spectral bands were confirmed by the same analysis applied on field reflectance and MSS data.

The interclass variations for passive detection in the nadir appeared to be wider than compared to active detection in the hot spot under an oblique angle of  $51.8^\circ$ . This is related with the elimination of the shadow observed and the weaker contrast influence of the bounding soil brought about by the hot spot conditions mentioned.

The possibility of discriminating between crops on the basis of differences between spectral reflectance by means of a decision rule, with a small probability of misclassification, depends on the stochastic behaviour of the reflectance values measured, the number and the selection of spectral bands. A criterion for the probability of misclassification, using statistical parameters has been

applied to illustrate the separability between potatoes and sugarbeets during the growing season. Field spectrometer data in four spectral bands were used. It appeared that the spectral band in the water absorption region at 1650 nm is a good discriminator for sugarbeets, because of the significant difference in the water content of the single leaf.

## SAMENVATTING

Relaties tussen de morfologische eigenschappen van homogene gewassen, de optische eigenschappen van de bladeren en de reflectie van kortgolvlige straling in het zichtbare licht en het nabije infrarood door gewassen vormen het onderwerp van dit proefschrift.

De studie had tot doel potentiële toepassingen van multispectrale scanning voor landbouwkundige doeleinden nader te onderzoeken vanuit een fundamentele benadering. Multispectrale scanning is een moderne luchtopname-techniek, gebaseerd op het gelijktijdig meten van door het aardoppervlak gereflecteerde straling binnen een aantal discrete golflengte-banden. Deze golflengte-banden zijn verdeeld over het golflengtebereik wat het zichtbare licht en het nabije reflectie-infrarood omvat. Toepassingen gebruikmakende van thermische infraroodstraling en gereflecteerde of uitgezonden microgolflstraling zijn buiten beschouwing gelaten.

Hoofdstuk 1 geeft een algemene inleiding in de samenhang tussen lucht-fotografie, remote sensing en multispectrale scanning in het bijzonder. Voorts wordt het doel van het verrichte onderzoek beschreven en in verband gebracht met potentiële toepassingen in de landbouw.

In hoofdstuk 2 wordt eerst ingegaan op de fysische relaties die een rol spelen bij het detecteren van door het aardoppervlak gereflecteerde straling op afstand.

De momenteel beschikbare kennis betreffende reflectie, transmissie en absorptie van kortgolvlige straling door bladeren is samengevat. Hierbij is het optisch gedrag in relatie gebracht met de blad-anatomie en de aanwezige pigmenten en het celvocht. Na de belangrijkste factoren te hebben genoemd welke de reflectie door kale bodem bepalen, wordt overgegaan op reflectie van straling door gewassen.

Onder gebruikmaking van een beschrijvingswijze van de structurele opbouw en de optische eigenschappen van de bladeren als belangrijkste componenten, zijn verschillende mathematische gewasreflectie-modellen behandeld. Het uit 1972 daterende deterministische model volgens G. H. SUITS is voor deze studie overgenomen en verder uitgewerkt. Uit een vergelijkend onderzoek met een numeriek model volgens GOUDRIAAN en DE WIT bleek dat een vergaande vereenvoudiging van de gewassenstructuur vooraf tot ongeveer dezelfde resultaten leidt als wanneer in het gedetailleerde numerieke model achteraf vereenvoudigingen worden aangebracht. De werkelijke bladhoekdistributie-functie wordt in het model volgens Suits gekarakteriseerd door slechts een getal. Het reflectiegedrag kan als functie van de gewasparameters en de richtingen van opvallende straling en observatie geheel analytisch worden uitgewerkt. Dit

geldt ook voor de hiermee samenhangende reciprociteitsrelaties, eerder door Goudriaan gevonden.

Met behulp van het Suits model wordt in hoofdstuk 3 een gevoeligheidsanalyse uitgevoerd voor het verband tussen de reflectie als functie van de golflengte en gewasvariabelen zoals de hoeveelheid bladoppervlak, de bladstandverdeling, de bladkleur en de bodemreflectie. Informatiedistributies berekend uit eigen meetresultaten worden bevestigd door modelvoorspellingen. Rekening houdend met selectieve absorptie van straling door de atmosfeer zijn spectrale gebieden gekozen, welke voor de gewasreflectie een grote gevoeligheid vertonen voor variaties van gewasparameters. De reflectie in het groen bij 550 nm, in het rood bij 670 nm, in het reflectie-infraroodplateau bij 870 nm en in het waterabsorptiegebied bij 1650 nm en 2200 nm zijn gekozen voor een nadere studie. De reflectie bij deze golflengten staat in direct verband met de bladpigmenten, de bladmorphologie en het watergehalte.

De gevoeligheid van de gemeten gewasreflectie voor variaties van de gewasstructuur in afhankelijkheid van de spectrale bandbreedte is onderzocht in het groen, het rood en het nabije infraroodplateau.

In het rood bij 670 nm als centrale golflengte bleek een breedte van 20 nm acceptabel te zijn bij verlies aan variantie als voor de toegenomen covariantie met de spectrale band in het groen van gelijke breedte. In het nabije infrarood mag de bandbreedte groter zijn, zeker 100 nm, in verband met de geringe spectrale variatie van de optische eigenschappen van de bladeren in het infraroodplateau.

Hoofdstuk 4 geeft een beschrijving van de te Wageningen uitgevoerde gewasreflectie metingen tijdens de groei met behulp van een hiervoor gebouwde spectrometer. Via een comparatieve methode wordt de reflectiecoëfficiënt gemeten bij 153 golflengtewaarden tussen 361 en 2360 nm. De optische stralingang en het principe van de spectrometer is besproken. Van in het veld gemeten gewasvariabelen zoals de bedekkingsgraad, de bladoppervlakte-index en de biomassa worden voorbeelden gegeven.

Ten slotte wordt in dit hoofdstuk het principe van multispectrale scanning nader toegelicht. Ook wordt ingegaan op relaties die verband houden met grondresolutie, spectrale resolutie, het stralingsniveau, de eigenschappen van de detector en beperkingen ten gevolge van detector-ruis.

Uit hoofdstuk 2 bleek dat de reflectie van straling door gewassen op complexe wijze samenhangt met de optische parameters van de gewascomponenten en de structuur.

In hoofdstuk 5 is door algebraïsch combineren van reflectiewaarden van homogene groene gewassen uit verschillende golflengte-banden gezocht naar nieuwe spectrale parameters welke optimaal gevoelig zijn voor een gezochte gewasvariabele en zoveel mogelijk invariant zijn voor de overige variabelen.

De systematische samenhang tussen de reflectie bij verschillende golflengten, veroorzaakt door de gewasstructuur en de correlaties binnen de optische

eigenschappen van bladeren en bodem is onderzocht.

Voor twee combinaties van de reflectie in het groen, het rood en het nabije infraroodplateau is een bruikbaar verband gevonden met de bedekkingsgraad. Dit verband is ongevoelig voor variaties van de zonnestand en de bodemvochtigheid. Uit dezelfde drie reflectiewaarden zijn combinaties te vormen welke bij niet te hoge bedekking gevoelig zijn voor het detecteren van bodemvochtigheidsvariaties alleen, of bij hoge bedekking voor bestaande verschillen in bladstanddistributie.

Door onder een hoek van  $75^\circ$  ten opzichte van de vertikaal het gewas waar te nemen, is voor de meest voorkomende gewassen de invloed van de bodem op de reflectie in het zichtbare licht te verwaarlozen. Uit een verhouding van de reflectie in het rood en het groen is afgeleid dat variatie van deze parameter tijdens de groei eenduidig aan kleurvariatie van de gewascomponenten kan worden toegeschreven. Met behulp van de reflectie in de drie genoemde golflengtebanden kan op non-destructieve wijze een structuurparameter, een bodemkarakteristiek en een kleurindicator van de gewascomponenten in de loop van het groeiseizoen gevolgd worden en voor landbouwkundige toepassingen worden aangewend.

Door gebruik te maken van de analytische uitdrukking voor gewasreflectie is gevonden dat detectie in de 'hot spot' (instralings- en waarnemingsrichting vallen dan samen) de relatie tussen multispectrale reflectie en gewasvariabelen aanmerkelijk vereenvoudigt. Detectie loodrecht op het aardoppervlak of onder een hoek van  $51,8^\circ$  maakt de reflectie als functie van de bedekking onafhankelijk van de bladstand-verdeling. Combinaties van reflectiewaarden in het groen, rood en nabij infrarood leveren een goed verband met de bedekkingsgraad, de bladoppervlakte-index en bodemvochtigheidsverschillen.

De verhouding van de reflectie in het rood en het groen wordt onder deze hoeken onafhankelijk van de structuur en een functie van de bladkleur alleen.

Conisch scannen van het aardoppervlak onder een hoek van  $51,8^\circ$  met behulp van een actieve bron en daarvoor geschikte sensoren vanuit een vliegtuig biedt de mogelijkheid ook bij bewolkt weer gewasgegevens in te winnen, waarbij de storende invloed van de atmosfeer in belangrijke mate geëlimineerd kan worden.

In hoofdstuk 6 is geanalyseerd welke en hoeveel spectrale banden, gekozen binnen de atmosferische vensters, minimaal nodig zijn om groene gewassen met uiteenlopende structuur, bladkleur en bodemreflectie van elkaar te onderscheiden. Hierbij is gebruik gemaakt van multi-regressie analyse waarbij door weglating van spectrale banden minder dan 1% informatie verloren mocht gaan. Uitgaande van de gekozen banden in het groen, rood en het nabije infraroodplateau, bleek zowel voor passieve detectie loodrecht op het aardoppervlak als voor actieve detectie in de hot spot onder een hoek van  $51,8^\circ$ , toevoeging van een vierde band bij 1650 nm in het waterabsorptiegebied meer dan 99% van de totaal beschikbare informatie te leveren. De gekozen spectrale banden bleken door analyses op spectrometer- en MSS gegevens bevestigd te worden. Bij passieve detectie loodrecht op het aardoppervlak is de

inter-klasse variatie groter dan bij actieve detectie in de hot spot onder  $51.8^\circ$ . Dit hangt samen met het elimineren van geobserveerde schaduw en de geringe contrastinvloed van de bodem als gevolg van de genoemde hot spot condities.

De mogelijkheid om gewassen op grond van verschillen in spectrale reflectie met behulp van een beslissingsregel met een geringe kans op misklassificatie onderling goed van elkaar te onderscheiden hangt af van het stochastisch gedrag van de gemeten reflectiewaarde, het aantal en de keuze van de spectrale banden. Een criterium voor de kans op misklassificatie, gebruikmakend van statistische parameters, is ter illustratie gebruikt om de onderscheidbaarheid tussen aardappelen en suikerbieten in de loop van het groeiseizoen te onderzoeken.

Hierbij is gebruik gemaakt van spectrometergegevens opgenomen in vier spectrale banden. De spectrale band in het waterabsorptiegebied bij 1650 nm bleek voor suikerbieten een goede discriminator te zijn, vanwege het significante verschil in het watergehalte van het enkele blad.

## ACKNOWLEDGEMENTS

I express my appreciation to:

Prof. dr. ir. C. T. de Wit and prof. ir. H. G. de Winter for their support and inspiration during the preparation of the manuscript.

Dr. ir. G. P. de Loor, prof. dr. ir. J. Schenk and ir. Th. A. de Boer for their co-operation in the initiation and in the realization of this thesis.

Ing. W. Verhoef for his indispensable assistance in the work reported.

All staff members who belonged to or were concerned in the NIWARS project, of the Centre for Agrobiological Research (CABO) and of the Agricultural University who offered technical support in the research, in the realization and in editing this report.

## REFERENCES

- ANDERSON, T. W., 1958. An introduction to multivariate statistical analysis. John Wiley & Sons, New York.
- ALLEN, W. A. and A. J. RICHARDSON, 1968. Interaction of light with a plant canopy. *J. Opt. Soc. Am.*, **58**(8): 1023-1028.
- ALLEN, W. A. *et al.*, 1969. Interaction of light with a compact plant leaf. *J. Opt. Soc. Am.*, **59**(10): 1376-1379.
- ALLEN, W. A. *et al.*, 1970. Plant canopy irradiance specified by the Duntley equations. *J. Opt. Soc. Am.*, **60**(3): 372-376.
- ALLEN, W. A. *et al.*, 1970. Mean effective optical constants of cotton leaves. *J. Opt. Soc. Am.*, **60**(4): 542-547.
- ALLEN, W. A. *et al.*, 1973. Willstätter-Stoll theory of leaf reflectance evaluated by ray tracing. *Applied Optics*, **12**(10): 2448-2453.
- BEERS, J. N. P., 1975. Analysis of significance within crop spectra. NIWARS, Delft, publ. No. 30.
- BHATTACHARYYA, A., 1943. On a measure of divergence between two statistical populations defined by their probability distributions. *Bull. Calcutta Math. Soc.*, **35**, 99-100.
- BOWERS, S. A. and R. J. HANKS, 1965. Reflection of radiant energy from soils. *Soil Science*, **100**(2): 130-138.
- BREECE, H. T., and R. A. HOLMES, 1971. Bidirectional scattering characteristics of healthy green soybean and corn leaves *in vivo*. *Applied Optics*, **10**(1): 119-127.
- BUNNIK, N. J. J. and W. VERHOEF, 1974. The spectral reflectance of agricultural crops. NIWARS, Delft, publ. No. 23.
- BUNNIK, N. J. J. *et al.*, 1977. Onderzoek naar de toepassingsmogelijkheden van multispectrale scanning. NIWARS, Delft, publ. No. 44.
- CHANDRASEKHAR, S., 1960. Radiative transfer, Dover Publications, New York.
- CIPRA, J. E., *et al.*, 1971. Measuring radiance characteristics of soil with a field spectrometer. *Soil Science Soc. of Am.*, proc. vol. 35.
- COLWELL, J. E. and G. H. SUITS, 1975. Yield prediction by analysis of multispectral scanner data. Environmental Research Institute of Michigan, rep. No. NASA CR-ERIM 109600-17-F on NASA contract No. NAS 9-14123.
- COLWELL, R. N., 1965. Determining the prevalence of certain cereal crop diseases by means of aerial photography. *Hilgardia*, **26**(5): 223-286.
- DUNTLEY, S. Q., 1942. The optical properties of diffusing materials. *J. Opt. Soc. Am.*, **32**: 61-70.
- FUKUNAGA, K., 1972. Introduction to statistical pattern recognition. Academic Press, New York.
- GATES, D. M., 1965. Spectral properties of plants. *Applied Optics*, **4**(1): 11-20.
- GAUSMAN, H. W. *et al.*, 1970. Relation of light reflectance to histological and physical evaluations of cotton leaf maturity. *Applied Optics*, **9**: 545-552.
- GAUSMAN, H. W. *et al.*, 1971. The leaf mesophylls of twenty crops, their light spectra and optical and geometrical parameters. Spectral Survey of irrigated region crops and soils. Annual report, Dept. of Agriculture, Weslaco, Texas.
- GAUSMAN, H. W. *et al.*, 1976. Infinite reflectance of dead compared with live vegetation. *Agronomy Journal*, **68**: 295-296.
- GOUDRIAAN, J., 1973. A calculation model and descriptive formulas for the extinction and reflection of radiation in leaf canopies. Proc. The sun in service of mankind, Paris.
- GOUDRIAAN, J., 1977. Crop micrometeorology: a simulation study, thesis. Centre for Agricultural Publishing and Documentation (PUDOC), Wageningen.
- HARALICK, R. M., 1970. Principal component analysis. Remote Sensing Laboratory, Centre for Research in Engineering Science - University of Kansas, Technical Memorandum, 177-5.



- HIGHAM, A. D. *et al.*, 1972. Multispectral scanning systems and their potential application to earth resource surveys. Vol 1. Basic physics and technology. Prepared under ESRO contract No. ESTEC 1673/72 EL.
- IDSO, S. A. and C. T. DE WIT, 1970, Light relations in plant canopies. *Applied Optics*, 9(1): 177-184.
- KAUTH, R. J. and G. S. THOMAS, 1976. The tasseled cap - a graphic description of spectral-temporal development of agricultural crops as seen by Landsat. Symp. Proc. Machine Processing of Remotely Sensed Data. LARS-Purdue. IEEE cat. 76 CH 1103-01 MPRSD.
- KORTUM, G., 1969. Reflectance spectroscopy. Springer Verlag, Berlin.
- KUBELKA, P. and F. MUNK, 1931. Ein Beitrag zur Optik der Farbanstriche. *A. Techn. Physik*, 11: 593-601.
- KUMAR, R. and L. SILVA, 1973. Reflectance model of a plant leaf. LARS information note No. 022473.
- LEMASTER, E. W., 1975. Further tests of plant canopy reflectance models and investigation of non-Lambertian properties of plant canopies. NASA report CR-145615.
- Laboratory for Agricultural Remote Sensing, 1970. (LARS), Res. Bulletin 873.
- MALILA, W. A. *et al.*, 1972. Information extraction techniques for multispectral scanner data. Willow Run Laboratories, NASA report WRL-31650-74-T.
- MALILA, W. A., 1974. Multi-aspect techniques in remote sensing. Proc. 9th Intern. Symp. Remote Sensing of Environment. Ann Arbor, Michigan.
- MELAMED, N. T., 1963. *J. Appl. Phys.*, 34: 560.
- MILLER, J. B., 1964. An integral equation from phytology. *Journ. Aust. Math. Soc.*, 4: 397-402.
- MONSI, M. and T. SAEKI, 1953. Über den Lichtfactor in den Pflanzengesellschaft und seine Bedeutung für die Stoffproduktion. *Jap. Journ. Bot.*, 14: 22-52.
- MONTEITH, J. L., 1965. Light distribution and photosynthesis in field crops. *Ann. Bot.*, 29(113): 17-37.
- MYERS, V. I. *et al.*, 1966. Proc. 4th Intern. Symp. Remote Sensing of Environment, Ann Arbor, Michigan: 801.
- NALEPKA, R. F. *et al.*, 1977. Wheat productivity estimates using Landsat data. Type II, progress report. Environmental Research Institute of Michigan. Report No. 114800-31-L on NASA contract No. NAS-22389.
- NICHIPOROVICH, A. A., 1961. Properties of plant crops as an optical system. *Soviet Pl. Physiol.*, 8: 428-435.
- NILSON, T., 1971. A theoretical analysis of the frequency of gaps in plant stands. *Agr. Meteorol.*, 8: 25-38.
- OLIVER, R. E. and J. A. SMITH, 1973. Vegetation canopy reflectance models. Final report. U.S. Army Research Office-Durham. DA-ARO-D-31-124-71-G 165. Colorado State University, Fort Collins, Colorado 80521.
- OLIVER, R. E. and J. A. SMITH, 1974. A stochastic canopy model of diurnal reflectance. Final report, U.S. Army Research Office-Durham. DAH-CO4-74-G0001. Colorado State University, Fort Collins, Colorado 80521.
- REEVES, R. G. (Editor-in Chief), 1975. Manual of Remote Sensing, American Society of Photogrammetry, Falls Church, Virginia.
- ROSS, J. and T. NILSON, 1974. Radiation exchange in plant canopies. Proc. Int. Centre for Heat and Mass Transfer.
- SCHUSTER, A., 1905. *Astrophys. Journ.* 21: 1.
- SHULL'GIN, I. A. and A. F. KLESHNIN, 1959. Correlation between optical properties of plant leaves and their chlorophyll content. *ABIS Doklady*, 125: 199-221.
- SINCLAIR, T. R., 1971. Reflectance and internal structure of leaves from several crops during a growing season. *Agr. Journ.*, 63: 864-868.
- SINCLAIR, T. R., 1973. Diffuse reflectance hypothesis for the pathway of solar radiation through leaves. *Agr. Journ.*, 65: 276-283.
- STOKES, G. G., 1862. *Proc. Roy. Soc. (London)*, 11: 545.
- SUITS, G. H., 1972. The calculation of the directional reflectance of a vegetative canopy.

- Remote sensing of environment, 2: 117-125.
- SUITS, G. H., 1972. The cause of azimuthal variations in directional reflectance of vegetative canopies. Remote sensing of environment, 2: 175-182.
- SUITS, G. H. and G. R. SAFIR, 1972. Verification of a reflectance model for mature corn with application to corn blight detection. Remote sensing of environment, 2: 183-192.
- TURNER, R. E., 1974. Radiative transfer in real atmospheres. Environmental Institute of Michigan, report No. NASA-CR-ERIM-190100-24-T on NASA contract No. NAS9-9784.
- VERHOEF, W. and N. J. J. BUNNIK, 1975. A model study on the relations between crop characteristics and canopy spectral reflectance. NIWARS, Delft, publ. No. 33.
- VERHOEF, W. and N. J. J. BUNNIK, 1976. The directional reflectance of row crops. NIWARS, Delft, publ. No. 35.
- WARREN WILSON, J., 1965. Stand structure and light penetration I. Analysis by point quadrats. Journ. of Appl. Ecology, 2(2): 383-390.
- WENDLANDT, W. WM. and H. G. HECHT, 1966. Reflectance spectroscopy. John Wiley and Sons, New York.
- WERNER, W., 1970. Imaging properties of diffraction gratings, thesis. Waltman, Delft.
- WILLSTÄTTER, R. and A. STOLL, 1918. Untersuchungen über die Assimilation der Kohlensäure. Springer Verlag, Berlin.
- WIT, C. T. de, 1965. Photosynthesis of leaf canopies. Agr. Res. Report 663, Centre for Agricultural Publications and Documentation (PUDOC), Wageningen.

## APPENDIX A

### BIDIRECTIONAL SCATTERING OF DIRECT RADIANT FLUX

A homogeneous canopy is considered consisting of horizontally and vertically oriented Lambertian reflectors in accordance with Suits' assumptions. A layer with thickness,  $\Delta x$ , at depth,  $x$ , is irradiated by direct radiant flux,  $E_s^0(x)$ , perpendicular to the ray direction given by  $(\theta_s, \phi_s)$ . In this appendix a detailed description is presented of the relation between radiance from this layer into direction,  $(\theta_o, \phi_o)$ , resulting from direct bidirectional scattering of the incoming direct flux by the canopy components.

The radiant intensity is composed from the contributions of the horizontal and vertical scattering components.

$$\Delta I(\theta_o, \phi_o) = \Delta I_h(\theta_o, \phi_o) + \Delta I_v(\theta_o, \phi_o) \quad (\text{A.1})$$

The radiant intensity of a horizontal component with area,  $a_h$ , in upward direction along the normal vector of the component is given by:

$$I_h(0) = \frac{\rho}{\pi} a_h E_s^0(x) \cos \theta_s \quad (\text{A.2})$$

The resulting intensity in direction,  $(\theta_o, \phi_o)$ , due to  $n_h \Delta x$  horizontal components is found by applying the Lambertian cosine law.

$$\Delta I_h(\theta_o, \phi_o) = \frac{\rho}{\pi} a_h n_h E_s^0(x) \cos \theta_s \cos \theta_o \Delta x \quad (\text{A.3})$$

The presence of vertical components causes an azimuthal variation, since the relative azimuth angle,  $\psi$ , between the directions of incoming flux and observation determines the fraction of vertical components radiating by transmittance in the observation direction. The azimuth angle is defined by:

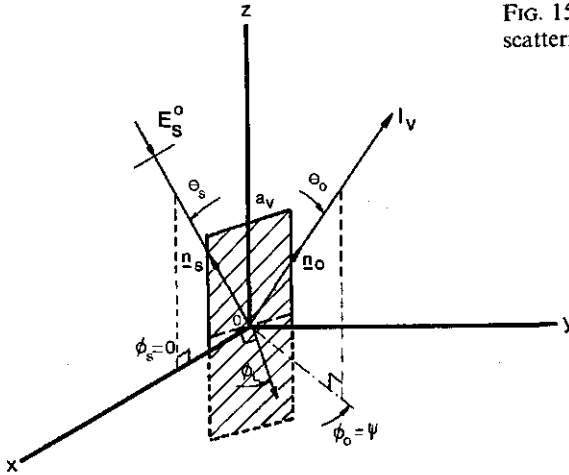
$$\begin{aligned} \psi &= |\phi_o - \phi_s|; 0 \leq |\phi_o - \phi_s| \leq \pi \\ \psi &= 2\pi - |\phi_o - \phi_s|; \pi < |\phi_o - \phi_s| < 2\pi \end{aligned} \quad (\text{A.4})$$

Fig. 152 shows a vertical component with normal vector,  $\underline{n}_L$  and irradiated by the incoming flux,  $E_s^0(x)$ . For simplicity  $\phi_s$  is considered to be zero. The directions of the incoming flux and observation are defined by the normalized vectors,  $\underline{n}_s$  and  $\underline{n}_o$ .

$$\left. \begin{aligned} \underline{n}_L &= (\cos \phi_L, \sin \phi_L, 0) \\ \underline{n}_s &= (\sin \theta_s, 0, \cos \theta_s) \\ \underline{n}_o &= (\cos \psi \sin \theta_o, \sin \psi \sin \theta_o, \cos \theta_o) \end{aligned} \right\} \quad (\text{A.5})$$

The radiant intensity,  $I_v(0)$ , in the direction of  $\underline{n}_L$  caused by the scattering of the vertical component depends on the azimuthal orientation of this component

FIG. 152. Geometry of the bidirectional scattering of a vertical canopy component.



$$I_v(0) = \frac{\rho}{\pi} a_v E_s^0(x) |\underline{n}_L \cdot \underline{n}_s|; \quad -\frac{\pi}{2} < \phi_L < \frac{\pi}{2} \quad (\text{A.6.})$$

$$I_v(0) = \frac{\tau}{\pi} a_v E_s^0(x) |\underline{n}_L \cdot \underline{n}_s|; \quad \frac{\pi}{2} < \phi_L < \frac{3\pi}{2}$$

The intensity in direction,  $(\theta_o, \psi)$ , follows from (A.6.) by applying the cosinus law.

$$I_v(\theta_o, \psi) = I_v(0) |\underline{n}_L \cdot \underline{n}_o| \quad (\text{A.7.})$$

In assuming a uniform distribution of the azimuthal orientation of the vertical components, the contribution,  $\Delta I_v(\theta_o, \psi)$ , is found by averaging the radiant intensity of the single components. This average intensity is determined by averaging the azimuthal orientation of the components.

$$\Delta I_v(\theta_o, \psi) = \frac{1}{2\pi} \int_0^{2\pi} I_v(\theta_o, \psi) d\phi_L n_v \Delta x \quad (\text{A.8.})$$

After determining the intervals of  $\phi_L$  belonging to reflectance or transmittance by the vertical components in the observation direction, substituting (A.5.) in (A.6.) and (A.7.) gives the following formula:

$$\Delta I_v(\theta_o, \psi) = \frac{n_v a_v}{\pi} E_s^0(x) \sin \theta_s \sin \theta_o \Phi(\psi) \Delta x \quad (\text{A.9.a.})$$

$$\Phi(\psi) = \frac{1}{2\pi} \left\{ \rho \left( \int_0^{\pi/2} d\phi_L + \int_{\pi/2+\psi}^{3\pi/2} d\phi_L + \int_{3\pi/2+\psi}^{2\pi} d\phi_L \right) |\cos \phi_L| + \right. \quad (\text{A.9.b.})$$

$$\left. * |\cos(\phi_L - \psi)| + \tau \left( \int_{\pi/2}^{\pi/2+\psi} d\phi_L + \int_{3\pi/2}^{3\pi/2+\psi} d\phi_L \right) |\cos \phi_L| |\cos(\phi_L - \psi)| \right\}$$

After solving the integrals of  $\Phi(\psi)$ , the next formula for  $\Delta I_e$  is found.

$$\Delta I_e(\theta_o, \psi) = \frac{n_v a_v}{\pi} E_s(x) \sin \theta_s \sin \theta_o \left\{ \frac{\rho}{2\pi} (\sin \psi + (\pi - \psi) \cos \psi) + \right. \\ \left. + \frac{\tau}{2\pi} (\sin \psi - \psi \cos \psi) \right\} \Delta x \quad (\text{A.10.})$$

The radiance contribution from the layer with thickness,  $\Delta x$ , is calculated by dividing the radiant intensity by the projected unit area in direction,  $(\theta_o, \psi)$ .

$$\Delta L(\theta_o, \psi) = \sec \theta_o (\Delta I_h(\theta_o, \psi) + \Delta I_v(\theta_o, \psi)) \quad (\text{A.11.})$$

Substituting (A.3.) and (A.10.) in (A.11.) gives:

$$\Delta L = \left( \frac{\rho}{\pi} H' + V' \frac{F(\theta_s, \psi)}{\pi} \text{tg } \theta_o \right) E_s(x) \Delta x \quad (\text{A.12.})$$

In this final result, expression (2.50.a.) has been used. The factor,  $F(\theta_s, \psi)$ , introduced in section 2.4.6.2., is given by:

$$F(\theta_s, \psi) = \left\{ \frac{\rho}{2\pi} (\sin \psi + (\pi - \psi) \cos \psi) + \frac{\tau}{2\pi} (\sin \psi - \psi \cos \psi) \right\} \text{tg } \theta_s \quad (\text{A.13.})$$

The bidirectional scattering coefficient,  $w(\theta_o, \theta_s, \psi)$ , follows from (A.12.).

$$w(\theta_o, \theta_s, \psi) = H' \rho + V' F(\theta_s, \psi) \text{tg } \theta_o \quad (\text{A.14.})$$

## APPENDIX B

### THE RECIPROCITY RELATION FOR BIDIRECTIONAL CANOPY REFLECTANCE

From equation (2.58.) for reflectance of a homogeneous canopy and the relations (2.39.a.) and (2.39.b.) follows that all the constants in the Suits' model may be written as a function of the total horizontal leaf area index,  $H$  and the total vertical leaf area index,  $V$ , instead of the leaf area densities,  $H'$  and  $V'$ . The integration constants,  $A$  and  $B$ , without diffuse sky irradiance,  $E_-(0)$ , are determined by the boundary conditions and are given by:

$$A = \frac{-D(1 - h^{-1}\rho_s)e^m - h^{-1}\{\rho_s(D+1) - C\}e^{-k}}{N} E_s(0) \quad (\text{B.1.a.})$$

$$B = \frac{D(1 - h\rho_s)e^{-m} + h\{\rho_s(D+1) - C\}e^{-k}}{N} E_s(0) \quad (\text{B.1.b.})$$

$$N = (h - \rho_s)e^m - (h^{-1} - \rho_s)e^{-m} \quad (\text{B.1.c.})$$

Substituting  $A$  and  $B$  in the canopy reflectance equation yields:

$$\begin{aligned} Nr(\theta_o, \theta_s, \psi) = & -\frac{u+hv}{K+m} \{D(1 - h^{-1}\rho_s)e^m + h^{-1}\{\rho_s(D+1) - C\}e^{-k}\} * \\ & * (1 - e^{-(K+m)}) + \frac{u+h^{-1}v}{K-m} \{h(\rho_s(D+1) - C) * \\ & * e^{-k} + D(1 - h\rho_s)e^{-m}\} (1 - e^{-(K-m)}) + \frac{N(uC+vD)}{K+k} * \\ & * (1 - e^{-(K+k)}) + \rho_s N(D+1)e^{-(K+k)} - \rho_s h * \\ & * \{D(1 - h^{-1}\rho_s)e^m + h^{-1}(\rho_s(D+1) - C)e^{-k}\} e^{-(K+m)} + \\ & + \rho_s h^{-1} \{h(\rho_s(D+1) - C)e^{-k} + \\ & + D(1 - h\rho_s)e^{-m}\} e^{-(K-m)} + \\ & + \frac{w}{K+k} (1 - e^{-(K+k)}) \end{aligned} \quad (\text{B.2.})$$

This equation is rewritten as a linear combination of the present exponential functions.

$$\begin{aligned} Nr(\theta_o, \theta_s, \psi) = & \left\{ \frac{u+hv}{K+m} [-D(1 - h^{-1}\rho_s)] + \frac{uC+vD}{K+k} (h - \rho_s) \right\} e^m + \\ & + \frac{w}{K+k} (1 - e^{-(K+k)}) + \left\{ \frac{u+h^{-1}v}{K-m} [D(1 - h\rho_s)] + \right. \\ & \left. - \frac{uC+vD}{K+k} (h^{-1} - \rho_s) \right\} e^{-m} + \end{aligned}$$

$$\begin{aligned}
& + \left\{ -\frac{u + hv}{K + m} [h^{-1}(\rho_s(D+1) - C)] + \right. \\
& + \frac{u + h^{-1}v}{K - m} h(\rho_s(D+1) - C) \left. \right\} e^{-k} + \left\{ \frac{u + hv}{K + m} * \right. \\
& * D(1 - h^{-1}\rho_s) - \frac{u + h^{-1}v}{K - m} D(1 - h\rho_s) + \\
& - \rho_s h D(1 - h^{-1}\rho_s) + \rho_s h^{-1} D(1 - h\rho_s) \left. \right\} e^{-K} + \\
& + \left\{ \frac{u + hv}{K + m} h^{-1}(\rho_s(D+1) - C) + \right. \\
& + \frac{uC + vD}{K + k} (h^{-1} - \rho_s) - \rho_s(\rho_s(D+1) - C) + \\
& - \rho_s(D+1) (h^{-1} - \rho_s) \left. \right\} e^{-(K+k+m)} + \\
& + \left\{ \frac{u + hv}{K - m} h(\rho_s(D+1) - C) + \frac{uC + vD}{K + k} (h - \rho_s) + \right. \\
& + \rho_s(\rho_s(D+1) - C) + \rho_s(D+1) (h - \rho_s) \left. \right\} e^{-(K+k-m)} \quad (B.3.)
\end{aligned}$$

The first term of (B.3.) is reduced to a function of infinite canopy reflectance.

$$\left( -\frac{u + hv}{K + m} \frac{D}{h} + \frac{uC + vD}{K + k} \right) (h - \rho_s) e^m = \left( r_\infty - \frac{w}{K + k} \right) (h - \rho_s) e^m \quad (B.4.)$$

In section 2.4.8. it has been demonstrated that  $r_\infty$  remains unchanged when the view and solar zenith angle are exchanged. If  $m$  in (B.4.) is replaced by  $-m$ , the same reciprocity is valid for the third term.

The factors of the fourth and fifth term with  $e^{-k}$  and  $e^{-K}$ , respectively, are both a linear function of soil reflectance,  $\rho_s$ . The terms of both exponential functions without  $\rho_s$  are taken together with substitution of the expressions (2.49.) for  $C$  and  $D$ .

$$\begin{aligned}
& \left( \frac{h^{-1}u + v}{K + m} - \frac{hu + v}{K - m} \right) \frac{s\sigma - s'(k-a)}{m^2 - k^2} e^{-k} + \\
& + \left( \frac{u + hv}{K + m} - \frac{u + h^{-1}v}{K - m} \right) \frac{s'\sigma + s(k+a)}{m^2 - k^2} e^{-K} \quad (B.5.)
\end{aligned}$$

Substitution of  $h$  by (2.48.) in (B.5.) leads to the following result.

$$\frac{-2m(u(K+a) + \sigma v)(s\sigma - s'(k-a))e^{-k} + 2m(s(k+a) + s'\sigma)(v(K-a) - \sigma u)e^{-K}}{\sigma(K+m)(K-m)(m-k)(m+k)} \quad (B.6.)$$

The numerator of (B.6.) shows symmetry when  $K$  and  $k$ ,  $u$  and  $s$  and  $v$  and  $s'$  are exchanged, respectively.

The soil term of both exponential functions is:

$$\rho_s(D+1)\left(-\frac{u+ hv}{h(K+m)} + \frac{hu+ v}{K-m}\right)e^{-k} - \rho_s D\left(h^{-1}\frac{u+ hv}{K+m} + \frac{(hu+ v)}{K-m} + (h+h^{-1})\right)e^{-K} \quad (\text{B.7.})$$

This function also may be written as:

$$-\rho_s D\left(\frac{u+ hv}{h(K+m)} - \frac{hu+ v}{K-m}\right)(e^{-k} + e^{-K}) - \rho_s\left\{\left(\frac{u+ hv}{h(K+m)} + \frac{hu+ v}{K-m}\right)e^{-k} + D(h+h^{-1})\right\}e^{-K} \quad (\text{B.8.})$$

Substitution of  $D$  by (2.49.b.) and of  $h$  by (2.48.) in (B.8.) yields the following symmetrical function for  $\theta_o$  and  $\theta_s$ .

$$\rho_s \frac{2m\{(k+a)s+s'\sigma\}\{(K+a)u+v\sigma\}}{\sigma(m-k)(m+k)(K+m)(K-m)}(e^{-k} + e^{-K}) + \rho_s \frac{2m(u(a+k) + \sigma v)e^{-(K+k)}}{\sigma(K+m)(K-m)} + \rho_s \frac{2m(s(a+k) + s'\sigma)}{\sigma(k+m)(k-m)}e^{-(K+k)} \quad (\text{B.9.})$$

The sixth and seventh exponential function is considered of formula (B.3.) and the terms with and without  $\rho_s$  separated. The expression in the factor of the exponential function,  $\exp\{-(K+k+m)\}$ , without  $\rho_s$ , written as a function of parameters of  $\theta_o$  and  $\theta_s$  is:

$$\frac{1}{h}\left(-C\frac{u+ hv}{K+m} + \frac{uC+ vD}{K+k}\right)e^{-(K+k+m)} = \frac{\sigma^2(us+vs') + \sigma\{us'(a-k) + vs(a-K)\} - (a+m)(K+k)vs'}{h\sigma(K+m)(k+m)(K+k)}e^{-(K+k+m)} \quad (\text{B.10.})$$

Function (B.10.) yields the term without  $\rho_s$  in the factor of the seventh exponential function by replacing  $m$  by  $-m$  and  $h^{-1}$  by  $h$ . Both terms together exchange when  $\theta_o$  and  $\theta_s$  are exchanged.

The term multiplied with  $\rho_s$  in the factor of the sixth exponential function of (B.3.) is written as follows.

$$\rho_s\left\{\frac{u+ hv}{K+m} \cdot \frac{D}{h} - \frac{uC+ vD}{K+k} + \frac{u+ hv}{h(K+m)} + C - h^{-1}(D+1)\right\}e^{-(K+k+m)} \quad (\text{B.11.})$$



The first two terms in (B.11.) are related with infinite canopy reflectance and are symmetrical; if  $m$  and  $h^{-1}$  are replaced by  $-m$  and  $h$ , symmetry has also been proved for the corresponding term of the last exponential function. The remaining part of (B.11.) is written as:

$$\rho_s \left\{ \frac{u + hv}{h(K + m)} + C - h^{-1}(D + 1) \right\} e^{-(K+k+m)} =$$

$$\rho_s \left\{ \frac{(k+m)(\sigma u + (a+m)v) + (K+m)(\sigma s + (a+m)s)}{(K+m)(k+m)(a+m)} - h^{-1} \right\} e^{-(K+k+m)} \quad (\text{B.12.})$$

This function is symmetrical for exchange of  $\theta_o$  and  $\theta_s$ . In an analogous way symmetry of the soil term of the seventh exponential function has been demonstrated.

The final conclusion is that the reciprocity relation for the canopy reflectance model has been proved analytically. It was also shown that reciprocity is no longer valid, if diffuse sky irradiance is present. The procedure given in this appendix can be applied to the more general cases of multilayer canopies, which means that reciprocity is a general canopy property and not restricted to a homogeneous canopy.

## CURRICULUM VITAE

Nico Bunnik werd geboren op 22 juni 1942 te Rijswijk (Z.H.). Te 's-Gravenhage behaalde hij het diploma HBS-b in 1961. Aan de Hogere Technische School te Dordrecht verwierf hij het diploma Fysische Techniek in 1965 en daarop, na vervulling van zijn militaire dienstplicht, aan de afdeling der Technische Natuurkunde van de Technische Hogeschool te Delft in 1972 het ingenieursdiploma in de vakgroep Magnetische Resonantie. In november 1972 trad hij als wetenschappelijk ambtenaar in dienst van de Nederlandse Interdepartementale Werkgemeenschap voor het Applicatie-onderzoek van Remote Sensing technieken (NIWARS) te Delft. Zijn werk op het gebied van reflectie door gewassen van licht en nabije infraroodstraling leidde tot dit proefschrift. Sedert 1 september 1977 is hij werkzaam in dienst van het Nationaal Lucht- en Ruimtevaartlaboratorium te Amsterdam.